

Modeling, Advanced Temperature Measurement, and Control Algorithms in Thermoforming

Rahi Modirnia



Department of Electrical and Computer Engineering
McGill University, Montréal

March 2016

A thesis submitted to McGill University in partial fulfillment of the requirements
of the degree of Doctor of Philosophy

© Rahi Modirnia

To my parents who gave me all the love in the world!

ABSTRACT

A thermoforming process consists of three major phases: heating, forming, and cooling. During the heating phase, the sheet is heated to a certain forming temperature, where it will start to experience sagging. Proper forming could only occur if the plastic sheet has reached the precise temperature set-point (profile) at which it is flexible enough to be molded. Moreover, often, because of the complexity of the shape of the final product, uneven temperature set-points or non-uniform temperature profiles are required across the plastic sheet. Therefore, it is crucial to systematically control the heaters' temperatures so that the exact temperature profile is achieved across and through the depth of the plastic sheet. There have been several advancements in the modeling and closed-loop control of the thermoforming heating phase. However, there are still a number of problems yet to be accounted for, which pose a barrier on the efficiency, precision, productivity, and autonomy of the process.

In the first part of this thesis, advanced temperature measurement algorithms are developed, namely model-based virtual sensors (MBVS) and core-temperature observers. The need to develop virtual measurement techniques arises from the fact the thermoforming control process requires a large number of feedback measurements in order to accurately control the temperature profile across the plastic sheet, and this is costly to implement using only infrared sensors. The concept of MBVSs allows for additional surface-temperature measurement points in addition to the existing infrared sensors. This leads to improved observability of the plastic sheet temperature and increased accuracy in achieving uneven temperature profiles, thus eliminating the use of extra infrared sensors and significantly reducing the cost of the control system. Additionally, core-temperature observers are developed in order to precisely monitor the core-temperature of the plastic sheet since it is crucial for the center-plane of the sheet to be within the forming temperature window at the end of the cycle. Virtual core-temperature observers are introduced since insertion of temperature measurement tools, such as thermocouples, in the plastic sheet is not permitted, and it is not possible to establish any kind of physical contact with the plastic sheet during the heating phase.

In the second part of this thesis, the application of the Watanabe-modified Smith predictor control technique (an internal-model control technique) is developed for the thermoforming heating phase in order to reduce the heating-cycle time of the process. The

performance of the system involving the new method was compared with existing control methods, and a significantly faster response was observed.

The third part of the thesis addresses the control of multilayered plastic sheets in the heating phase. Thermoforming of multilayered sheets has proven to be quite challenging due to the fact that different plastic materials have different rheological properties and distinctive forming temperatures. In this thesis, a dynamical temperature evolution model of multilayered plastic sheets is presented, followed by a proposed discrete-time model predictive control (DTMPC) algorithm to solve, for the first time, the non-uniform temperature tracking problem of all the layers, while incorporating the nonlinear dynamics of the actuators in the design. The DTMPC method is shown to provide superior tracking performance as well as lower energy consumption compared to classical control methods.

Finally, the last part of this thesis covers the important problem of parameter variations in thermoforming. During the thermoforming heating phase, temperature evolution models of plastic sheets consist of nonlinear temperature-dependent parameters, which have yet to be accounted for when solving the temperature tracking problem. These equations are subsequently modeled in the hybrid systems framework based on the segmentization of the parameter varying elements. Employing a proposed constrained hybrid optimal control (HOC) algorithm based on the Hybrid Minimum Principle (HMP), which contains the nonlinear actuator constraints of the heating phase, the temperature tracking problem is solved for this parameter varying system, for the first time. The HOC algorithm is also designed to minimize the energy consumption of the heaters during the heating phase. Moreover, a closed-loop hybrid controller (CLHC) is developed, based on the proposed HOC, to provide robustness against perturbations. Successful application of the proposed HOC algorithm also serves as a proof of concept to show that HMP based HOCs can be implemented on large-scaled nonlinear industrial processes, containing parameter variations and nonlinear actuator constraints.

RÉSUMÉ

Un procédé de thermoformage se compose de trois grandes phases: le chauffage, le formage, et le refroidissement. Pendant la phase de chauffage, la feuille est chauffée à une température de formage prédéterminée, où elle commence à subir de l'affaissement. Un formage approprié ne peut s'effectuer que si la feuille de plastique a atteint le point de consigne de température précise (profil) à laquelle elle devient suffisamment souple pour être moulée. En outre, souvent en raison de la complexité de la forme du produit final, un profil de température de consigne inégal ou non uniforme est nécessaire selon la position sur la feuille de plastique. Par conséquent, il est crucial de contrôler systématiquement les températures des éléments de chauffage de telle sorte que le profil de température exact puisse être obtenu à différentes positions et profondeurs de la feuille de plastique. Il y a eu plusieurs avancées dans la modélisation et le contrôle en boucle fermée de la phase de chauffage du thermoformage. Cependant, il y a encore un certain nombre de problèmes à prendre en compte, qui constituent une barrière pour l'efficacité, la précision, la productivité et l'autonomie du processus.

Dans la première partie de cette thèse, des algorithmes de mesure de température de pointe sont développés, à savoir des capteurs virtuels basés sur des modèles (MBVS) et des observateurs de température interne. La nécessité de développer des techniques de mesure virtuelles se pose du fait que le processus de contrôle de thermoformage nécessite un grand nombre de mesures de rétroaction afin de contrôler avec précision le profil de température sur toute la surface de la feuille de plastique, ce qui est coûteux à mettre en œuvre en utilisant uniquement des capteurs infrarouges. Le concept de MBVS permet d'obtenir des points supplémentaires de mesure de température en surface, en plus des capteurs infrarouges existants. Cela conduit à l'amélioration de la gouvernabilité de la température de la feuille de matière plastique et une plus grande précision dans la réalisation de profils de température inégaux, ce qui évite aussi l'utilisation de capteurs infrarouges d'appoint et réduit considérablement le coût du système de commande. En outre, les observateurs de température interne sont conçus pour contrôler précisément la température interne de la feuille de matière plastique, ce qui est essentiel pour le plan médian à l'intérieur de la feuille qui doit être dans la fenêtre de température de formage à la fin du cycle. Les observateurs de température interne sont introduits puisque les capteurs de température physiques devant être insérés dans la feuille de plastique, tels que des

thermocouples, sont interdits, et il est impossible d'établir le moindre contact physique avec la feuille de plastique au cours de la phase de chauffage.

Dans la deuxième partie de cette thèse, l'application de la technique de contrôle prédictif de Smith modifiée selon la technique de Watanabe (une technique de contrôle à modèle interne) est élaborée pour la phase de chauffage de thermoformage afin de réduire le temps de cycle de chauffage du processus. La performance du système comportant la nouvelle méthode a été comparée à des méthodes de contrôle existantes, et une réponse beaucoup plus rapide a été observée.

La troisième partie de la thèse porte sur le contrôle des feuilles de plastique multicouches dans la phase de chauffage. Le thermoformage de feuilles multicouches s'est révélé être très difficile en raison du fait que différentes matières plastiques ont des propriétés rhéologiques et des températures distinctes de formage. Dans cette thèse, un modèle dynamique de l'évolution de la température des feuilles de plastique multi-couches est présenté, suivi d'un algorithme de commande prédictive en temps discret (DTMPC) pour résoudre, pour la première fois, le problème d'asservissement de températures non uniformes de toutes les couches de la feuille, tout en intégrant la dynamique non-linéaire des actionneurs dans la conception. On démontre que la méthode DTMPC présente une performance d'asservissement supérieure ainsi qu'une consommation d'énergie inférieure par rapport aux méthodes de contrôle classiques.

Enfin, la dernière partie de cette thèse traite du problème important de variation de paramètres dans le thermoformage. Pendant la phase de chauffage de thermoformage, les modèles d'évolution de la température de feuilles de plastique se composent de paramètres non-linéaires dépendant de la température, qui doivent être pris en compte lors de la résolution du problème de suivi de la température. Ces équations sont ensuite modélisées dans le cadre des systèmes hybrides sur la base de la segmentation des paramètres variables. L'utilisation d'un algorithme de commande hybride optimale (HOC) basé sur le principe minimum hybride (HMP), qui contient les contraintes d'actionneurs non-linéaires de la phase de chauffage, le problème d'asservissement de la température est résolu pour ce système à paramètres variables, et ceci pour la première fois. L'algorithme de HOC est également conçu pour minimiser la consommation d'énergie des éléments de chauffage pendant la phase de chauffage. En outre, un contrôleur hybride en boucle fermée (CLHC) est développé, sur la base du HOC proposé, pour donner une robustesse contre les perturbations. L'application réussie de l'algorithme de HOC

proposé sert aussi de démonstration de faisabilité de la HMP HOC qui peut être mise en œuvre sur des procédés industriels non linéaires à grande échelle, ayant des variations de paramètres et des contraintes d'actionneurs non-linéaires.

ACKNOWLEDGMENTS

During my PhD studies, I have been extremely lucky to be accompanied with the support of some of the best people I have encountered in my life. These amazing people include a number of McGill professors, colleagues, friends, and family, who have all pushed me to towards being a better engineer, and most importantly, a better person.

I would like to first start by thanking my thesis supervisor, Professor Benoit Boulet, who fully supported and trusted me throughout this journey. I will never forget his positive encouragements and his patience regarding all of our scientific work. It was because of his trust and excellent professional guidance that we have worked and published peer-reviewed articles on numerous inter-disciplinary side projects, in addition to the PhD thesis. His kind and friendly attitude makes him such a joy to interact with, inside and outside the work domain. His vision and approach towards directing my studies has definitely made me a better engineer, and I would like to especially thank him for that. It has been an absolute pleasure to work with Professor Benoit, and I sincerely hope that we can always keep in touch and continue our great relationship.

I would also like to thank my PhD advisory committee, Professors Peter Kabal and Peter Radziszewski, for their commitment and support during my studies at McGill.

Additionally, I would also like to thank Professor Martin Rochette for his involvement and support in the photonics related project as his open-minded view of his research domain, opened the door for the experimental application of sophisticated control problems in the field of photonics, which have been rarely attempted so far.

Thanks also goes to Professor Peter Caines, his former student Mr. Farzin Taringoo, and his current PhD student Mr. Ali Pakniyat for their commitment and scientific support with regards to the concept of “hybrid optimal control”, which has lead to the successful completion of Chapter 4 of this thesis.

Special thanks to former graduate students working in the thermoforming research group for their contributions and for developing a thermoforming simulator, which has been further developed and expanded upon in this thesis. Many thanks goes to Ben Moore, Mark Ajersch, Guy Gauthier, Alexandre Boyer, and Gino Lalli for their many important contributions.

I would like to thank my colleagues for making this an incredible journey. Many thanks goes to Ahmad Haidar, Vahid Raissi Dehkordi, Farzin Taringoo, Marwan Kanaan, Ali Pakniyat,

Mahyiar Abdolhosseini, Omar Abdelfattah, Mojtaba Nourian, and many other great colleagues at the Centre for Intelligent Machines (CIM) for their incredible support. Special thanks goes to my Foosball buddies, Ahmad, Marwan, and Farzin, for all the moments of excitement and laughter in the CIM lounge.

I would like to thank the staff of CIM and the McGill ECE graduate affairs office for providing me with an excellent research environment. I would especially like to thank Mr. Jan Binder, and Ms. Cynthia Davidson, and Ms. Marguerite Dexter for their incredible work ethic and commitment. I would also like to thank McConnell Building's fourth floor janitor Mr. Labelle, one of the most committed people working in McGill, for his exemplary work ethic in making sure that our offices and our work environment are always spotless.

I would also like to thank my friends outside of our academic environment. I am biologically an only child, but there have some amazing people who have been more than siblings to me, and I would like to thank them from the bottom of my heart. Amir Pourteymour, Sepideh Bakhtiari, Nasim Sedaghat, and YaC Sedaghat have all been the greatest siblings anyone could wish for. Most especially, I would like to thank my brother Ashkan Golzar who has been with me through thick and thin and has continuously and kindly supported me during this period. I would also like to thank Fariborz, Nazanin Aslani, Padideh, Peiman, Amin Damyar, Shahab, Firoozeh, Amin Mirzadeh, Pegah, Shahin, Navid, Saba, Farnood, Sam Sadighi, and all my other friends, which I cannot mention because of lack of space, for being some of most supportive, fun, and enjoyable people I have ever met.

Thanks to all my friends in Iran, California, and all over the world, especially Mahmoud, Ali and Sadegh, who have always inspired me to continue on my path stronger than ever before.

Special thanks to comedian Louis C.K. for making me laugh when I was down and tired during the sleepless nights. Louis you are hilarious! You are so hilarious “that I almost went INSANE”, and you are so funny that “you almost ruined my life” in the greatest way possible. I really hope to meet you one day and give you a big hug to show my appreciation.

I would like to thank my relatives, my aunts and uncles, and my grandparents. Special thanks goes to Mohammad Reza Kojouri, Fatemeh Davatolhagh, Badri Ghajar, Javad Modirnia, Farideh, Farhad, Farzaneh and Farzam Kojouri, Gita, Mahin, and my uncles Hamid and Kamal, for all their love and support. I would like to thank my two cousins Pirooz and Pouyan, who I grew up with, for welcoming me in and treating me like their own. To my cousins, Roya, Reza,

Anita, Mehrnoush, and all the other beautiful ones, I would like to say thanks for being there. I would also like to thank all my other relatives who made me experience lovely moments in life.

Lastly, I want to thank my parents, Fariba Kojouri and Mohammad Modirnia, who have sacrificed everything for me to get here. My parents, both successful Doctors in their own domains, gave up their careers to lift me up as a human being. More important than providing me with everything that I could have asked for, they gave me the most precious gift in life that I will always cherish and carry with me forever: true and genuine love. You guys are my role models, my best friends, and my everything! I would like to express my eternal gratitude to you and tell you that I love you very much!

CLAIMS OF ORIGINALITY

The contributions of this thesis are summarized as follows:

In Chapter 2:

- Model-based virtual sensors (MVBS) and core-temperature observers are developed as new surface and center-plane temperature estimation methods to improve observability and result in accurate temperature zoning of plastic sheets, while producing a cost-effective control system.

In Chapter 3:

- Application of the Watanabe-modified Smith predictor technique (an internal-model control method) is presented to improve the performance and robustness of the in-cycle temperature tracking problem (equivalent to reducing the heating cycle time).

In Chapter 4:

- A state-space temperature evolution model of multilayered plastic sheets is developed, which can be utilized in various control schemes.
- A discrete-time model predictive control (DTMPC) algorithm is developed and applied to the thermoforming heating phase to solve the multilayer temperature tracking problem. The superior performance and energy efficiency of the DTMPC algorithm, compared to conventional control methods, is shown.
- Energy efficiency analysis is conducted for the first time in thermoforming.

In Chapter 5:

- Temperature-dependent material properties are introduced and accounted for in the control problem of the heating phase.
- A Hybrid Minimum Principle (HMP) based constrained hybrid optimal control (HOC) algorithm is implemented to solve the temperature tracking problem of plastic sheets in the presence of temperature-varying model parameters.

- A closed-loop hybrid control (CLHC) block diagram is developed, based on the HOC, to provide robustness against perturbations and facilitate industrial applicability.
- A proof of concept is provided to show that HMP based hybrid optimal controllers can be implemented on complex industrial processes, which are large-scaled, containing nonlinear constraints and parameter variations.

The abovementioned contributions have resulted in the following peer-reviewed publications:

- *Papers published*

1. R. Modirnia and B. Boulet, "Model-Based Virtual Sensors and Core-Temperature Observers in Thermoforming Applications," *IEEE Transactions on Industry Applications*, vol. 49, no. 2, pp. 721-730, Mar. 2013.

- **Authors contributions:**

- 1) Rahi Modirnia: the author of the thesis is responsible for the development of the sensing algorithm, implementation and interpretation of the results. The thesis author is also responsible for writing the manuscript.
- 2) Benoit Boulet: supervised the work and edited the manuscript.

2. R. Modirnia and B. Boulet, "Application of the Watanabe-modified Smith predictor control technique in thermoforming, " in *American Control Conf. (ACC)*, Montreal, Canada, 2012, pp. 6448-6454.

- **Authors contributions:**

- 1) Rahi Modirnia: the author of the thesis is responsible for the design and development of the control technique, implementation, and interpretation of the results. The thesis author is also responsible for writing the manuscript.
- 2) Benoit Boulet: supervised the work and edited the manuscript.

3. R. Modirnia and B. Boulet, "Model-based virtual sensors and core temperature observers in thermoforming applications," in *2011 IEEE Industry Applications Society Annual Meeting (IAS)*, Orlando, FL, Oct. 2011, pp.1-8.

➤ **Authors contributions:**

- 1) Rahi Modirnia: the author of the thesis is responsible for the development of the sensing algorithm, implementation and interpretation of the results. The thesis author is also responsible for writing the manuscript.
- 2) Benoit Boulet: supervised the work and edited the manuscript.

- *Papers submitted for publication*

4. R. Modirnia, M. Abdolhosseini, and B. Boulet, " Modeling and Model Predictive Control of Multilayered Plastic Sheets in Thermoforming," *IEEE Transactions on Control System Technology*, submitted and under review (Submission number: TCST-2015-0664).

➤ **Authors contributions:**

- 1) Rahi Modirnia: the author of the thesis is responsible for the development and implementation of the model predictive controller in collaboration with Mahyar Abdolhosseini. In addition, the thesis author is responsible for conducting the energy efficiency analysis interpreting the results. The thesis author is also responsible for writing the manuscript.
- 2) Mahyar Abdolhosseini: significantly contributed to the design of the model predictive control algorithm. He also partially wrote the manuscript.
- 3) Benoit Boulet: supervised the work and edited the manuscript.

5. R. Modirnia, A. Pakniyat, and B. Boulet, "Application of Hybrid Optimal Control and Closed-Loop Hybrid Control to Manage Temperature-Dependent Parameters in Thermoforming," *IEEE Transactions on Control System Technology*, submitted and under review (Submission number: TCST-2015-1011).

➤ **Authors contributions:**

- 1) Rahi Modirnia: the author of the thesis is responsible for the implementation of the hybrid optimal controller on the thermoforming heating process. The thesis author is also responsible for developing and implementing the closed-loop hybrid controller in the heating phase. In addition, the thesis author is responsible for the interpretation of the results. The thesis author is also responsible for writing the manuscript.
- 2) Ali Pakniyat: responsible for providing the theoretical framework of the hybrid optimal control technique. He also partially wrote the manuscript.
- 3) Benoit Boulet: supervised the work and edited the manuscript.

This thesis is a manuscript-based thesis, based on papers 1, 2, 4, and 5.

TABLE OF CONTENTS

ABSTRACT	iii
RÉSUMÉ	v
ACKNOWLEDGMENTS	viii
CLAIMS OF ORIGINALITY	xi
TABLE OF CONTENTS	xv
LIST OF FIGURES	xix
LIST OF TABLES	xxiii
1 Introduction	1
1.1 Literature Review and Motivation	1
1.2 New Surface and Core-Temperature Estimation Methods	8
1.3 A Control Method to Reduce the Heating Cycle Time	11
1.4 Thermoforming of Multilayer Plastic Sheets	13
1.5 Temperature-Dependent Material Properties and Hybrid Control	14
1.6 Thesis Organization	16
2 Model-Based Virtual Sensors and Core-Temperature Observers in Thermoforming	18
2.1 Abstract	19
2.2 Introduction	19
2.3 Modeling of The Heating Phase in Thermoforming	22
2.4 Description of the Existing Control System	25
2.5 Implementation of MVBSs	26
2.6 Application of the Luenberger Core Temperature Observer	29
2.6.1 Closed-Loop Luenberger State Observer	29
2.6.2 Application of the Luenberger Observer in a Thermoforming Process	31
2.7 Simulation Results	33
2.7.1 Simulation Under Ordinary Conditions	35
2.7.2 Simulation Under Uncertainty in Material Properties	38
2.8 Conclusion	40

3 Application of the Watanabe-Modified Smith Predictor Technique in Thermoforming	41
3.1 Abstract	42
3.2 Introduction	42
3.3 Description of the Existing Control System	44
3.4 The Smith Predictor Control Technique: an Overview	46
3.5 Application of the Watanabe-Modified Smith Predictor to the Thermoforming Heating Phase	48
3.5.1 Justifying the Use of the Smith Predictor Technique.....	48
3.5.2 Controller Design	49
3.6 Simulation Results	51
3.6.1 Simulation under ideal conditions	55
3.6.2 Simulation under uncertainty in material properties.....	58
3.7 Conclusion	60
4 Modeling and Model Predictive Control of Multilayered Plastic Sheets in Thermoforming	61
4.1 Abstract	62
4.2 Introduction	62
4.3 Modeling of the Heating Phase of Thermoforming in the Presence of Multilayered Plastic Sheets	65
4.3.1 Horizontal Conduction.....	72
4.4 Model Predictive Control: an Overview	73
4.5 Heating Phase Control Problem: Proposed DTMPC	80
4.5.1 Linear State-Space Model	83
4.5.2 Incorporating the Actuator Constraints.....	84
4.5.3 Establishing the DTMPC Optimization.....	86
4.6 Simulation Results	86
4.6.1 Tracking Performance Simulation.....	88
4.6.2 Energy Performance Simulation	96
4.7 Conclusion	98
5 Application of Hybrid Optimal Control and Closed-Loop Hybrid Control to Manage Temperature-Dependent Material Properties in Thermoforming	100

5.1	Abstract.....	102
5.2	Introduction	102
5.3	Description of the Existing Model and Block Diagram	105
5.3.1	Modeling of the Heating Phase.....	106
5.3.2	Temperature Dependent Material Properties.....	109
5.4	HMP-Based HOC Algorithm	112
5.4.1	The HMP with Constraints	113
5.4.2	HMP-Based HOC Algorithm	115
5.5	Design of the HOC for the Heating Process	116
5.5.1	Segmentation of the Specific heat capacity.....	117
5.5.2	Linear State-Space Model	118
5.5.3	State Constraints	120
5.5.4	Actuator Constraints.....	120
5.5.5	HOC Design to Solve the Thermoforming Tracking Problem	122
5.5.6	Design Results	124
5.6	Simulation Results	126
5.6.1	Open-Loop HOC	127
5.6.2	Closed-Loop Hybrid Controller (CLHC).....	127
5.7	Conclusion.....	137
6	Conclusion	138
6.1	Thesis Summary.....	138
6.2	Future Research.....	141
6.2.1	Inclusion of the Sag Effect in the Heat Transfer Model.....	141
6.2.2	Future Research on Temperature-Dependent Material Properties.....	142
6.2.3	Cycle-to-Cycle Control.....	143
6.2.4	Thermoplastic Composite Thermoforming and Welding Processes	143
7	References	144
Appendix A	The Industrial Thermoforming Machine Simulator	152
A.1	The Thermoforming Simulator Blocks	153
A.1.1	The Heaters Block.....	155
A.1.2	The Heating Phase Model Block	157
A.1.3	The Ambient Air Blocks	162

A.1.4	Luenberger Observer Blocks	162
A.2	Chapter 2 Simulator Blocks	163
A.3	Chapter 3 Simulator Blocks	166
A.4	Chapter 4 Simulator Blocks	167
A.5	Chapter 5 Simulator Blocks	168
A.6	Table of Material Properties	169
A.7	Simulator Discussion	170

LIST OF FIGURES

Figure 1.1. The thermoforming heating and forming phase [8].....	2
Figure 1.2. Block diagram of the closed-loop system containing the heating phase.....	7
Figure 1.3. The thermoforming oven, exhibiting the heaters, the plastic sheet, and the measurement zones.....	11
Figure 2.1. Block diagram of the closed-loop system.....	26
Figure 2.2. Updated controller block in the presence of MBVSs.....	27
Figure 2.3. Closed-loop block diagram of the system containing the virtual sensors	29
Figure 2.4. Block diagram of a closed-loop Luenberger state estimator	30
Figure 2.5. Complete block diagram of the system containing the MBVSs and the observers..	33
Figure 2.6. Desired zoned temperature setpoints (profile).....	35
Figure 2.7. 2-D position grid of the real IR sensors and the virtual sensors relative to the heaters	35
Figure 2.8. (a) Ramp response of the real sensors to the zoned ramp inputs shown in red dotted lines. (b) Ramp response of the MVBSs to the zoned ramp inputs. (c) Estimated core-temperature response to the zones ramp inputs. (d) Final surface temperatures of the measurement zones.....	38
Figure 2.9. In the presence of 20% material uncertainty: (a) Ramp response of the real sensors to the zoned ramp inputs shown in red dotted lines. (b) Ramp response of the MBVSs to the zoned ramp inputs. (c) Estimated core-temperature response to the zones ramp inputs. (d) Final surface temperatures of the measurement zones.....	40
Figure 3.1. Block diagram of the closed-loop control system	46
Figure 3.2. Watanabe-modified Smith predictor	47
Figure 3.3. The open-loop surface temperature response of an HDPE plastic	49
Figure 3.4. The 2D position grid of the real IR sensors and the virtual sensors relative to the heaters	53
Figure 3.5. Open-loop response of the measurement zones on a plastic sheet in simulation shown in gray, along with the fitted response shown in red.....	55
Figure 3.6. Desired zoned temperature set-points (profile)	56
Figure 3.7. (a) Averaged closed-loop step response of all the IR measurement zones to the zoned set-points using the Smith predictor method, shown in blue, and using PI controllers,	

shown in red (dotted plot). (b) Averaged step response of all the virtual measurement zones to the zoned set-points points using the Smith predictor method, shown in blue, and using PI controllers, shown in red (dotted plot). (c) Averaged estimated core-temperature response to the zoned set-points points using the Smith predictor method, shown in blue, and using PI controllers, shown in red (dotted plot)..... 57

Figure 3.8. In the presence of 30% material uncertainty: (a) Averaged closed-loop step response of all the IR measurement zones to the zoned set-points using the Smith predictor method, shown in blue, and using PI controllers, shown in red (dotted plot). (b) Averaged step response of all the virtual measurement zones to the zoned set-points points using the Smith predictor method, shown in blue, and using PI controllers, shown in red (dotted plot). (c) Averaged estimated core-temperature response to the zoned set-points points using the Smith predictor method, shown in blue, and using PI controllers, shown in red (dotted plot). 59

Figure 4.1. Block diagram of the closed-loop system..... 66

Figure 4.2. The multilayer plastic sheet composed of acrylic and ABS layers 68

Figure 4.3. A two-layer, two-zone plastic sheet 73

Figure 4.4. The heating and cooling curves of a ceramic heater with the heaters operating at 100% during the heating period, and turned off during the cooling period..... 86

Figure 4.5. Desired zoned temperature set-points (profile) 88

Figure 4.6. 2-D position grid of IR and virtual sensors relative to the heaters..... 88

Figure 4.7. Closed-loop step response of IR and virtual measurement zones to the zoned temperature set-points using the IR (shown in blue) DTMPC (shown in red) methods: (a) left side top surface profile of 180°C, (b) left side bottom surface profile of 170°C, (c) left side core temperature profile of 170°C, (d) right side top surface profile of 160°C, (e) right side bottom surface profile of 150°C, (f) right side core temperature profile of 150°C. 93

Figure 4.8. Using the DTMPC method: (a) Control output generated by the DTMPC controller. (b) The response of the heaters to the generated control output. (c) The difference between the heaters' response and the control output..... 94

Figure 4.9. Using PI controllers: (a) Control output generated by the DTMPC controller. (b) The response of the heaters to the generated control output. (c) The difference between the heaters' response and the control output..... 95

Figure 4.10. Using PI controllers: (a) the temperature response of the heaters, (b) the average power consumption of ceramic heaters.....	97
Figure 4.11. Using the DTMPC method: (a) the temperature response of the heaters, (b) the average power consumption of ceramic heaters.....	98
Figure 5.1. Block diagram of the closed-loop system.....	109
Figure 5.2. Temperature variation curve of the specific heat capacity.....	110
Figure 5.3. Temperature response of a measurement zone in open-loop: 1) when the specific heat capacity is kept constant, 2) when it is varying with temperature of the measurement zone. Substantial difference is observed.....	112
Figure 5.4. The heating and cooling curves of a ceramic heater with the heaters operating at 100% during the heating period, and turned off during the cooling period.....	121
Figure 5.5. 2-D position grid of IR and virtual sensors relative to the heaters.....	125
Figure 5.6. Open-loop block diagram containing the hybrid optimal control inputs.....	130
Figure 5.7. Proposed CLHC block diagram, providing robustness against perturbations.....	130
Figure 5.8. Open-loop response of the real and virtual measurement zones using the HOC generated control inputs: (a) under 15% uncertainty in C_p . (b) under 20% uncertainty in C_p . .	130
Figure 5.9. Using the open-loop HOC setup: The Difference between the optimal temperature trajectories and the temperature response of the real and virtual measurement zones. The difference remains in the $\pm 10^\circ\text{C}$ bound.....	131
Figure 5.10. Using the CLHC setup: The Difference between the optimal temperature trajectories and the temperature response of the real and virtual measurement zones. Maximum difference is 6°C and showing close tracking.....	131
Figure 5.11. Proposed flowchart of the HOC algorithm used to solve the thermoforming heating phase tracking problem.....	132
Figure 5.12. Resulting from the HOC algorithm: (a) The Hamiltonian plot of the three segments. (b) The Langrangian of the Hamiltonian for the three segments. (c) Total cost minimization curve.....	133
Figure 5.13. Resulting from the HOC algorithm: (a) the optimal temperature trajectories of the measurement zones. (b) Optimal control inputs for the heaters.....	134
Figure 5.14. Simulating the HOC generated control inputs in open-loop: (a) The temperature response of the real and virtual measurement zones, closely tracking the optimal trajectories. (b)	

The response of the heaters to the HOC inputs. (c) The percentage error between the heaters' response and HOC generated control inputs, which shows 95% accuracy. 135

Figure 5.15. Under 20% uncertainty, simulating the HOC generated optimal temperature trajectories and control inputs using the proposed CLHC diagram: (a) The temperature response of the real and virtual measurement zones, closely tracking the optimal trajectories. (b) The response of the heaters. (c) The percentage error between the heaters' response and HOC generated control input, showing 85% accuracy, which means that the heaters are behaving similarly to HOC generated control inputs. 136

Figure A.1. The General Simulator Schematic 155

Figure A.2. The Heaters Block 156

Figure A.3. Heating and Cooling rate saturation blocks 156

Figure A.4. The block of the heating phase model 157

Figure A.5. The heat transfer model block for every measurement zone divided in five fictitious layers 158

Figure A.6. The heat transfer model block for every measurement zone divided in fictitious layers (continued)..... 158

Figure A.7. The heat transfer model of the first layer..... 159

Figure A.8. The heat transfer model of the second layer 160

Figure A.9. The heat transfer model of the third layer 160

Figure A.10. The heat transfer model of the fourth layer 161

Figure A.11. The heat transfer model of the fifth layer 161

Figure A.12. Inside the ambient air block..... 162

Figure A.13. Inside the observers block 163

Figure A.14. The simulator in the presence of PI controllers 164

Figure A.15. Inside the PI control block..... 165

Figure A.16. The PI controllers blocks designated for each measurement zone 165

Figure A.17. The Smith predictor setup along with PI controllers designed for each measurement zone..... 166

Figure A.18. Inside the block of each Smith predictor scheme 167

Figure A.19. The simulator in the presence of the discrete time model predictive controller.. 167

Figure A.20. The simulator in the presence of the hybrid optimal and feedback controllers... 169

LIST OF TABLES

Table 5-1 List of Operating Points for Each Segment	119
Table 5-2 Parameter Values Used in the Algorithm	124
Table A-1 Table of tuned material properties for HDPE	169
Table A-2 Table of tuned material properties for Acrylic	170
Table A-3 Table of tuned material properties for ABS.....	170

1 Introduction

1.1 Literature Review and Motivation

The plastics industry is one of the largest manufacturing industries in the world, employing more than 4 million and generating global annual revenues of \$ 800 billion [1]. The plastics industry is also one of the fastest growing, with an annual growth rate of 2.5% from 2010 to 2015 [1]. In the United States alone, this industry is considered as the third largest manufacturing industry, generating more than \$380 billion in annual shipments, having grown 2.4% per year from 1980 to 2011 [2]. The productivity growth rate of 2.4% in the United States is better than the 1.7% per year productivity growth for manufacturing as a whole, signifying the importance of this industry in the United States' economy [2]. The plastics industry is also an important part of the Canadian economy, generating annual shipments valued at \$29.2 billion, with over 3000 companies employing 95,000 workers [3].

The underlying cause of the increase in plastic production is due to the fact that plastic parts are gradually replacing the more traditional types of materials, such as wood, glass, aluminum, and other metal products. Plastic products are more cost effective and durable, and they are also recyclable as some plastics can be recycled without losing any chemical properties. In the automotive industry, automakers are now using plastics and polymer-based components for lightweighting to optimize fuel efficiency [4]. In 1970, plastics only accounted for 6% of the average vehicle weight. In 2010, plastics accounted for 16% of the vehicle weight, and this number is expected to increase to 18% in 2020 [4].

Overall, annual plastic consumption in North America has reached approximately 45 billion kilograms (100 billion pounds), which is approximately a third of the world consumption [5]. The increased use of plastic products, however, has resulted in concerns with (1) the increased consumption of natural resources such as oil, (2) the toxicity associated with their manufacture and use, and (3) the environmental impact arising from discarded plastics [6]. Therefore, it is crucial for researchers to optimize all plastic production methods in order to improve efficiency and productivity while simultaneously reducing manufacturing costs.

Thermoforming is one of the oldest and most important methods in producing plastic parts. In 2007, the North American thermoforming industry produced more than 2.7 billion

kilograms (6 billion pounds) of thermoformed products, with an estimated value of \$ 13 billion [5]. By 2019, the global plastic thermoformed product market is expected to grow to 4.25 billion kilograms (9.4 billion pounds), with a five-year compound annual growth rate (CAGR) of 4.3% [7]. In fact today, in comparison with injection molding and other plastic processes, thermoformed plastics are competing more favourably in several key applications, namely in the automotive, building products, appliances, and a wide range of other consumer and industrial products [7]. Thus, in order for this process to keep up with the market demand, it is imperative to develop more efficient and cost effective techniques to ensure productivity improvement. Improved technologies will more importantly result in waste reduction, reducing the negative environmental impacts of the plastic processing industries.

In order to become more familiar with the existing challenges of the thermoforming process, a brief overview of this particular plastic manufacturing process along with a detailed literature survey of the associated technological advancements is presented.

The thermoforming process consists of three phases: heating, forming, and cooling. In the heating phase, a plastic sheet is inserted in a thermoforming machine (oven) and is heated to a precise temperature profile (set-point) without mechanical manipulation. The heating phase of thermoforming is the most important stage of the process since successful completion of the remaining phases largely depends on the outcome of this phase. Once the required temperature profile is achieved, the plastic sheet starts to sag, indicating that it is flexible enough and ready for the forming process. This is when the sheet is draped on a mold to take a certain predetermined shape. In the final phase of the process, the sheet is cooled and excess material around the actual product is trimmed. Fig. 1.1 graphically describes the different elements involved in the heating and forming phase.

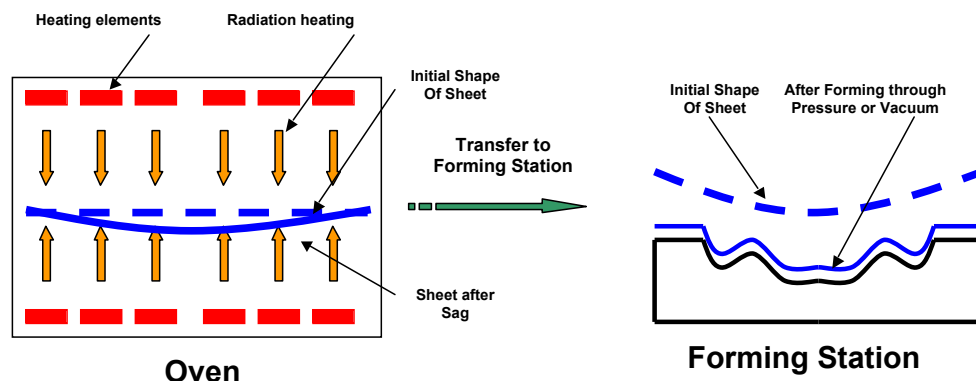


Figure 1.1. The thermoforming heating and forming phase [8]

The thermoforming process is often categorized according to the thickness or gauge of the plastic sheet. If the sheet thickness is less than 1.5 mm, the process is called thin-gauge or light-gauge thermoforming, and if the sheet thickness is more than 3 mm, the process is called thick-gauge or heavy-gauge thermoforming [5]. Another way of classifying the thermoforming process is by the type and form of the plastic sheet. If the sheet is thin, it is usually initially extruded into rolls and fed continuously into certain types of thermoforming machines called roll-fed machines. On the other hand, if the sheet is too thick to be rolled, it is cut into discrete pieces and fed, either manually or automatically, into cut-sheet machines.

Today, there are two main types of plastic sheets being regularly used in thermoforming applications: monolayer and multilayer plastic sheets. Monolayer plastic sheets consist of only one type of plastic material, whereas multilayer plastic sheets are made of different layers of plastic materials (between 2 to 9 layers), each with different material (rheological) properties [9]. The popularity of multilayer plastic sheets is ever growing in thermoforming since these sheets provide certain characteristics, which are not attainable when using monolayer plastic sheet. For example, in order to achieve the characteristics of stiffness, moisture barrier, and oil resistance in a plastic part, polystyrene (PS) may be laminated with polyolefin (PO) [9]. Today, thermoformed multilayer plastic parts are being used as vehicular components, construction products, and sanitary products.

As it was previously alluded to, proper forming could only occur if the precise temperature set-point (profile) is achieved across and through the depth of the plastic sheet, at which point it is flexible enough to be molded. Often in thermoforming, because of the shape complexity of the desired product, uneven temperature (zoned temperature) set-points or non-uniform temperature profiles are desired across and through the depth of the plastic sheet. Therefore, it is imperative to systematically control the heaters temperatures in order to achieve the exact temperature profile required for any particular type of sheet.

Research in process modeling and control of plastic manufacturing processes first started with the extrusion blow molding and injection molding processes. With regards to extrusion blow molding, Diraddo *et al.* first introduced an adaptive closed-loop control scheme to control the parison thickness profile in 1991 [10]. Diraddo and Garcia-Rejon then presented in-cycle deterministic and stochastic models of extrusion blow molding and demonstrated the effectiveness of in-cycle control by performing a series of control simulations [11]. Later,

advanced numerical modeling became the topic of interest in this field, as the focus was turned in developing accurate industrial simulators to predict and optimize the parison thickness and other related performance parameters. In [12], Laroche *et al.* used advance numerical modeling techniques to predict part thickness and conducted an optimization analysis to minimize the part weight in blow molding. Currently, accurate simulators have been developed in this field and studies for specific parts are being conducted. In one of the more control related developments, a study was published in 2007 by Huang *et al.*, in which a hybrid combination of Finite element method, artificial neural network, and genetic algorithm were utilized to optimize the parison thickness distribution of a blow molded part [13].

Modeling and application of sophisticated control techniques in the injection molding process has also been extensively studied. Research in this area was first started by Kamal *et al.* and Gomes *et al.* in a two part study, presented in [14] and [15]. In [14], Kamal *et al.* presented a preliminary understanding of the effect of a step input in heating power on melt and barrel temperatures, and deterministic and stochastic models were derived. Subsequently, in [15] Gomes *et al.* used different control strategies in injection molding, namely PID control of barrel temperature, Dahlin control, and Smith predictor control of melt temperature. Later in [16], Dubay *et al.* presented “single-input single-output” (SISO) and “multi-input multi-output” (MIMO) model predictive control (MPC) strategies to control the temperature of the plastic melt in an injection molding machine and showed improved results compared to conventional control methods. This was followed by another study in [17], where Dubay *et al.* investigated the model predictive control of plastic melt temperature on an insulated injection molding machine barrel. In 2004, a comprehensive two part study of temperature control in injection molding was presented by Diduch *et al.* in [18] and Dubay *et al.* in [19]. In the first part of this study, a more comprehensive mathematical model of the temperature dynamics of a plastic injection molding machine, to be used as a basis for control system design, was presented [18]. This model included the effects of zone interaction and backpressure, as opposed to lumping them into a disturbance signal. In [19], as the second part of the study, Dubay *et al.* developed and implemented a model predictive controller for the improved mathematical model presented in [18]. In related studies, Gerber *et al.* used transient CFD simulations to develop a dynamic process model and used MPC to control the set-point changes in melt temperature [20]. Also in [21], Anbarasan *et al.* applied fuzzy tuned PI-PD controllers to reduce the overshoot and settling

time in the control of the melt temperature in the barrel. Alternatively in [22], Tao *et al.* applied an IMC method to control the barrel temperature of an injection molding machine. Finally, in addition to developing model-based techniques to control the process model, the control of the actuators of an injection molding machine, which include the screw position and velocity, was also studied by Dubay *et al.* in [23], where two MPCs were implemented in real-time to control the screw injection velocity and position. It should be noted that in this thesis, the models and methods used to control the thermoforming heating phase exhibited closer similarities to the injection molding process in comparison with the blow molding process.

While the research efforts were well underway to automate the blow molding injection molding process, less attention was paid to the control of the thermoforming process until early in 2000s. The application of advanced model-based control methods in thermal processes, comprising of similar attributes to the thermoforming process, were well documented, and the results of which were used as a starting point for the control of the thermoforming heating phase. For instance, Rapid thermal processing (RTP) of semiconductor materials is one of the most studied thermal processes while being comparable to the thermoforming heating phase. In RTP, semiconductor wafers are heated using high temperature radiation heating lamps, and it is necessary to precisely control the wafer temperature in order to achieve the desired material properties. Modeling and model-based control strategies for temperature tracking in RTP were first introduced by Park *et al.* in [24], followed by Schaper *et al.* in [25] and [26], who utilized internal-model control based techniques to control the wafer temperature. Later in this field, nonlinear system identification techniques and adaptive model-based control were presented by Tian *et al.* in [27], while Cho *et al.* used nonlinear model identification and nonlinear predictive controllers to control the wafer temperature [28]. Recently, robust control of rapid thermal processes applied to vapor deposition processes, which are widely used in semi conductor production, has also been investigated by Aranovsky *et al.* in [29]. Finally in the most recent study, Junghwan *et al.* investigated the modeling and optimal design of a glass RTP, where an iterative learning control technique was used to solve the temperature tracking problem [30].

Therefore, with regards to the thermoforming process, the goal was to employ the ideas utilized in the disciplines of rapid thermal processing and the injection molding process (presented in all the abovementioned studies) in order to develop a model and a control structure for the thermoforming heating phase.

The process of automating the heating phase started with modeling the temperature evolution of plastic sheets during the heating stage. In this front, Moore *et al.* first developed the heating phase model of a thick plastic sheet by discretizing the layers across the thickness of the plastic into a finite number of nodes [31, 32]. Moore also developed H-infinity and model predictive in-cycle controllers in a simulation environment using the already developed model in [31]. In [33], Yousefi *et al.* further improved the FEM modeling, performed by Moore in [31], by the uncertainty treatment of several thermoforming machine parameters.

The first real-time in-cycle closed-loop control study to control the temperature of a plastic sheet in thermoforming was conducted by Ajersch in [34]. Ajersch controlled the surface of a plastic sheet using empirical models of the heating phase, and subsequently tuned several PI controllers for these models. The PI controllers were then utilized in real-time in a feedback setup, where infrared sensors were placed above and below the plastic sheet to provide feedback measurements. The block diagram of this setup is shown in Fig. 1.2. Ajersch also validated the model introduced by Moore in [31], and concluded that the finite-element heating phase model accurately represents the actual dynamics of a plastic sheet during the heating phase.

Several studies have also suggested improvements to the heating phase model of the plastic sheet by considering the radiation absorption properties of transparent sheets (see [35] and [34]), yet for the more opaque plastic sheets, the model developed by Moore in [31] is deemed to be accurate enough. Moreover in [36] and [37], Thomson *et al.*, and subsequently Khan *et al.*, presented and experimentally validated an improved heat transfer model of the heating phase, which considered temperature dependent properties, radiation transmission through the depth of the sheet, sheet color, and operating conditions.

Analysis later established that the use of feedback control in thermoforming would result in productivity improvement, especially in reducing scrap rates, improving the heating cycle time, reducing energy consumption, and maximizing heater life [38]. Chy *et al.* continued the efforts to produce more efficient results by introducing a model predictive control (MPC) technique for monolayer plastic sheets [39]. Chy *et al.* also attempted to increase the number of feedback measurements by introducing Fast Fourier Transform (FFT) based interpolation methods to estimate the surface temperature across the plastic sheet in [40] and [41].

In addition to the development of in-cycle controllers for the heating phase, cycle-to-cycle controllers were also developed in order to further increase the productivity and autonomy

of the heating phase control problem. Gauthier first introduced terminal iterative learning control (TILC) as a cycle-to-cycle controller in thermoforming in [42], and subsequently presented robust design of TILC with H-infinity mixed-sensitivity approach for a thermoforming oven in [43]. A study by Girard *et al.* in [8] also investigated the implementation of an on-line adaptive controller for in-cycle and cycle-to-cycle control of large thermoplastic sheets. The cycle-to-cycle approach provides an additional avenue in increasing the throughput of the thermoforming process while simultaneously reducing the scrap rates in the process.

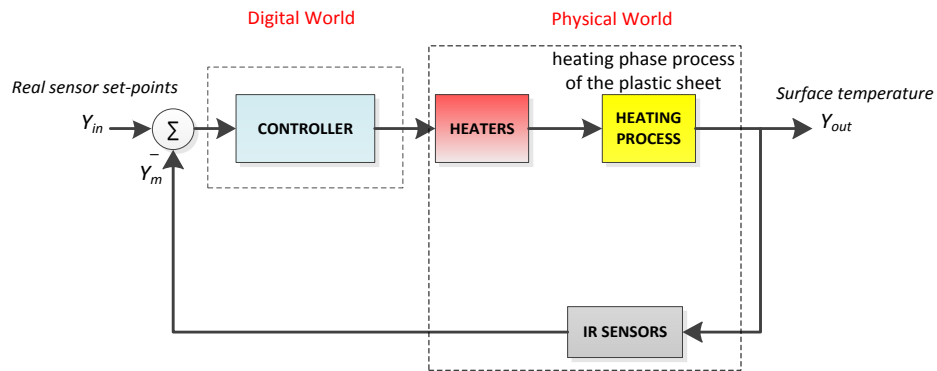


Figure 1.2. Block diagram of the closed-loop system containing the heating phase

The above summary describes all the control-related advancements in the heating phase of the thermoforming process. Although much progress has been made towards automating the cut-sheet thermoforming process through in-cycle and cycle-to-cycle control methods, there are still a key number of questions yet to be answered.

The first question to be answered is: how can the number of feedback measurement points be increased to improve the precision, observability, and productivity of the process in a way that uneven temperature profiles can be achieved across the surface and through the depth of the plastic sheet?

The second question to be addressed is: can the heating time (cycle time) be further improved using new control methods in thermoforming?

The third question to be answered is: can a control method be developed to control the temperatures of all the layers of multilayer plastic sheets, considering all the nonlinearities associated with the heating phase of the thermoforming process?

Finally, the fourth question to be answered is: Can the heating phase model be further improved by incorporating the temperature-dependent material properties of the

plastic sheet? More importantly can a novel Hybrid Minimum Principle (HMP) based hybrid optimal control method be applied for the first time to a large-scale nonlinear industrial process, namely thermoforming, to solve the temperature tracking problem of a plastic sheet under the presence of temperature-variant material properties?

The answers to the above questions constitute the contents of this thesis as they will be briefly introduced and discussed in the following subsections.

1.2 New Surface and Core-Temperature Estimation Methods

In thermoforming, a plastic sheet is inserted into a thermoforming oven, which contains a number of heaters above and below the plastic sheet, as shown in Fig. 1.3. In most cases, the number of heaters placed above and below the sheet is equal. The number of heaters used in a thermoforming oven is dependent on the size of the thermoforming machine. Medium scale thermoforming ovens usually consist of 30 heating banks (15 placed on top and 15 on the bottom of the oven), while the larger scale ovens contain more than 100 heaters in total.

As it was previously discussed, in the feedback control setup shown in Fig. 1.2, IR sensors are also placed above and below the plastic sheet, pointing towards areas on the sheet called measurement zones. This is shown in Fig. 1.3, and the temperature of these measurement zones is then compared to the sheet temperature set-points and a control signal is produced to act on the actuators of the process, which are indeed the heaters.

Theoretically, to be able to achieve total control of the temperature set-points across the plastic sheet, there needs to be an equal number of infrared sensors relative to the number of heaters in the oven, which is difficult to have in practice due to the high cost of IR sensors. Therefore, the number of IR sensors used should be limited to maintain the cost efficiency of the overall control system. On the other hand, in order to achieve accurate temperature profiles, there is a need to have extra measurement points in addition to the actual infrared sensors readings. This is particularly the case when non-uniform temperature profiles are desired across the plastic sheet. There have been two interpolation methods developed to estimate the surface temperature of the plastic sheet. First one is the work done by Chy *et al.* in [40], which estimates the surface temperature at different points using a Fast-Fourier Transform (FFT) approach. In order for this method to be effective, the heaters and the IR sensors have to be equally spaced to be able to apply Fourier Transform to obtain an estimation of the temperature profile across the sheet. Later in a second study, Chy *et al.* proposed a surface temperature estimation method using Non-

Uniform Fast Fourier Transform (NUFFT) for non-equidistant temperature sensors (see [41]) although the non-equidistant placement of heaters were still not considered in the study.

In Chapter 2 of this thesis, the concept of model-based virtual sensors (MBVSs) introduces a new proposed measurement method. The method of temperature measurement in MBVSs is based on the heat transfer model of the heating phase presented in [35]. Similar to IR sensors, the proposed virtual sensors are considered to have the freedom of being virtually placed anywhere above or below the sheet. For these sensors, it is assumed that the actual heating process is taking place with respect to their position in the oven; however, the measurements are actually generated online using the mathematical model of the heating process. The control system then acts on these measurements, as if they were actual IR sensor readings, adjusting the heaters' temperatures according to the virtual sensor estimations.

The MBVS does not require the condition of evenly distributed heaters or sensors. Heaters and IR sensors can be placed in the oven with any type of geometrical attributes, independent of where the virtual sensors are placed, since the heat transfer model used in the MBVSs algorithm is not dependent on the particular distribution of the elements. Thus, the proposed method allows for non-equidistant placement of the heaters or any other geometric distribution thereof. Finally, the significant advantage of MBVSs is that their algorithm does not rely on prediction and interpolation techniques as this is the case in [40] and [41]. Rather, these sensors utilize the actual model-based dynamics of the process, which are validated to be within 2% accuracy of the physical system in [34].

The second estimation problem that has to be addressed to improve the efficiency and productivity of the process is monitoring the center-plane or core temperature of the plastic sheet during the heating phase. As mentioned before, in thermoforming, at the moment when the heating phase is completed and the sheet is ready to be draped on a mold, it is very important to achieve the desired temperature profile across and through the entire depth of the plastic sheet for the sheet to mold correctly, especially when dealing with thick gauge plastic sheets. Naturally, the core temperature is always cooler than the surface temperature, and if it is not the case that the core of the polymer is within the same forming temperature window as the surface, the interior of the plastic sheet will crack during the molding phase, resulting in the part being scrapped and rejected. Therefore, there needs to be a mechanism to measure the core temperature during the heating phase. Conventionally, the direct method to measure the center-plane

temperature of a plastic sheet is to insert thermocouple pins into the sheet. However, in thermoforming, mechanical manipulation is prohibited since inserting thermocouple pins will result in the surface quality degradation and introduction of holes in the plastic sheet (discussed in the later sections). Thus, an estimation technique is required to estimate the core temperature.

In Chapter 2 of this thesis, the implementation of a closed-loop Luenberger core-temperature observer is proposed to accurately estimate the core temperature of a plastic sheet during the heating phase. Using this method, the core temperature can be actively and accurately estimated during the heating phase based on the IR and MVBS readings. It should be noted that the estimation methods proposed in [40] and [41] do not take into account the core-temperature estimation of the plastic sheet.

The two proposed methods of MBVS and core-temperature observers are then included in the control system setup to form a new observer-based control system for the thermoforming heating phase. The two proposed estimation methods improve the observability and cost efficiency of the system as non-uniform temperature profiles can be easily achieved using a minimum number of IR sensors and a high number of MBVSs. The only cost associated to the MBVSs is a computer device to perform the online model-based temperature estimation. The core-temperature observers are also beneficial in terms of reducing the scrap rates and improving the productivity of the process. During the heating phase, the center-plane of the plastic sheet can be monitored and the process could be accordingly adjusted so that core temperature can reach the required temperature forming window by the end of the cycle. This will solve the potential problems posed during the forming stage, resulting in scrap rate reduction.

In order to test the performance and robustness of the new control system containing the MVBSs and the core-temperature estimators, the overall system is tested on an industrial thermoforming machine simulator. First, temperature tracking is tested for zoned temperature profiles using ramp-shaped inputs, followed by the robustness examination of the new system in the presence of perturbation in material properties. As previously mentioned, unlike IR sensors, virtual sensors do not directly measure the surface temperature as they utilize the model of the heating process, in which the material properties of any type of plastic sheet has to be included and quantified. The material property specifications for certain types of plastic sheets (HDPE for example) are often temperature dependent, as it has been shown in [36] by Thomson *et al.* and in [37] by Khan *et al.*, and may lie within a 20% range or more according to [36], [37], [5] and

[116]. In addition to the temperature variability factor, the data sheets provided by different companies, often contain different values for the same type of plastic sheet. This has been discussed by Sepe in [117], in which it is argued that values of the material properties are not generated under equivalent test conditions as there currently exist a variety set of standard test conditions (such as ASTM, DIN and JIS) that are regionally specific, and each one produces a unique set of numbers. The interested reader can refer to [117] for a more detailed analysis. Therefore, since virtual sensors deal with material properties in the estimation of the surface temperature, and since these quantified values can be 20% inaccurate, it is important for the virtual sensors to be tested under perturbation to make sure they can still provide acceptable estimations.

The industrial thermoforming machine simulator is described in detail in Appendix A.

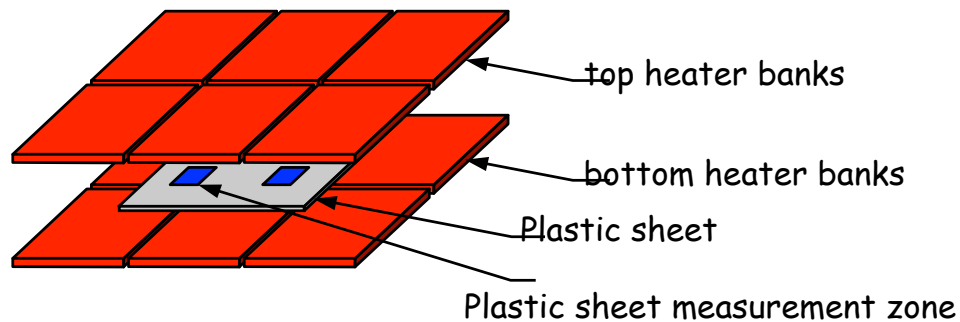


Figure 1.3. The thermoforming oven, exhibiting the heaters, the plastic sheet, and the measurement zones

1.3 A Control Method to Reduce the Heating Cycle Time

One of the problems addressed in this thesis is to investigate the application of a control method, which can reduce the in-cycle heating time (sheet temperature tracking time) when compared to the PI controllers used in the process. Reducing the temperature tracking time results in improved throughput of the thermoforming process since more plastic parts can be produced within a fixed time frame, and so it is important to introduce a control technique for this purpose.

In thermoforming, it has been observed that the temperature response of a plastic sheet exhibits an input delay type of behavior due to the heaters' dynamics and other environmental factors. In general, the reason that the temperature response of the plastic sheet experiences an

input delay is due to the slow rate of change in the heaters' temperatures as it takes a considerable amount of time for the ceramic heaters to exhibit an increase or decrease in their temperatures from a particular set-point to another. Therefore, since the heaters are not fast enough to immediately provide desired temperature set-points, the plastic sheet would not receive the required amount of heat in time, displaying a delay-like attribute in increasing the surface temperature. More detailed analysis is given in Chapter 3.

Another reason for the existence of the input delay is due to the energy of the heater banks not being entirely concentrated in raising the temperature of the plastic sheet at the beginning of the heating phase. Certain types of thermoforming machines are placed in an open environment, allowing for the ambient air to circulate in and out of the machine. Thus, the ambient air temperature is always considerably lower than the heater banks' temperatures when the heating phase begins. This difference in temperatures requires the heaters to dedicate some of their energy to in order to increase the temperature of the ambient air, at the beginning of the heating phase.

Combining the above factors, it can be observed that the step response of the surface temperature of the plastic sheet exhibits an input delay-like behavior at the beginning of its temperature rise. Therefore, a delay compensation control technique is suggested to improve the performance of the closed-loop system.

In Chapter 3 of this thesis, a special type of internal-model controller called the Smith predictor control scheme is proposed to compensate for the input delay while improving the performance, robustness, and tunability of the system. The Smith predictor technique, introduced by Smith in 1957, is aimed at improving the performance and robustness of systems containing time delays [44]. In the literature, the application of the Smith predictor control scheme has been studied for a number of thermal systems. In [45], the Smith predictor controller is utilized to control the temperature of a solar collector field. Similarly, the temperature control in solar air conditioning plants has been studied using the Smith predictive techniques in [46] while a similar internal-model control technique has also been applied to heat exchangers (based on an artificial neural networks driven model) to solve the air temperature control problem in [47].

The Smith predictor method has been the subject of much modification since it was first introduced in order to accommodate specific properties of certain systems. For instance in [48], Watanabe *et al.* improved the performance of a system with an integrator and long dead-time.

Astrom *et al.* further developed Watanabe's method such that the tracking performance and disturbance rejection are independently improved [49]. Subsequently, based on the works of Watanabe and Astrom, Zhang *et al.* proposed a modified Smith predictor to deal with first-order plus time-delay processes [50]. In this thesis, the method of interest is derived from the work of Watanabe *et al.* since only the tracking performance is of interest, and disturbance rejection is not considered.

In Chapter 3, the Watanabe-modified Smith predictor technique is introduced and applied to the control block diagram of the heating phase (updated in Chapter 2), which contains all the nonlinear heat transfer equations of the process, and tested on an industrial thermoforming machine simulator. In the simulation study, the performance of the system and robustness to variations in material properties are investigated, and results from the Watanabe-modified Smith predictor method are compared to existing control methods.

1.4 Thermoforming of Multilayer Plastic Sheets

Another question answered in this thesis is: can the forming process of multilayered plastic sheets be automatically controlled?

Multilayer plastic sheets are made of different types of plastic materials with different rheological properties. The popularity of multilayer sheets is ever growing in thermoforming as they are especially used in vehicular components, construction products, and sanitary products [9]. As it was stated in the previous subsections, it is crucial for all the layers of a plastic sheet to be within the temperature forming window at the end of the cycle. It is however a complex task to form multilayer plastic sheets since for each particular layer, the forming temperature and the associated heating time may be different. Failure to achieve the right temperature set-point for each layer results in fractures when the plastic is being molded. As a consequence, the part fails to pass the quality-control phase in production.

At the moment and to the best of our knowledge, there has been no research in designing a systematic control method, which can take the type and forming temperature of each layer into account. There has however been some research conducted in numerical modeling of multilayered plastic sheets in thermoforming, in [51] and [52], yet no control method is discussed. Moreover, because of their specific numerical nature and complexity, the models and analysis presented in [51] and [52] are not suitable to be used in a control algorithm.

In Chapter 4 of this thesis, a practical model of the heating phase of multilayer plastic sheets, which can easily be linearized and used in various control schemes, is presented. This model is a generalized model in the sense that it can account for any number or combination of plastic materials in a multilayer sheet. Additionally, a new discrete-time model predictive controller (DTMPC) is presented to solve, for the first time, the temperature tracking problem of multilayer plastic sheets in thermoforming.

MPC methods have been studied in various thermal processes, namely in rapid thermal processing [53, 54], building Heating Ventilation and Air Conditioning systems (HVAC) [55, 56], and in plastic injection molding [17, 20, 23]. Also, in the thermoforming literature, Chy *et al.* developed an MPC method in [39] to control the temperature of monolayer plastic sheets.

In this thesis, the proposed DTMPC method takes all the different plastic layers along with their respective rheological properties into account and solves the tracking problem for all the layers of multilayer plastic sheets. Apart from the novelty in its application, the new DTMPC method is quite different from the monolayer MPC controller proposed by Chy *et al.* in [39] since it considers the complete model of the system in each step of the optimization while taking the nonlinear dynamics of heaters completely into consideration, and it is more importantly able to provide non-uniform temperature profile tracking. The differences between the proposed DTMPC method and the monolayer MPC are further discussed in Chapter 4, in which the superior and comprehensive capabilities of the proposed DTMPC are showcased.

The DTMPC is finally added to the updated closed-loop thermoforming block diagram (developed in Chapter 2) and tested on an industrial thermoforming machine simulator, which includes all the nonlinear dynamics and geometrical attributes associated with the thermoforming process. In the simulation study, the tracking performance and the energy efficiency of the proposed control method are compared to classical PI controllers to show the superiority of the new method to these alternatives. Finally, it is to be noted that energy efficiency analysis is being conducted for the first time in thermoforming.

1.5 Temperature-Dependent Material Properties and Hybrid Control

So far in thermoforming, all the control methods discussed in the literature have been based on linearized temperature evolution models of the heating phase presented in [34] and [42], in which the rheological (material) properties of the plastic materials are held constant in order to represent the actual process. However in reality, certain material properties, most

notable of which being the specific heat capacity (C_p) of the plastic sheet, are dependent on the temperature of the sheet and may vary up to 9 times their starting value [57]. In all the previous works, the value of C_p had to be tuned in order to represent the actual process. This indeed limits the autonomy of the system, as each temperature profile requires a set of distinctively tuned values of material properties. Thus, it is desired to incorporate the temperature varying material properties into the models of the heating phase in order to increase the autonomy, accuracy, and reliability of the entire system.

As it was previously alluded to, the heaters, used as actuators in the process, contain nonlinear dynamics in the forms of saturation limits and rate-saturation limits, which have to be considered. In addition, the heating phase of the thermoforming process is a large-scale system because of the high number of heaters (used as actuators) placed in the thermoforming oven, and the large number of measurement zones, which are treated as the states of the system. Therefore, a new control algorithm has to be developed to take all the abovementioned factors into account.

The control of parameter-varying models has been addressed in the literature using a number of well-known methods. One of these methods is to linearize the system around several operating points and use the method of robust gain scheduling for linear parameter varying (LPV) systems, as described in [58-63]. Alternatively, the nonlinear model predictive control (NMPC) technique has been used in [64] in controlling heat pump systems. A study of a neural network based hybrid controller in wind induction generation applications has also been conducted in [65]. Additionally, in related studies, Karer *et al.* in [66] solve temperature control problem in a batch reactor using hybrid fuzzy modeling and an MPC control algorithm. Hybrid fuzzy logic controllers are also employed in multiphase industrial processes, namely in gas phase propylene copolymerization, where these controllers are used to control the reactor temperature [67].

In Chapter 5 of this thesis, an optimal class of hybrid controllers is the subject of interest. In this chapter, a hybrid systems formulation of the thermoforming heating phase problem is introduced, based on linearization around several operating points with autonomous switchings associated with the change of operating points. The minimization of the power consumption of the heaters and the sheet temperature tracking cost is considered in the hybrid optimal control framework, which is gaining popularity in applied control studies as hybrid controllers improve

performance measures [68]. Examples are in the areas of automotive industry and in the aerospace industry to obtain optimal flight path trajectories [69-72].

The majority of research on the optimal control of hybrid systems is focused on the Hybrid Minimum Principle (HMP), presented in [73-78], which is the generalization of the Pontryagin Minimum Principle. The results of the HMP for the hybrid system formulation in study provide the necessary conditions for the optimality of the control inputs and the optimal state trajectories. In order to solve for the optimal solutions, several HMP based control algorithms have been proposed (see, e.g., [76, 77, 79]). These algorithms have been applied to some unconstrained low-dimensional systems in [72, 80] and [81-83] in order to obtain optimal state and control solutions. However, the application of these HMP control algorithms has not yet been reported for large-scale systems with mixed state and control constraints. Therefore, a constrained HMP based HOC algorithm is presented in this thesis to solve the large-scale and constrained problem of temperature tracking in thermoforming. Successful application of the proposed HOC algorithm would provide a proof of concept, showing that these HMP-based hybrid optimal controllers could actually be implemented on complex industrial processes, which are large-scale and comprise nonlinear constraints, and parameter variations.

In Chapter 5, in addition to the design of the HOC, a closed-loop hybrid control (CLHC) setup is presented, based on the results obtained using the HOC algorithm, to provide robustness against perturbations. Industrial applicability is a major concern when HMP-based HOC algorithms are being utilized, as these are open-loop controllers by nature. In this thesis, a CLHC setup is proposed to overcome the industrial applicability barrier of HOC algorithms. Similar to the HOC, the CLHC produces optimal control inputs under nominal conditions. Under perturbed conditions, the CLHC produces feedback control inputs, added to the optimal control inputs, so that the system can track optimal temperature path trajectories.

The performance, efficiency, and robustness of the HOC and the CLHC are tested on an industrial thermoforming machine simulator, which includes all the nonlinear dynamics, temperature-varying properties, and geometrical attributes of the thermoforming process.

1.6 Thesis Organization

This organization of this manuscript-based thesis is as follows:

In Chapter 2, the notion of model-based virtual sensors (MBVSs) and virtual core-temperature observers are presented. These two concepts are then combined to form an overall

observer-based closed-loop system. The functionality, performance, and robustness of the new system are investigated through a simulation study of an industrial thermoforming machine.

In Chapter 3, the application of Watanabe-modified Smith predictor control technique in the thermoforming heating phase is presented. The Watanabe-modified Smith predictor control technique is included in the control diagram of the system, tuned, and tested on an industrial thermoforming machine simulator. The performance and robustness of the new control technique is then compared to the existing PI controllers in simulation.

In Chapter 4, a dynamical temperature evolution model of multilayered plastic sheets in the thermoforming heating phase is presented, followed by a proposed discrete-time model predictive control algorithm (DTMPC) to control the surface and core temperatures of multilayered sheets. This control method is then implemented and tested on an industrial thermoforming machine simulator, where the tracking performance and energy efficiency of the proposed DTMPC is tested against conventional PI controllers.

In Chapter 5, the temperature-dependent material properties of polymer sheets are incorporated in the temperature evolution equations of the heating phase. These equations are subsequently modeled in the hybrid optimal control framework based on the segmentation of the parameter-varying elements. A hybrid optimal control (HOC) algorithm based on the Hybrid Minimum Principle (HMP) is then presented, which takes into account the nonlinear actuator constraints of the thermoforming process and solves the temperature tracking problem for the parameter-varying system. A closed-loop hybrid controller (CLHC) is also developed, based on the proposed HOC, to provide robustness against perturbations. The HOC and the CLHC are then tested on an industrial thermoforming machine simulator to evaluate the tracking performance and robustness of the system.

In Chapter 6, the conclusion of the research is given, and possible future work in thermoforming and other thermal applications is discussed.

Finally in Appendix A of this thesis, the industrial thermoforming machine simulator is described in detail, and the various block diagrams used in each of the above Chapters are presented.

It has to be noted again that this thesis is a manuscript-based thesis, and so the flow of this kind of thesis does not necessarily follow a linear progression in terms of the development of analysis of the models, design techniques, and results.

2 Model-Based Virtual Sensors and Core-Temperature Observers in Thermoforming

How can the number of feedback measurement points be increased to improve the accuracy, observability, and productivity of the process in a way that even non-uniform temperature profiles can be achieved across the surface and depth of the plastic sheet?

In this chapter, advanced temperature measurement methods are developed for the thermoforming heating phase. The notion of model-based virtual sensors (MBVSs) is presented, followed by the development of virtual core-temperature observers. These concepts are then combined and a new control system block diagram is proposed. The new block diagram is simulated on a thermoforming machine simulator and the results are discussed. The proposed control block diagram of the thermoforming heating phase will be utilized in the subsequent chapters, as well.

This chapter has been adapted from: R. Modirnia and B. Boulet, "Model-Based Virtual Sensors and Core-Temperature Observers in Thermoforming Applications," *IEEE Transactions on Industry Applications*, vol. 49, no. 2, pp. 721-730, Mar. 2013.

➤ **Authors contributions:**

- 1) Rahi Modirnia: the author of the thesis is responsible for the development of the sensing algorithms, implementation and interpretation of the results. The thesis author is also responsible for writing the manuscript.
- 2) Benoit Boulet: supervised the work and edited the manuscript.

2.1 Abstract

In this chapter, we present the notion of model-based virtual sensors and virtual core temperature observers in a thermoforming process. The concept of model-based virtual sensors allows for additional surface temperature measurement points in addition to the already existing infrared sensors. This leads to improved observability of the plastic sheet temperature as well as increased accuracy in temperature zoning, thus eliminating the use of extra infrared sensors, which significantly reduces the cost of the control system. The problem of core sheet temperature measurement is also addressed through the application of a closed-loop Luenberger core temperature observer to estimate the center-plane temperature of the plastic sheet since it is not practical to have any kind of actual core temperature measurement during the heating process. The two concepts of virtual sensors and virtual core temperature observers are then combined to form an overall observer based closed-loop control system. Finally, the functionality, performance, and robustness of the new system is investigated through simulation of an industrial-type thermoforming machine.

2.2 Introduction

Thermoforming is a generic term describing many techniques for producing useful plastic parts from a flat sheet. In the process of thermoforming, a plastic sheet is heated to a certain temperature, and then is formed on an open mold. This process is used in automotive, aerospace, refrigeration, and packaging industries. Because plastic products are gradually replacing traditional materials, such as aluminum, glass, wood, and paper, the plastic manufacturing industry occupies a strategic place and is considered among the rising manufacturing sectors. This encourages researchers to develop more efficient and cost-effective techniques for the thermoforming process, which carries a significant weight in the plastic manufacturing sector [40].

A thermoforming process is divided into three major phases: heating, forming, and cooling [34]. The first part of this process is the heating phase, in which the sheet is heated to be brought up into a softening temperature. This phase of the thermoforming process is the most important one since the remaining phases depend largely on its outcome. By the end of the heating phase, it is very important to obtain a specified temperature profile (set-points) over the whole sheet because the rheological properties of the polymer, such as fluid behavior index, and

fluid viscosity, largely depend on the temperature of the sheet [84-87]. The second phase of the thermoforming process is the forming phase, where because of the rheological properties, the plastic sheet is deformed over the mould to take on a desired shape [84-87]. Most often, uneven temperature profiles or zoned temperature profiles are required to influence the mechanical formability of the plastic based on the desired shape of the plastic object. Therefore, it is very important to control the heaters of a thermoforming machine to ensure that the required sheet temperature profile is achieved.

Previously, the heater temperature adjustments were based on trial and error, obviously not an efficient way to obtain desired sheet temperature set-points. Thus, the concept of closed-loop control is deemed useful for a thermoforming process as it will automate the changes in heater temperatures to obtain desired temperature profiles. This was first proposed by Mark Ajersch in [34], who acquired an empirical model of the thermoforming heating process and used PI controllers to control the sheet's surface temperature. In this setup, the control loop is closed by placing a number of infrared (IR) sensors between the heaters. Theoretically, to be able to perfectly control the temperature set-points across the plastic sheet, there needs to be an equal number of infrared sensors relative to the number of heaters in every oven, which is difficult to have in practice due to the high cost of IR sensors. Therefore, the number of IR sensors used should be limited to maintain the cost efficiency of the overall control system. On the other hand, to achieve accurate temperature profiles, there is a need to have extra measurement points in addition to the actual infrared sensors readings. Several methods have been proposed in the past, one involving a weighted average method of measurement, and the other one involving a DFT estimation method [40].

The concept of model-based virtual sensors leads to a new method proposed in this chapter. Just like the real IR sensors, the proposed virtual sensors are considered to have the freedom of being virtually placed anywhere above the sheet, and their method of measurement is based on the developed heat transfer model of the heating phase in [35]. In other words, for these sensors, it is assumed that the actual heating process is taking place with respect to their position in the oven, however, the measurements are actually generated online using the mathematical model of the heating process. The control system then acts on these measurements, as if they were real IR sensor readings, adjusting the heater temperatures according to the virtual sensor estimations.

In this chapter, through simulation on an industrial thermoforming machine, the functionality of the new algorithm is put to the test. It will be shown that using virtual model-based sensors, accurate estimations of the surface temperature are obtained, and the temperature zoning control problem will also be solved. Also, by showing the accuracy of the new method, it will be concluded that the number of real IR sensors can be kept at a minimum.

In addition to simulation under idle conditions, the virtual sensors are also tested in the presence of perturbations in material properties. Virtual sensors, unlike real IR sensors, do not directly measure the surface temperature, dealing with the model of the heating process, in which the material properties of any type of plastic sheet has to be included and quantified. However, the material property specifications for certain types of plastic sheets (HDPE for example) are often temperature dependent, as it has been shown in [36] by Thomson *et al.* and in [37] by Khan *et al.*, and may lie within a 20% range or more according to [36], [37], [5] and [116]. In addition to the temperature variability factor, the data sheets provided by different companies often contain different values for the same type of plastic sheet. This has been discussed by Sepe in [117], where it is stated that the values of these properties are not generated under equivalent test conditions since a variety of standard test conditions (such as ASTM, DIN and JIS) that are regionally specific are being used, and everyone one of these standards produces a unique set of numbers. The interested reader can refer to [117] for a more detailed analysis. Therefore, since virtual sensors deal with material properties in the estimation of the surface temperature and since these quantified values can approximately in a 20% range above or below their nominal values, it is important for the system to undergo simulation with the presence of perturbations to make sure that they can still provide acceptable estimations.

It will also be shown that the proposed algorithm, compared to the aforementioned estimation methods, will provide more flexibility in terms of temperature zoning, observability, and also in terms of freedom of application on different types of thermoforming machines with different heater configurations.

The second problem addressed in this chapter is monitoring the center-plane or core temperature of the plastic sheet, during the heating phase, as the temperature of the sheet is rising. In thermoforming, when the heating phase is completed and the sheet is to be draped on a mold, it is very important to achieve the desired temperature profile across the entire depth of the plastic sheet for the sheet to mold correctly, especially when dealing with thick gauge plastic

sheets. Naturally, the core temperature is always cooler than the surface temperature, so if it is not the case that the core of the plastic has the same forming temperature as the surface, the interior of the plastic sheet will crack during the molding phases, resulting in scrap parts and rejection of the material. Therefore, there needs to be a mechanism to measure the core temperature during the heating phase. Conventionally, the direct method to measure the center-plane temperature of a plastic sheet is to insert thermocouple pins deep into the sheet. However, in thermoforming, this may not be possible during the heating phase since inserting thermocouple pins will result in the surface quality degradation and introduction of holes in the plastic sheet (discussed in the later sections), thus requiring some kind of core-temperature estimation method.

In this chapter, the implementation of a closed-loop Luenberger state observer is proposed to accurately estimate the core temperature of the plastic sheet. Using this method, the core temperature can be actively and accurately estimated during the heating phase based on the real IR and virtual sensor readings. The two proposed methods of virtual model-based sensors and core temperature observers are then included in the control system setup to form a new observer-based control system.

Finally, to verify the validity of the results, and to test the performance and robustness of the new control system, the overall system is tested on an industrial thermoforming machine simulator. First, tracking of temperature is tested for zoned temperature profiles using a ramp shaped input. Then, the robustness of the new system is tested in the presence of perturbation in material properties for the reasons described before.

2.3 Modeling of The Heating Phase in Thermoforming

The heating phase model used in this chapter has been developed by several researchers, the most recent of which is presented in [34] by Ajersch and by Gauthier *et al.* in [35]. The model has also been further developed by Thomson *et al.* in [36] and by Khan *et al.* in [37], where temperature dependent properties, sheet color, and other operating conditions have been experimentally investigated. The model used in the implementation of virtual sensors and core temperature observers is based on the heat transfer model developed by Gauthier *et al.* in [35]. A brief presentation of the method is provided in this section. In this model, the thermoforming machine consists of $2H$ heaters, H on top and H on the bottom, and the plastic sheet is placed in-between with an equal distance from the top and bottom heaters. There are also a total of $2S$

sensors, with S sensors on top, and S on the bottom. It is important to note that the top and bottom heaters and the sensors are respectively placed to be directly facing each other in the oven. The sensors read the surface temperature of the plastic sheet. The plastic sheet is divided into $2S$ measurement zones, each zone corresponding to the area around which a sensor is pointing. The thickness of the plastic sheet is divided into N equally spaced layers with a corresponding node for each layer.

In this model, it is determined that there are three methods by which heat is transferred to a plastic sheet: radiation, conduction, and convection. It is also assumed that within the sheet, heat transfer only occurs vertically, between the layers of the plastic, and that there is no energy interaction between adjacent measurement zones. Moreover, it is assumed that the heat radiated from the heaters gets transmitted through all the layers of the plastic depending on the transmissivity factor of the plastic sheet while convection only has an effect on the surface of the sheet because of the interaction of the oven's ambient air with the surface of the plastic.

Combining the aforementioned modes of heat transfer, for $2H$ number of heaters, $2S$ number of measurements zones, and N number of layer nodes for each zone, the heat transfer model for the top and bottom surface nodes of the k -th zone is

$$\frac{dT_{k,1}}{dt} = \frac{2}{\rho V C_p} \left\{ \frac{kA}{\Delta z} \{T_{k,2} - T_{k,1}\} + h \{T_\infty - T_{k,1}\} + \beta_1 Q_{RT_k} + \beta_1 (1 - \beta_1) (1 - \beta_2)^3 Q_{RB_k} \right\}, \quad (1)$$

$$\frac{dT_{k,N}}{dt} = \frac{2}{\rho V C_p} \left\{ \frac{kA}{\Delta z} \{T_{k,N-1} - T_{k,N}\} + h \{T_\infty - T_{k,N}\} + \beta_1 Q_{RB_k} + \beta_1 (1 - \beta_1) (1 - \beta_2)^3 Q_{RT_k} \right\}, \quad (2)$$

where ρ the density of the plastic sheet, C_p is the specific heat capacity of the sheet, k is the heat conduction constant, Δz is the layer thickness, A is the zone area, V is the volume of the layer, h is the convection coefficient, T_∞ is the ambient air temperature, Q_{RT_n} is the total radiant energy from the top heaters affecting k th measurement zone, Q_{RB_n} is the total radiant energy from the bottom heaters affecting the n th measurement zone, β_1 is the absorbed fraction of radiant energy for the top and bottom surface layers, and β_2 is the absorbed fraction of radiant energy for the internal layers. Q_{RT_n} , Q_{RB_n} , β_1 , β_2 are defined in (6).

It should be noted that in (1) and (2), the first term corresponds to conduction, the second term corresponds to convection, and the third term corresponds to radiation.

In this chapter, we define five layers for the plastic sheet ($N=5$); therefore, the heat transfer model for the three internal zones is

$$\frac{dT_{k,2}}{dt} = \frac{1}{\rho VC_p} \left\{ \frac{kA}{\Delta z} \{T_{k,1} - 2T_{k,2} + T_{k,3}\} + \beta_2 (1 - \beta_1) \{Q_{RT_k} + (1 - \beta_2)^2 Q_{RB_k}\} \right\}, \quad (3)$$

$$\frac{dT_{k,3}}{dt} = \frac{1}{\rho VC_p} \left\{ \frac{kA}{\Delta z} \{T_{k,2} - 2T_{k,3} + T_{k,4}\} + \beta_2 (1 - \beta_1) (1 - \beta_2) \{Q_{RT_k} + Q_{RB_k}\} \right\}, \quad (4)$$

$$\frac{dT_{k,4}}{dt} = \frac{1}{\rho VC_p} \left\{ \frac{kA}{\Delta z} \{T_{k,3} - 2T_{k,4} + T_{k,5}\} + \beta_2 (1 - \beta_1) \{(1 - \beta_2)^2 Q_{RT_k} + Q_{RB_k}\} \right\}, \quad (5)$$

where

$$\begin{aligned} \beta_1 &:= 1 - e^{-A_{av} \Delta z / 2} \\ \beta_2 &:= 1 - e^{-A_{av} \Delta z} \\ Q_{RT_k} &= \sigma \varepsilon_{eff} A_h \sum_{j=1}^H F_{kj} \{ \theta_j^4 - T_{k,1}^4 \}, \\ Q_{RB_k} &= \sigma \varepsilon_{eff} A_h \sum_{j=H+1}^{2H} F_{kj} \{ \theta_j^4 - T_{k,N}^4 \} \end{aligned} \quad (6)$$

where A_{av} is the average absorptivity, and it is defined by taking the average absorption of the plastic sheet over the spectrum range (for example $2 - 4 \mu\text{m}$) at which the heaters are operating. The (Fourier transform infrared spectroscopy) FTIR spectroscopy of the plastic in study would provide the transmission or absorption percentages across the spectrum of interest, and the average absorptivity can be calculated accordingly. σ is the Stefan Boltzmann constant, ε_{eff} is the effective emissivity, A_h is the area of the heater bank, F_{kj} is the view factor between the j th heater bank and the k th measurement zone, θ_j is the j th heater bank temperature. Note that in the right-hand side of (3), (4), and (5), the first term represents conduction between nodes while the second term represents radiation through the layers. Details of the above equations and methods for obtaining the effective emissivity and view factors can be found in [42] and [34]. Finally, it needs to be mentioned that the developed model of the heating phase has been shown to be accurate and close to the actual process in the thermoforming machine during the heating phase [42].

2.4 Description of the Existing Control System

In this section, the original setup of the closed-loop block diagram is discussed. The control diagram is shown in Fig. 1.1 The set-points of this control diagram are defined as the desired sheet temperature profile, or in other words, the desired sensor measurements at all the zones of the plastic sheet. In this setup, the heaters are treated as actuators while the heating phase is considered as the plant. The sensors then measure the surface temperatures, feeding them back to the controller. Each of these sensors measures a certain area on the surface of the sheet, and as it was mentioned, we consider the zone that the sensor directly points to as a measurement zone on the sheet. The controller part consists of individual controllers corresponding to each sensor measurement zone, and also of a coupling matrix with a dimension of $2H \times 2S$, which transforms measurement-zone heat fluxes to heater temperatures since there are fewer measurement zones than there are heaters.

The coupling matrix consists of view-factor elements, which are useful parameters to determine the fraction of the radiant energy exchanged between two surfaces having different areas and orientations [42]. The view factors provide a method to convert the energy needed to heat each measurement zone on the sheet to the amount of radiation needed for each heater in the thermoforming machine. The evaluation of the view factor from a measurement zone to each heater is derived by considering of having two parallel surface areas A_1 and A_2 , with the perpendicular distance between the two being z . The mathematical and geometrical details on how to obtain the view-factor are extensively covered in [42]. In order to calculate all the view-factor entries of the coupling matrix, the location of all the heater banks and sensors (IR or virtual) has to be mapped on a Cartesian plot. Therefore, all the heaters and sensors zones are placed on a two-dimensional grid, and appropriate coordinates are defined for all. The vertical distance z between the sensor measurement zones and the heaters has also been taken into account, but considering that this value is constant for all the heater banks and sensors, the grid will be two dimensional for simplicity. Fig. 2.7 shows an example of a two dimensional grid with 54 heaters and 22 sensors.

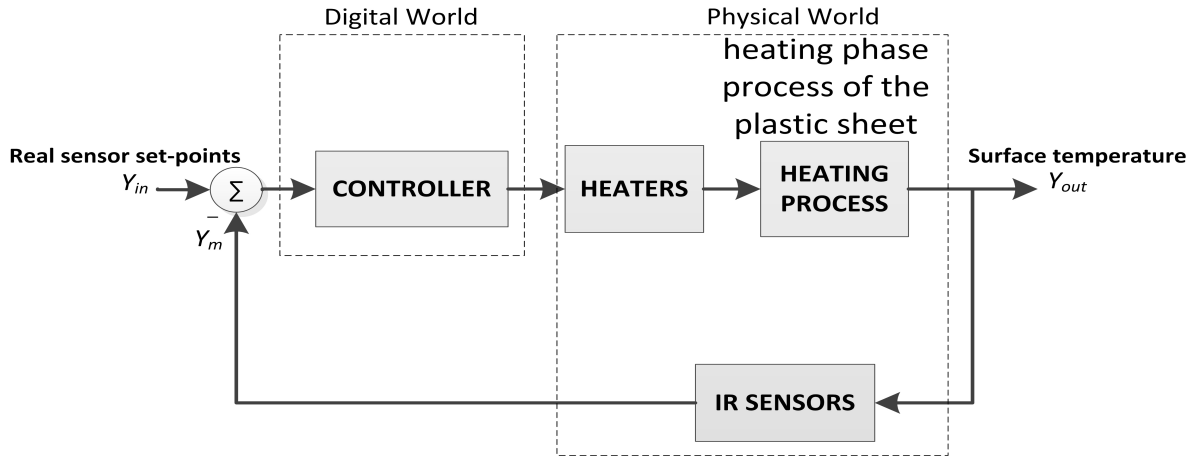


Figure 2.1. Block diagram of the closed-loop system

2.5 Implementation of MVBSs

In this section, implementation of MVBSs is discussed and comparisons are made with other measurements methods. As it was mentioned, the usage of real IR sensors is costly, thus requiring limited usage in order to keep the control system cost efficient. However, if the number of these sensors is kept at a minimum, there will be inaccuracy in measuring the surface temperature throughout the sheet's surface, resulting in the ineffectiveness of the feedback, and eventually poor controllability and observability. The use of a limited number of sensors also reduces the possibility of controlling zoned temperature profiles accurately. To solve the IR sensor limitation problem, the method of MVBSs is proposed, adding many more measurement points of the surface temperature at virtually no cost.

In the implementation of MVBSs, each virtual sensor is placed on the aforementioned grid of sensors with total freedom of placement, generating virtual sensor measurement zones on the plastic sheet. Therefore, just like real IR sensors, coordinates are generated on the Cartesian grid for each of the virtual sensors, thus requiring a set of view-factors from all the heaters to each virtual sensor on the sheet so that the heaters can use the virtual sensor reading to adjust their temperature in the control environment.

The algorithm of a MBVS can be summarized as follows:

- 1) Define Cartesian coordinates for $2V$ virtual sensors and $2Z$ real IR sensors on the grid, and obtain the view-factors from all the heaters to each of the virtual sensors.

- 2) Use the model's surface measurement formulas (1) and (2) to measure actively the surface temperature of each virtual measurement zone in parallel; the actual heating phase is taking place.
- 3) Define and tune a number of virtual zone controllers $2V$ equal to the number of virtual sensor zones, and combine the output of the virtual zone controllers with the output of the $2Z$ real zone controllers calling the overall vector C_{out} .
- 4) Generate the coupling matrix G by combining the virtual sensor view-factor matrix with the real sensor view-factor matrix.
- 5) Feed the overall controller output C_{out} to the coupling matrix G in order to obtain the heater temperature set-points with respect to all the sensor zones as shown in Fig. 2.2.

The method proves to provide an accurate estimation of the surface temperature and increase observability since a virtual sensor uses the actual heater values, then utilizes the surface heat transfer equations (1) and (2), which are already proven to be accurate, to determine the temperature at that particular zone on the sheet relative to where it is located on the grid. In addition, since the virtual sensors increase the number of measurement points, thus providing the controller with more information, the controller can provide more accurate heater set-points for the heaters resulting in improved observability, accurate temperature zoning, and providing a faster trend to reach the desired set-points.

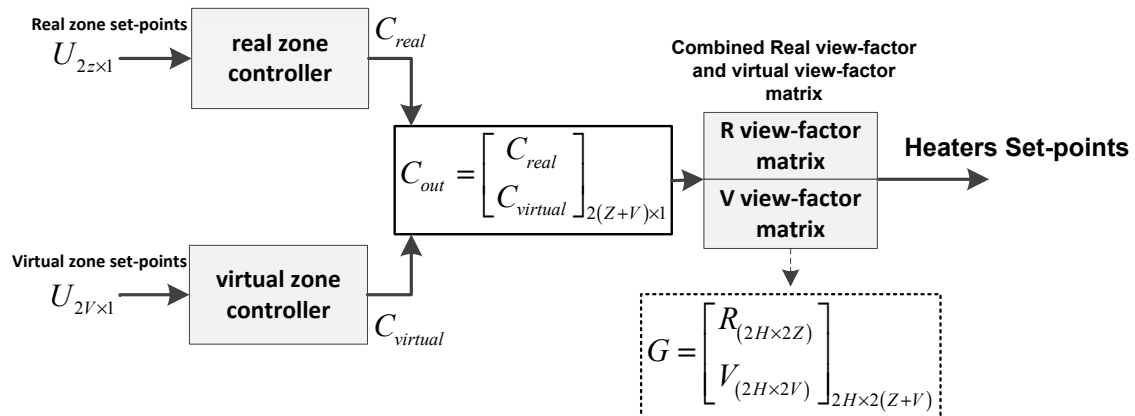


Figure 2.2. Updated controller block in the presence of MBVSSs

The virtual model-based sensor is added to the existing control block diagram and is shown in Fig. 2.3. The performance and robustness of the proposed method will be investigated in the simulation section, in detail, through implementation of the algorithm on an industrial thermoforming machine simulator.

Recently, there have been two other methods developed to estimate the surface temperature of the plastic sheet. First one is the work done by Chy *et al.* in [40], which estimates the surface temperature at different points using a Fast-Fourier Transform approach. However, in order for this method to be effective, the heaters and the real IR sensors have to be equally spaced to be able to apply the Fourier Transform to obtain an estimation of the temperature profile across the sheet. The virtual model-based sensor, however, does not require the condition of evenly distributed heaters and sensors. Heaters and real IR sensors can be placed anywhere on the grid independent of where the virtual sensors are placed because the heat transfer model used in the algorithm is not dependent on the particular distribution of the elements. The only position dependent parameter is the view-factor, which does not pose any limitation on the particular arrangement of heaters and sensors. Therefore, comparing the proposed method to the FFT algorithm in [41], virtual model-based sensors remove the existing practical limitations in the application of an estimation algorithm.

Later, Chy *et al.* proposed a surface temperature estimation method for non-equidistant temperature sensors in [41]. Comparing the methods proposed in [41] with the one proposed in this chapter, it should be noted that the placement of heaters are still not considered while in the proposed method of this chapter allows for non-equidistant placement of the heaters or any other geometric distribution. Moreover, the methods proposed in [41] uses advanced interpolators and predictors whereas the virtual sensors proposed in this chapter are model-based and deal with the actual dynamics of the system. Lastly, the estimation methods proposed in [41] are only limited to surface temperature estimations while core temperature measurements are not considered. This chapter, on the other hand, introduces a novel core-temperature estimation method for the first time, which will be presented in the next section.

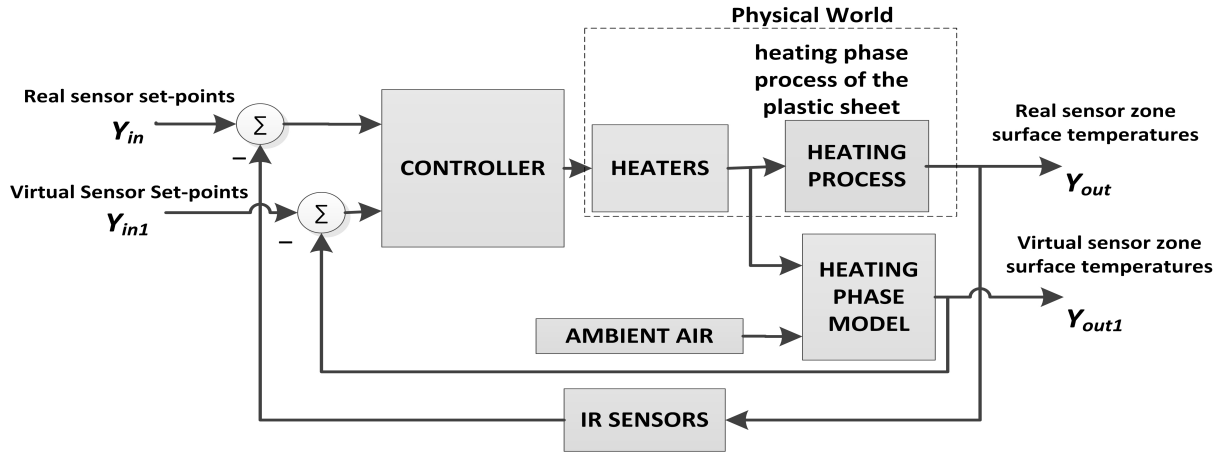


Figure 2.3. Closed-loop block diagram of the system containing the virtual sensors

2.6 Application of the Luenberger Core Temperature Observer

In thermoforming, one of the most important aspects during the heating phase is to monitor the core temperature of the plastic sheet. It was stated before that if the center-plane temperature is not correctly monitored and equal to the surface temperature, the plastic sheet can break during the molding phase.

Typically, to measure the center-plane temperature of a plastic sheet, pin thermocouples have to be inserted in the plastic sheet. However, during the heating phase in a thermoforming process, inserting thermocouples will degrade the surface quality of the sheet, and introduce holes in it resulting in creation of bubbles and small cracks after the sheet is formed. Most often, a formed plastic part exhibiting these conditions would be rejected, and so there can be no physical interaction with the plastic sheet to determine the core temperature during the heating phase. This only leaves estimation or predictive methods as available tools to measure the center-plane temperature of the plastic sheet.

To accurately estimate the core temperature, the method of closed-loop Luenberger state observer is implemented since an accurate state-space model of the heating phase exists. The concept of Luenberger state estimator is extensively described in [88]. A brief presentation is given here, and the block diagram is shown in Fig. 2.4.

2.6.1 Closed-Loop Luenberger State Observer

Suppose that the state space system describing the dynamics of the system is described as

$$\begin{aligned} \dot{x} &= Ax + Bu + w \\ y &= Cx + v \end{aligned} \quad (7)$$

The Luenberger observer with gain L is used to produce an estimate of the state characterized as $\hat{x}(t)$. The state-space system describing the dynamics of the observer is as follows:

$$\begin{aligned} \dot{\hat{x}} &= (A - LC)\hat{x} + Ly + Bu \\ \hat{y} &= C\hat{x} \end{aligned} \quad (8)$$

The goal is design L such that the state estimate will track the state. This can be expressed in terms of the state-space system governing the evolution of the error $e(t) = x(t) - \hat{x}(t)$, and $\dot{e} = (A - LC)e + w + lv$. Therefore, it suffices to find a matrix L such that all eigenvalues of $A - LC$ (the poles of the observer) are in the open left-half plane to ensure that the error will tend to zero when the noises are zero.

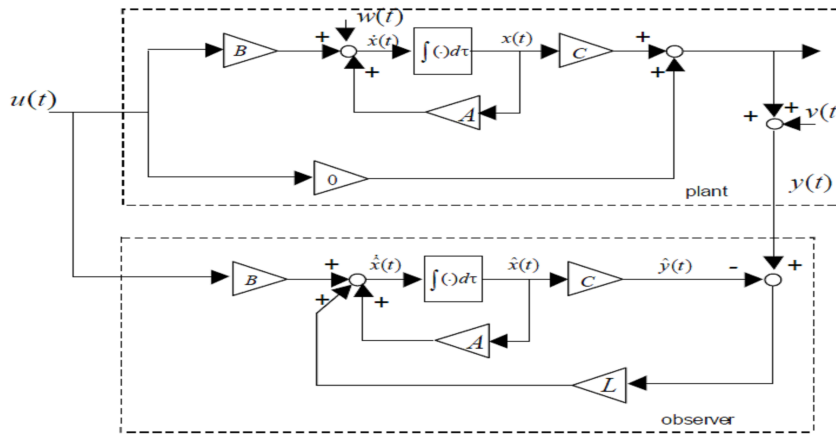


Figure 2.4. Block diagram of a closed-loop Luenberger state estimator

2.6.2 Application of the Luenberger Observer in a Thermoforming Process

As aforementioned, the state-space equations of the heating process of the polymer are developed. If those can be reformed to resemble the block diagram structure in Fig. 2.4, then a Luenberger observer can be applied to estimate the core temperature of the plastic sheet.

Equations (1)-(5) can be combined to form a state space model of the system, for which the standard arrangement is described in (7). Looking at the model equations (1)-(5), for the k th measurement zone, the state-space representation of this system is

$$\dot{X}_k = AX_k + B_\infty T_\infty + B_{R_k} Q_{R_k} \quad (9)$$

where X_k is the vector representing the surface temperatures of the N layers in the k th measurement zone, B_∞ is the matrix which introduces the ambient air as an input to the system, T_∞ is the ambient temperature vector, B_{R_k} is the matrix representing the radiation effect in the model, and Q_{R_k} is the total radiation input for the k th zone.

Expanding Q_{R_k} , we have

$$\dot{X}_k = AX_k + B_\infty T_\infty + B_{R_k} \theta - B_{R_k} \begin{bmatrix} x_{k,1} \\ x_{k,5} \end{bmatrix} \quad (10)$$

where θ is the vector of all the heater temperatures, $x_{k,1}$, and $x_{k,5}$ are the surface temperatures of the k th zone.

It should be noted that the C matrix can be chosen depending on the available readings of the states. In this case, since only the top and bottom surface temperature readings are available, for the k th measurement zone, we have

$$Y_k = \begin{bmatrix} 1 & 0 & 0 & 0 & 1 \end{bmatrix} \dot{X}_k. \quad (11)$$

Finally, (10) and (11) are linearized around an operating point. The reader can refer to [34] and [42] for the linearized state-space representation of the system. In addition, to apply the

Luenberger observer, it has to be ensured that the system is observable. The observability matrix Q of this system has full rank, ensuring that the overall system is observable.

In the implementation of the observer, since there now exist two types of sensors, the observer is divided into: 1) a real zone observer, which corresponds to the estimation of the core temperature for real sensor zones of the sheet; and 2) a virtual zone observer dealing with the estimation of the core temperature for virtual zones of the sheet.

To estimate the core temperature of the plastic sheet, the linearized state-space model of (10) and (11) are used, and we are interested in the temperature of the third layer, i.e., the third state in each sensor measurement zone, as the core temperature of the plastic sheet. Next, the input U , output Y , and the matrices A , B , C , and D are identified.

- The inputs are chosen as:
 - 1) The actual surface temperature readings from the real sensors, in case of the real zone observer, and the virtual sensors, in case of the virtual zone observer.
 - 2) The heater temperature, which will later be multiplied by the inverse view factor matrix to decouple the system for each sensor measurement zone.
 - 3) The ambient temperature inside the thermoforming machine.
- Matrices A and B are stated in (10) and the matrix C is chosen so that the outputs are the surface temperatures of the plastic sheet since they are the only measurable and visible states shown in (11), and Matrix D is set to zero.

In this arrangement, the gain matrix L is chosen so that the eigenvalues of $A-LC$ have all negative real parts, so that the error will approach zero, guarantying that all estimated states will converge to the actual states. Therefore, it can be ensured that the third state in each zone, which is the center-plane temperature, will provide an accurate estimate of the actual core temperature of the plastic.

Once the two observers are designed, they will be added to the block diagram of the system updated in the last section (Fig. 2.3). Fig. 2.5 shows the new block diagram of the system that has the MVBSs and the observers incorporated. Observing Fig. 2.5, it is important to notice that the second feedback, previously being generated from the virtual sensor block, will now be replaced with the surface temperature estimate from the virtual observer creating an observer based control setup for the virtual environment. The observer is actively trying to reduce the

error between the model estimate and its own generated estimate making the end estimated result more reliable. Therefore, the surface-temperature reading from the virtual observer is preferred since it also has a corrective action on the model inaccuracies existing in the heating-phase model block meanwhile not affecting the overall transfer function between the set-points and the output [88].

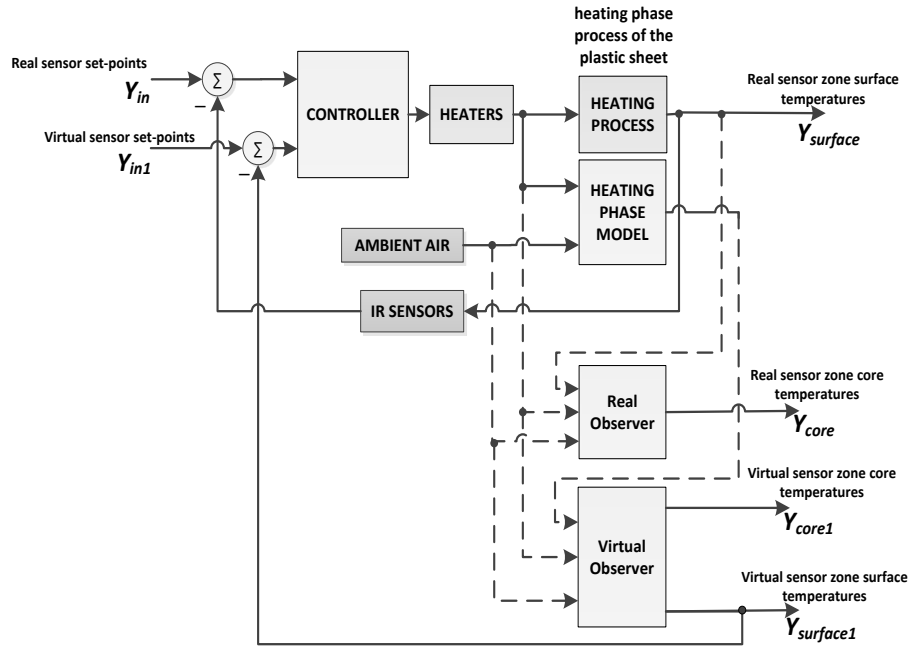


Figure 2.5. Complete block diagram of the system containing the MBVSs and the observers

2.7 Simulation Results

In this section, the updated control setup shown in Fig. 2.5, which includes the MVBSs and the core-temperature observers, is simulated in real-time, on a standard industrial rotary thermoforming machine simulator. This machine is configured with the exact specifications of an industrial machine used in production lines, which contains 108 heating zones (54 on top and 54 on the bottom), uses ceramic-type heaters, and can fit sheets with dimensions of 1.5mX2m. The sheet used in this simulation is a commonly used black high-density polyethylene (HDPE) sheet with 1.5mX2m dimensions and 8mm thickness, which fits in the thick-gauge thermoforming category. Black HDPE plastics are widely used to produce parts in a variety of industries and applications, including automotive, roadside equipment, household products, and

many others [120]. For instance, in the automotive industry, black HDPE plastics are widely used in producing plastic fuel tanks for cars and recreational vehicles as stated in [120] and [121], while they are also used in producing inner fender panels [122]. The black HDPE sheet, according to [36] and [37], has a dynamically more accurate heat transfer model if it is considered to be opaque to the transmittance of the radiant energy. Therefore, we consider $\beta_1 = 1$ and $\beta_2 = 1$, implying that the radiation energy is only absorbed by the top and bottom surface layers of the plastic sheet. It is important to note that the algorithms of MVBSs and the core-temperature observers can incorporate any types of plastic sheets, with or without radiation transmission, since the nature of the model does not affect the methodologies used in developing the MVBSs and core-temperature observers.

In total, considering top and bottom levels, there are 20 real IR sensors (10 on top and 10 below the plastic sheet) and 24 MVBSs (12 on top and 12 below the plastic sheet), creating 44 sensor measurement zones on the sheet for temperature measurement.

The 2D position grid of the real IR sensors and the virtual sensors relative to the heaters is shown in Fig. 2.7. Note that the real IR sensors are not equally distanced from each other. Also, there are a total of 44 identical PI controllers used relative to the number of sensor zones (20 for real IR sensor zones, and 24 for virtual IR sensor zones).

The simulation is conducted in two parts: simulation under ideal conditions, and simulation in the presence of uncertainty in material properties. Also, the type of input used in this simulation is a ramp-type input to address the needs of the industry. In thermoforming, the goal is to reach the forming temperature as soon as possible and to rapidly start the forming process, eliminating the need to monitor both the overshoot and the settling time. Therefore, the ramp-type input is introduced to rapidly bring the sheet's temperature to the forming window. To achieve an appropriate ramp-type input, the system was operated in open-loop, and the heater temperatures were changed from their initial temperature to 100°C higher in order to monitor the rate of temperature increase in the plastic sheet. The ramp-type input is then chosen as a slightly more conservative version of the temperature-increase curve obtained in open-loop testing. The ramp input is chosen in this manner to account for limiting factors, such as the physical limitation of the heaters, and the delay of the plastic sheet in reacting to the heat.

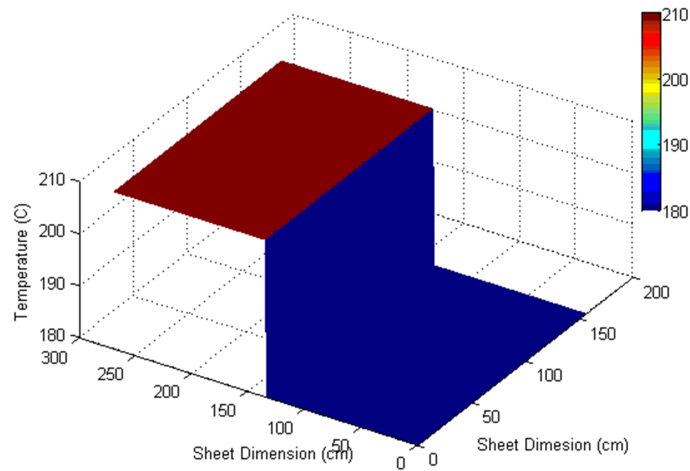


Figure 2.6. Desired zoned temperature setpoints (profile)

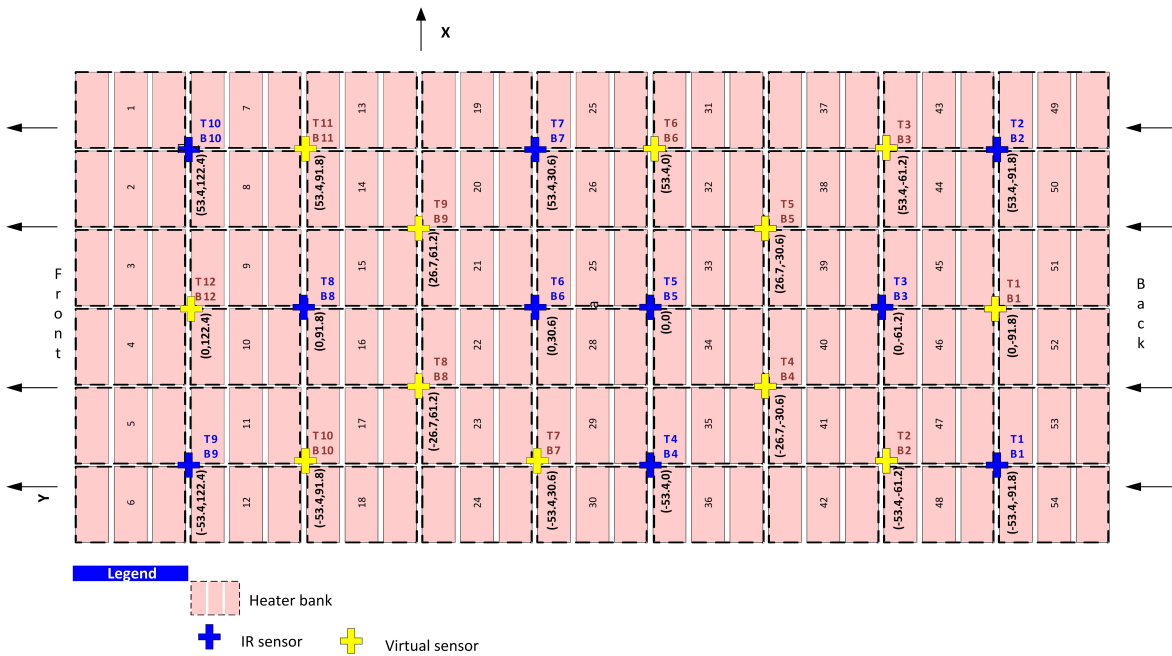


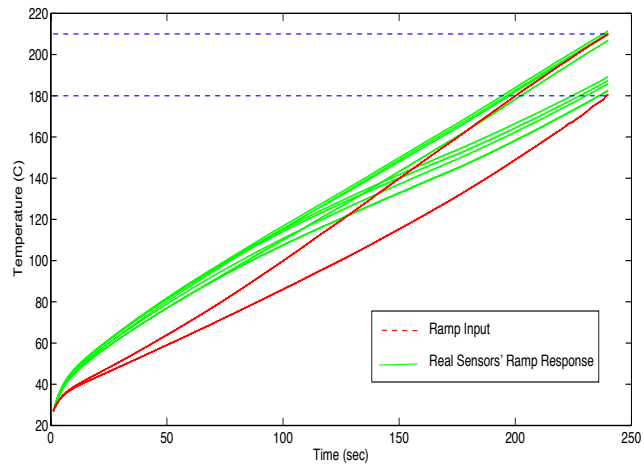
Figure 2.7. 2-D position grid of the real IR sensors and the virtual sensors relative to the heaters

2.7.1 Simulation Under Ordinary Conditions

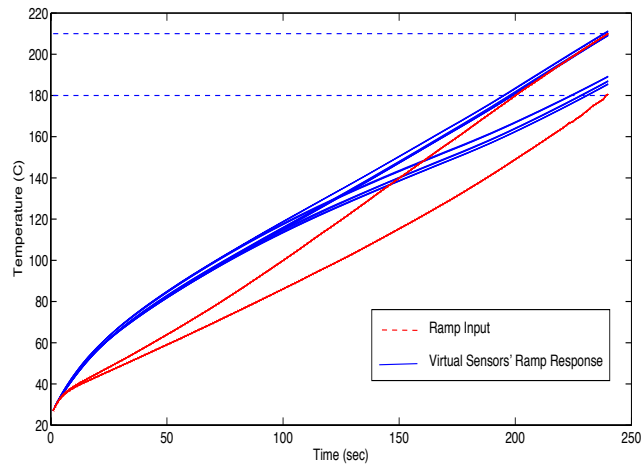
The simulation is conducted for zoned temperature set-points shown in Fig. 2.6. In thermoforming, it is often needed to have one area of the sheet in a certain temperature, and the other area at lower temperature with a difference of 20°C to 30°C. Here, the set-point

temperature profile requires one area of the sheet to have a temperature of 210°C, and the other area to be at 180°C. As shown in Fig. 2.7, in terms of sensor zone set-points, real sensors 1-5 (top and bottom) along with virtual sensors 1-6 (top and bottom) will have 210°C set-points while real sensors 6-10 (top and bottom) and virtual sensors 7-12 (top and bottom) are required to have 180°C set-points. During the heating process, the sheet temperature should never exceed the set-point temperature by more than 10°C since the plastic starts to melt, resulting into a rejected part.

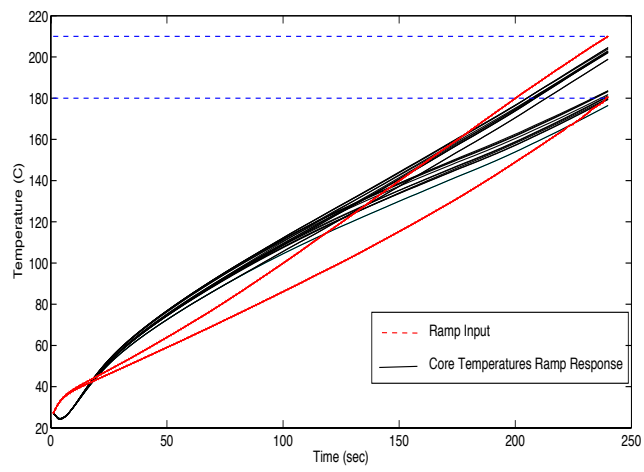
The ramp-shaped input is then applied containing the temperature set-point profile in Fig. 2.6. The simulation results for the ramp-type input are shown in Fig. 2.8. Observing Fig. 2.8(a)-(d) the virtual sensors are behaving like the real sensors trying to track the ramp input to get to the desired set-points, meaning that the virtual measurement zones are being accurately controlled. Moreover, Fig. 2.8(c) shows that the estimated center-plane temperatures are tracking their surface temperature set-points, indicating the functionality of the observers. Using the ramp input, the sheet reaches its forming temperature in 235 s while never going over the 10°C overshoot window. In addition, when applying the ramp input, if the surface temperature is at its forming temperature (e.g. 210°C), the core temperature, since it is lagging the surface temperature, has to be no less than 10°C cooler than the surface temperature. Otherwise, the center-plane temperature is not in the temperature forming window, and the sheet cannot be formed. Observing Fig. 2.8(c), it can be seen that the core temperature of the plastic sheet is, in fact, within the 10°C window, and so the sheet can be successfully formed.



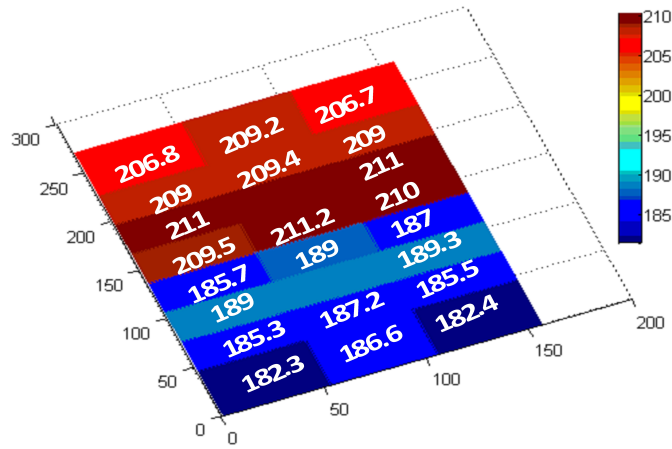
(a)



(b)



(c)



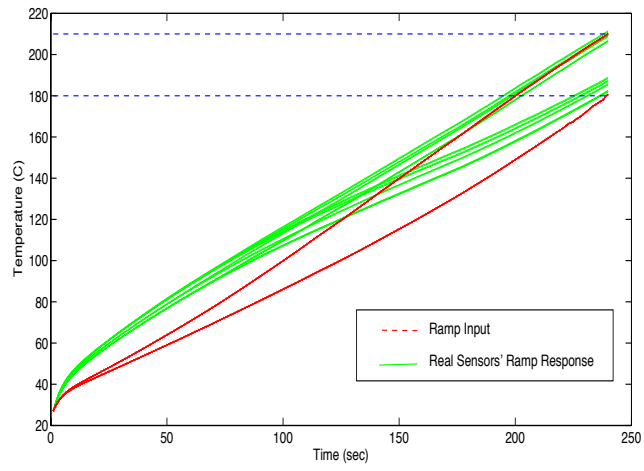
(d)

Figure 2.8. (a) Ramp response of the real sensors to the zoned ramp inputs shown in red dotted lines. (b) Ramp response of the MVBSs to the zoned ramp inputs. (c) Estimated core-temperature response to the zones ramp inputs. (d) Final surface temperatures of the measurement zones.

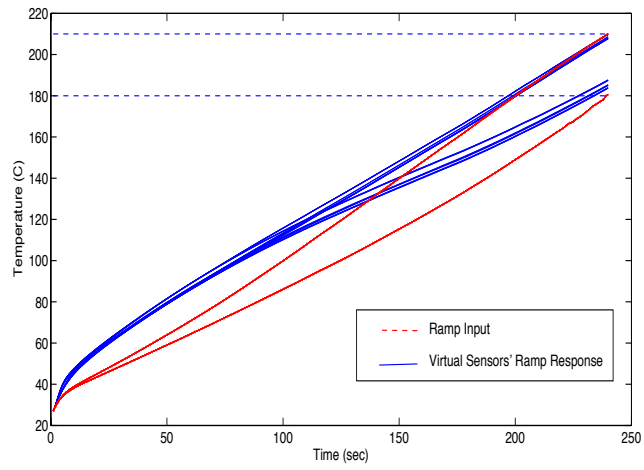
2.7.2 Simulation Under Uncertainty in Material Properties

As aforementioned, material properties could be 20% uncertain in practice. This uncertainty could affect the MVBSs since those parameters are used in estimation of the surface temperature. Therefore, the robustness of the virtual sensors and the entire control system is investigated under an existing 20% perturbation in material property values, namely the specific heat capacity, the density, the effective emissivity, the conduction coefficient, and the convection coefficient, for an HDPE plastic sheet.

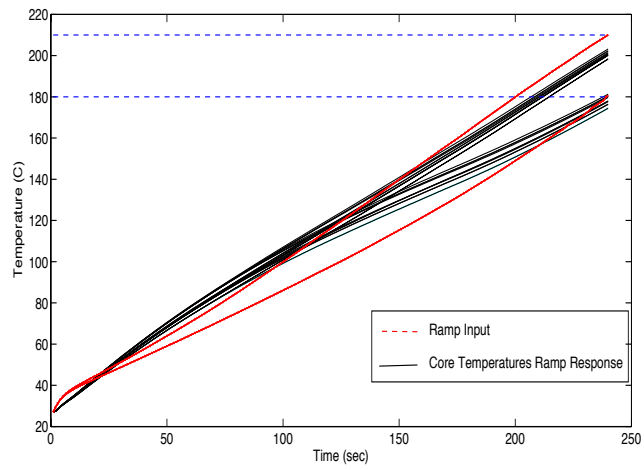
The ramp-type input is applied to the system with perturbed virtual sensors. Fig. 2.9 shows the simulation results, and it can be seen from Fig. 2.9 (a)-(d) that the real sensors final temperature along with the virtual sensors and the center-plane final temperatures are all in the 10°C temperature forming window. In addition, the tracking pattern is similar to the case of “simulation under ordinary conditions” with the virtual sensors and the core-temperature estimator tracking the ramp input just like the real sensors are. Moreover, the system is still able to bring the plastic sheet temperature to the forming window in 235 s, similar to the perturbation-free conditions. Therefore, it is established that the virtual sensors along with the core temperature observers are robust to uncertainties in material properties as they are still delivering accurate estimations.



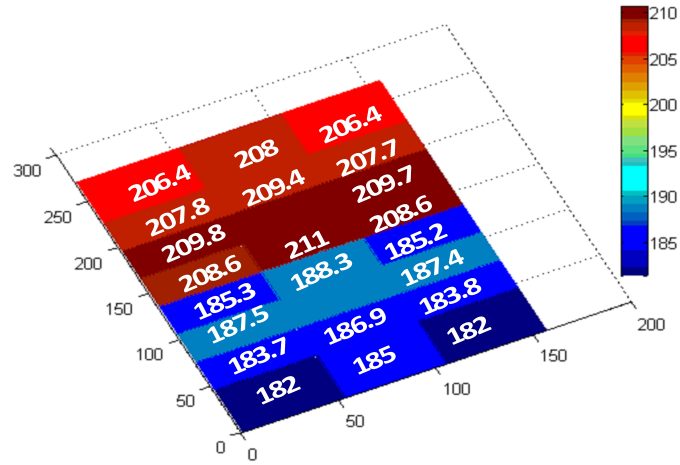
(a)



(b)



(c)



(d)

Figure 2.9. In the presence of 20% material uncertainty: (a) Ramp response of the real sensors to the zoned ramp inputs shown in red dotted lines. (b) Ramp response of the MBVSs to the zoned ramp inputs. (c) Estimated core-temperature response to the zones ramp inputs. (d) Final surface temperatures of the measurement zones.

2.8 Conclusion

MVBSs were proposed as a new estimation method of the surface temperature, and controllers were developed for the virtual sensors. Also, closed-loop Luenberger observers were applied to estimate the core temperature of the plastic sheet. The two methods were then combined, creating a new closed-loop control diagram for a thermoforming process. The performance and robustness of the new system, containing the MVBSs and the core-temperature observers, is verified through simulation.

The proposed closed-loop control diagram is utilized in Chapter 3, where the Watanabe-modified Smith predictor is implemented to improve the heating cycle time of the thermoforming heating phase.

3 Application of the Watanabe-Modified Smith Predictor Technique in Thermoforming

Can the heating time (cycle time) be further improved using new control methods in thermoforming?

In this chapter, the application of the Watanabe-modified Smith predictor technique is presented in order to improve the cycle time of the heating phase. This chapter describes the motivation behind the application of this control scheme, followed by the controller design study. The proposed control scheme is then implemented on the updated block diagram of the control system containing the MVBSs and core-temperature observers, which was presented in Chapter 2. A simulation study is also conducted to compare the performance and robustness of the proposed control scheme with conventional controllers.

This chapter has been adapted from: R. Modirnia and B. Boulet, "Application of the Watanabe-modified Smith predictor control technique in thermoforming, " in *American Control Conf. (ACC)*, Montreal, Canada, 2012, pp. 6448-6454.

➤ **Authors contributions:**

- 1) Rahi Modirnia: the author of the thesis is responsible for the design and development of the control technique, implementation, and interpretation of the results. The thesis author is also responsible for writing the manuscript.
- 2) Benoit Boulet: supervised the work and edited the manuscript.

3.1 Abstract

In this chapter, the application of the Watanabe-modified Smith predictor control technique in a thermoforming heating process is presented. It has been observed that the temperature rise of a plastic sheet exhibits an input delay-like behavior due to heater lags and other environmental parameters. Therefore, the modified Smith predictor technique is applied to compensate for this delay, allowing for improved tunability, performance, and robustness to parameter variations in the system, compared to the existing controllers. The Watanabe-modified Smith predictor control technique is then included in the control diagram of the system, tuned, and tested on an industrial thermoforming machine simulator. The performance and robustness of the new control technique is then compared to the existing PI controllers in simulation.

3.2 Introduction

Thermoforming is an industrial process in which plastic sheets are heated and then formed into useful parts, mainly utilized in the automotive, aerospace, refrigeration, medical and packaging industries [5, 89-91]. Today, the extensive growth of the plastic manufacturing industry worldwide is faster than any other manufacturing industries, stressing the ever important presence of the plastics industry in the world's economy. An example of this trend lies in the automotive industry, where the percentage of plastic materials used per vehicle has increase by 75% between 1977 and 2007 while the percentage of ferrous materials used has been decreased by 20%. Looking ahead to 2020, the world's plastic industries will more than double their production, indicating that polymer processing will play increasingly important roles in the future [91]. Thermoforming is one of the most important plastic forming processes; therefore it is important to develop more efficient and cost-effective techniques for this process to ensure productivity improvement.

A thermoforming process consists of three major phases: heating, forming, and cooling [34]. During the heating phase, the sheet is heated to a certain forming temperature, where it will start to experience sagging. Once the forming temperature is reached, the sheet is placed on a mold to take on the required shape. It is important to reach the forming temperature or the set-point temperature profile during the heating phase in order to achieve the right rheological properties of the polymer so the sheet can be formed properly [84-87]. Moreover, in order for the plastic to take on different shapes, uneven temperature profiles or zoned temperature profiles are

often required across the plastic sheet. Therefore, it becomes crucial to systematically control the heaters temperatures in a thermoforming machine to ensure that the required sheet temperature profile is attained.

This was previously done in an open-loop mode, where the heaters temperatures were manually adjusted throughout the heating phase so that the plastic sheet would reach its desired temperature profile. This method was based on trial and error and, naturally, was also not an efficient way to obtain the set-point profile on the plastic sheet. Later, closed-loop control methods were proposed in order to generate some type of feedback measurement and to automate the system. This was first proposed by Mark Ajersch in [34], who controlled the plastic sheet's surface temperature through an empirical model of the thermoforming process and PI controllers while infrared (IR) sensors were used in the feedback to measure the surface temperature of the plastic sheet at various locations. It was then shown in later studies that a closed-loop control system will result in productivity improvement, in particular, reducing part reject rates, cutting the heating phase time, reducing energy costs and maximizing heater life [38].

In this chapter, a new type of internal control technique for the thermoforming heating process is proposed to improve performance, robustness, and tunability of the system. This internal control method is based on the Smith predictor technique, introduced by Smith in 1957, and is aimed at improving the performance and robustness of systems containing time delays [44]. The Smith predictor method was later modified by Watanabe *et al.* to improve the performance of a system with an integrator and long dead-time [48]. Astrom *et al.* further developed Watanabe's method such that the tracking performance and disturbance rejection are independently improved [49]. Subsequently, based on the works of Watanabe and Astrom, Zhang *et al.* proposed a modified Smith predictor to deal with first-order plus time-delay processes [50]. The method used in this chapter is derived from the work of Watanabe *et al.* since only tracking performance is of interest while disturbance rejection is not considered here.

The Smith predictor delay compensation technique is of interest because during the heating phase, the sheet temperature output is initially delayed. This is mainly because of the delay in the heaters, which are sluggish in changing their temperature to a higher and lower set-point, as well as other environmental factors [34]. This was verified in simulation and experimentally, and it was determined that the value of this delay is substantial, requiring the use

of a time-delay compensation method. In this chapter, the applicability of the Smith predictor technique in a thermoforming process is presented, and tuning formulas are also discussed. The Watanabe-modified Smith predictor technique is then applied to the existing control block diagram of the heating phase, which contains all the complex heat transfer equations of the process, and tested on an industrial thermoforming machine simulator. In the simulation section, the performance of the system and robustness to variations in material properties are investigated, and results from the Watanabe-modified Smith predictor method are compared to existing control methods.

3.3 Description of the Existing Control System

In this section, the existing block diagram of the heating phase, introduced by Modirnia *et al.* in [92], is briefly presented. The block diagram of this control system is shown in Fig. 3.1. The set-points of this control system are defined as the desired sheet temperature profile, or in other words, the desired temperature of the measurement zones on the plastic sheet which are discussed later in this section. In this setup, heaters are treated as actuators, and the heating phase of the plastic sheet is considered as the plant. There are two types of sensors measuring and feeding the surface temperatures back to the control side: real IR and virtual model-based sensors. The real IR sensors are placed in the thermoforming machine, measuring the surface temperature of the sheet during the actual heating process, while the virtual model-based sensors use the model of the heating phase in thermoforming, developed in [34] and [35], to actively estimate the surface temperature, in parallel with the actual process taking place. In Fig. 3.1, this operation is being performed in the “heating phase model” block, where the entire complex heat transfer equations, developed in [34] and [35], are present. Therefore, we consider the zone on the plastic sheet over which each of the real or virtual sensors directly point to as a sensor measurement zone, thus having two sets of inputs: real sensor and virtual sensor set-points.

A thermoforming machine generally consists of $2H$ heaters, H being placed on top and H on the bottom, with the plastic sheet being placed in-between with an equal distance from the top and bottom heater banks. There are also a total $2Z$ IR and $2V$ virtual sensors for a total of $2(Z+V)$ sensors, $(Z+V)$ sensors placed on top, and $(Z+V)$ on the bottom. It is important to note that the top and bottom heaters and the sensors are respectively placed to be directly facing each other in the thermoforming oven.

The controller part consists of $2(Z+V)$ individual controllers corresponding to each sensor measurement zone, $2Z$ of which are designed for the real IR sensor measurement zones and $2V$ controllers for the virtual sensor measurement zones. In the controller block, a decoupling matrix is also defined after the controllers with the dimension $2H \times 2(Z+V)$, which transforms the measurement zones temperatures to heater banks temperatures since there are more heater banks than there are measurement zones. The decoupling matrix contains view-factor elements, which are defined to determine the fraction of the radiant energy exchanged between two surfaces having different areas and orientations [42]. The inversion of the view-factors indeed plays a decoupling role, converting the energy needed to heat each of the measurement zones to the amount of radiation needed for each of the heater banks during the heating phase.

The evaluation of the view-factor from a measurement zone to each heater is obtained by considering having two parallel surface areas A_1 and A_2 , with the perpendicular distance between them being z . The mathematical and geometrical details on how to obtain the view-factor are extensively covered in [42]. In order to calculate all the view-factor entries of the decoupling matrix, the location of all the heater banks and sensors (IR or virtual) has to be mapped on a Cartesian plot. Therefore, the heater banks, the real IR sensors, and the virtual model-based sensors are placed on a two-dimensional grid, and appropriate coordinates are defined for each of these elements while the vertical distance z is also taken into account. However, the reason for which a two-dimensional grid is chosen instead of a three-dimensional one is due to the fact that the distance z between the sensors measurement zones and the heater banks is always constant. Therefore, the two dimensional grid is chosen for simplicity.

The control system shown in Fig. 3.1 also contains two core-temperature estimator blocks: one designed for real sensor measurement zones, and the other aimed to deal with the virtual sensor measurement zones. These observer blocks contain closed-loop Luenberger state observers, using the state-space model of the heating phase developed in [42] and [34], in order to accurately estimate the core-temperature of the plastic sheet. It should be noted that the feedback designated for the virtual sensor set-points is taken from the virtual observer block since it takes corrective action on the model uncertainties in the “heating-phase model” block, producing more accurate surface temperature estimates of the virtual sensor measurement zones.

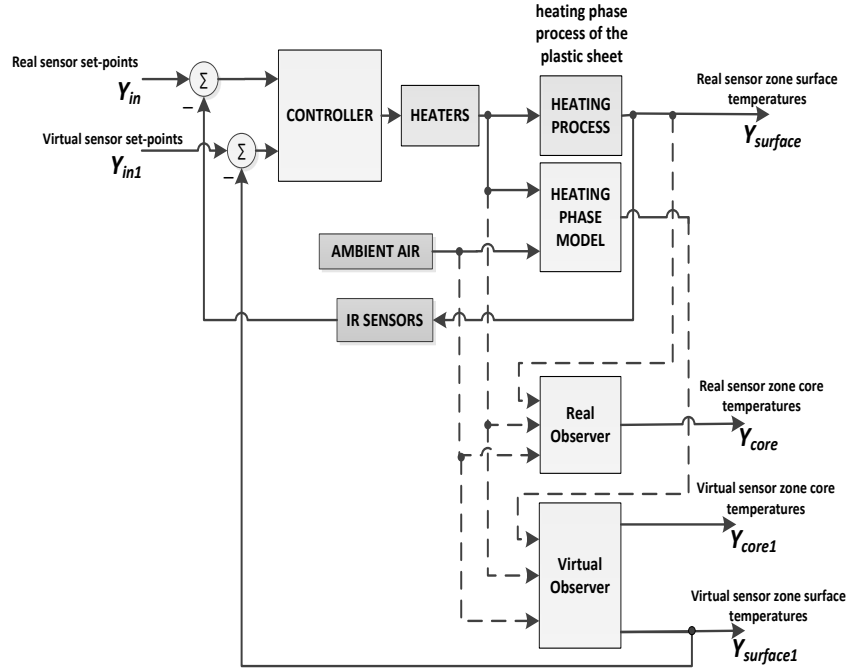


Figure 3.1. Block diagram of the closed-loop control system

3.4 The Smith Predictor Control Technique: an Overview

As mentioned before, the Smith predictor technique is a control strategy developed to deal with systems containing time delays. Details of this method can be found in [44], and a brief presentation of this method is given here.

Suppose that a model for the process $G_p(s)$ (s being the Laplace variable) is available, and described by

$$\tilde{G}_p(s) = \tilde{G}^*(s) e^{-\tilde{\theta}s}. \quad (1)$$

The process model is divided into two parts: the part without the time delay, $\tilde{G}^*(s)$ and the time-delay term of the process, $e^{-\tilde{\theta}s}$, when $\tilde{\theta}$ is the delay time. In the Smith predictor control scheme, the model of the process without the time delay ($\tilde{G}^*(s)$) is used to predict the effect of control actions on the non-delayed output. In other words, in case of perfect modeling, the controller responds to the error signal that would occur if no time delays were present.

Assuming that there is no model error ($G_p(s) = \tilde{G}_p(s)$), it can be shown that the closed-loop transfer function of a system containing the Smith predictor controller $G_c(s)$ is given by

$$\frac{Y}{Y_{sp}} = \frac{G_c \tilde{G}^* e^{-\tilde{\theta}s}}{1 + G_c \tilde{G}^*}, \quad (2)$$

in contrast to conventional feedback control

$$\frac{Y}{Y_{sp}} = \frac{G_c \tilde{G}^* e^{-\tilde{\theta}s}}{1 + G_c \tilde{G}^* e^{-\tilde{\theta}s}}. \quad (3)$$

Comparison of (2) and (3) indicates that the Smith predictor has the advantage of eliminating the time delay from the characteristic equation, thus greatly improving the performance over a conventional system. In case of the process model not being perfect, the Smith predictor can still provide improvement over conventional feedback control if the model parameters are within about $\pm 30\%$ of the actual values [93]. Therefore, if a certain type of controller is included into a Smith predictor loop, the performance and robustness of the closed-loop system will be superior to the one that has the controller used without the Smith predictor setup.

Watanabe *et al.* later improved the performance of the system using a modified version of the Smith predictor setup, shown in Fig. 3.2.

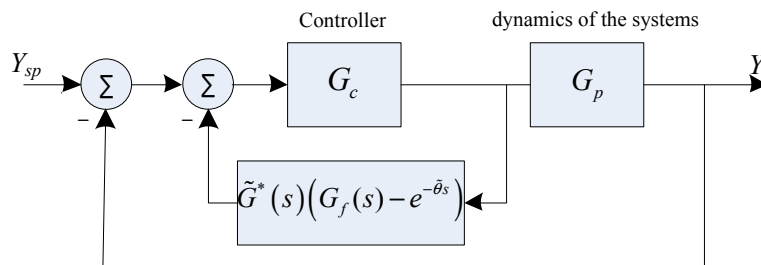


Figure 3.2. Watanabe-modified Smith predictor

In this method, a low-pass filter $G_f(s)$ is introduced in the feedback of the controller, which helps improve the tracking performance of the system, and in some cases helps reject the load disturbance [48]. $G_f(s)$ is often chosen as:

$$G_f(s) = \frac{1}{1+sL}, \quad (4)$$

where the time constant L is chosen depending on the aggressiveness of the design.

3.5 Application of the Watanabe-Modified Smith Predictor to the Thermoforming Heating Phase

In this section, an application of the Watanabe-modified Smith predictor to the heating phase of the thermoforming process is discussed. First, it will be shown that the temperature response of the plastic sheet contains a significant delay to justify the use of the Smith predictor, and then the controller design and the application of the Smith predictor technique will be presented.

3.5.1 Justifying the Use of the Smith Predictor Technique

In order for the Smith predictor to provide useful results, it has to be first determined if the open-loop output temperature response exhibits a certain amount of delay compared to the input. In general, the reason for which the temperature response of the plastic sheet experiences an input delay is due to the fact that the heaters are sluggish in temperature change, taking a considerable amount of time to increase or decrease their temperature from a particular set-point to another [34]. Different types of heaters may have different heating and cooling rates, but in the case of ceramic heaters, which are one of the most commonly used heaters in the thermoforming industry, it takes nearly 50 s for the heater temperature to have a 100°C increment in temperature and nearly 100 s to have a 100°C decrement in temperature. Therefore, since the heaters are not fast enough to immediately provide desired temperature set-points, the plastic sheet would not receive the required amount of heat in time, thus exhibiting a delay in increasing the surface temperature. Another reason for the existence of the delay is due to the energy of the heater banks not being entirely concentrated in raising the temperature of the plastic sheet at the beginning of the heating phase, instead having to dedicate some of their energy to heat the temperature of the ambient air. This is because certain types of thermoforming machines are placed in an open environment, allowing for the ambient air to circulate in and out of the machine. Thus, the ambient air temperature is always considerably lower than the heater banks temperatures when the heating phase begins. Combining the above factors, the step response of the surface temperature output of the plastic sheet exhibits a delay like behavior at the beginning

of its temperature rise, justifying the use of the Smith predictor control technique. Fig. 3.3 shows a high-density polyethylene (HDPE) plastic sheet simulated on an industrial thermoforming machine simulator in open-loop, exhibiting 50 s of delay at the beginning of its temperature response.

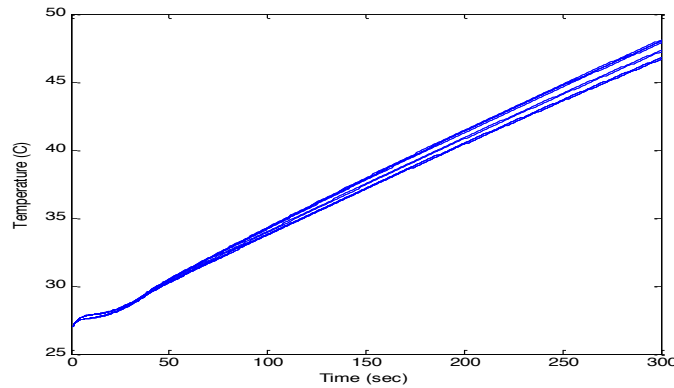


Figure 3.3. The open-loop surface temperature response of an HDPE plastic

3.5.2 Controller Design

As mentioned before, there are a total of $2(Z+V)$ measurement zones corresponding to the number of the real IR and virtual model-based sensors. Since the open-loop temperature response of all the measurement zones are approximately similar, having only minor differences, the goal is to design $2(Z+V)$ identical controllers for the measurement zones in order to keep the design process time efficient.

The first step is to represent the open-loop dynamics of the heating process of all the measurement zones by a single fitted open-loop response. Fig. 3.5 shows the open-loop temperature response of all the measurement zones with respect to a set-point change in all the heater banks, demonstrating that the heating process has first order dynamics plus an initial time delay. In Fig. 3.5, the fitted response representing the dynamics of all the measurement zones is also shown.

Assume that the dynamics of the fitted step response can also be represented using a “first order plus time delay” (FOPTD) response

$$G_p = \frac{K_p}{\tau_p s + 1} e^{-\theta_p s}, \quad (5)$$

where, K_p is the DC gain of the process, τ_p is the time constant and θ_p is the delay of the process.

Therefore, a controller will be designed for the fitted response and will be replicated to be used for all the measurement zones. To design the controller in the Smith predictor technique, the Direct Synthesis approach is used. In this approach, the desired closed-loop transfer function will be predetermined.

Assume that we are interested in having a desired FOPTD response with the following transfer function

$$\left(\frac{Y}{Y_{sp}} \right)_{desired} = \frac{e^{-\theta_p s}}{\tau_c s + 1}, \quad (6)$$

where, τ_c is the desired time constant of the closed-loop system, and θ_p , is the desired closed-loop time delay.

Also, as it was mentioned in (2), assuming that a perfect model is available ($G_p(s) = \tilde{G}_p(s)$, with $G_f(s) = 1$), the closed-loop transfer function for set-point changes is

$$\frac{Y}{Y_{sp}} = \frac{G_c \tilde{G}^* e^{-\theta_p s}}{1 + G_c \tilde{G}^*}. \quad (7)$$

Equating (6) and (7)

$$\frac{e^{-\theta_p s}}{\tau_c s + 1} = \frac{G_c \tilde{G}^* e^{-\theta_p s}}{1 + G_c \tilde{G}^*}, \quad (8)$$

the controller present in the Smith predictor structure can be obtained from (8) as

$$G_c(s) = \frac{1}{\tilde{G}^*} \frac{1}{\tau_c s}, \quad (9)$$

where \tilde{G}^* is the non-delayed part of the process in (5), represented as

$$\tilde{G}^*(s) = \frac{K_p}{\tau_p s + 1}. \quad (10)$$

Substituting (10) in (9), G_c is then given by

$$G_c(s) = \frac{\tau_p}{K_p \tau_c} \left(1 + \frac{1}{\tau_p s} \right). \quad (11)$$

It can be seen from (11) that the structure of G_c represents a PI controller, which has the form

$$G_{PI}(s) = P + \frac{I}{s}. \quad (12)$$

Comparing (11) and (12), the P and I tunings for G_c are

$$P = \frac{\tau_p}{K_p \tau_c}, \quad I = \frac{1}{K_p \tau_c}. \quad (13)$$

This also demonstrates that, in the case of a first-order process, if a first-order closed-loop response is desired, the controller in the Smith predictor setup will be a PI controller. Thus, the performance and robustness that this PI controller along with the Smith predictor setup can achieve is definitely superior to the performance and robustness that a PI controller without a Smith predictor setup can achieve since the Smith predictor eliminates the effect of the time delay from the characteristic equation of the closed-loop transfer function.

The Smith predictor method also allows for improved tunability. The range of tunings for the Smith predictor control parameters, while obtaining an overshoot of less than 10°C, is significantly larger than the other methods since the controller has an internal feedback loop, preventing the more unstable controller outputs to get fed to the heater banks.

Finally, $G_f(s)$ will be chosen as shown in (4) in order to provoke a faster step response in the system while making sure that the overshoot does not exceed the design requirements.

Once the controller is designed for the fitted process, the next step is to replicate this for all the measurement zones for a total of $2(Z+V)$ controllers. These controllers will be then included in the “controller” block shown in Fig. 3.1 and will be applied to the heating phase process which contains the actual heat-transfer dynamical equations, thus completing the application of the Watanabe-modified Smith predictor technique on the thermoforming heating phase.

3.6 Simulation Results

In this section, the Watanabe-modified Smith predictor applied to the control setup in Fig. 3.1 is tested on an industrial thermoforming machine simulator, and its performance and robustness to perturbations is compared to the PI control method. The goal is to design a

Watanabe-modified Smith predictor such that the step response of the closed-loop system has the fastest settling time while exhibiting an overshoot of less than 10°C.

The thermoforming machine simulator contains 108 heating zones or heater banks (54 on top and 54 on the bottom), uses ceramic-type heaters, and can fit sheets with dimensions of up to 1.5mX2m. In this simulation, we used a common black HDPE sheet of dimension 1.5mX2m and 8mm thickness, which fits in the thick-gauge thermoforming category. Black HDPE plastics are widely used to produce parts in a variety of industries and applications, including automotive, roadside equipment, household products, and many others [120]. More specifically, in the automotive domain, black HDPE plastics are widely used in producing plastic fuel tanks for cars and recreational vehicles as stated in [120] and [121], while they are also used in producing inner fender parts [122]. The black HDPE sheet, according to [36] and [37], has a more accurate heat transfer model if it is considered to be opaque to the transmittance of radiant energy. Therefore, we consider the radiation energy to be absorbed only by the top and bottom surface layers of the plastic sheet. It should be noted that the control algorithm designed in this chapter is universal for all types of plastic sheets containing different absorption coefficients since the heat transfer dynamics of the plastic sheet, with or without the absorption coefficients, can always be modeled using first-order dynamics with a time delay.

In total, considering top and bottom levels, there are 20 IR sensors (10 on top and 10 below the plastic sheet) and 24 model-based virtual sensors (12 on top and 12 below the plastic sheet), creating 44 sensor measurement zones on the sheet for temperature measurement. The 2D position grid of the real IR sensors and the virtual sensors relative to the heaters is shown in Fig. 3.4, noting that the sensors placed on top and bottom of the sheet are directly facing each other, thus having similar coordinates on the grid. Finally, there are a total of 44 identical controllers used relative to the number of sensors (20 for real IR sensor zones, and 24 for virtual IR sensor zones).

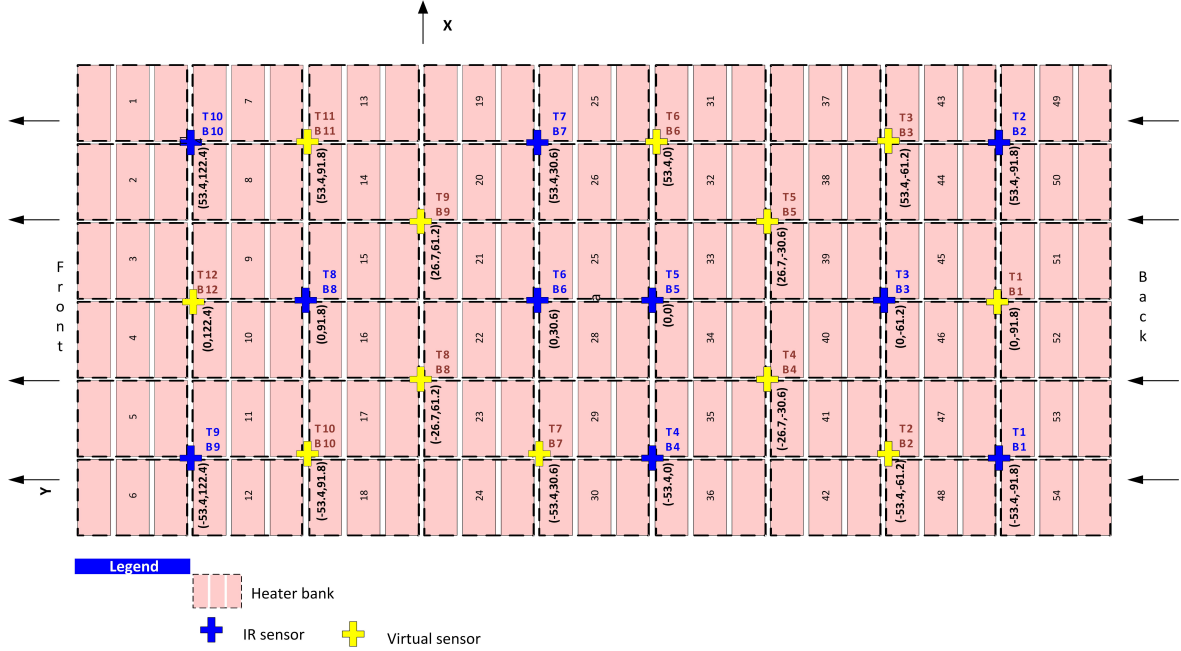


Figure 3.4. The 2D position grid of the real IR sensors and the virtual sensors relative to the heaters

The simulation is conducted in two phases: under ideal conditions and under the presence of uncertainties in material properties. Virtual sensors, unlike real IR sensors, do not directly measure the surface temperature. Instead, they deal with the model of the heating process, in which the material properties of any type of plastic sheet, such as the density of the plastic sheet ρ , the specific heat capacity of the sheet C_p , the thermal conduction k , and the emissivity ϵ_{eff} are included and quantified, thus having an important effect on the dynamics of the system. However, the material property specifications for certain types of plastic sheets (HDPE for example) are often temperature dependent, as it has been shown in [36] by Thomson *et al.* and in [37] by Khan *et al.*, and may lie within a 30% range (or more in the case of C_p) according to [36], [37], [5] and [116]. Additionally, for every identical type of plastic sheet (HDPE for example), the data sheets provided by different companies often contain different values. This has been discussed by Sepe in [117], stating that the material properties are not generated under equivalent test conditions due to the existence of a variety of standard test conditions such as (ASTM, DIN and JIS), which are regionally specific. Different companies use different standard test conditions, and this leads to nonidentical values of material properties for the same material. The interested reader can refer to [117] for more detailed discussion and analysis. Therefore, since virtual sensors deal with material properties in the estimation of the surface temperature

and since these quantified values can approximately vary in a 30% range above or below their nominal values, it is important for the system to undergo simulation with the presence of material properties perturbations in the “heating phase model” and the “virtual observer” blocks in Fig. 3.1 to make sure that the overall closed-loop system will maintain an acceptable performance. These parametric perturbations are used as a method to represent the variations of the material properties mentioned above, along with the convection coefficient h , being applied to the test robustness of the system.

Finally, we use a step input used in this simulation to facilitate the comparison of the Watanabe-modified Smith predictor technique with the existing PI method. To design the Watanabe-modified Smith predictor PI controller, the procedure described in the previous section is utilized. The system is first simulated under the open-loop condition with a step change in the heater banks temperatures from their initial value to 50°C higher. Fig. 3.5 shows the open-loop response of the measurement zones along with the fitted FOPTD response described by the following transfer function

$$G_p = \frac{K_p}{\tau_p s + 1} e^{-\theta_p s} = \frac{1}{220s + 1} e^{-90s}. \quad (14)$$

Note that the gain has been chosen as $K_p = 1$ because a 50°C step change in the heaters results into nearly a respective 53°C temperature increase in the plastic sheet’s temperature response, thus the ratio of the two changes is approximately $K_p = \frac{53}{50} \approx 1$.

Using the direct synthesis method, the desired closed-loop transfer function is chosen as

$$\left(\frac{Y}{Y_{sp}} \right)_{desired} = \frac{e^{-\theta_p s}}{\tau_c s + 1} = \frac{e^{-90s}}{54s + 1}. \quad (15)$$

Therefore, having determined the values of K_p , τ_p , and τ_c , the PI controller used in the Watanabe-modified Smith predictor technique has the P and I tunings of $P = \frac{\tau_p}{K_p \tau_c} = 4.07$ and

$I = \frac{1}{K_p \tau_c} = 0.0185$ according to (13). Finally, $G_f(s)$ is chosen as $G_f(s) = \frac{1}{1 + 6.5s}$, so that the

settling time of the system can be the fastest while the overshoot is less than the 10°C limit. The

Watanabe-modified Smith predictor is compared with existing PI controllers, which are also designed for the fastest settling time while achieving an overshoot of less than 10°C . The P and I tunings for these controllers are: $P = 1.867$ and $I = 6.67 \times 10^{-3}$.

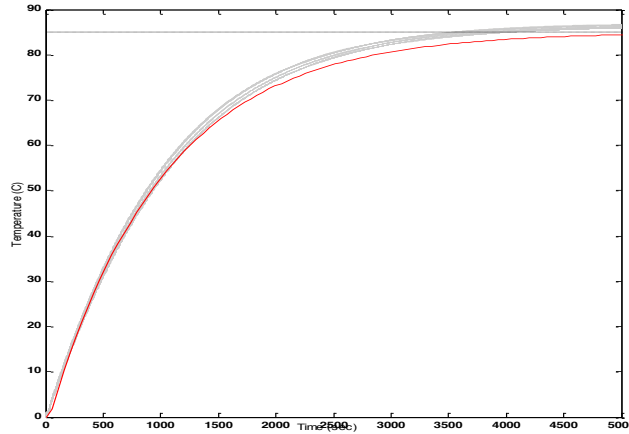


Figure 3.5. Open-loop response of the measurement zones on a plastic sheet in simulation shown in gray, along with the fitted response shown in red

3.6.1 Simulation under ideal conditions

The simulation is conducted for zoned temperature set-points, shown in Fig. 3.6. In thermoforming, it is often needed to have one end of the sheet at a certain forming temperature, and the other end at a lower forming temperature. Here, the set-point temperature profile requires one half of the sheet to have a temperature of 210°C , and the other half to reach 180°C . As shown in Fig. 3.4, in terms of sensor zone set-points, real sensors 1-5 (top and bottom) along with virtual sensors 1-6 (top and bottom) will have 210°C set-points while real sensors 6-10 (top and bottom) and virtual sensors 7-12 (top and bottom) are required to have 180°C set-points. During the heating phase, the sheet temperature should never exceed the set-point temperatures by more than 10°C since the plastic may start melting, resulting in a rejected part. Fig. 3.7 shows the step response of the system using the Watanabe-modified Smith predictor technique and the system using PI controllers alone, designed for the fastest settling time while keeping the overshoot under 10°C . Observing Fig. 3.7(a)-(c), it can be seen that the system with the Watanabe-modified Smith predictor technique has a faster performance with an average 5% settling time of 340 s, while never going over the 10°C overshoot bound, as opposed to the

system with the PI controllers, which has an average 5% settling time of 435 s. This is true for the real IR measurement zones, the virtual measurement zones, and the core temperature estimation of the measurement zones. Therefore, the Smith predictor technique will deliver an improved performance compared to the existing PI controller method.

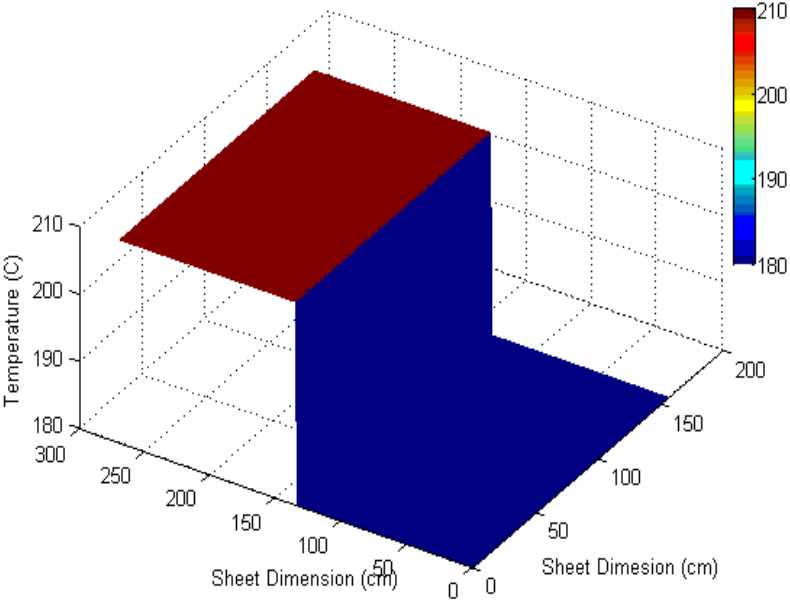
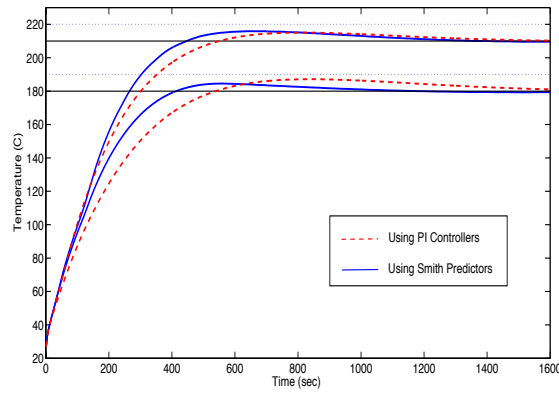
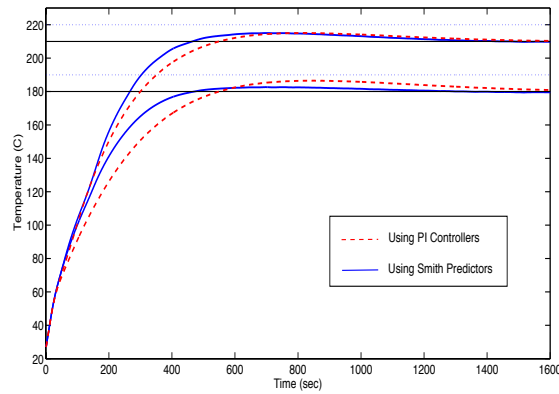


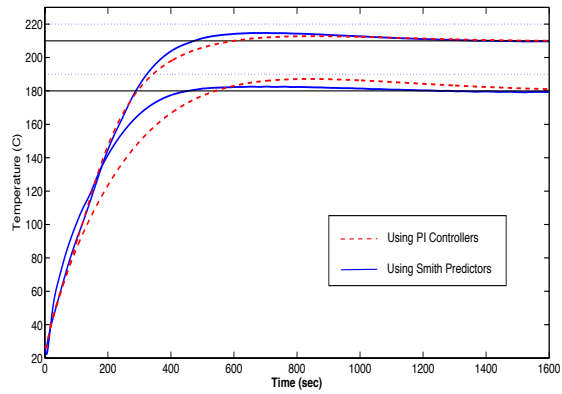
Figure 3.6. Desired zoned temperature set-points (profile)



(a)



(b)

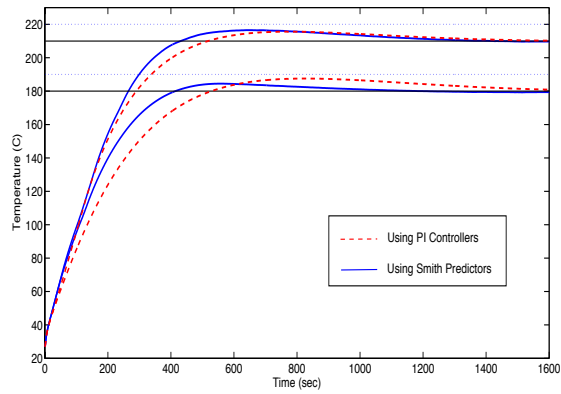


(c)

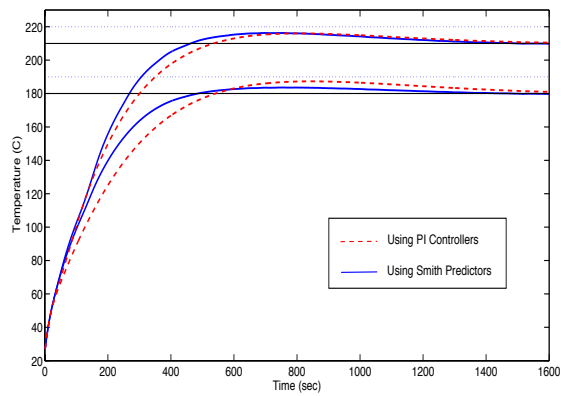
Figure 3.7. (a) Averaged closed-loop step response of all the IR measurement zones to the zoned set-points using the Smith predictor method, shown in blue, and using PI controllers, shown in red (dotted plot). (b) Averaged step response of all the virtual measurement zones to the zoned set-points points using the Smith predictor method, shown in blue, and using PI controllers, shown in red (dotted plot). (c) Averaged estimated core-temperature response to the zoned set-points points using the Smith predictor method, shown in blue, and using PI controllers, shown in red (dotted plot).

3.6.2 Simulation under uncertainty in material properties

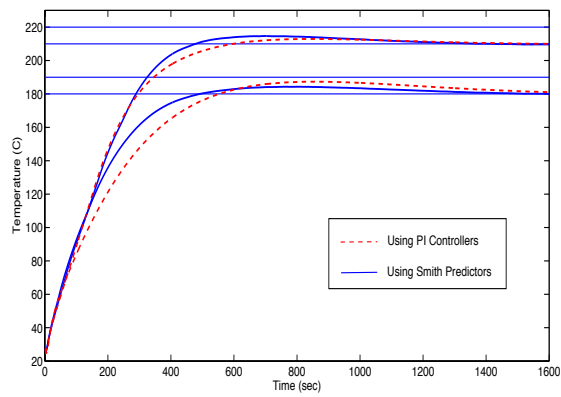
As it was discussed before, material properties of plastic sheets can be up to 30% uncertain in practice. Therefore, the robustness and tracking performance of the entire control system is investigated under a 30% perturbation in the “heating phase model” and the “virtual observer” blocks of the system. Fig. 3.8 shows the step response of the system, for zoned temperature set-points shown in Fig. 3.6, using the Watanabe-modified Smith predictor technique and using the existing PI controllers. Fig. 3.8(b) indicates accurate estimations by virtual sensor measurement zones in the presence of 30% perturbation in material properties, while the overshoot not exceeding the 10°C window, using any of the two control methods. Nevertheless, in the presence of this perturbation, the performance of the system containing the Smith predictor has been improved over the PI controller method with an average 5% settling time of 360 s for the Smith predictor method as opposed to an average 470 s when using the PI control method. Thus, it can be concluded that the Smith predictor technique is maintaining robustness when the material properties of the plastic sheet are uncertain while also improving the tracking performance, compared to the existing PI controllers.



(a)



(b)



(c)

Figure 3.8. In the presence of 30% material uncertainty: (a) Averaged closed-loop step response of all the IR measurement zones to the zoned set-points using the Smith predictor method, shown in blue, and using PI controllers, shown in red (dotted plot). (b) Averaged step response of all the virtual measurement zones to the zoned set-points points using the Smith predictor method, shown in blue, and using PI controllers, shown in red (dotted plot). (c) Averaged estimated core-temperature response to the zoned set-points points using the Smith predictor method, shown in blue, and using PI controllers, shown in red (dotted plot).

3.7 Conclusion

The Watanabe-modified Smith predictor has been applied to the heating phase of the thermoforming process to compensate for the time delay in the temperature response of the plastic sheet, improve the tracking performance under nominal and perturbed conditions, and to increase the tunability of the controllers. Direct Synthesis control design method was used to tune the controller parameters of the Smith predictor. The control setup, containing the Smith predictor controllers, was then simulated on an industrial thermoforming machine simulator, where it was shown that the Smith Predictor control technique provides improved performance and robustness to parameter variations compared to the PI control method.

In Chapter 4, modeling and control of multilayered plastic sheets is discussed.

4 Modeling and Model Predictive Control of Multilayered Plastic Sheets in Thermoforming

Can a control method be developed to control the temperatures of all the layers of multilayer plastic sheets during the heating phase, considering all the nonlinearities associated with the heating phase of the thermoforming process?

In this chapter, a control-oriented heat transfer model of the heating phase of multilayer plastic sheets is presented. A discrete-time model predictive control (DTMPC) algorithm is presented to solve the temperature tracking problem of all the layers in a multilayer plastic sheet. The DTMPC algorithm takes the nonlinearities of the heaters into account and solves the tracking problem for zoned temperature profiles. This control scheme is then incorporated in the block diagram of the control system containing the MVBSs and core-temperature observers, presented in Chapter 2. A simulation study is conducted to compare the tracking performance and the energy efficiency of the proposed control setup compared with conventional controllers.

This chapter has been adopted from: R. Modirnia, M. Abdolhosseini, and B. Boulet, "Modeling and Model Predictive Control of Multilayered Plastic Sheets in Thermoforming," *IEEE Transactions on Control System Technology*, submitted and under review (Submission number: TCST-2015-0664).

➤ **Authors contributions:**

- 1) Rahi Modirnia: the author of the thesis is responsible for the development and implementation of the model predictive controller in collaboration with Mahyar Abdolhosseini. In addition, the thesis author is responsible for conducting the energy efficiency analysis interpreting the results. The thesis author is also responsible for writing the manuscript.
- 2) Mahyar Abdolhosseini: significantly contributed to the design of the model predictive control algorithm. He also partially wrote the manuscript.
- 3) Benoit Boulet: supervised the work and edited the manuscript.

4.1 Abstract

In this chapter, we present a dynamical temperature evolution model of multilayered plastic sheets in the thermoforming heating phase, followed by a proposed discrete-time model predictive control algorithm (DTMPC) to control the surface and core temperatures of multilayered sheets. Multilayered plastic sheets are often used in vehicular components, construction, and sanitary products. However, thermoforming of these sheets has proven to be quite challenging due to the fact that different plastic materials have different rheological properties and different forming temperatures. Therefore, we propose a model predictive controller, designed based on newly developed models of multilayered plastic sheets in thermoforming, in order to solve the temperature tracking problem of such sheets. This control method is then implemented and tested on an industrial thermoforming machine simulator, where the tracking performance and energy efficiency of the proposed DTMPC is tested against conventional PI controllers. Energy efficiency analysis is conducted for the first time in thermoforming.

4.2 Introduction

Thermoforming is a plastic manufacturing process, in which a plastic sheet is heated to a precise temperature profile and formed into a useful part [89]. This process is used in automotive, appliance, construction, aerospace, and many other industries [5]. Today, in the United States, the plastic manufacturing industry is the third largest manufacturing industry as its productivity has grown 2.4% per year, which is better than the 1.7% per year productivity growth for manufacturing as a whole [2]. By the year 2020, the production of plastic materials is estimated to double the current amount, stressing the importance of polymer processing in the world's economy [94]. Thermoforming, being the oldest of plastic manufacturing processes, has had a rapid growth in recent years, attracting the interest of many plastic product manufacturers. According to a market study in 2007, the value of the world thermoforming market was estimated at US\$ 30,000 million, highlighting the important role of thermoforming in the growth of the plastic manufacturing industry [5]. With all the aforementioned facts and the promises of this particular plastic manufacturing process, it is imperative to develop more efficient and cost effective techniques to improve the productivity of the thermoforming process.

The thermoforming process is divided into three major phases: heating, forming, and cooling. In the heating phase of this process, the plastic sheet is inserted into a thermoforming machine and is heated to a precise forming temperature, which is indeed when the plastic sheet sags, indicating that it is ready for the forming phase of the process. In the forming phase, the sheet is draped on a mold to take a certain predetermined shape, subsequently being cooled in the final phase of the process. It should be noted that proper forming could only occur if the plastic sheet has reached the precise temperature set-point (profile) at which the sheet is flexible enough to be molded. Moreover, often, because of the complexity of the shape of the final product, uneven temperature set-points or non-uniform temperature profiles are required across the plastic sheet. Therefore, it is crucial to systematically control the heaters temperatures so that the exact temperature profile is achieved across the plastic sheet.

Previously, the heating phase of the process has been conducted in open-loop, inferring that the human operator would manually adjust the heaters' temperatures throughout the heating phase so that the plastic sheet would reach its required temperature profile. Indeed, this method is not an overall efficient method since it involves a heavy amount of trial and error. Later, closed-loop control was introduced by Ajersch in [34], where the surface temperature of the plastic sheet was controlled using an empirical model of the heating phase and classical PI controllers. The feedback of the control loop was provided by Infrared (IR) sensors, which were placed at various locations on top and bottom of the plastic sheet.

Analysis later confirmed that the use of feedback control in thermoforming would result in productivity improvement, especially in reducing scrap rates, improving the heating phase time, reducing energy consumption, and maximizing heater life [38]. In subsequent studies, Modirnia *et al.* introduced model-based virtual sensors in order to increase the number of feedback measurements for a more precise control effort and to achieve non-uniform temperature profiles across the plastic sheet [95]. Core temperature observers were also developed to provide an accurate real-time prediction of the core temperature during the process since it is also crucial for the core temperature of the sheet to be kept within the forming temperature range [95]. There have also been more sophisticated control efforts developed for the heating phase of monolayer plastic sheets (sheets consisting of only one type of plastic material) in order to improve the performance of the system, especially the heating time (tracking time). In [96], Modirnia *et al.* applied an internal-model control concept to the heating phase process, in the form of the Smith

predictor controller, considerably improving the heating time over the cycle. Chy *et al.* also applied model predictive control in [39] and have compared the MPC method with the more traditional controllers. MPC methods have also been used in controlling other plastic manufacturing processes such as injection molding. In [16] and [20], Dubay *et al.* and Gerber *et al.* discuss the application of MPC methods to control the temperature of the plastic melt in injection molding. Controlling the actuators of the process, which are the screw position and the velocity on an injection molding machine, is also discussed in [23] using MPC techniques. This signifies the increasing interest and favorability towards using the MPC method in various areas of the plastic manufacturing industry.

With regards to the thermoforming process, as it was mentioned above, although significant progress has been made towards improving the performance and efficiency of the thermoforming heating phase using monolayer sheets, there has been very limited research involving the thermoforming of multilayer plastics. Multilayer plastic sheets are made of different types of plastic materials with different rheological properties, the popularity of which is ever growing in thermoforming, being especially used in vehicular components, construction products, and sanitary products [9]. It is however a complex task to form multilayer plastic sheets since for each particular layer, the forming temperature and the heating time may be different. At the moment and to the best of our knowledge, there has been no research in designing a systematic control method, which can take the type and forming temperature of each layer into account. There has however been some research conducted in numerical modeling of multilayered plastic sheets in thermoforming, in [51] and [52], yet no control method is discussed. Moreover, because of their specific numerical nature and complexity, the models and analysis presented in [51] and [52] are not suitable to be used in a control algorithm.

In this chapter however, we present a practical model of the heating phase of multilayer plastic sheets, which can easily be linearized and used in various control schemes. This model is a generalized model in the sense that it can account for any number or combination of plastic materials in a multilayer sheet. We also present a new discrete-time model predictive controller (DTMPC) to solve, for the first time, the temperature tracking problem of multilayer plastic sheets in thermoforming. This method takes all the different plastic layers along with their respective rheological properties into account and solves the tracking problem for all the layers of the multilayer plastic sheet. Apart from the novelty in its application, the new DTMPC

method is quite different from the monolayer MPC controller proposed by Chy *et al.* in [39] since it considers the complete model of the system in each step of the optimization while taking the nonlinear dynamics of heaters completely into consideration, and it is more importantly able to provide non-uniform temperature profile tracking. These abovementioned differences are further discussed in the subsequent sections.

The organization of this chapter is as follows: In the first part, the modeling of the heating phase of a multilayer plastic sheet in thermoforming is discussed. The design and implementation of the DTMPC method to solve the temperature-tracking problem is the subject of the subsequent sections. Finally, the controller's performance and efficiency is tested on an industrial thermoforming machine simulator, which includes all the nonlinear dynamics and geometrical attributes of the thermoforming process and is tested to be within 2°C accuracy of an actual thermoforming machine [34]. Finally, the tracking performance and the energy efficiency of the proposed control method are compared to classical PI controllers to show the superiority of the new method to potential alternatives. It is to be noted that energy efficiency analysis is being conducted for the first time in thermoforming.

4.3 Modeling of the Heating Phase of Thermoforming in the Presence of Multilayer Plastic Sheets

Before introducing the heating phase model of multilayer plastic sheets, the existing block diagram of the heating phase, introduced by Modirnia *et al.* in [95], is discussed since it will be the studied block diagram in this chapter, as well. The block diagram of this control system is shown in Fig. 4.1, where the set-points are defined as the desired sheet temperature profile, or in other words, the desired temperature of the measurement zones on the plastic sheet (discussed later in this section). In this setup, heaters are treated as actuators, and the heating phase of the plastic sheet is considered as the plant. For cost reasons, there are two types of sensors measuring and feeding the surface temperatures back to the control side: real IR and model-based virtual sensors (MBVSs). The real IR sensors are placed in the thermoforming machine, measuring the surface temperature of the sheet during the actual heating process, while the MBVSs use the model of the heating phase in thermoforming, developed in this section, to actively estimate the surface temperature, in parallel with the actual process taking place. In Fig. 4.1, this operation is being performed in the “heating phase model” block, where all the complex

heat transfer equations developed in this chapter, are dynamically present. Therefore, we consider the zone on the plastic sheet over which each of the real or virtual sensors directly point to as a sensor measurement zone, thus having two sets of inputs: real sensor and virtual sensor set-points.

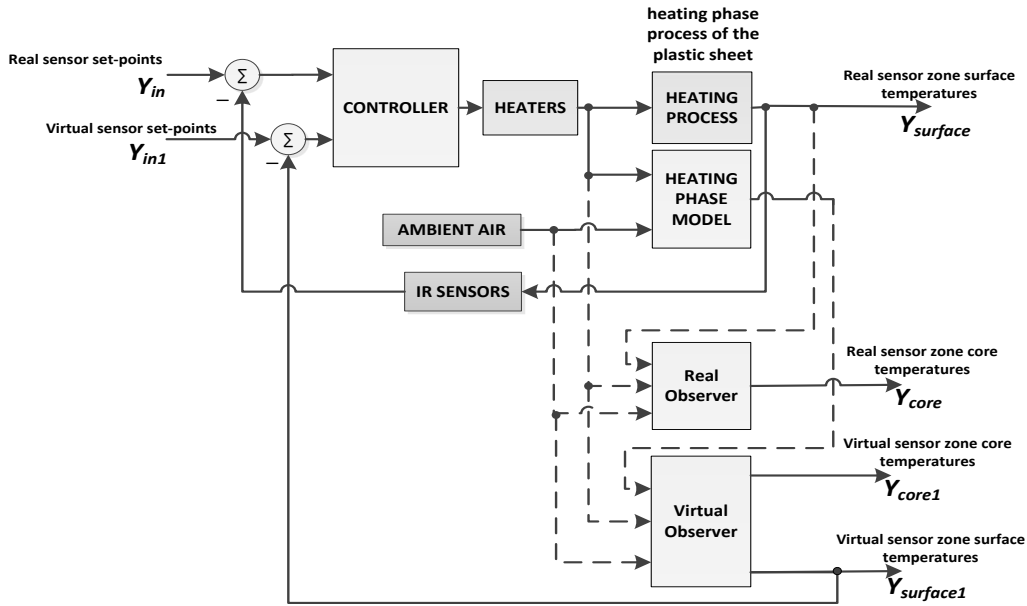


Figure 4.1. Block diagram of the closed-loop system

The thermoforming machine consists of $2H$ heaters, i.e., H on top and H on the bottom, and plastic sheet is placed in-between with an equal distance between the top and bottom sets of heaters. There are also a total of $2S$ (real and virtual) sensors, with S sensors placed on top, and S placed on the bottom. It is important to note that the top and bottom heaters and the sensors are respectively placed to be directly facing each other in the oven. The sensors read the surface temperature of the plastic sheet. The plastic sheet is divided into $2S$ measurement zones, each zone corresponding to the area around which a sensor is pointing. The thickness of the plastic sheet is divided into L equally spaced layers with a corresponding node for each layer.

In this section, the heating phase model of a multilayer plastic sheet is discussed. This model is based on the ideas used in developing the heating phase of the monolayer sheet, which was developed by several researchers, the most recent of which being presented in [34] and [35]. The model has also been further developed by Thomson *et al.* in [36] and by Khan *et al.* in [37],

where the effects of temperature dependent properties, sheet color, and other operating conditions have been experimentally investigated.

The monolayer heat transfer model has proven to be (on average) within 2% accuracy of the actual process, signifying its accuracy and reliability [34]. As it can be seen in [34] and [35], the model takes all the methods of heat transfer acting on the sheet into account and produces practical dynamical equations to be used in a state-space setup. Therefore, the foundation of the model used in [34] and [35] is utilized to develop a multilayer heat transfer model. As it was mentioned before, the multilayer models introduced in [51] and [52] are numerically developed for a special type of plastic, which are not suitable to use in a control scheme.

In the multilayer heating phase model, it is determined that there are three methods by which heat is transferred to a plastic sheet: radiation, conduction, and convection. Analysis also determined that within the sheet, heat transfer only occurs vertically, between the layers of the plastic, and that there is no energy interaction between adjacent measurement zones. This will be discussed in the next subsection.

Radiation occurs between the heaters and the surface layers and is also transmitted through the internal layers. This has been established by Thomson *et al.* in [36] and Khan *et al.* in [37], where the importance of radiation absorption coefficients for the internal layers of the plastic sheet was empirically demonstrated, particularly when the sheet color is not black. Therefore, since multilayer plastic sheets can be made of different combinations of plastic materials, we will consider radiation transmission for interior layers in order to avoid loss of generality. Conduction occurs between all the layers of the plastic sheet. However, Convection only occurs between the air in-between the heaters and the surface layers.

Realistically, for a multilayer plastic sheet, there could be many different combinations of plastic materials, but the heat transfer methods and the basic principles of the model remain unchanged. In this work, a multilayer plastic sheet with two different plastic types is studied. The sheet in study is made of layers of ABS (Acrylonitrile butadiene styrene) and acrylic, used actively in the automotive industry, with a thickness of 7.5mm, shown in Fig. 4.2 [9]. The acrylic layer is used as a cap layer with a thickness of 1.5mm, and the rest of the sheet is composed of ABS material that is 6mm thick. In order to obtain an exact temperature measurement from the entire depth of this sheet, we divide the sheet into five layers ($L=5$), i.e., one acrylic layer and four ABS layers, each being 1.5mm thick, as shown in Fig. 4.2. In the model's equations, the top

surface temperature of the n th measurement zone (the acrylic layer) is shown as $T_{n,1}$, and the temperature of the four ABS layers are represented by $T_{n,2}$, $T_{n,3}$, $T_{n,4}$, and $T_{n,5}$, respectively, where $T_{n,5}$ is the bottom surface temperature of the plastic sheet. On the same note, the thickness of the top surface acrylic layer is denoted as l_1 , and the thickness of the four ABS layers, the fourth layer being the bottom surface layer, are represented by l_2 , l_3 , l_4 , and l_5 , respectively. It has to be noted that the four layers of the ABS material have been fictitiously defined in order to obtain accurate temperature estimates from the entire depth of the ABS layer.

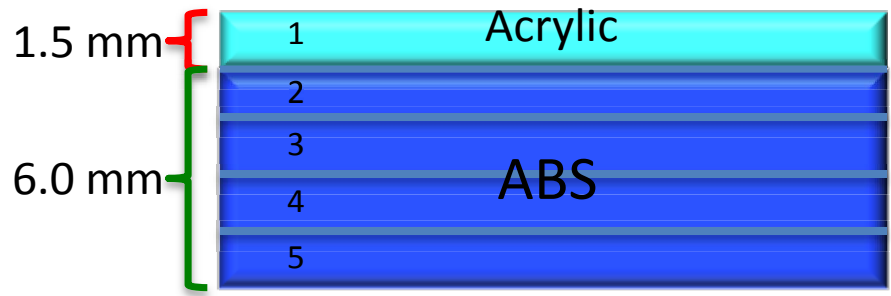


Figure 4.2. The multilayer plastic sheet composed of acrylic and ABS layers

In terms of radiation absorption, the fraction of the radiant energy absorbed by the acrylic layer is presented as

$$\beta_1 := \beta(l_1) = 1 - e^{-A_{av_1} l_1},$$

where A_{av_1} represents the average absorptivity of the acrylic material across its spectrum, the value for which can be found in [119]. In [119], The (Fourier transform infrared spectroscopy) FTIR spectroscopy of the acrylic suggests that within the wavelength over which the heaters are operational, i.e. $2-4 \mu\text{m}$, the percentage transmittance is 70%, resulting in an average absorptivity of $A_{av_1} = 300 \text{ m}^{-1}$ and $\beta_1 = 0.37$.

With regards to the ABS layer, since the thickness of the four layers are set to be equal at $l_2 = l_3 = l_4 = l_5$, the fractions of the absorbed radiant energy will also be equal for all these layers, meaning that

$$\beta_2 := \beta(l_2) = \beta(l_3) = \beta(l_4) = \beta(l_5) = 1 - e^{-A_{av_2} l_2},$$

where A_{av_2} represents the average absorptivity of the ABS material across its spectrum, the value for which can be found in [118]. In [118], The FTIR spectroscopy of the ABS suggests that within the wavelength over which the heaters will be operational, i.e. 2–4 μm , the percentage transmittance is 70%, resulting in an average absorptivity of $A_{av_2} = 300 \text{ m}^{-1}$ and $\beta_2 = 0.37$.

The heat equation for the top-surface node is:

$$\frac{dT_{n,1}}{dt} = \frac{1}{\rho_1 V C_{p1}} \times \left\{ \frac{A}{\left[\frac{l_1}{k_1} + \frac{l_2}{k_2} \right]} \left\{ T_{n,2} - T_{n,1} \right\} + h \left\{ T_{\infty, \text{top}} - T_{n,1} \right\} + \beta_1 Q_{RT_n} + \beta_1 (1 - \beta_2)^4 Q_{RB_n} \right\} \quad (1)$$

where Q_{RT_n} is the total radiant energy from the top heaters affecting n th measurement zone and is presented as,

$$Q_{RT_n} = \sigma \epsilon_{\text{eff}} A_h \sum_{j=1}^H F_{nj} \left\{ \theta_j^4 - T_{n,1}^4 \right\}, \quad (2)$$

and where Q_{RB_n} is the total radiant energy from the bottom heaters affecting the n th measurement zone and is defined in (7). ρ_1 is the density of acrylic, C_{p1} is the specific heat capacity of acrylic, k_1 is the heat conduction constant of acrylic, k_2 is the heat conduction constant of ABS, A is the area of the measurement zone, V is the volume of the layer, h his the convection coefficient, $T_{\infty, \text{top}}$ is the ambient air temperature trapped between the top placed heaters and the top surface of the plastic sheet, σ is the Stefan Boltzmann constant, ϵ_{eff} is the effective emissivity, A_H is the area of the heater bank, F_{nj} is the view factor between the j th heater bank and the n th measurement zone, θ_j is the j th heater bank temperature.

It should be noted that in (1), the first term corresponds to conduction between the acrylic and the ABS layer, the second term corresponds to convection, the third and fourth terms correspond to radiation.

The heat equation of the first ABS layer in direct contact with the acrylic surface is presented as,

$$\frac{dT_{n,2}}{dt} = \frac{1}{\rho_2 V C_{p_2}} \times \left\{ \frac{A}{\left[\frac{l_1}{k_1} + \frac{l_2}{k_2} \right]} \{ T_{n,1} - T_{n,2} \} + \frac{k_2 A}{l_2} \{ T_{n,3} - T_{n,2} \} + \beta_2 (1 - \beta_1) Q_{RT_n} + \beta_2 (1 - \beta_2)^3 Q_{RB_n} \right\} \quad (3)$$

where ρ_2 is the density of ABS, and C_{p_2} is the specific heat capacity of ABS. In (3), the first term relates to conduction between the surface acrylic layer and the first ABS layer, the second term relates to conduction between the first and second ABS layers, while the third and fourth terms represent transmitted radiation from the top heaters and bottom heaters.

The heat equations of the interior layers of the same ABS material is presented as,

$$\frac{dT_{n,3}}{dt} = \frac{1}{\rho_2 V C_{p_2}} \times \left\{ \frac{k_2 A}{l_3} \{ T_{n,2} - 2T_{n,3} + T_{n,4} \} + \beta_2 (1 - \beta_1)(1 - \beta_2) Q_{RT_n} + \beta_2 (1 - \beta_2)^2 Q_{RB_n} \right\} \quad (4)$$

$$\frac{dT_{n,4}}{dt} = \frac{1}{\rho_2 V C_{p_2}} \times \left\{ \frac{k_2 A}{l_4} \{ T_{n,3} - 2T_{n,4} + T_{n,5} \} + \beta_2 (1 - \beta_1)(1 - \beta_2)^2 Q_{RT_n} + \beta_2 (1 - \beta_2) Q_{RB_n} \right\} \quad (5)$$

Finally, the bottom surface equation of the ABS layer is shown as,

$$\frac{dT_{n,5}}{dt} = \frac{1}{\rho_2 V C_{p_2}} \times \left\{ \frac{k_2 A}{l_5} \{ T_{n,4} - T_{n,5} \} + h \{ T_{\infty,bot} - T_{n,5} \} + \beta_2 (1 - \beta_1)(1 - \beta_2)^3 Q_{RT_n} + \beta_2 Q_{RB_n} \right\} \quad (6)$$

where $T_{\infty,bot}$ is the ambient air temperature trapped between the bottom placed heaters and the bottom surface of the plastic sheet, and Q_{RB_n} is the total radiant energy from the bottom heaters affecting the n th measurement zone

$$Q_{RB_n} = \sigma \varepsilon_{eff} A_h \sum_{j=H+1}^{2H} F_{nj} \{ \theta_j^4 - T_{n,5}^4 \}. \quad (7)$$

In order to form a linear state-space model, the above equations will be linearized. Also, since the goal is to use the model in the design process of the DTMPC, it is desired to only use the heaters' temperature as inputs in the state-space model, indicating that the top and bottom ambient air temperatures should be treated as states. Therefore, the heat equations for the top and bottom ambient air is developed as,

$$\frac{dT_{\infty,top}}{dt} = \frac{2\sigma}{\rho_{air} C_{p,air} \Delta z} \times \left\{ \varepsilon (\theta_{av,top}^4 - T_{\infty,top}^4) + \varepsilon_1 (T_{av,top}^4 - T_{\infty,top}^4) \right\}, \quad (8)$$

$$\frac{dT_{\infty,bot}}{dt} = \frac{2\sigma}{\rho_{air} C_{p,air} \Delta z} \times \left\{ \varepsilon (\theta_{av,bot}^4 - T_{\infty,bot}^4) + \varepsilon_1 (T_{av,bot}^4 - T_{\infty,bot}^4) \right\}, \quad (9)$$

where ρ_{air} is the air density, $C_{p,air}$ is the specific heat capacity of air, Δz is the distance between the heaters and the plastic sheet where the ambient air lies, ε is the effective emissivity that combines the emissivity of air and ceramic heaters, and ε_1 is the effective emissivity that combines the emissivity of air and the plastic sheet. Also, $\theta_{av,top}$, $\theta_{av,bot}$, $T_{av,top}$, and $T_{av,bot}$ are defined as,

$$\begin{aligned} \theta_{av,top} &= \frac{\theta_{1,top} + \theta_{2,top} + \dots + \theta_{H,top}}{H} \\ \theta_{av,bot} &= \frac{\theta_{1,bot} + \theta_{2,bot} + \dots + \theta_{H,bot}}{H} \\ T_{av,top} &= \frac{T_{1,1} + T_{2,1} + \dots + T_{S,1}}{S} \\ T_{av,bot} &= \frac{T_{1,5} + T_{2,5} + \dots + T_{S,5}}{S} \end{aligned}, \quad (10)$$

where $\theta_{1,top}, \theta_{2,top}, \dots, \theta_{H,top}$ are the top heaters' temperatures, $\theta_{1,bot}, \theta_{2,bot}, \dots, \theta_{H,bot}$ are the bottom heaters' temperatures while H is the number of heaters on top or bottom of the sheet. Also, $T_{1,1}, T_{2,1}, \dots, T_{S,1}$ are the top surface temperatures of the measurement zones, $T_{1,5}, T_{2,5}, \dots, T_{S,5}$ are the bottom surface temperatures of the measurement zones while S is the number of the

measurement zones on top or bottom of the sheet. Therefore $\theta_{av,top}$ and $\theta_{av,bot}$ are respectively the average of temperatures of the top and bottom heaters, and $T_{av,top}$ and $T_{av,bot}$ are the average top and bottom surface temperatures of the multilayer plastic sheet, respectively.

In (8) and (9), the first term of each equation corresponds to radiation between the heaters and the ambient air while the second term reflects the radiation between the ambient air and the plastic sheet.

4.3.1 Horizontal Conduction

In this part, the reason for which horizontal conduction is not incorporated into the model is explained. Consider two measurement zones, which are adjacent as shown in Fig. 4.3, each consisting of two layers. The heat transfer equation for the surface layer of the first measurement zone, when adding horizontal conduction as a heating method, is

$$\frac{dT_{1,1}}{dt} = \frac{1}{\rho VC_p} \times \left\{ \frac{kA_1}{l} \{T_{1,1} - T_{1,2}\} + \frac{kA_2}{d} \{T_{1,1} - T_{2,1}\} + Q_{ambient} + Q_{heater} \right\}, \quad (11)$$

where $V = A_1 \cdot l$, $A_1 = d \cdot d$, $A_2 = d \cdot l$, $Q_{ambient}$ is the convection heat, and Q_{heater} is the radiation heat. In this analysis, the convection and radiation terms are irrelevant since cross conduction with adjacent layers does not influence their values. Examining (11), it can be deduced that the first two terms are the determining factors on the importance of cross conduction. Substituting V , A_1 , and A_2 into (11), we get the following for the vertical conduction term:

$$\frac{k}{\rho C_p l^2} \{T_{1,1} - T_{2,1}\}, \quad (12)$$

and the following for the horizontal conduction term:

$$\frac{k}{\rho C_p d^2} \{T_{1,1} - T_{2,1}\}, \quad (13)$$

Examining (12) and (13), it can be deduced that the horizontal conduction coefficient is highly dependent on the space between measurement zones. Thus, as this space is typically between 20cm to 40cm in a realistic thermoforming configuration, the coefficient corresponding

to the horizontal conduction term becomes too small compared to the vertical conduction term, where the depth of the plastic sheet in thick-gauge thermoforming is 1cm at its maximum. In other words,

$$\frac{1}{l^2} \gg \frac{1}{d^2} .$$

Therefore, in this type of model, the effect of horizontal conduction is negligible compared to vertical conduction; consequently this term can be dropped from the model equations.

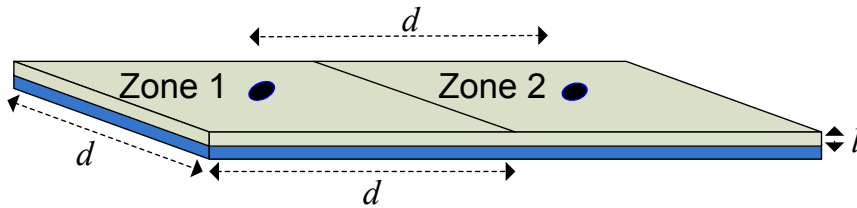


Figure 4.3. A two-layer, two-zone plastic sheet

4.4 Model Predictive Control: an Overview

Model Predictive Control (MPC) is one of the most widely used controllers in the process control industry. MPC uses the dynamical model of the system to predict the output of the system over a certain horizon, called the prediction horizon, and produces a control effort minimizing the error between the predicted output and the set-point. The capability of routinely dealing with operational constraints, as well as the straightforwardness of the concept behind has rendered MPC as a versatile and favoured control technique among control system design engineers, next to PID. MPC is able to consider saturation limits of actuators involved in a control system. It can also take into account the maximum rate at which an actuator can respond to a change in the drive signal, and that there exists no instantaneous change of position, temperature, current, etc. Furthermore, there are circumstances under which the output of a control system should always stay within a predefined range disregarding how satisfactory or unsatisfactory performance of the control system is [97]. Therefore, MPC is capable of systematic handling of operational constraints existing on: a) *Amplitude of the control signals*, b) *Rate of change of the control signals*, and c) *System's output/state variables*, and generating a

control signal that drives the plant towards the desired status while being cautious with constraints prevalent in that control system.

In this chapter, the focus is on discrete-time model-predictive controllers (DTMPC), which are used for tracking problems, and a brief presentation is given. For a more detailed description of this control scheme, the reader can refer to [97] and [98].

Assuming that the process is dynamically modeled as a state-space representation and described by:

$$\begin{aligned} x_m(k+1) &= A_m x_m(k) + B_m u(k) \\ y(k) &= C_m x_m(k) \end{aligned}, \quad (14)$$

where $u \in \mathbb{R}^p$ is the control signal or input variable, $y \in \mathbb{R}^q$ is the process output, $x_m \in \mathbb{R}^n$ is the state variable vector with assumed dimension n , and the subscript m is used to represent the plant model.

To meet the offset-free tracking requirement, it is desired to rewrite the state-space equations in the form of difference state-variables. The model has also been rewritten so that an integral action is embedded into the structure of the model in order to achieve the design purpose of offset-free tracking. Taking a difference operation on both sides of (14) yields:

$$\begin{aligned} x_m(k+1) - x_m(k) &= A_m (x_m(k) - x_m(k-1)) \\ &\quad + B_m (u(k) - u(k-1)) \end{aligned}. \quad (15)$$

Also by denoting the difference of the state variable and the control variable by:

$$\begin{aligned} \Delta x_m(k) &= x_m(k) - x_m(k-1) \\ \Delta u_m(k) &= u(k) - u(k-1) \end{aligned}, \quad (16)$$

respectively, as the increments of the variables $x_m(k)$ and $u(k)$, the finite difference representation of the state-space equation is given by:

$$\Delta x_m(k+1) = A_m \Delta x_m(k) - B_m \Delta u(k), \quad (17)$$

where the input to the state-space model is $\Delta u(k)$. The next step is to connect $\Delta x_m(k)$ to the output $y(k)$. To this end, a new state variable vector is introduced as:

$$x(k) = \begin{bmatrix} \Delta x_m(k) \\ y(k) \end{bmatrix}^T.$$

Following the same procedure as before yields:

$$\begin{aligned}
y(k+1) - y(k) &= C_m (x_m(k+1) - x_m(k)) \\
&= C_m \Delta x_m(k+1) \\
&= C_m A_m \Delta x_m(k) + C_m B_m \Delta u(k)
\end{aligned} \tag{18}$$

Putting together (16) with (18) leads to the following augmented state-space model:

$$\begin{aligned}
\begin{bmatrix} \Delta x_m(k+1) \\ y(k+1) \end{bmatrix} &= \begin{bmatrix} A_m & O_{n \times q} \\ C_m A_m & I_{q \times q} \end{bmatrix} \begin{bmatrix} \Delta x_m(k) \\ y(k) \end{bmatrix} + \begin{bmatrix} B_m \\ C_m B_m \end{bmatrix} \Delta u(k) \\
y(k) &= \begin{bmatrix} O_{1 \times n} & I_{1 \times q} \end{bmatrix} \begin{bmatrix} \Delta x_m(k) \\ y(k) \end{bmatrix}
\end{aligned} \tag{19}$$

The characteristic polynomial equation of the augmented model in (19) is:

$$C(\lambda) = \det \begin{bmatrix} \lambda I - A_m & O_m^T \\ -C_m A_m & (\lambda - 1) I_{q \times q} \end{bmatrix}, \tag{20}$$

where q is the number of outputs of the original model prior to augmentation, described in (14). Equation (20) is obtained using the property in which the determinant of a block lower triangular matrix equals the product of the determinants of the matrices on the diagonal. Obtaining the eigenvalues from (20), it is shown that the eigenvalues of the augmented model are the union of the eigenvalues of the plant model and the q eigenvalues of $\lambda = 1$. This shows that there are q integrators embedded into the augmented design model, which is indicative of how the integral action is incorporated into an MPC system [99].

Upon formation of the new state-space model, the next step is to calculate the predicted plant output as being driven by the calculated future control signal acting as the adjustable variable. Here, it is assumed that the current time is labeled k_i and the length of the optimization window is N_p number of samples. It has been assumed that at the sampling instant k_i , $k_i > 0$, the state variable vector $x(k_i)$ is available through direct measurement or estimation; this provides the current plant information necessary for prediction of future state and output trajectories. The future control trajectory is denoted by:

$$\Delta u(k_i), \Delta u(k_i + 1), \Delta u(k_i + 2), \dots, \Delta u(k_i + N_c - 1),$$

where N_c is called the control horizon, indicating the number of parameters used to build the future control trajectory. With the given information $x(k_i)$ as the current measurement of the process, the future state variables are predicted for N_p number of samples, where N_p is called the prediction horizon. The control horizon N_c is chosen to be less than (or equal to) the prediction horizon N_p .

Having computed the future control trajectory, only the first element of the trajectory will be applied as the input control signal to the plant while the rest are discarded. The entire sequence of events, which encompasses output measurement, prediction, and control trajectory computation, is then repeated on the next sampling interval.

Denoting the future state-vector by $x(k_i+l|k_i)$ which contains predicted state-variables at k_i+l with the given current plant information $x(k_i)$ provided by measurement, based on the augmented state-space model (A,B,C), the future state vectors are calculated sequentially using the set of future control parameters as:

$$\begin{aligned}
x(k_i+1|k_i) &= Ax(k_i) + B\Delta u(k_i) \\
x(k_i+2|k_i) &= Ax(k_i+1|k_i) + B\Delta u(k_i+1) \\
&= A^2x(k_i) + AB\Delta u(k_i) + B\Delta u(k_i+1) \\
&\vdots \\
x(k_i+N_p|k_i) &= A^{N_p}x(k_i) + A^{N_p-1}B\Delta u(k_i) \\
&\quad + A^{N_p-2}B\Delta u(k_i+1) + \dots \\
&\quad + A^{N_p-N_c}B\Delta u(k_i+N_c-1)
\end{aligned}$$

The predicted output variables are obtained from the predicted state variables, by substitution of corresponding state variables as:

$$\begin{aligned}
y(k_i+1|k_i) &= CAx(k_i) + CB\Delta u(k_i) \\
y(k_i+2|k_i) &= CA^2x(k_i) + CAB\Delta u(k_i) + CB\Delta u(k_i+1) \\
y(k_i+3|k_i) &= CA^3x(k_i) + CA^2B\Delta u(k_i) + CAB\Delta u(k_i+1) \\
&\quad + CB\Delta u(k_i+2) \\
&\vdots \\
y(k_i+N_p|k_i) &= CA^{N_p}x(k_i) + CA^{N_p-1}B\Delta u(k_i) \\
&\quad + CA^{N_p-2}B\Delta u(k_i+1) + \dots \\
&\quad + CA^{N_p-N_c}B\Delta u(k_i+N_c-1)
\end{aligned} \tag{21}$$

Also, by defining vectors Y and ΔU as:

$$Y = \begin{bmatrix} (k_i + 1 | k_i) \\ y(k_i + 2 | k_i) \\ y(k_i + 3 | k_i) \\ \vdots \\ y(k_i + N_p | k_i) \end{bmatrix}; \quad \Delta U = \begin{bmatrix} \Delta u(k_i) \\ \Delta u(k_i + 1) \\ \Delta u(k_i + 2) \\ \vdots \\ \Delta u(k_i + N_c - 1) \end{bmatrix},$$

(21) can be rewritten in a compact matrix form as:

$$Y = Fx(k_i) + \Phi \Delta U, \quad (22)$$

where

$$F = \begin{bmatrix} CA \\ CA_2 \\ CA^3 \\ \vdots \\ CA^{N_p} \end{bmatrix}$$

$$\Phi = \begin{bmatrix} CB & 0 & 0 & \dots & 0 \\ CAB & CB & 0 & \dots & 0 \\ CA^2B & CAB & CB & \dots & 0 \\ \vdots & \vdots & \vdots & \vdots & \vdots \\ CA^{N_p-1}B & CA^{N_p-2}B & CA^{N_p-3}B & \dots & CA^{N_p-N_c}B \end{bmatrix}.$$

Upon forming the predicted plant output and having defined a set-point signal or a desired output $r(k_i)$, the objective of the MPC at sample time k_i is to bring the predicted output as close as possible to the set-point signal. It is assumed that the set-point signal is frozen to its value at sample time k_i over the prediction horizon or the optimization window. This objective is then mathematically translated into finding a control signal vector ΔU such that a cost function containing an error indicating the discrepancy between the set-point signal and the predicted output, is minimized. That is to say:

$$\min J = (R_s - Y)^T (R_s - Y) + \Delta U^T \bar{R} \Delta U,$$

where J denotes the cost function in which the first term is linked to the objective of minimizing the discrepancy mentioned, whereas the second term refers to reducing the control effort while achieving this objective, and

$$R_s = [11\dots 1]_{(q.N_p) \times 1} \cdot r(k_i),$$

is the data vector that contains information regarding the set-point signal. Also, in this expression \bar{R} is a diagonal matrix in the form of

$$\bar{R} = r_w I_{(p.N_c) \times (p.N_c)} (r_w \geq 0),$$

where r_w is used as a tuning parameter acting on the control effort for the desired closed-loop performance. By substitution of the predicted output expressed by (22), the cost function J is expanded as:

$$J = (R_s - Fx(k_i))^T (R_s - Fx(k_i)) - 2\Delta U^T \Phi^T (R_s - Fx(k_i)) + \Delta U^T (\Phi^T \Phi + \bar{R}) \Delta U \quad (23)$$

The first term, though constant, explains how the optimal solution of the control signal is tightly linked to the set-point signal $r(k_i)$ and the state variables $x(k_i)$, which are fed back from the most recent measurements taken, leading to a closed-loop optimal control system.

Next is the consideration of operational constraints that are frequently encountered in the design of control systems. This is where MPC lends itself to the systematic handling of operational constraints. Such constraints are usually presented as linear equalities and inequalities of the control and plant variables. In practice, there are three major types of constraints frequently encountered:

- Constraints on the Control Variables Incremental Variation
- Constraints on the Amplitudes of the Control Variables
- Constraints on the Outputs or State Variables

from which the first two deal with the constraints imposed on the control variables $u(k)$, and the third deals with those on the outputs $y(k)$ or state variables $x(k)$. Having expressed operational constraints prevalent in a control system in terms of linear inequalities, it is required to relate them to the original MPC problem. To this end, the set of equalities and inequalities reflecting constraints should be parameterized using the same parameter vector ΔU appearing in the cost function in the design of MPC.

For the case of constraints on the *Control Variables Incremental Variation*, this will be expressed by two inequalities as follows:

$$\begin{aligned} -\Delta U &\leq -\Delta U^{min} \\ \Delta U &\leq \Delta U^{max} \end{aligned}$$

In the matrix form, this becomes:

$$\begin{bmatrix} -I \\ I \end{bmatrix} \Delta U \leq \begin{bmatrix} -\Delta U^{min} \\ \Delta U^{max} \end{bmatrix}.$$

Also, for the case of constraints on the *Amplitudes of the Control Variables*, since

$$\Delta u(k) = u(k) - u(k-1),$$

and the control trajectory $u(k_i)_{i=1,2,\dots,N_c-1}$ can be expressed in terms of u as:

$$\begin{aligned} \begin{bmatrix} u(k_i) \\ u(k_i+1) \\ u(k_i+2) \\ \vdots \\ u(k_i+N_c-1) \end{bmatrix} &= \begin{bmatrix} I \\ I \\ I \\ \vdots \\ I \end{bmatrix} u(k_i-1) \\ &+ \begin{bmatrix} I & 0 & 0 & \dots & 0 \\ I & I & 0 & \dots & 0 \\ I & I & I & \dots & 0 \\ \vdots & & & & \\ I & I & \dots & I & I \end{bmatrix} \begin{bmatrix} \Delta u(k_i) \\ \Delta u(k_i+1) \\ \Delta u(k_i+2) \\ \vdots \\ \Delta u(k_i+N_c-1) \end{bmatrix}. \end{aligned} \quad (24)$$

Rewriting (24) in a compact matrix form, with C_1 and C_2 corresponding to the appropriate matrices, the constraints on the *Amplitudes of the Control Variables* is imposed as:

$$\begin{aligned} -(C_1 u(k_i-1) + C_2 \Delta U) &\leq -U^{min} \\ (C_1 u(k_i-1) + C_2 \Delta U) &\leq U^{max} \end{aligned}$$

The same procedure applies to constraints on the *Outputs*, yielding:

$$\begin{aligned} -(Fx(k_i) + \Phi \Delta U) &\leq -Y^{min} \\ (Fx(k_i) + \Phi \Delta U) &\leq Y^{max} \end{aligned}$$

As the optimal solution will be obtained using quadratic programming, the constraints needed to be decomposed into two parts to indicate the lower limit and the upper limit with opposite signs. Finally, in the presence of hard constraints, the MPC controller is proposed as finding the parameter vector ΔU that minimizes:

$$\begin{aligned}
J = & (R_s - Fx(k_i))^T (R_s - Fx(k_i)) \\
& -2\Delta U^T \Phi^T (R_s - Fx(k_i)) + \Delta U^T (\Phi^T \Phi + \bar{R}) \Delta U \quad ,
\end{aligned} \tag{25}$$

subject to the inequality constraints:

$$\begin{bmatrix} M_1 \\ M_2 \\ M_3 \end{bmatrix} \Delta U \leq \begin{bmatrix} N_1 \\ N_2 \\ N_3 \end{bmatrix} \tag{26}$$

where the data matrices are:

$$\begin{aligned}
M_1 &= \begin{bmatrix} -C_2 \\ C_2 \end{bmatrix}; & N_1 &= \begin{bmatrix} -U^{min} + C_1 u(k_i - 1) \\ U^{max} - C_1 u(k_i - 1) \end{bmatrix}; \\
M_2 &= \begin{bmatrix} -I \\ I \end{bmatrix}; & N_2 &= \begin{bmatrix} -\Delta U^{min} \\ \Delta U^{max} \end{bmatrix}; \\
M_3 &= \begin{bmatrix} -\Phi \\ \Phi \end{bmatrix}; & N_3 &= \begin{bmatrix} -Y^{min} + Fx(k_i) \\ Y^{min} - Fx(k_i) \end{bmatrix} .
\end{aligned}$$

The optimization cost, defined in (25), provides set-point tracking, as the first and second terms of (25) are indicatives of set-point tracking, as well resulting in the minimization of the energy of the control outputs as the term $\Delta U^T (\Phi^T \Phi + \bar{R}) \Delta U$ forces the minimization of the control effort.

4.5 Heating Phase Control Problem: Proposed DTMPC

Having briefly discussed the optimization performed in the DTMPC and the constraints that can be incorporated in the design of the controller, we address the problems encountered in the set-point temperature tracking of multilayer plastic sheets during the thermoforming heating-phase.

As mentioned before, because we are dealing with a multilayer plastic sheet, all the different layers should reach a precise forming temperature profile to achieve successful molding. During the forming phase, if the temperature of one of the layers is not at the precise forming temperature, particularly one of the middle layers, fractures will occur when the plastic is being molded. This results in the part failing to pass the quality-control phase in production. This is especially difficult to achieve when dealing with multilayer plastic sheets since each layer

has a different forming temperature. Therefore, one of the objectives of the new control law is controlling the temperatures of all the layers of the plastic sheet.

The second issue to be considered during the heating phase of a multilayer sheet is non-uniform or zoned control. As mentioned before, the required temperature profile of a plastic sheet is very often non-uniform across the sheet as some areas of the sheet need to be at higher or lower temperatures depending on the desired shape of the final product. Therefore, it is crucial for the DTMPC to produce control signals, which will result in precisely achieving uneven temperature profiles across the sheet. It is also important for the DTMPC algorithm to consider the entire model of the system, not just a localized part of which, in order to be able to produce those kinds of control signals.

Lastly, ceramic heaters, which are the actuators of this process, are extremely nonlinear because of two important sets of limitations. The first aspect of nonlinearity is the upper and lower saturation limits as ceramic heaters' temperatures cannot exceed 450 °C, and they indeed cannot fall below room temperature. In addition to upper and lower temperature saturation limits, there is also rate saturation limits. In other words, the rate of temperature rise and fall of the heaters varies over time according to the current temperature of the heaters, which means that the heaters' temperatures can only be increased or decreased by a limited margin at any given time. As these limitations pose significant concerns in achieving a high performance tracking solution, the nonlinear dynamics of the heaters need to be recognized by the controller and be respected as operational constraints in order to achieve success in the implementation of the developed control system.

Prior to starting the design process of the proposed DTMPC for multilayer plastic sheets, the MPC controller developed in [39] by Chy *et al.* for monolayer sheets was reviewed for potential applicability, but the following issues were encountered:

- 1) The controller is not designed for the system as a whole. In other words, for each pair of heaters, a different MPC is designed. Therefore, if there exist $2H$ heaters in the thermoforming machine, there will be H controllers. In [39], it is considered that for each zone, for which the controller is designed,, only the two closest (top and bottom) heaters are considered to have an effect on the temperature evolution of that zone, which may be an unrealistic assumption. Although it is mentioned in the study that each heater can only have its temperature varied 3°C at every sample, the collection of all the heaters which are not

being considered may play an important role in determining the temperature of each zone on the plastic sheet. Moreover, as it can be seen in Fig. 4.6, the heaters are very closely placed next to each other, making it systematically and practically difficult not to consider the effect of the adjacent heaters on each measurement zone.

- 2) The design becomes extremely machine dependent. In the design of the MPC in [39], because we are dealing with a number of MPC controllers, a weight matrix has to be designed for the controllers. This will be difficult to consider in a practical mass industrial application for different thermoforming machines since the geometry and placement of heaters is different in each brand of machine. Therefore, there needs to be manual tuning with respect to the geometry of every single machine to achieve the right type of weight matrix.
- 3) Non-uniform temperature tracking is not possible. Again, since there is a specific controller designed for each zone and due to the fact that the system is not considered as a whole, non-uniform profiles may be impossible to achieve. It might be misleading to think that since there exist multiple controllers, then designing for zoned temperature profiles becomes an easier task. However, because the controllers designed for each zone do not consider all the heater inputs affecting that particular zone, and due to the close proximity of all the heaters, it is very difficult to separate and designate different tracking set-points to each zone. This is why in [39], only uniform tracking simulations are discussed and presented.
- 4) In [39], the dynamics of the heaters are not actively varied with temperature over time. Instead, the entire operating range of the heaters is divided into different sub-ranges and different maximum heating and cooling rate constraints are incorporated. In practice, this type of approximation may result in the heaters not following the actual control command at certain instances.

Thus, having described the issues to be considered in the design of the multilayer MPC controller and the shortcomings of the monolayer controller in [39], a new DTMPC controller will be designed in the next section that will address all the above issues. In other words, a DTMPC will be designed to achieve uneven temperature tracking for all the layers of a multilayer plastic sheet while fully accounting for all the actuator nonlinearities.

Finally, The design of the DTMPC is universal, meaning that it can account for any types of multilayer plastic sheets. The only essential requirement is a heat transfer model of the plastic sheet.

4.5.1 Linear State-Space Model

First, the state-space model of the system has to be developed. This state-space model is generated from the nonlinear heat-transfer equations of a multilayer plastic sheet, developed earlier. Indeed, there is a need for linearization of the previously developed equations, first. Examining (1), (3), (4), (5), (6), (8), and (9), it can be determined that the top surface, bottom surface, top ambient, and bottom ambient heat equations are nonlinear due to the radiation terms present in these equations. The heat equations of the middle layers however remain linear since conduction is the only governing factor in these equations. Therefore, (1), (6), (8), and (9) are to be linearized around the operating point of the existing nonlinear parameters, which are indeed T , θ , and T_∞ due to their presence in the radiation terms.

The operating points are defined as follows: $T_o = 200 \text{ }^\circ\text{C}$, $\theta_o = 200 \text{ }^\circ\text{C}$, and $T_\infty_o = 200 \text{ }^\circ\text{C}$. These operating points are chosen as $\theta_o = T_\infty_o = T_o$ since it has been shown in [42] that control structures, applied to models containing this linearization condition, result in promising experimental results. Next, the nonlinear parameters are linearized using the following linear approximations:

$$\begin{aligned}
 T^4 &\approx T_o^4 - 4T_o^3(T - T_o) \\
 &\approx 4T_o^3T - 3T_o^4, \\
 \theta^4 &\approx \theta_o^4 - 4\theta_o^3(\theta - \theta_o) \\
 &\approx 4\theta_o^3\theta - 3\theta_o^4, \text{ and} \\
 T_\infty^4 &\approx T_\infty_o^4 - 4T_\infty_o^3(T_\infty - T_\infty_o) \\
 &\approx 4T_\infty_o^3T_\infty - 3T_\infty_o^4.
 \end{aligned}$$

This approximation has been shown to be accurate in the case of monolayer plastic sheets as the percentage error corresponding to the above linear approximations is less than 2% in comparison with the nonlinear model [34].

Once the nonlinear parameters in (1), (3), (4), (5), (6) are replaced by their abovementioned linear approximations, the linear state-space model of a single measurement zone is produced. Stacking the state-space model of all the measurement zones, followed by the linearized ambient-air heat equations obtained from (8) and (9), the linear state-state space model for the heating phase of the entirety of the multilayer plastic sheet is produced. This model is then sampled to get the following:

$$\begin{aligned} X_m(k+1) &= A_m X_m(k) + B_m U(k) \\ Y_m(k) &= C_m X_m(k) + D_m U(k) \end{aligned} \quad (31)$$

where $A_m \in \mathbb{R}^{(2S \times N + 2) \times (2S \times N + 2)}$, $B_m \in \mathbb{R}^{(2S \times N + 2) \times 2H}$, $C_m \in \mathbb{R}^{2S \times 2H}$, and $D = 0$.
 $X_m(k) = \begin{bmatrix} X_1 & X_2 & \cdots & X_{2S} & T_{\infty, top} & T_{\infty, bot} \end{bmatrix}^T$, in which $X_n = \begin{bmatrix} T_{n,1} & T_{n,2} & \cdots & T_{n,N} \end{bmatrix}^T$.
 $Y_n = \begin{bmatrix} Y_1 & Y_2 & \cdots & Y_{2S} \end{bmatrix}^T$, in which $Y_n = \begin{bmatrix} T_{n,1} & T_{n,2} & \cdots & T_{n,N} \end{bmatrix}^T$, and
 $u_i(k) = \begin{bmatrix} \theta_1 & \theta_2 & \cdots & \theta_{2H} \end{bmatrix}^T$.

In (31):

- The states are the temperatures of all the layers of the measurement zones, plus the two top and bottom level ambient temperatures.
- The inputs are the heater temperatures
- The outputs are the temperatures of all the layers. The temperatures of surface layers are measured by infrared and virtual sensors while the temperatures of mid-layers are measured by core-temperature estimators developed in [8].

Finally, the controllability matrix R of this system has full rank, ensuring that the overall system is controllable.

4.5.2 Incorporating the Actuator Constraints

After the state-space model is developed and identified, the next step is to incorporate the actuator constraints. As mentioned before, there are two sets of constraints in this problem:

- 1) A ceramic heater, along with all other sorts of heaters, has lower and upper temperature saturation limits, meaning that the heater's temperature cannot be lower than room

temperature and cannot be higher than a certain maximum temperature. In a typical ceramic heater, The upper and lower temperature saturation limits are:

$$\begin{aligned}\theta_{\min} &= 27 \\ \theta_{\max} &= 450\end{aligned}\quad (32)$$

The above constraint has to be transformed into a constraint in the form of (26), which is the set of constraints used to solve the DTMPC optimization problem. As mentioned before, the heater temperatures are considered as the inputs to the system, implying that $\theta(k) = u(k)$. Now, if (32) is transformed into a constraint in terms of $\Delta u(k) = u(k) - u(k-1)$, the following is achieved:

$$\begin{aligned}\Delta u(k) &> 27 - u(k-1) \\ \Delta u(k) &< 450 - u(k-1)\end{aligned}\quad (33)$$

- 2) Heating and cooling rate saturation limits. In fact, the heating and cooling rates of a heater are dynamically varying with the current temperature of the heater, over time. In the case of the ceramic heaters used in this setup, Fig. 4.4 shows the heating/cooling rate curve. This curve is achieved by setting the heaters' temperature to maximum power until saturation is reached, and subsequently shutting them off until they reach room temperature. Thus, this curve shows the maximum and minimum rates of increase and decrease in the temperature of the heaters, at each instant. After a close observation of Fig. 4.4, it was deduced that the variation in the heating and cooling rate is significant at different heater temperatures. The heating rate is decreasing as the temperature of heaters are increased (the slope of the heating curve is decreasing) whereas the cooling rate is decreasing as the temperature of the heaters are decreased (the slope of the cooling curve is decreasing). The slopes of the heating and cooling curves have been characterized by the following equations:

$$\begin{aligned}\dot{\theta}_{h_rise} &= -0.005\theta(t) + 3 \\ \dot{\theta}_{h_fall} &= -0.0018\theta(t) + 0.06\end{aligned}\quad (34)$$

which are obtained from Fig. 4.4 to determine the rate of change in the temperature of each heater with respect to the current temperature of the heater at each instant. Consequently, the dynamic heating and cooling rates depicted in (34) should be considered as the second set of

constraints. Just as in the previous set of constraints, (34) has to be discretized, transformed in the form of (26), and be presented as:

$$\begin{aligned} \Delta u(k) &< T_s (-0.005 \cdot u(k-1) + 3) \\ \Delta u(k) &> T_s (-0.0018 \cdot u(k-1) + 0.06) \end{aligned} \quad (35)$$

where T_s is the fundamental sampling period.

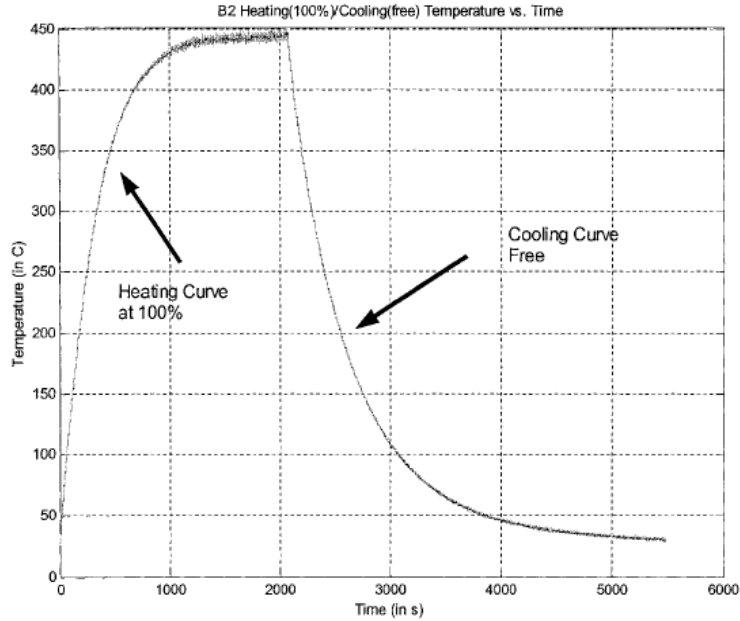


Figure 4.4. The heating and cooling curves of a ceramic heater with the heaters operating at 100% during the heating period, and turned off during the cooling period

4.5.3 Establishing the DTMPC Optimization

After the linearized and discretized state-space model is developed and presented in (31), and the abovementioned constraints are considered in the form of (33) and (35), the formulation of the DTMPC optimization presented in (25) and (26) can be completed. This optimization problem is solved using Hildreth's Quadratic Programming (QP) procedure (discussed in [97-99]), which proves to be computationally effective, and control efforts are subsequently produced.

4.6 Simulation Results

In this section, the proposed DTMPC, applied to the control setup shown in Fig. 4.1, is simulated on an industrial thermoforming machine simulator, which contains all the

nonlinearities of the actual process, along with all the specific geometric configurations. As mentioned before, this simulator is tested to be within 2°C accuracy of the actual thermoforming machine [34].

The thermoforming machine simulator contains 108 heating zones or heater banks (54 on top and 54 on the bottom), uses ceramic-type heaters, and can fit sheets with dimensions of up to 1.5mX2m. The multilayer sheet used in this simulation is the 7.5mm thick acrylic/ABS multilayer sheet, shown in Fig. 4.2, with a dimension of 1.5mX2m. In total, considering top and bottom levels, there are 20 IR sensors (10 on top and 10 below the plastic sheet) and 24 model-based virtual sensors (12 on top and 12 below the plastic sheet), creating 44 sensor measurement zones on the sheet for temperature measurement. The 2D position grid of the real IR sensors and the virtual sensors relative to the heaters is shown in Fig. 4.6, noting that the sensors placed on top and bottom of the sheet are directly facing each other, thus having similar coordinates on the grid.

This simulation is also conducted using conventional PI controllers as a measure of comparison. There are a total of 44 identical controllers used relative to the number of sensors (20 for real IR sensor zones, and 24 for virtual IR sensor zones) along with a coupling matrix as discussed in [95].

The goal of this simulation is to: 1) determine the fastest response time of the closed-loop system, and 2) to determine the least amount of energy consumed by the machine's heaters. The tracking performance and energy consumption results obtained using the DTMPC method are compared to results attained using PI controllers to determine the feasibility of the DTMPC method.

As for the input of the process, a step input is used in this simulation to facilitate the comparison of the DTMPC technique with the PI method. The criterion is to track the uneven temperature profile, shown in Fig. 4.5, while not exceeding the maximum top and bottom surface temperature set-points by more than 10°C. In this study, as shown in Fig. 4.5, the maximum top surface temperature set-point (acrylic material) is 180°C (thus should not exceed 190°C), whereas the maximum bottom surface temperature set-point (ABS material) is 170°C (thus should not exceed 180°C). This is to avoid damage to the quality of plastic as we look to prevent surface degradation. The core temperature should also follow the criterion that is set for the bottom surface temperature since it consists of the same type of material (ABS).

Finally, the simulation results are compared when all the top and bottom surface temperatures have settled to within $\pm 2\%$ of their corresponding set-points. This is used as a tracking performance measure to systematically compare the tracking performances of the two methods. We consider the system's overall settling time to be the slowest settling time of all of the measurement zones since the end of the cycle has to be marked by all of the measurement zones settling to within $\pm 2\%$ of their corresponding temperature set-points. Another reason for using the $\pm 2\%$ criteria is to be as precise as possible in simulation so that the results could also be admissible in practice.

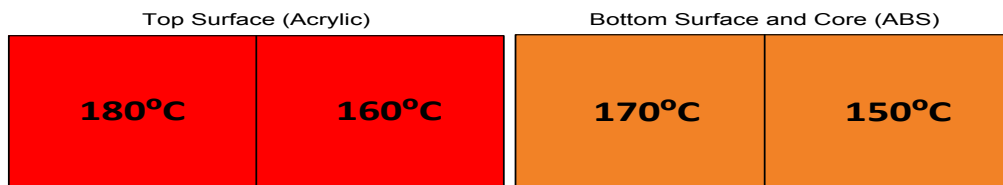


Figure 4.5. Desired zoned temperature set-points (profile)

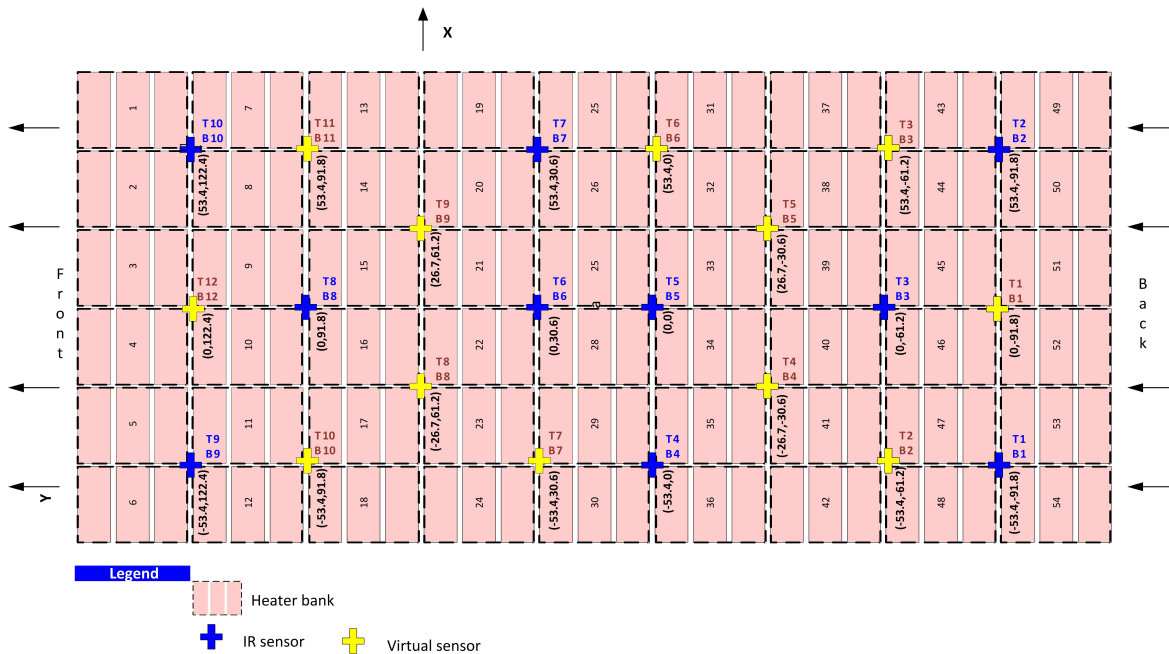


Figure 4.6. 2-D position grid of IR and virtual sensors relative to the heaters

4.6.1 Tracking Performance Simulation

In this part of the simulation process, the goal is to determine the fastest response time of the closed-loop system, in terms of the $\pm 2\%$ settling time, using the proposed DTMPC method

and the PI controllers while the above mentioned simulation criteria are in effect. Fig. 4.7 shows the step responses of the system using the PI and DTMPC methods, as Fig. 4.7 (a)-(c) show the temperature tracking responses for the 180°C and 170°C set-points at the left side of the sheet, whereas Fig. 4.7 (d)-(f) show the temperature tracking responses for the 160°C and 150°C set-points at the right side of the sheet. As we closely examine the top and bottom surface tracking responses in Fig. 4.7 (a), (b), (d), and (e), the 2% settling times of the system using the PI controllers for the 180 °C, 170 °C, 160 °C, and 150°C set-points are respectively at 580 s, 950 s, 750 s, and 1086 s, indicating that it takes a total of time 1086 s for all the top and bottom surface zones to settle within $\pm 2\%$ of the set-points. On the other hand, as we observe the top and bottom surface tracking responses in Fig. 4.7 (a), (b), (d), and (e), the 2% settling times of the system using the DTMPC algorithm for the 180°C, 170°C, 160°C, and 150°C set-points are respectively at 610 s, 520 s, 615s, and 430s, indicating that it takes a total time of 615 s for all the top and bottom surface zones to settle within 2% of the set-points. This suggests that the 2% settling time of the system will be improved by 471 s when employing the DTMPC algorithm instead of PI controllers, which is quite significant. The reason for this significant improvement can be found in two of the most important characteristics of the DTMPC algorithm: the prediction horizon and the incorporation of the heater dynamics in terms of optimization constraints. As it was shown in Section 4.4 and in (22), the algorithm comprises of a prediction horizon N_p and a control horizon N_c . If the prediction and control horizons are set to large numbers, in our case 70 for N_p and 12 for N_c , then the optimization cost in (23) will produce a more precise and efficient control effort since it is taking the future behavior of the states into account. Moreover, the optimization cost in the DTMPC will also consider the sluggish heating and cooling dynamics of the heaters in producing the control outputs. This can be well observed in Fig. 4.8 as the DTMPC does not dramatically increase the heaters' temperatures from their initial temperatures. The DTMPC is predicting that if at the beginning of the cycle, the heaters are taken to high temperatures (past 350°C for example), then later in the cycle, it will take a considerably longer amount of time to decrease the heaters temperatures to lower values, which could potentially result in an overshoot in the sheet's temperature response and could eventually result in a slower performance, which is exactly what happens when the PI controllers are controlling the system. Fig. 4.9 shows that initially, PI controllers increase the heaters temperatures to values higher than those produced by

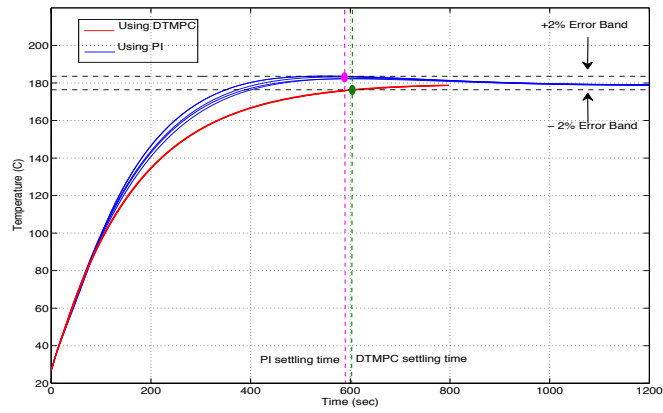
the DTMPC method, thus taking the heaters longer to reach lower values by the end of the cycle. This creates an overshoot in the temperature response of the measurement zones as shown in Fig. 4.7 and so the response cannot settle to within the 2% window in a reasonable amount of time. Therefore, we can state that the DTMPC compensates for the sluggish dynamics of the heaters, producing control efforts shown in Fig. 4.8 that are more dynamically responsive than the PI control outputs presented in Fig. 4.9.

In addition to the major improvement in the tracking performance, it can be observed in Fig. 4.7 that the tracking responses generated using the DTMPC algorithm are all rising with similar rates and time constants, without any overshoot. However, when observing the generated tracking responses using the PI controllers, we can see that the time constants of different measurement zones are quite different for the same tracking profile (see Fig. 4.7 (d) for example) while overshoot is also a factor. This shows the superiority of the DTMPC design since the control algorithm can operate within the bounds of its actuator limits, producing faster responses while forcing identical time constants and avoiding overshoots in tracking.

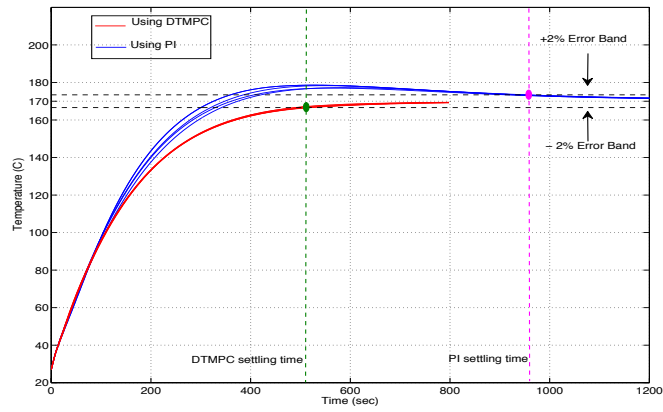
As for the core-temperature responses shown in Fig 4.7 (c) and (e), the PI control method is not able to direct the core temperatures towards a settling window of $\pm 2\%$, yet the DTMPC provides 2% settling times of 450 s and 430 s for the 170°C and 150°C core-temperature set-points, respectively. As mentioned before, the DTMPC acts on the entire state-space model of the plastic sheet in order to produce the control signals. This means that the DTMPC not only provides for surface temperature tracking, but it also systematically forces the interior states to track their respective set-points, which is a major advantage for multilayer plastic sheets. This is done by providing the required surface and interior set-points to the vector R_s in (25), regardless of the number of materials used in the multilayer plastic sheet. The DTMPC then acts on the cost function in (23) and provides control outputs to control all the states of the system. However, in the case of PI controllers, since there is only one controller tuned for each measurement zone, explicitly designed for the surface state in each zone, there is no systematic control on the interior states of the measurement zone. This becomes particularly significant when the multilayer plastic sheet is composed of multiple types of materials, i.e. for a sheet composed of six different layers, used to produce fuel tanks, it is necessary to utilize the DTMPC algorithm to provide set-point tracking for all the layers.

In addition to the response figures, Fig. 4.8 shows the control outputs generated by the DTMPC, the heaters' response, and the difference between the heaters' response and the control outputs generated by the DTMPC. Furthermore, Fig. 4.9 shows the control output generated by the PI controllers, the heaters' response of the system, and the difference between the PI generated control signals and the heaters' response. Observing and comparing Fig. 4.8(a) and Fig. 4.8(b), it can be stated that in the case of the DTMPC method, the difference between the control signal and the heater response is practically non-existent as Fig. 4.8(c) confirms this. This shows that the controller accounted for all the nonlinearities and varying dynamics of the heaters, which were presented in (33) and (35), through its optimization constraints shown in (26). The same, however, cannot be said about PI controllers as the significant difference between the control outputs and the heaters' response can be seen in Fig. 4.9(c). Therefore, this verifies our claim that the DTPMC method effectively produces control signals which take the limitations and nonlinearities of the actuators into account, and as it was shown in Fig. 4.7, this results in a much faster tracking response than other conventional control methods.

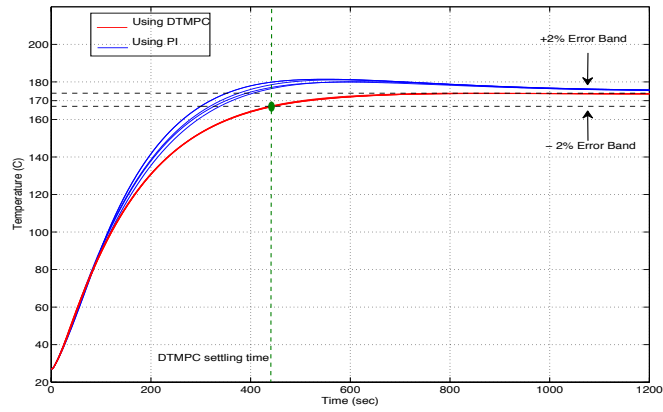
It is to be noted that the proposed DTMPC method is not compared with the MPC method proposed in [39] since the previous MPC (developed in [39]) is only limited to controlling the surface temperatures while also not being able to track uneven temperature profiles because of its particular design architecture (mentioned in Section 4.5).



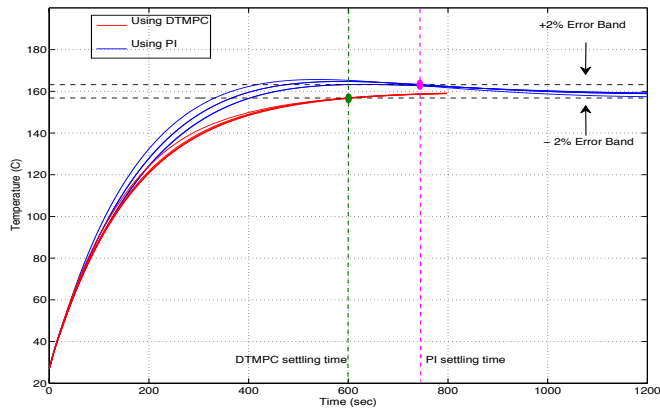
(a)



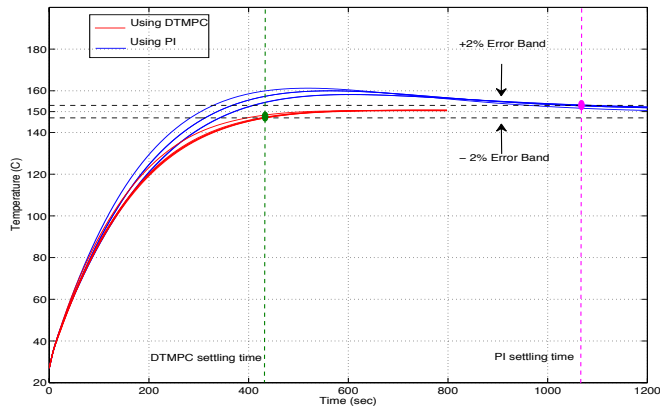
(b)



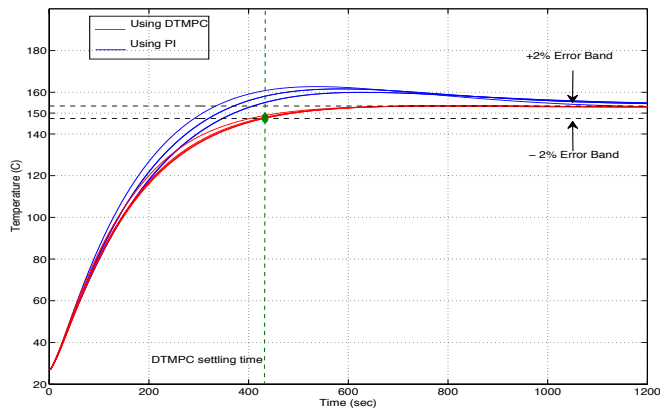
(c)



(d)

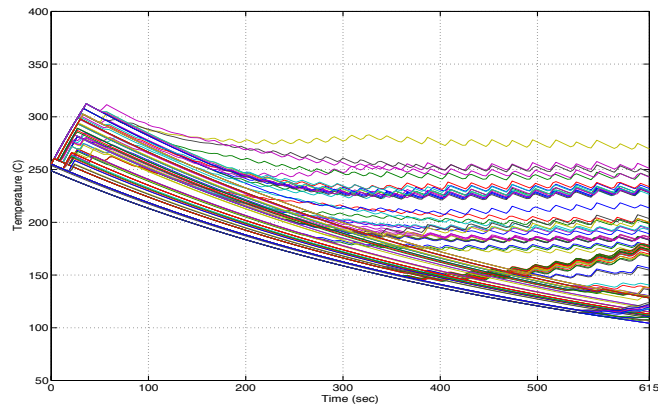


(e)

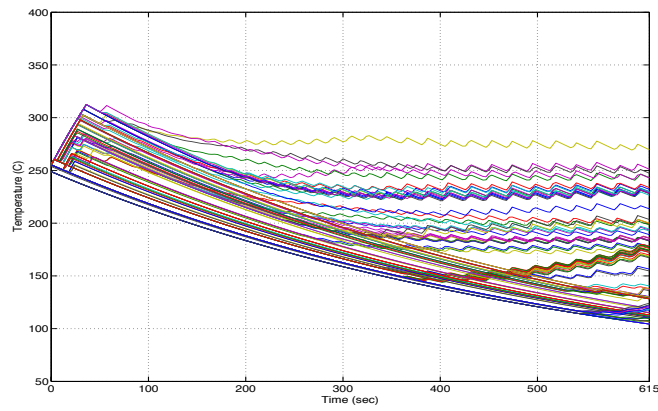


(f)

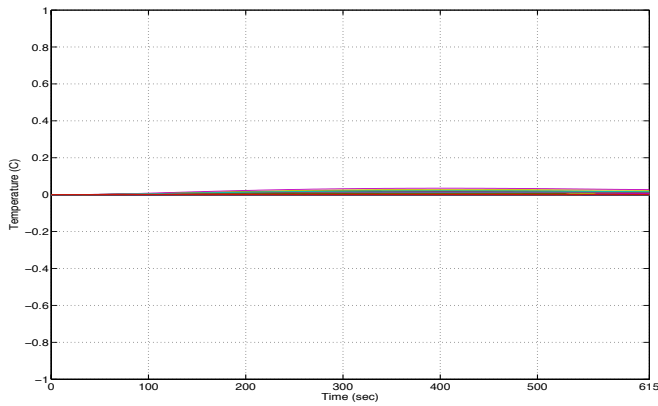
Figure 4.7. Closed-loop step response of IR and virtual measurement zones to the zoned temperature set-points using the IR (shown in blue) DTMPC (shown in red) methods: (a) left side top surface profile of 180°C, (b) left side bottom surface profile of 170°C, (c) left side core temperature profile of 170°C, (d) right side top surface profile of 160°C, (e) right side bottom surface profile of 150°C, (f) right side core temperature profile of 150°C.



(a)

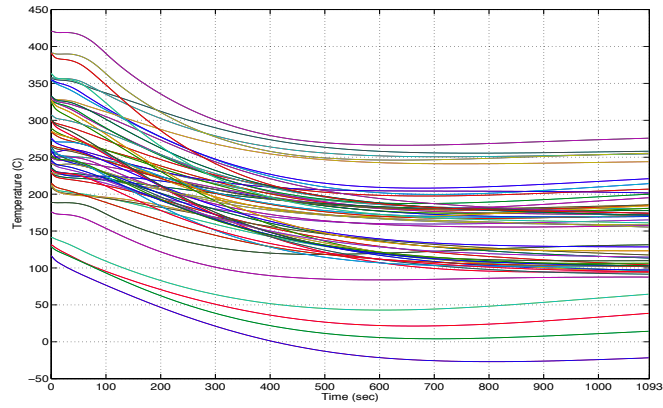


(b)

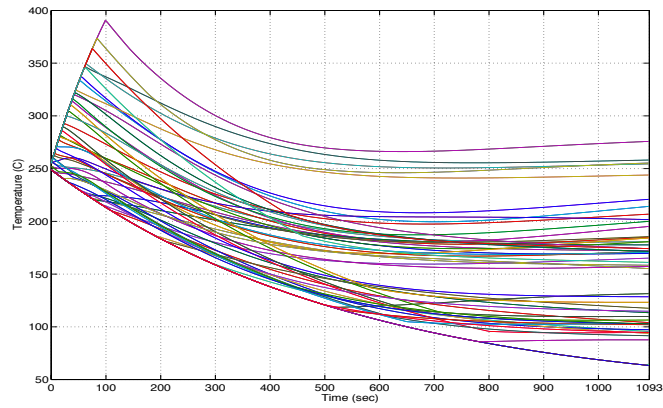


(c)

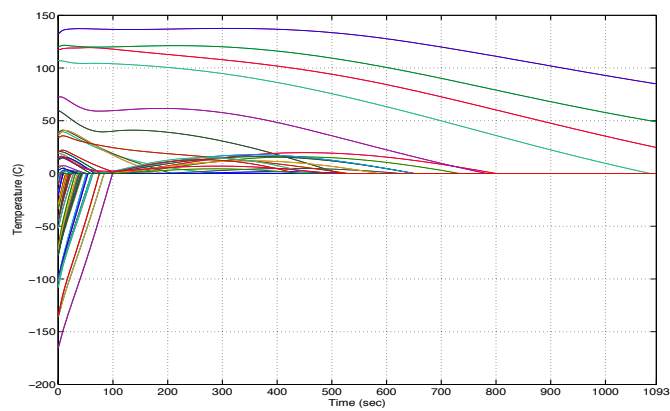
Figure 4.8. Using the DTMPC method: (a) Control output generated by the DTMPC controller. (b) The response of the heaters to the generated control output. (c) The difference between the heaters' response and the control output.



(a)



(b)



(c)

Figure 4.9. Using PI controllers: (a) Control output generated by the DTMPC controller. (b) The response of the heaters to the generated control output. (c) The difference between the heaters' response and the control output.

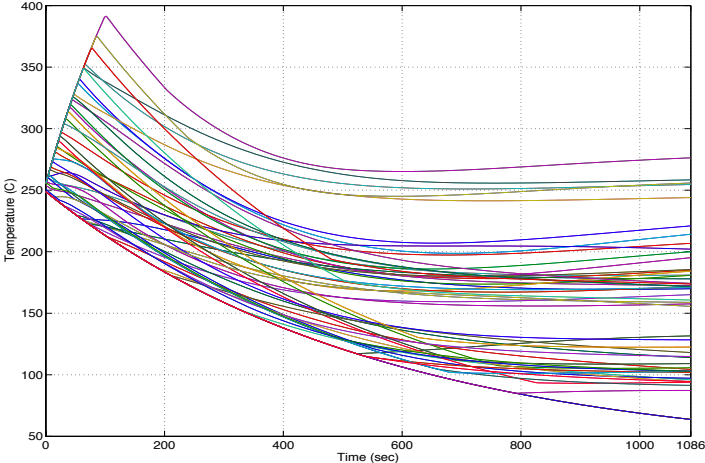
4.6.2 Energy Performance Simulation

Aside from a considerably faster tracking response, the DTMPC method also results in lower energy consumption by the heaters. Fig. 4.10 and Fig. 4.11 show the heaters' response and total power consumption using the DTMPC and PI control methods, respectively. The tuning of the controllers is identical to the performance test, with both controllers set to achieve the maximum performance in terms of achieving the fastest 2% settling time. As mentioned before, the simulation is stopped once the top and bottom surface temperatures have all settled to within $\pm 2\%$ of their corresponding set-points (shown in Fig. 4.5).

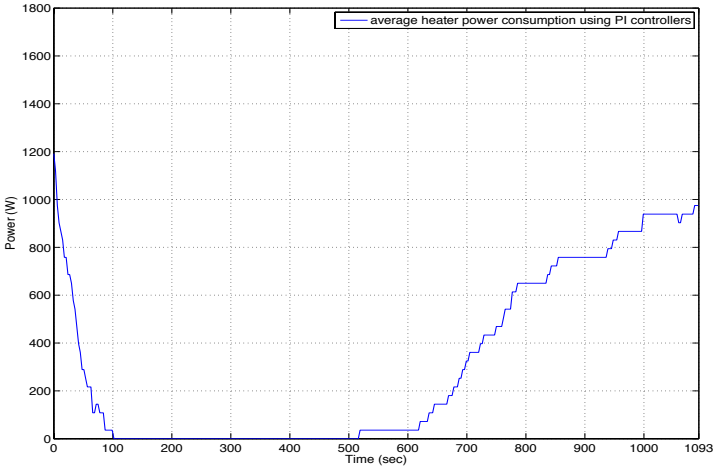
The power consumption plots shown in Fig. 4.10(b) and Fig. 4.11(b) are obtained by superposing the power consumption curves of all 108 ceramic heaters, followed by taking the average. The average energy consumption is obtained by calculating the area under both curves, which amounts to 1.62×10^5 Joules using the DTMPC method as opposed to 3.45×10^5 Joules using the PI technique. This is in fact a 55% decrease in energy consumption over a single cycle, which results in substantial energy savings for an entire batch of plastic sheets, thus increasing the economic profitability of the process. As it was shown before in Fig. 4.7, the overall settling time of the system using the PI control method is considerably slower than the DTMPC method. This is because the heaters' temperatures are raised to higher values using the PI method, subsequently taking a longer amount of time to drop to lower temperatures, thus creating overshoot and slower sheet temperature response. Fig. 4.10 (b) is also consistent with this claim, where it can be seen that the heaters are taken to high temperatures in the first 100 s, then are completely switched off for 400 s (between 100 s and 500 s), and later turned back on for 593 s to complete the cycle. This however is not the case when the DTMPC method is employed, where it can be seen in Fig. 11 (b) that because of the inclusion of the nonlinear dynamics of the heaters and the existence of the prediction and control horizons, the heaters are dynamically responsive. The heaters never seem to be in complete turn-off mode during the entire cycle as shown in Fig. 11 (b), as their temperatures are constantly being slightly varied by the DTMPC algorithm, as shown in Fig. 11 (a). These slight increments and decrements are the key to achieving a faster response as exhibited by the DTMPC method.

More importantly, the inclusion of the $\Delta U^T(\Phi^T\Phi + \bar{R})\Delta U$ term in the cost function, presented in (25), forces the minimization of the control outputs. The above term provides a

systematic reason as to why the DTMPC algorithm improves the energy performance of the system.

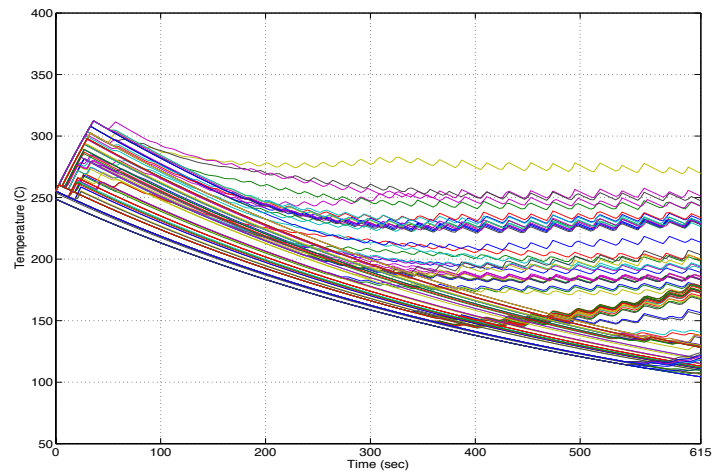


(a)

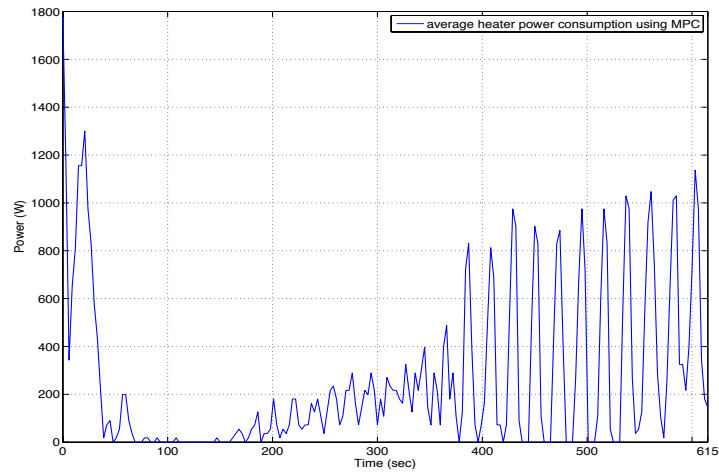


(b)

Figure 4.10. Using PI controllers: (a) the temperature response of the heaters, (b) the average power consumption of ceramic heaters.



(a)



(b)

Figure 4.11. Using the DTMPC method: (a) the temperature response of the heaters, (b) the average power consumption of ceramic heaters.

4.7 Conclusion

In this chapter, a generalized heat transfer model was developed for the heating phase of a multilayer plastic sheet in thermoforming. A DTMPC design method was then proposed for multilayer plastic sheets to solve, for the first time, the surface and core temperatures tracking problem in the presence of uneven temperature profiles. The DTMPC algorithm can be implemented for all types of multilayer plastic sheets without any type of limitation. The DTMPC method took into account the entire heat transfer model of the multilayer plastic sheet,

along with actuator nonlinearities, and successfully addressed the tracking problem. Finally, the control setup containing the DTMPC method was simulated on an industrial thermoforming machine simulator, where it was shown that the proposed method provides superior tracking performance as well as lower energy consumption compared to classical control methods.

In Chapter 5, the effects of temperature-dependent material properties of polymers in thermoforming is investigated, and a control structure is presented to solve the temperature tracking problem in the presence of temperature-varying parameters.

5 Application of Hybrid Optimal Control and Closed-Loop Hybrid Control to Manage Temperature-Dependent Material Properties in Thermoforming

Can the heating phase model be further improved by incorporating the temperature-variant material properties of plastic sheets? More importantly, can a novel method be applied to a large-scale nonlinear industrial process, namely thermoforming, to solve the temperature tracking problem of a plastic sheet under the presence of temperature-dependent material properties?

In this chapter, the inclusion of the temperature-dependent material properties in the heating phase model of plastic sheets is studied. A hybrid systems formulation of the thermoforming heating phase problem is presented to take the parameter variations of the model into account. A Hybrid Minimum Principle (HMP) based hybrid optimal algorithm (HOC) is then developed to solve the temperature tracking problem of the heating phase in the presence of temperature-varying parameters and actuator nonlinearities. This is followed by the presentation of a closed-loop hybrid controller (CLHC) to provide robustness under perturbed conditions. The HOC and the CLHC are simulated on an industrial thermoforming machine simulator to evaluate their performance and robustness. The MVBSs developed in Chapter 2 are used in the control setups presented in this chapter.

This chapter was adapted from: R. Modirnia, A. Pakniyat, and B. Boulet, " Application of Hybrid Optimal Control and Closed-Loop Hybrid Control to Manage Temperature-Dependent Parameters in Thermoforming," *IEEE Transactions on Control System Technology*, submitted and under review (Submission number: TCST-2015-1011).

➤ **Authors contributions:**

- 1) Rahi Modirnia: the author of the thesis is responsible for the implementation of the hybrid optimal controller on the thermoforming heating process. The thesis author is also responsible for developing and implementing the closed-loop

hybrid controller in the heating phase. In addition, the thesis author is responsible for the interpretation of the results. The thesis author is also responsible for writing the manuscript.

- 2) Ali Pakniyat: responsible for providing the theoretical framework of the hybrid optimal control technique. He also partially wrote the manuscript.
- 3) Benoit Boulet: supervised the work and edited the manuscript.

5.1 Abstract

In this chapter, we present a hybrid optimal control (HOC) algorithm to control the temperature of plastic sheets and to minimize power consumption in thermoforming. During the thermoforming heating phase, temperature evolution models of plastic sheets consist of nonlinear temperature dependent parameters, which have been segmented and modeled in the hybrid optimal control framework. Employing the proposed HOC algorithm based on the Hybrid Minimum Principle (HMP), which takes into account the nonlinear actuator constraints of the thermoforming process, the temperature tracking problem is solved for this parameter varying system, for the first time. Moreover, a closed-loop hybrid controller (CLHC) is developed, based on the proposed HOC, to provide robustness against perturbations. The HOC and the CLHC are then tested on an industrial thermoforming machine simulator to evaluate the tracking performance and robustness of the system. This chapter also serves as a proof of concept to show that HMP based HOC algorithms can be practically applied to large-scaled and constrained industrial processes to solve in-cycle control problems.

5.2 Introduction

Thermoforming is a type of plastic manufacturing process, in which plastic sheets are heated and formed into useful parts [89]. Thermoformed plastic parts are mainly utilized in automotive, aerospace, refrigeration, medical and packaging industries. The North American thermoforming market was valued at US\$ 13,000 million in 2007, while currently the estimated global market value stands at US\$ 30,000 million [5]. In 2012, the consumption of thermoformed products was estimated at 3.15 billion kg, and this figure is projected to increase to 3.85 billion kg by 2017 [100]. Thus, as the usage of thermoformed products increases in the upcoming years, it is important to develop more efficient and cost effective techniques for this process to ensure productivity improvement.

The thermoforming process consists of three major phases: heating, forming, and cooling. In the heating phase of this process, the plastic sheet is inserted into a thermoforming machine and is heated to a precise forming temperature, at which point the plastic sheet sags, indicating that it is ready to enter the forming phase. During the forming phase, the sheet is draped on a mold to take a certain predetermined shape, and subsequently cooled in the final phase of the process. Proper forming could only occur if the plastic sheet has reached the precise temperature

set-point (profile) at which it is flexible enough to be molded. Moreover, often, because of the complexity of the shape of the final product, uneven temperature set-points or non-uniform temperature profiles are required across the plastic sheet. Therefore, it is crucial to systematically control the heaters' temperatures so that the exact temperature profile is achieved across the plastic sheet.

In typical industrial operations, the heating phase of the process has been conducted in an open-loop process, meaning that the heaters' temperatures would be manually adjusted by the human operator throughout the heating phase, so that the plastic sheet would reach its required temperature profile. Consequently, this method is an inefficient method since it involves a heavy amount of trial and error and results in high scrap rates. Closed-loop control was introduced by Ajersch in [34], where the surface temperature of the plastic sheet was controlled using an empirical model of the heating phase and classical PI controllers. The feedback of the control loop was provided by Infrared (IR) sensors, which were placed at various locations above and below the plastic sheet.

Analysis later confirmed that the use of feedback control in thermoforming would result in productivity improvement, especially in reducing scrap rates, improving the heating phase time, reducing energy consumption, and maximizing heater life [38]. In subsequent studies, Modirnia *et al.* introduced model-based virtual sensors in order to increase the number of feedback measurements (in a cost effective manner) for a more precise control effort and to achieve non-uniform temperature profiles across the plastic sheet [95]. Core temperature observers were also developed to provide an accurate real-time prediction of the core temperature during the process, as it is invariably crucial for the core temperature of the sheet to be kept within the forming temperature range [95]. There have also been more sophisticated control efforts developed for the heating phase of monolayer (sheets consisting of only one type of plastic material) and multilayer (made of different types of plastic materials with different rheological properties) plastic sheets. These methods, which include internal-model control and model predictive control (MPC) techniques, are presented in [96] and [101], in order to improve the performance of the system, especially the heating time (tracking time).

However, all these control methods have been based on linearized temperature evolution models of the heating phase presented in [34] and [42], in which the rheological (material) properties of the plastic materials are held constant in order to represent the actual process.

Nevertheless in reality, certain material properties, most notable of which being the specific heat capacity (C_p) of the plastic sheet, are dependent on the temperature of the sheet and may vary up to 10 times their starting value [57]. In all the previous works, the value of C_p has been tuned to a single constant value in order to represent the actual process. This indeed limits the autonomy of the system, as each temperature profile requires a set of distinctively tuned values of material properties. Thus, it is desired to incorporate temperature varying material properties into the models of the heating phase to increase the autonomy, precision, and reliability of the system. In addition to the varying parameters in the model, the heaters, used as actuators in the process, have nonlinear dynamics, which cannot be neglected. Thus, a new control algorithm has to be developed to take all the abovementioned factors into account.

Control of parameter varying models has been addressed in the literature using a number of well-known methods. One of these methods is to linearize the system around several operating points and use the method of robust gain scheduling for linear parameter varying (LPV) systems, as described in [58, 60, 61, 63]. Alternatively, nonlinear model predictive control (NMPC) has been used in [64] in heat pump systems, as well as certain neural networks based hybrid controllers in wind induction generation applications [65].

In this chapter, we introduce a hybrid systems formulation of the thermoforming heating phase problem, based on linearization around several operating points with autonomous switchings associated with the change of operating points. The minimization of the power consumption of the heaters and the sheet temperature tracking cost is considered in the hybrid optimal control framework, which is gaining popularity in applied control studies as hybrid controllers have shown improvement in performance measures [68]. Examples are in the areas of automotive industry and in the aerospace industry to obtain optimal flight path trajectories [69-72].

The majority of research on the optimal control of hybrid systems is focused on the Hybrid Minimum Principle (HMP), presented for instance in [73-77], which is the generalization of the Pontryagin Minimum Principle. The results of the HMP for the hybrid system formulation in study provide the necessary conditions for the optimality of the control inputs and the optimal state trajectories. In order to solve for the optimal solutions, several HMP based algorithms have been proposed (see e.g. [76, 77, 79]). These algorithms have been applied to some unconstrained low-dimensional systems in [72, 81, 82] in order to obtain optimal state and control solutions.

However, the application of these HMP control algorithms has not yet been reported for large-scale systems with mixed state and control constraints. Therefore, a constrained HMP based hybrid optimal control (HOC) algorithm is presented in this chapter to solve the large-scale and constrained problem of temperature tracking in thermoforming. Successful application of the proposed HOC algorithm would show that such HMP based hybrid optimal controllers could actually be implemented on complex industrial processes, which are large-scaled, comprise of nonlinear constraints, and parameter variations.

The organization of this chapter is as follows: In the first section, the heating phase modeling of a monolayer plastic sheet in thermoforming is discussed, followed by the inclusion of the temperature dependent variables in the model. The design and implementation of the HOC algorithm is the subject of the subsequent sections. It should be noted that the thermoforming temperature tracking problem, which includes state-dependent parameter variations in the models, is being solved for the first time. In addition to the design of the HOC, a closed-loop hybrid controller (CLHC) is developed, based on the results obtained using the HOC algorithm, to provide robustness against perturbations. Finally, the performance, efficiency, and robustness of the HOC and the CLHC is tested on an industrial thermoforming machine simulator, which includes all the nonlinear dynamics, temperature varying properties, and geometrical attributes of the thermoforming process. This simulator was tested to be within 2°C accuracy of an actual thermoforming machine [34].

5.3 Description of the Existing Model and Block Diagram

Before introducing the heating phase model of multilayer plastic sheets, the existing block diagram of the heating phase, introduced by Modirnia *et al.* in [95], is discussed since it will be the studied block diagram in this chapter, as well. The block diagram of this control system is shown in Fig. 5.1., where the set-points are defined as the desired sheet temperature profile, or in other words, the desired temperature of the measurement zones on the plastic sheet (discussed later in this section). In this setup, heaters are treated as actuators, and the heating phase of the plastic sheet is considered as the plant. For cost reasons, there are two types of sensors measuring and feeding the surface temperatures back to the control side: real IR and model-based virtual sensors (MBVSs). The real IR sensors are placed in the thermoforming machine, measuring the surface temperature of the sheet during the actual heating process, while the MBVSs use the model of the heating phase in thermoforming, developed in this section, to

actively estimate the surface temperature, in parallel with the actual process taking place. In Fig. 5.1, this operation is being performed in the “heating phase model” block, where all the complex heat transfer equations developed in this chapter, are dynamically present. Therefore, we consider the zone on the plastic sheet over which each of the real or virtual sensors directly point to as a sensor measurement zone, thus having two sets of inputs: real sensor and virtual sensor set-points.

The thermoforming machine consists of $2H$ heaters, i.e., H on top and H on the bottom, and plastic sheet is placed in-between with an equal distance between the top and bottom sets of heaters. There are also a total of $2S$ (real and virtual) sensors, with S sensors placed on top, and S placed on the bottom. It is important to note that the top and bottom heaters and the sensors are respectively placed to be directly facing each other in the oven. The sensors read the surface temperature of the plastic sheet. The plastic sheet is divided into $2S$ measurement zones, each zone corresponding to the area around which a sensor is pointing. The thickness of the plastic sheet is divided into L equally spaced layers with a corresponding node for each layer.

5.3.1 Modeling of the Heating Phase

Several researchers have developed the heating phase model of monolayer plastic sheets, the most recent of which is presented in [34] and [35] by Ajersch and Gauthier. The model has also been further developed by Thomson *et al.* in [36] and by Khan *et al.* in [37], where the effects of temperature dependent properties, sheet color, and other operating conditions have been experimentally investigated. These investigations, which provide the essential motivation of this chapter, will be discussed in more detail in the next section.

The monolayer heat transfer model presented [34] and [35] takes the material properties of plastic sheets as constant values, but for special cases, these values have been tuned to achieve an accurate model, with only $\pm 2\%$ error with respect to the actual process. The model validation has been showcased in [34].

In the monolayer heating phase model, it is determined that there are three methods by which heat is transferred to a plastic sheet: radiation, conduction, and convection. Analysis also determined that within the sheet, heat transfer only occurs vertically, between the layers of the plastic, and that there is no energy interaction between adjacent measurement zones [101].

Radiation occurs between the heaters and the surface layers and is also transmitted through the internal layers. This has been established by Thomson *et al.* in [36] and Khan *et al.*

in [37], where the importance to include the radiation absorption coefficients for the internal layers of the plastic sheet was empirically demonstrated, particularly when the sheet color is not black. Conduction occurs between all the layers of the plastic sheet. However, Convection only occurs between the air in-between the heaters and the surface layers.

In this chapter, the plastic sheet under study is a high-density polyethylene (HDPE) sheet, which is very popular in thick-gauge thermoforming and has a thickness of 7.5mm [5]. In order to obtain an accurate temperature estimate from the entire depth of this sheet, we divide the sheet into three layers ($L=3$), for which the thickness of the top and bottom surface are half of the middle layer's thickness. In the model's equations, the top surface temperature of the n th measurement zone is shown as $T_{n,1}$, the temperature of the mid-layer is presented as $T_{n,2}$ while $T_{n,3}$ is the bottom surface temperature of the plastic sheet.

In terms of radiation absorption, the fraction of the radiant energy absorbed by the top and bottom surface layers is presented as,

$$\beta_1 := \beta(\Delta z/2) = 1 - e^{-A_{av}\Delta z/2},$$

where A_{av} represents the average absorptivity of the material across its spectrum of interest, and $\Delta z/2$ is the thickness of the top and bottom surface layers. With regards to the internal layer, the fraction of the absorbed radiant energy is presented as,

$$\beta_2 := \beta(\Delta z) = 1 - e^{-A_{av}\Delta z},$$

where Δz is the thickness of the internal layer.

Thus, the heat equation of the of the top-surface node of the n th measurement zone is

$$\frac{dT_{n,1}}{dt} = \frac{2}{\rho V C_p} \left\{ \frac{kA}{\Delta z} \{T_{n,2} - T_{n,1}\} + h \{T_\infty - T_{n,1}\} + \beta_1 Q_{RT_n} + \beta_1 (1 - \beta_1) (1 - \beta_2) Q_{RB_n} \right\}, \quad (1)$$

where Q_{RT_n} is the total radiant energy from the top heaters affecting n th measurement zone and is presented as,

$$Q_{RT_n} = \sigma \epsilon_{eff} A_h \sum_{j=1}^H F_{nj} \{ \theta_j^4 - T_{n,1}^4 \},$$

where ρ the density of the plastic sheet, C_p is the specific heat capacity of the sheet, k is the heat conduction constant, Δz is the layer thickness, A is the zone area, V is the volume of the layer, h is the convection coefficient, T_∞ is the ambient air temperature, σ is the Stefan Boltzmann constant, ε_{eff} is the effective emissivity, A_h is the area of the heater bank, F_{nj} is the view factor between the j th heater bank and the n th measurement zone, θ_j is the j th heater bank temperature.

It should be noted that in (1), the first term corresponds to conduction, the second term corresponds to convection, and the third and fourth terms correspond to radiation.

The heat equation of the internal layer is presented as,

$$\frac{dT_{n,2}}{dt} = \frac{1}{\rho V C_p} \left\{ \frac{kA}{\Delta z} \{T_{n,1} - 2T_{n,2} + T_{n,3}\} + \beta_2 (1 - \beta_1) \{Q_{RT_n} + Q_{RB_n}\} \right\}. \quad (2)$$

Finally, the heat transfer equation of the bottom surface node of the n th measurement zone is

$$\frac{dT_{n,3}}{dt} = \frac{2}{\rho V C_p} \left\{ \frac{kA}{\Delta z} \{T_{n,2} - T_{n,3}\} + h \{T_\infty - T_{n,3}\} + \beta_1 Q_{RB_n} + \beta_1 (1 - \beta_1) (1 - \beta_2) Q_{RT_n} \right\} \quad (3)$$

where Q_{RB_n} is the total radiant energy from the bottom heaters affecting the n th measurement zone shown as

$$Q_{RB_n} = \sigma \varepsilon_{eff} A_h \sum_{j=H+1}^{2H} F_{nj} \{ \theta_j^4 - T_{n,3}^4 \}.$$

In order to form a state-space model, for which the HOC can be applied, it is desired to only use the heaters' temperature as inputs in the state-space model, indicating that the ambient air temperature should be treated as a state. Therefore, the heat equation for the ambient air is developed as,

$$\frac{dT_\infty}{dt} = \frac{2\sigma}{\rho_{air} C_{p,air} \Delta d} \left\{ \varepsilon (\theta_{av}^4 - T_\infty^4) + \varepsilon_1 (T_{av}^4 - T_\infty^4) \right\} \quad (4)$$

where ρ_{air} is the air density, $C_{p,air}$ is the specific heat capacity of air, Δd is the distance between the heaters and the plastic sheet where the ambient air lies, ε is the effective emissivity

that combines the emissivity of air and ceramic heaters, and ε_1 is the effective emissivity that combines the emissivity of air and the plastic sheet. In addition, $\theta_{av}(t)$ is the average of the heaters' temperatures of all the $2H$ heaters banks, and $T_{av}(t)$ is defined as the average of the surface temperatures of all the measurement zones.

The effects of the temperature dependent material properties are investigated next.

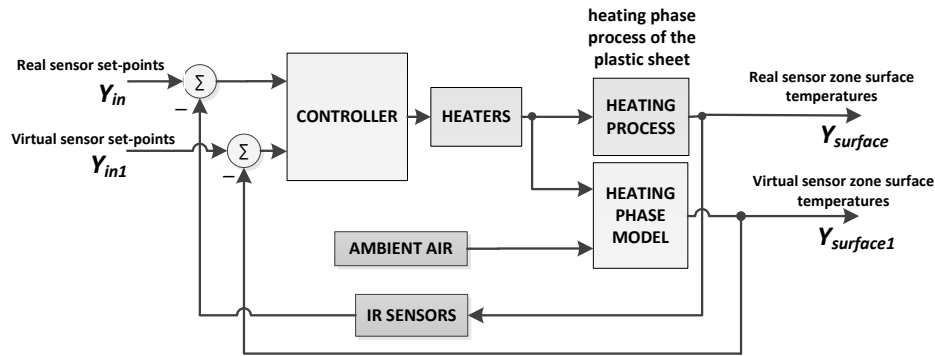


Figure 5.1. Block diagram of the closed-loop system

5.3.2 Temperature Dependent Material Properties

As mentioned before and as stated in previous studies (see [34] and [35]), the values of all the rheological properties of the plastic sheet were kept constant throughout the heating process. More specifically, in order for the models presented in (1), (2), and (3) to mimic the actual process, these values had to be carefully tuned. However, in reality, some of these material properties vary with the temperature of the plastic sheet, as described in [36], [37], and [57]. More importantly, it is recommended in [36], [37], and [57], to include these variations in the heat transfer models to achieve a more precise heating phase model. In addition to the improvement of model precision, the inclusion of temperature variant models will indeed increase the autonomy of the system since tuning the values of the material properties will no longer be necessary.

As it is analyzed in [36], [37] and [57], several rheological properties, such as the specific heat capacity (C_p), the density (ρ), and thermal conductivity (k), are temperature variant. Based on the analysis performed in [57], it has been determined that the specific heat capacity, due to its large variations, causes the largest deviation between the actual process and the model of the heating phase. In fact, the specific heat capacity of crystalline polymers, which include HDPE,

varies dramatically with the temperature of the sheet as shown in Fig. 5.2. As it is shown in [57], although other material properties are temperature-dependent, the variations in their values are overshadowed by the variation in the specific heat capacity. Therefore, in this chapter, only the specific heat capacity (C_p) will be considered as a temperature varying parameter, and the rest are kept constant.

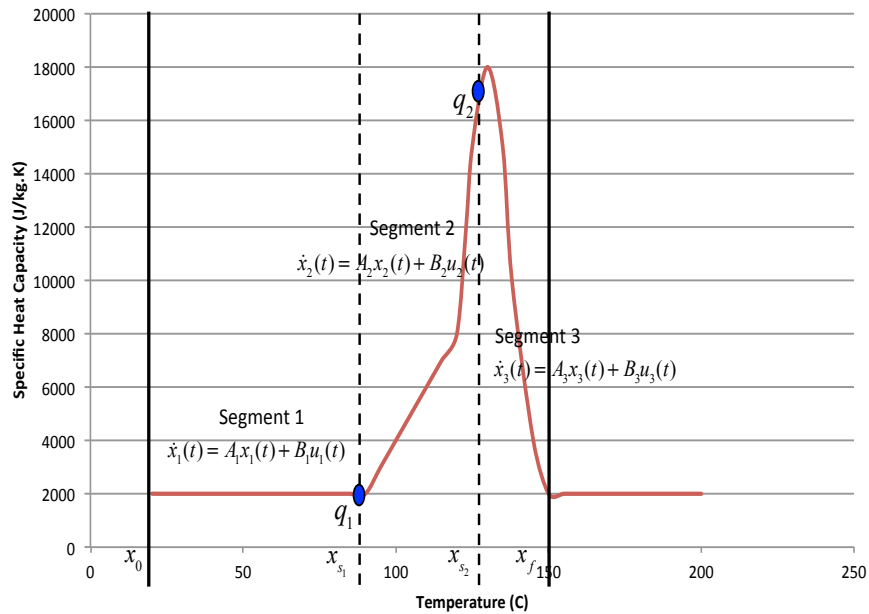


Figure 5.2. Temperature variation curve of the specific heat capacity

Observing Fig. 5.2, it can be seen that initially the specific heat capacity value is at 2000 J/(kg.K), but then this value is increased to nine times its initial value at 18000 J/(kg.K), while eventually settling back down to 2000 J/(kg.K). In case of an HDPE sheet, the forming temperature is at 150°C, and Fig. 5.2 shows the presence of the dramatically varied part of the curve in the heating phase. Therefore, if the models are not tuned properly, a significant deviation in the temperature response of the plastic sheet could manifest. Fig. 5.3 shows the temperature responses of one of the measurement zones on the plastic sheet, one with C_p held constant (blue curve) at its initial value of 2000 J/(kg.K), and the other with the variant C_p (red curve) shown in Fig. 5.2. The temperature responses in Fig. 5.3 are achieved by setting the value of the heaters to a constant temperature of 500°C in open-loop over a fixed time interval of 500 s. Fig. 5.3 shows the significant discrepancy of the two responses, indicating that if the specific heat capacity is set as a constant value of 2000 J/(kg.K) (not tuned properly), the model will

wrongly predict that the plastic sheet has actually melted (at 300°C), while in reality the surface temperature of the plastic sheet will be exactly at its forming temperature (at 150°C). Therefore, it can be concluded that C_p plays a major part in determining the temperature response of the system. Including C_p in the equations of the models, the heat transfer equations of the heating phase are presented as,

$$\frac{dT_{n,1}}{dt} = \frac{2}{\rho V(C_p(T_{n,1}))} \left\{ \frac{kA}{\Delta z} \{T_{n,2} - T_{n,1}\} + h\{T_\infty - T_{n,1}\} + \beta_1 Q_{RT_n} + \beta_1(1 - \beta_1)(1 - \beta_2) Q_{RB_n} \right\}, \quad (5)$$

$$\frac{dT_{n,2}}{dt} = \frac{2}{\rho V(C_p(T_{n,2}))} \left\{ \frac{kA}{\Delta z} \{T_{n,1} - 2T_{n,2} + T_{n,3}\} + \beta_2(1 - \beta_1) \{Q_{RT_n} + Q_{RB_n}\} \right\}, \quad (6)$$

$$\frac{dT_{n,3}}{dt} = \frac{2}{\rho V(C_p(T_{n,3}))} \left\{ \frac{kA}{\Delta z} \{T_{n,2} - T_{n,3}\} + h\{T_\infty - T_{n,3}\} + \beta_1(1 - \beta_1)(1 - \beta_2) Q_{RT_n} + \beta_1 Q_{RB_n} \right\}. \quad (7)$$

In order to increase precision of the model, the specific heat capacity of each layer of every measurement zone has been chosen to vary with the temperature of the same exact layer in that measurement zone. Also, it should be noted that the ambient air equations would not be affected by the temperature variant specific heat capacity of the plastic, thus remaining at the same exact form of (4).

The above model equations ((5), (6), and (7)), along with (4), provide the basis for the HOC design, presented in the next section.

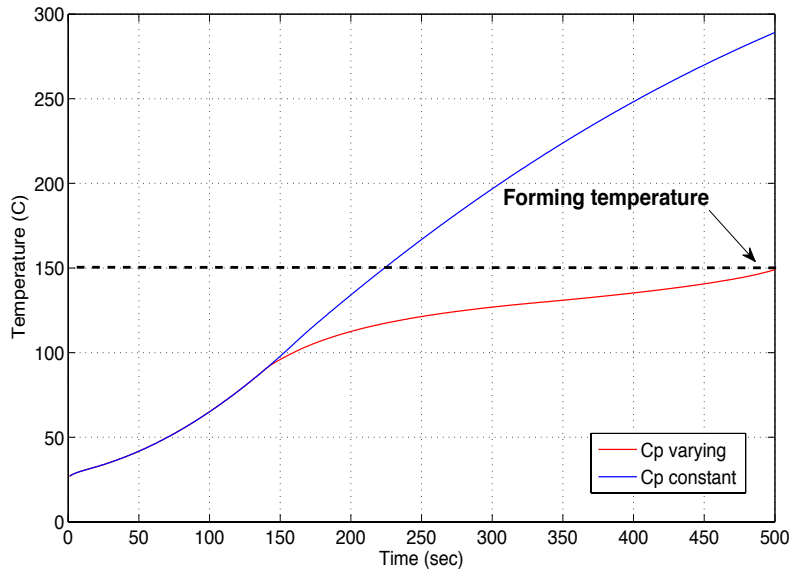


Figure 5.3. Temperature response of a measurement zone in open-loop: 1) when the specific heat capacity is kept constant, 2) when it is varying with temperature of the measurement zone. Substantial difference is observed.

5.4 HMP-Based HOC Algorithm

The consideration of the temperature dependent parameter C_p , as a piecewise constant function of the temperature, results in a hybrid systems formulation of the thermoforming process where the dynamics of the continuous states depend on a discrete state that corresponds to the present value of C_p . The generalization of the optimal control theory for systems that undergo changes in their dynamics (i.e. hybrid systems) has been the subject of a large number of studies (see e.g. [73-77, 79, 102-108]). On one hand, the generalizations of the Pontryagin Minimum Principle (PMP) result in the Hybrid Minimum Principle (HMP) [73-76, 79, 104, 107], that provides necessary conditions for the optimality of the control inputs and the corresponding trajectories of a hybrid system with a given initial conditions and a sequence of autonomous or controlled switchings. On the other hand, the generalization of Dynamic Programming for hybrid systems results in Hybrid Dynamic Programming (HDP) based upon the Principle of Optimality, which introduces the value function as the optimal cost-to-go [102, 103, 105, 108]. While the two approaches are equivalent under certain general assumptions (see e.g. [106]), the determination of optimal control from HDP requires solving a partial differential equation known as the Hamilton–Jacobi–Bellman (HJB) equation together with the corresponding boundary conditions expressed at the terminal and switching instants. On the

other hand, the HMP results in a boundary value problem on the ordinary differential equations for the state and the adjoint process, coupled by the Hamiltonian minimization condition. In this chapter, multiple autonomous switchings, as described in [76], are considered in the hybrid systems formulation of the problem, and the HMP is employed in order to determine the necessary conditions satisfied by the optimal control inputs and the corresponding optimal trajectories subject to the state and control input constraints. The HMP results are then employed to formulate the HMP based HOC algorithm.

5.4.1 The HMP with Constraints

Consider the following performance function with two switching times:

$$J(t_0, t_f, r_0, r_{s_1}, r_{s_2}, r_f; u, t_{s_1}, t_{s_2}) = \sum_{i=1}^3 E_i + \sum_{i=1}^3 \int_{t_{i-1}}^{t_i} l_i(x_i(s), u(s)) ds, \quad (8)$$

where for the discrete states $i = 1, 2, 3$, the running costs $l_i(x, u)$ are $l_i(x, u) = \frac{1}{2} u^T R_i u + \frac{1}{2} x^T Q_i x$, the endpoint costs E_i are $E_1 = \frac{1}{2} [x(t_{s_1}) - r_{s_1}]^T [x(t_{s_1}) - r_{s_1}]$, $E_2 = \frac{1}{2} [x(t_{s_2}) - r_{s_2}]^T [x(t_{s_2}) - r_{s_2}]$, and $E_3 = \frac{1}{2} [x(t_f) - r_f]^T [x(t_f) - r_f]$ for each segment. $R_i = R_i^T$ and $Q_i = Q_i^T$, subject to the system dynamics presented as $\dot{x}_i = f_i(x_i, u) = A_i x_i + B_i u$, with state and control input box constraints shown as,

$$\begin{aligned} x^L &\leq x(t) \leq x^U \\ u^L &\leq u(t) \leq u^U \end{aligned} \quad (9)$$

and the path constraints,

$$h^L \leq h(x(t), u(t), t) \leq h^U. \quad (10)$$

The initial and boundary conditions for the continuous state are $x_1(t_0) = r_0$, $x_2(t_{s_1}) = x_1(t_{s_1}^-) = r_{s_1}$, $x_3(t_{s_2}) = x_2(t_{s_2}^-) = r_{s_2}$, and $x_3(t_f) = r_f$.

The Hamiltonians are formed as

$$\begin{aligned}
H_i(x, \lambda, u) &= \lambda^T f_i(x, u) + l_i(x, u) \\
&= \lambda^T [A_i x_i + B_i u] + \frac{1}{2} u^T R_i u + \frac{1}{2} x^T Q_i x
\end{aligned} \tag{11}$$

Based on the HMP, there exists an adjoint process λ^* along an optimal trajectory x^* corresponding to the optimal control input u^* such that

$$\dot{x}^* = \frac{\partial H_{q_i}^*}{\partial \lambda} (x^*, \lambda^*, u^*) = A_i x^* + B_i u^* ,$$

subject to the boundary conditions

$$\begin{aligned}
x_1^*(t_0) &= r_0 \quad , \quad x_1^*(t_{s_1}^-) = r_{s_1} \\
x_2^*(t_{s_1}) &= r_{s_1} \quad , \quad x_2^*(t_{s_2}^-) = r_{s_2} \quad , \\
x_3^*(t_{s_2}) &= r_{s_2} \quad , \quad x_3^*(t_f) = r_f
\end{aligned}$$

and where at the switching instants t_{s_1} and t_{s_2} , the Hamiltonian continuity conditions hold, i.e.

$$\begin{aligned}
H_1(x_1^*(t_{s_1}^-), \lambda^*(t_{s_1}^-), u^*(t_{s_1}^-)) &\equiv H_1(r_{s_1}, \lambda^*(t_{s_1}), u^*(t_{s_1})) \\
&= H_2(r_{s_1}, \lambda^*(t_{s_1}^+), u^*(t_{s_1}^+)) \equiv H_2(x^*(t_{s_1}^+), \lambda^*(t_{s_1}^+), u^*(t_{s_1}^+)) \\
H_2(x_2^*(t_{s_2}^-), \lambda^*(t_{s_2}^-), u^*(t_{s_2}^-)) &\equiv H_2(r_{s_2}, \lambda^*(t_{s_2}), u^*(t_{s_2})) \\
&= H_3(r_{s_2}, \lambda^*(t_{s_2}^+), u^*(t_{s_2}^+)) \equiv H_3(x^*(t_{s_2}^+), \lambda^*(t_{s_2}^+), u^*(t_{s_2}^+))
\end{aligned}$$

Furthermore, the Hamiltonian is minimized with respect to the control input, i.e.

$$H_{q^*}^*(x^*, \lambda^*, u^*) \leq H_{q^*}^*(x^*, \lambda^*, u) ,$$

for all the admissible control inputs $u \in U$ satisfying the constraints described in (9) and (10).

This is equivalent to

$$\frac{\partial \bar{H}_{q^*}^*(x^*, \lambda^*, \mu^*, u^*)}{\partial u} = 0 , \tag{12}$$

where \bar{H} is the Lagrangian of the Hamiltonian H defined as

$$\bar{H}_i(x, \lambda, \mu, u) = H_i(x, \lambda, u) + \mu_h^T h(x, u, t) + \mu_x^T x + \mu_u^T u , \tag{13}$$

where

$$\mu_{h,j} \begin{cases} \leq 0 & \text{if } h_j(x,u,t) = h_j^L \\ = 0 & \text{if } h_j^L \leq h_j(x,u,t) \leq h_j^U \\ \geq 0 & \text{if } h_j(x,u,t) = h_j^U \\ \text{unrestricted} & \text{if } h_j^L = h_j^U \end{cases}, \quad (14)$$

$$\mu_{u,j} \begin{cases} \leq 0 & \text{if } u_j = u_j^L \\ = 0 & \text{if } u_j^L \leq u_j \leq u_j^U \\ \geq 0 & \text{if } u_j = u_j^U \\ \text{unrestricted} & \text{if } u_j^L = u_j^U \end{cases}, \quad (15)$$

and $\mu_{x,j}$ is define as in (15), where u is replaced by x .

5.4.2 HMP-Based HOC Algorithm

In order to find the optimal solution from the necessary conditions presented above, the following algorithm is developed based on the HMP algorithm proposed by Shaikh and Caines in [76], as well as Taringoo and Caines in [77].

- (0) Fix $\varepsilon > 0$ and $0 < \alpha < 1$. Set the iteration counter $m = 0$ and set the switching times at this iteration equal to the arbitrary nominal values t_1^0, t_2^0 with $t_0 < t_1^0 < t_2^0 < t_f$. Compute the optimal control inputs for the three segments, i.e. $u_1^0(t), t_0^0 = t_0 \leq t \leq t_1$; $u_2^0(t), t_1^0 \leq t \leq t_2^0$, and $u_3^0(t), t_2^0 \leq t \leq t_3^0 = t_f$, along with the corresponding trajectories $x_i(t), i = 1, 2, 3$, and associated adjoint processes $\lambda_i(t)$ for the constrained optimal control problems in the intervals $[t_{i-1}^0, t_i^0]$ with boundary state pairs $(x_i(t_{i-1}^0), x(t_i^0)) = (r_{i-1}, r_i)$.

- (1) Increment k by 1. Set

$$\begin{aligned} t_1^m &= t_1^{m-1} - \alpha_m (H_1(t_1^{m-1}) - H_2(t_1^{m-1})) \\ t_2^m &= t_2^{m-1} - \alpha_m (H_2(t_2^{m-1}) - H_3(t_2^{m-1})) \end{aligned} \quad (16)$$

- (2) Compute the optimal control inputs for the three segments as $u_1^m(t), t_0^m = t_0 \leq t \leq t_1^m$; $u_2^m(t), t_1^m \leq t \leq t_2^m$ and $u_3^m(t), t_2^m \leq t \leq t_3^m = t_f$ the corresponding trajectories $x_i(t)$ and

associated adjoint processes $\lambda_i(t)$ for the constraint optimal control problems in the intervals $[t_{i-1}^m, t_i^m]$ with boundary state pairs $(x_i(t_{i-1}^m), x(t_i^m)) = (r_{i-1}, r_i)$.

(3) If the inequality

$$\Delta H = \left| H_1(t_1^{m-1}) - H_2(t_1^{m-1}) \right| + \left| H_2(t_2^{m-1}) - H_3(t_2^{m-1}) \right| < \epsilon \quad (17)$$

is achieved, then STOP, else go to step1.

In order to solve the boundary value problem in each segment, DIDO optimal control software is used. This software solves optimal control problems based on pseudospectral theories [109-111], in which a pseudospectral discretization of constrained nonlinear optimal control problems is performed to produce optimal control signals and state trajectories. Also, the Covector mapping theorem is used to produce the Hamiltonian and adjoints for the boundary value problem [110]. The interested reader can refer to [109-111] for more information about pseudospectral methods and the DIDO optimal control software.

DIDO is an attractive method for the implementation of our problem since constraints can be conveniently defined. As far as the thermoforming heating phase is concerned, we deal with special types of actuator constraints, which will be covered in the next section. Also, since we are dealing with a high order system and a large number of control inputs, the numerical methods used in solving the optimization problem of each segment are computationally time-efficient. Finally, being provided by the Hamiltonian of each segment is extremely important as the HMP algorithm compares the Hamiltonians of the three segments.

5.5 Design of the HOC for the Heating Process

As previously stated, the control design is performed for a 7.5mm thick black HDPE plastic sheet. Although the design process can be generalized to all types of plastic sheets with different thicknesses, we specifically focus on the black HDPE sheet to showcase the design methodology in detail. Black HDPE plastics are widely used to produce parts in a variety of industries and applications, including automotive, roadside equipment, household products, and many others [120]. In the automotive domain, black HDPE plastics are widely used in producing plastic fuel tanks for cars and recreational vehicles as stated in [120] and [121], while they are also used in producing car bumpers [122].

It has been determined in [36] and [37] that black colored plastic sheets are considered to be opaque to the transmission of radiant energy, and thus all the radiant heat will be absorbed by the top and bottom surface layers, meaning that $\beta_1 = 1$ and $\beta_2 = 1$. Nevertheless, It should again be mentioned that the control algorithm is universal to all types of plastic sheets, whether radiation transmission exists or not, since the inclusion of the absorption coefficient will only change some of the elements of the state-space matrix (A) and the input matrix (B) of the system from zeros to nonzero elements, but in doing so, it does not increase the dimension or change the general structure of the system.

The design criterion is for the sheet top and bottom surface temperatures to track a uniform temperature profile (set-points) of 150°C while remaining within a $\pm 10^\circ\text{C}$ range of the set-point temperature. The temperature profile could be generalized to both uniform and non-uniform, yet we choose a uniform temperature profile to focus exclusively on the control design process rather than rheological technicalities.

The above design criteria will provide an adequate proof of concept, demonstrating that the abovementioned HOC algorithm can be applied to a large-scale industrial process with actuator nonlinearities and in-cycle parameter variations.

In this section, we tailor the HMP based HOC to our problem. In the first step, the model of the heating phase of the plastic sheet is presented in the hybrid systems framework. The goal is to divide the temperature variation curve of C_p into a number of segments and to linearize the state equations (4), (5), (6), and (7) around appropriate operating points, for each segment. The goal is to then use the HOC algorithm to switch from one segment to another as the sheet temperature is rising. Thus, in the first part of this section, we discuss the segmentation of the temperature dependent (state-dependent) material property (C_p) as follows.

5.5.1 Segmentation of the Specific heat capacity

The forming temperature of an HDPE plastic sheet is 150°C , which means all the variations of C_p within $27^\circ\text{C} \leq T \leq 150^\circ\text{C}$ have to be considered. Therefore, the idea is to divide the temperature variation curve of C_p into a number of segments, where C_p will have a constant value for each of the segments. In this chapter, we divide the variation curve into three segments as shown in Fig. 5.2. These segments are defined as follows,

1. Segment 1: $27^{\circ}\text{C} \leq T \leq 90^{\circ}\text{C}$: In this range, C_p is constant and so $C_p = 2000 \text{ J}/(\text{kg}\cdot\text{K})$ is assigned for this segment.
2. Segment 2: $90^{\circ}\text{C} < T \leq 130^{\circ}\text{C}$: For this range, we choose the midpoint temperature of this interval ($T=110^{\circ}\text{C}$) and assign its C_p value for the segment at $C_p = 6000 \text{ J}/(\text{kg}\cdot\text{K})$.
3. Segment 3: $130^{\circ}\text{C} < T \leq 150^{\circ}\text{C}$: For this range, we also choose the midpoint temperature of the interval ($T=140^{\circ}\text{C}$) and assign its C_p value for this segment at $C_p = 7000 \text{ J}/(\text{kg}\cdot\text{K})$.

After dividing the C_p curve into the abovementioned segments and assigning corresponding values for each segment, the heating equations of the system are linearized as follows.

5.5.2 Linear State-Space Model

Examining (4), (5), and (7), it is determined that the top surface, bottom surface, and ambient-air heat equations are nonlinear due to the radiation terms present in these equations. In this chapter, for the sake of computational efficiency (4), (5), and (7) will be linearized around the operating point of the existing nonlinear terms T^4 , θ^4 , and T_{∞}^4 , which appear in the radiation terms.

For each of the segments introduced in the previous subsection, which correspond to the discrete states ($i = 1, 2, 3$) of the hybrid system formulation, the following linear approximations are employed:

$$\begin{aligned}
 T^4 &\approx T_o^4 - 4T_o^3(T - T_o) = 4T_o^3T - 3T_o^4 \\
 \theta^4 &\approx \theta_o^4 - 4\theta_o^3(\theta - \theta_o) = 4\theta_o^3\theta - 3\theta_o^4 \\
 T_{\infty}^4 &\approx T_{\infty_o}^4 - 4T_{\infty_o}^3(T - T_o) = 4T_{\infty_o}^3T - 3T_{\infty_o}^4
 \end{aligned} \tag{18}$$

This approximation has been shown to be accurate in the case of monolayer plastic sheets as the percentage error corresponding to the above linear approximations is less than 2% in comparison with the nonlinear model [34].

The heat equation of the middle layer (shown in (6)) retains its linear form and is only segmented with reference to the value of C_p in each hybrid discrete state. This is due to the fact that conduction is considered as the only governing factor in this equation.

Table I presents the list of operating point for each segment, exhibiting that the values of T_o are chosen based on the segmentation intervals of $C_p(T)$, described earlier. In fact for each segment, the lower bound of T is chosen as the value of T_o . Moreover, the operating points for θ and T_∞ are chosen as $\theta_o = T_\infty = T_o$ since it has been shown in [42] that control structures, applied to models containing this linearization condition, result in promising experimental results.

Combining the linearized version of (5), (6), and (7), the linear state-space model of a single measurement zone is produced. Stacking the state-space model of all the measurement zones, followed by the linearized ambient-air heat equation obtained from (4), the linear state-space model for the heating phase of the entirety of the plastic sheet is produced as

$$\dot{x}_i(t) = A_i x_i(t) + B_i u_i(t), \quad (19)$$

where, $i = 1, 2, 3$ are considered as the discrete states for the hybrid system, labeling the state-space equations representing each segment. S , L , and H as previously defined are as follows: $2S$ is the number of measurement zones, L is the number of the layers for each measurement zone, and $2H$ is the number of heaters. Also, $A_m \in \mathbb{R}^{(2S \times L+1) \times (2S \times L+1)}$ and $B_m \in \mathbb{R}^{(2S \times L+1) \times 2H}$.

$$x_i(t) = \begin{bmatrix} x_{i_1} & x_{i_2} & \cdots & x_{i_{2S}} & T_\infty \end{bmatrix}^T, \text{ with } x_{i_n} = \begin{bmatrix} T_{n,1} & \cdots & T_{n,L} \end{bmatrix}^T, \text{ and } u_i(t) = \begin{bmatrix} \theta_1 & \theta_2 & \cdots & \theta_{2H} \end{bmatrix}^T.$$

In (19):

- The states are the temperatures of all the layers of the measurement zones, as well as the ambient temperature.
- The inputs are the heater temperatures.

It should be noted that in each segment, the controllability matrix R of this system has full rank, ensuring that the overall system is controllable.

Thus, after obtaining the state-space model of each segment and assigning the autonomous switching points as $x(t_{s_1}) = 90^\circ\text{C}$ and $x(t_{s_2}) = 130^\circ\text{C}$, we will define the constraints as follows.

Table 5-1 List of Operating Points for Each Segment

Segment	T_o ($^\circ\text{C}$)	θ_o ($^\circ\text{C}$)	T_∞ ($^\circ\text{C}$)	C_{p_o} (J/(kg.K))
1	27	27	27	2000
2	90	90	90	6000
3	130	130	130	7000

5.5.3 State Constraints

As it was previously stated, as a design requirement, the temperatures of the measurement zones are required to start from a certain temperature while not exceeding the set point temperature by more than 10°C in each segment. Therefore, we define the states box constraint as,

$$x_i^L \leq x_i(t) < x_i^U + 10, \quad (20)$$

where in each segment ($i = 1, 2, 3$), x_i^L represents the starting temperature of the measurement zones, and x_i^U represents the set-point tracking temperature.

5.5.4 Actuator Constraints

After defining the states box constraint, the next step is to incorporate the actuator constraints. There are two sets of actuator constraints in this problem:

5.5.4.1 Box Saturation Limits

A ceramic heater, along with all other sorts of heaters, has lower and upper temperature saturation limits, meaning that the heater's temperature cannot be lower than room temperature and cannot be higher than a certain maximum temperature. For the ceramic heater used in this study, the upper and lower temperature saturation limits are $\theta_{\min} = 27^\circ\text{C}$ and $\theta_{\max} = 600^\circ\text{C}$. These limits, when transformed into a constraint in terms of $u(t)$, will result in:

$$27 \leq u(t) \leq 600. \quad (21)$$

5.5.4.2 Heating and Cooling Rate Saturation Limits

The heating and cooling rates of a heater are dynamically varying with the current temperature of the heater, over time. In the case of the ceramic heaters used in this setup, Fig. 5.4 shows the heating/cooling curve of the heater. This curve is produced by setting the heater's power to maximum until the saturation temperature is reached, then shutting it off until room temperature is reached. After a close observation of Fig. 5.4, it is deduced that the variation in the heating and cooling rates is nonlinear due to the varying slope at different heater temperatures. The heating rate is decreasing as the temperature of the heater is increased whereas the cooling rate is decreasing as the temperature of the heater is decreased. The slopes of the heating and cooling curves have been characterized by the following equations:

$$\begin{aligned}\dot{\theta}_{h_rise} &= -0.005\theta(t) + 3 \\ \dot{\theta}_{h_fall} &= -0.0018\theta(t) + 0.06\end{aligned}\quad (22)$$

which are obtained from Fig. 5.4 to determine the rate of change in the temperature of each heater with respect to the current temperature of the heater at each instant. The dynamic heating and cooling rates, presented in (22), is not modeled and included in the state-space model as the dynamics of the actuators. This is because there are no external inputs driving the heaters during the cooling mode, when the heaters are off. Hence, the dynamic heating and cooling rates are considered as an additional set of actuator constraints. These constraints can be modeled as path constraints using the DIDO optimal control software. Rearranging (22) and replacing the change in the heaters' temperatures with the derivative of the control input $u(t)$, we get:

$$-0.0018u(t) + 0.06 \leq \frac{du(t)}{dt} \leq -0.005u(t) + 3. \quad (23)$$

Thus, the set of admissible control inputs $u(t) \in U$ is characterized by taking the constraints in (21) and (23) into account.

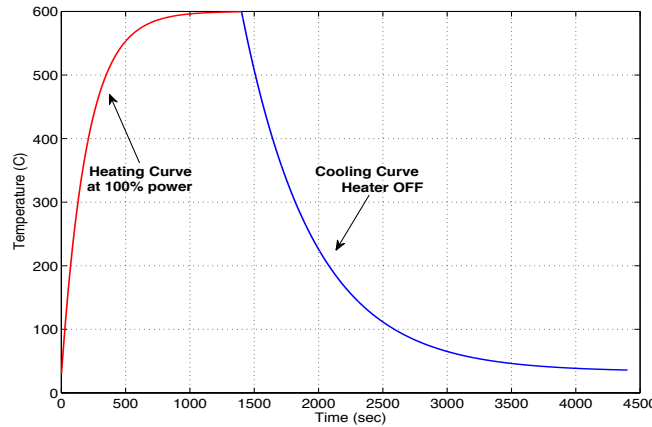


Figure 5.4. The heating and cooling curves of a ceramic heater with the heaters operating at 100% during the heating period, and turned off during the cooling period

5.5.4.3 Implementing Actuator Constraints on DIDO

When using DIDO, the path constraints have to be defined as a single inequality with time-invariant upper and a lower bounds as this control optimization software is not able to handle a number of path constraints twice the amount of control inputs.

In order to represent the heating and cooling rate saturation limits as a single inequality with an upper and a lower bound, we will replace the limits $-0.0018u(t)+0.06$ and $-0.005u(t)+3$ in (23) by constant terms for each segment of the hybrid problem, i.e. the heating and cooling curves shown in Fig. 5.4 will be replaced by linear ones, with a different slope in each of the three segments. This is can presented as,

$$decR_i \leq \frac{du(t)}{dt} \leq incR_i, \quad (24)$$

where $i=1,2,3$ indicates that these rates are different for each particular segment. In each segment, $incR_i$ and $decR_i$ will be conservatively chosen so that the heaters track the actual heating and cooling rates in (22) as closely as possible.

The next issue to be considered is the derivative term. As it was mentioned before, DIDO optimal control software is being used in this chapter, in which the system is discretized using pseudospectral methods. This means that the time interval, for which the optimization problem is being solved, is divided into a number of predetermined nodes called the Legendre-Gauss-Lobatto (LGL) points [110]. The distances between these points, although not uniform, are a priori known, and this can be used to replace $u(t)$ with $u(p)$, where p is the index for each node. Thus, the implementation of (22) in DIDO will be represented with:

$$decR_i \leq \frac{u_i(p) - u_i(p-1)}{t_p - t_{p-1}} \leq incR_i. \quad (25)$$

Thus for every LGL point p in the specified time interval, the constraint shown in (25) has to hold in order to replicate the continuous constraint of (24).

5.5.5 HOC Design to Solve the Thermoforming Tracking Problem

Having defined the linearized system in (19) along with the states and actuator constraints, we will use the HMP based HOC to solve the temperature tracking problem. The final formulation of the HOC algorithm along with the optimization of each segment is shown as a flowchart in Fig. 5.11.

As it is shown in Fig. 5.11, in order to solve the temperature tracking problem in the thermoforming heating phase, for a fixed final time and in the presence of parameter variations, we divide the heating cycle into three linearized segments, for each plastic sheet. These segments

are based on the variation of the most dominant temperature-dependent material property, identified as Cp , as the system is linearized around three sets of operating points as mentioned before. Therefore during the heating cycle, we define two switching sets at $(x(t_{s_1}), t_{s_1})$ and $(x(t_{s_2}), t_{s_2})$ so that the dynamics of the system can switch from the first to the second segment, and from second to the third segment, as the temperature of the sheet is rising. $x(t_{s_1})$ and $x(t_{s_2})$ will both be fixed as the temperatures at which Cp changes values autonomously, indicating Autonomous Switchings in the hybrid system presentation and the corresponding HOC algorithm.

Thus, the goal of the HOC design is to find the optimal control input (for each segment) to minimize the cost function of that particular segment while also determining optimal switching times for the two switching sets in order to minimize the total cost function of the three segments combined, shown in (8). In doing so, the HOC will also minimize the energy consumed by the heaters throughout the entire cycle since the term $\frac{1}{2}u^T R_i u$ is included as a running cost in the cost function (described in (8)) to minimize the control effort.

In the execution of the algorithm, it is required in each segment for the temperatures of the measurement zones to reach the respective switching points of $x(t_{s_1}) = r_{s_1}$, $x(t_{s_2}) = r_{s_2}$, and $x(t_f) = r_f$, while never exceeding an overshoot limit of 10°C (as incorporated in (20)). In addition in each segment, it is also naturally required for the initial sheet temperatures to start from the final temperatures of the previous segment. Although it is required for the sheet temperature to track the mentioned references, the ambient-temperature state is not forced to track a set-point in any segment (designated weight in the running and endpoint cost set to zero), yet in each segment, it is also required for the initial value of the ambient air to equal its final value from the previous segment.

For the control inputs, an initial value $u(t_0)$ is assigned to the input control signals in the first segment, i.e. the heaters' starting temperature is fixed for this segment. Also, for the second and third segments, it is required that the heaters start from the final temperature of the previous segment, i.e. $u_2(t_{s_1}) = u_1(t_{s_1}^-)$ and $u_3(t_{s_2}) = u_2(t_{s_2}^-)$ in order to avoid discontinuities in the control input signal. This is done so that the control signals could be implemented in practice.

Finally as shown in Fig. 5.11, at the end of each iteration, the Hamiltonians obtained from the optimal results of each of the segments are compared, as depicted in (17), in order to determine whether or not the HOC algorithm has found the optimal switching times. If not, the switching times will be updated based on the equations presented in (16) and shown in Fig. 5.11, where α is selected to adjust the convergence rate of the algorithm.

Table II shows the assigned values for the parameters shown in the flowchart, which are needed to solve our specific problem. It should also be noted that the number of computation nodes (LGL points), chosen in the DIDO program, is set as $P = 30$, for each segment. Thus, applying all the above points, along with the values of table II, to the hybrid setup, the algorithm shown in Fig. 5.11 is implemented.

Table 5-2 Parameter Values Used in the Algorithm

Time Related		State Related (fixed)		Control Related (fixed)	
t_0 fixed	0 s	$x(t_0)$	27°C	$u(t_0)$	150°C
t_{s_1} initial	310 s	$x(t_{s_1})$	90°C	$decR_1$	0.2
t_{s_2} initial	510 s	$x(t_{s_2})$	130°C	$incR_1$	2.17
t_f fixed	820 s	$x(t_f)$	150°C	$decR_2$	0.1
				$incR_2$	2.0
				$decR_3$	0.15
				$incR_3$	2.0

5.5.6 Design Results

The particular thermoforming machine, on which we will implement the HOC algorithm contains 36 heating zones or heater banks (18 on top and 18 on the bottom), uses ceramic-type heaters, and can fit sheets with dimensions of up to 1.5mX0.9m. As mentioned before, The HDPE sheet used in this simulation is the 7.5mm with a dimension of 1.5mX0.9m. In total, considering top and bottom levels, there are 6 IR sensors (3 on top and 3 below the plastic sheet) and 6 model-based virtual sensors (3 on top and 3 below the plastic sheet), creating 13 sensor measurement zones on the sheet for temperature measurement. The 2D position grid of the real IR sensors and the virtual sensors relative to the heaters is shown in Fig. 5.5, noting that the sensors placed on top and bottom of the sheet are directly facing each other thus having similar coordinates on the grid.

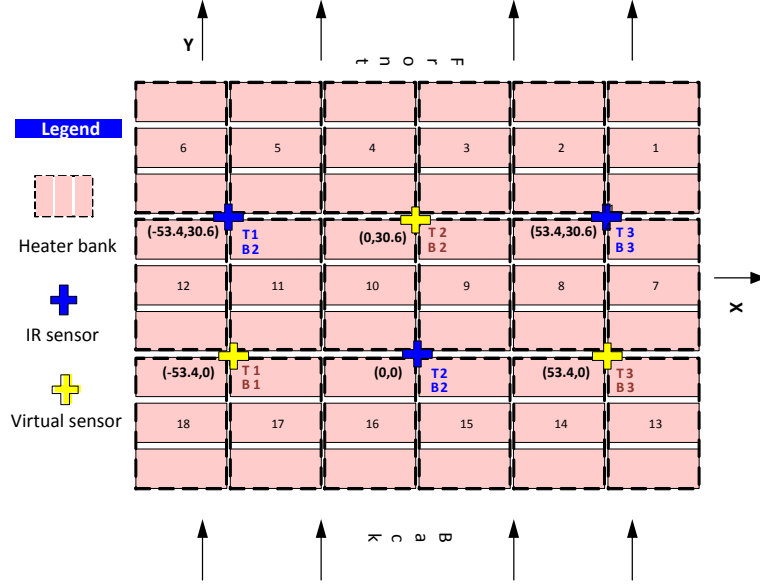


Figure 5.5. 2-D position grid of IR and virtual sensors relative to the heaters

Considering the abovementioned features of the thermoforming machine, the A and B matrices presented in (16) have the dimensions $A_i \in \mathbb{R}^{37 \times 37}$ and $B_i \in \mathbb{R}^{37 \times 36}$, for each segment.

After the implementation of the HOC algorithm, we obtain the optimal control inputs along with the state trajectories, after a number of iterations. Optimal results are achieved since ΔH defined in (17) is determined to be 4×10^5 , which is two decimal points lower than the Hamiltonians of each section. The Hamiltonians (H defined in (11)) of the three segments are shown in Fig. 5.10(a), where a constant line is nearly achieved, signifying that a hybrid optimal solution is reached. In addition, Fig. 5.10(b) shows the Lagrangian of the Hamiltonian, \bar{H} , previously defined in (13), of the three segments, where it can be seen that \bar{H} is also nearly a constant line for each segment, signifying that (12) holds and that optimal solution is achieved for each segment. It should be noted that in Fig. 5.12(a) and 5.12(b) the \bar{H} and the Hamiltonian curve contain some imperfections specially at the beginning and end of each segment, yet this is completely normal since numerical computations of DIDO in determining \bar{H} and H for a large scale system, such as ours, will lead to some errors and imperfections, based on the number of computation (LGL) nodes ($P = 30$ in our case). Accuracy in the results could be improved even further if the number of LGL nodes for each segment is increased; yet this will increase the computation time. With regards to our problem, these small variations are negligible, and results are indeed acceptable. Hybrid optimality is also confirmed by showing that in Fig. 5.12(c), the

total cost (presented in (8)) is being minimized as the algorithm converges to optimal switching times.

Finally, Fig. 5.13(a) and Fig. 5.13(b) show the resulting state trajectories and control inputs, respectively, which are applied to the industrial simulator, described in the next section of this chapter.

5.6 Simulation Results

In this section, the hybrid optimal control signals obtained in the design stage will be implemented, in real-time, on a standard rotary thermoforming machine simulator in open-loop and closed-loop settings, shown in Fig. 5.6 and Fig. 5.7, respectively. The simulator contains all the nonlinearities of the actual process, including the nonlinearities resulting from the infrared heating method (shown in (4), (5), and (7)) and the nonlinearities of the ceramic heaters (actuators), along with all the specific geometric configurations. The simulator is tested to be within 2°C accuracy of the actual thermoforming machine [4]. It should be noted that the temperature-varying curve of the specific heat capacity, shown in Fig. 5.2, is fully incorporated as the value of C_p is changing in real-time.

The goal of this simulation is to determine whether the control signals, produced using the HOC algorithm, can meet the design requirements and solve the tracking problem of thermoforming heating phase under the presence of temperature varying material properties, in an open-loop setting (shown in Fig. 5.6). This would imply that the HOC algorithm has successfully taken the temperature-varying dynamics of the system, along with actuator nonlinearities and already mentioned constraints, into consideration. Moreover, successful implementation of the HOC algorithm in an open-loop setting would provide a proof of concept, showing that hybrid optimal algorithms can be applied to high-dimension, nonlinear, and parameter varying industrial processes.

In this section, we also propose a new control structure, based on the HOC produced control inputs and using feedback control as shown in Fig. 5.7, to compensate for potential perturbations, such as uncertainty in the value of the specific heat capacity C_p . The new structure will be described later in detail while its robustness to perturbations will be examined.

As stated before, the design criteria is for the surface measurement zones to track a uniform temperature profile of 150°C in 820 s. The results are demonstrated below.

5.6.1 Open-Loop HOC

In the first part of the simulation phase, the control inputs obtained in Fig. 13(b) are applied to the simulation setup shown in Fig. 5.6. Fig. 14 (a) shows the resulting temperature response of the measurement zones along with the optimal trajectories produced by the HOC (also shown in Fig. 13(a)). It can be observed that the measurement zones are closely tracking the optimal trajectories, eventually reaching the desired 150°C temperature profile. In order to examine the tracking performance in a more precise manner, we show the difference between the optimal trajectories and the actual responses in Fig. 5.9, demonstrating that this difference never exceeds the $\pm 10^\circ\text{C}$ window. Fig. 5.9 also shows that the measurement zone temperatures have also accurately tracked the set-points of 90°C and 130°C at the end of each segment (switching points), validating the linearization of the model in the three already mentioned segments.

Moreover, Fig. 5.14(b) shows the response of the heaters to the control inputs. Note that the heaters' block contains all the nonlinear dynamics of the heaters, which was shown in Fig. 5.4. Fig. 5.14(c) shows the difference between the optimal control inputs and the actual heaters' temperatures during the entire cycle, demonstrating that the maximum percentage error does not exceed the 5% mark. This implies that the linearization of the heating and cooling rate-saturation limits for the three segments has successfully captured the nonlinear dynamics of the ceramic heaters since the actual heaters' response is following the optimal control inputs with 95% accuracy.

Therefore, it can be concluded that the control inputs obtained from the HOC algorithm solve the tracking problem of the thermoforming heating phase in the presence of temperature varying parameters. It should be noted that if we increase the number of linearized segments, we could achieve even more accuracy in our results since the system will be able to catch more of the nonlinear dynamics. However the tradeoff is that more segmentation results in a heavier computation load.

5.6.2 Closed-Loop Hybrid Controller (CLHC)

The specific heat capacity (C_p), which is a material property of plastic sheets, can be uncertain in terms of its indicated value. The material property specifications for certain types of plastic sheets (HDPE for example) provided by companies are often inaccurate and may lie within a 20% range of the specified values. Also, the same plastic materials produced by different companies are never perfectly identical because of various manufacturing factors, thus

having slightly different material properties [6]. This uncertainty could affect the model-based virtual sensors since the values of the material properties are used in the estimation of the surface temperature. Therefore, the robustness of the virtual sensors and the entire control system has to be investigated under a perturbation in material property values for an HDPE plastic sheet. In this chapter, we consider uncertainties affecting the specific heat capacity (Cp), since it is the temperature varying parameter. We start by adding the perturbation to the open-loop setup (shown in Fig. 5.6) in order to determine how much uncertainty could actually be problematic. The criterion used in analyzing the robustness of the system is the final surface temperatures of the measurement zones. For a given percentage uncertainty, if the surface temperatures remain within a $\pm 10^\circ\text{C}$ window of the set-points, then we consider the system to be robust enough for that amount of uncertainty. Fig. 5.8(a) and 5.8(b) show the temperature response of the measurement zones, when the uncertainty of the specific heat capacity is set to be at +15% and +20% of its nominal variation curve (shown in Fig. 2), respectively. In fact, Fig. 5.8(a) shows that under +15% perturbation, the open-loop system containing only the HOC generated control inputs can still produce acceptable temperature responses, which are actually within the $\pm 10^\circ\text{C}$ range of the final set-point. This however is no longer the case for a +20% perturbation since the final surface temperatures are no longer within the $\pm 10^\circ\text{C}$ window of the 150°C set-point, as this can be observed in Fig. 5.8(b).

Thus, in order to deal with larger uncertainties, we propose the closed-loop feedback structure shown in Fig. 5.7. Fig. 5.7 shows that the control inputs, which are being fed to the heaters, are based on the HOC generated control inputs. However, under the presence of perturbations, a feedback controller is also implemented, which will compensate the difference between the HOC generated optimal trajectories (applied as the reference inputs) and the actual real and virtual temperature measurements. The feedback controller could be of any simple type, and so P controllers are utilized in this chapter. The output of the feedback controller will then be added to the optimal control inputs to produce suboptimal control inputs, shown as,

$$u_H(t) = u^*(t) + C_f(y_{out}(t) - y_{ref}^*(t)), \quad (26)$$

where, $u_H(t)$ represents the suboptimal control inputs, $u^*(t)$ and are the optimal control inputs generated by the HOC algorithm, $y_{ref}^*(t) = [x_r^* \quad x_v^*]^T$ are the optimal state trajectories of surface

temperatures for the real (x_r^*) and virtual (x_v^*) measurement zones combined, C_f is the feedback control block, and $y_{out}(t) = [y_s^* \ y_{s_1}^*]^T$ are the surface temperature outputs of the real (y_s^*) and virtual ($y_{s_1}^*$) measurement zones.

It can be realized from (26) that if there is no uncertainty in C_p , the optimal control inputs are the only inputs practically applied to the heaters block. Since it was shown in the open-loop study that under no uncertainty $y_{out}(t) - y_{ref}^*(t)$ is small throughout the cycle, the feedback controller will not produce significant control signals, as tracking is accurate enough.

Also from (26), it is deduced that these suboptimal control inputs have two important advantageous characteristics: 1) they behave similarly to the optimal control inputs, and 2) they force the system to track the optimal temperature trajectories produced by the HOC algorithm.

To show the effectiveness of the control setup shown in Fig. 5.7, the simulation is conducted incorporating +20% perturbation in the specific heat capacity. Fig. 5.15(a) shows that the surface temperatures are accurately tracking the optimal temperature trajectories as Fig. 5.10 demonstrates that the deviation is not more than 6°C. Fig. 5.15(b) also shows the control input signals comprising the added optimal and feedback control inputs. Comparing Fig. 5.15(b) and Fig. 5.13(b), it can be observed that the shape and behavior of both sets of signals nearly coincide. This claim that the suboptimal control signal is not significantly different from the optimal control input is further validated in Fig. 5.15(c), as it is shown that the maximum percentage difference during the entire cycle is 15%, which signifies that the heaters are tracking the optimal control inputs with an 85% accuracy under +20% perturbation acting on the system. Therefore, it can be stated that in the presence of significant perturbations, the proposed CLHC setup can provide a robust option, while in addition to the temperatures of the measurement zones closely tracking the optimal trajectories, the heaters also track the optimal control inputs with a significant degree of accuracy.

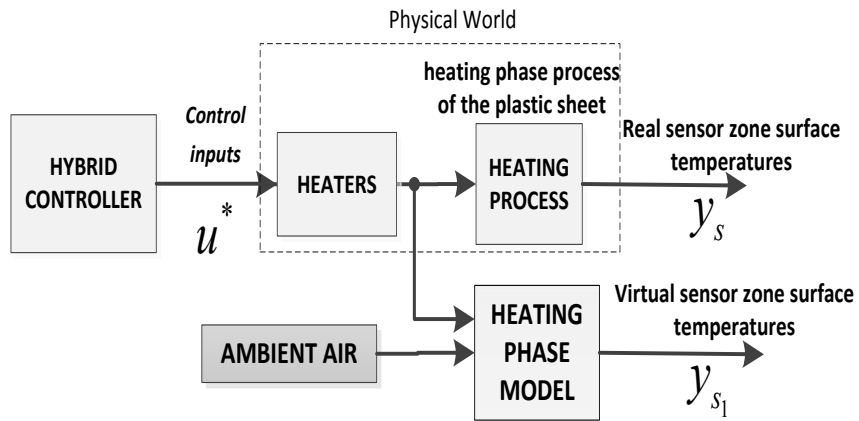


Figure 5.6. Open-loop block diagram containing the hybrid optimal control inputs

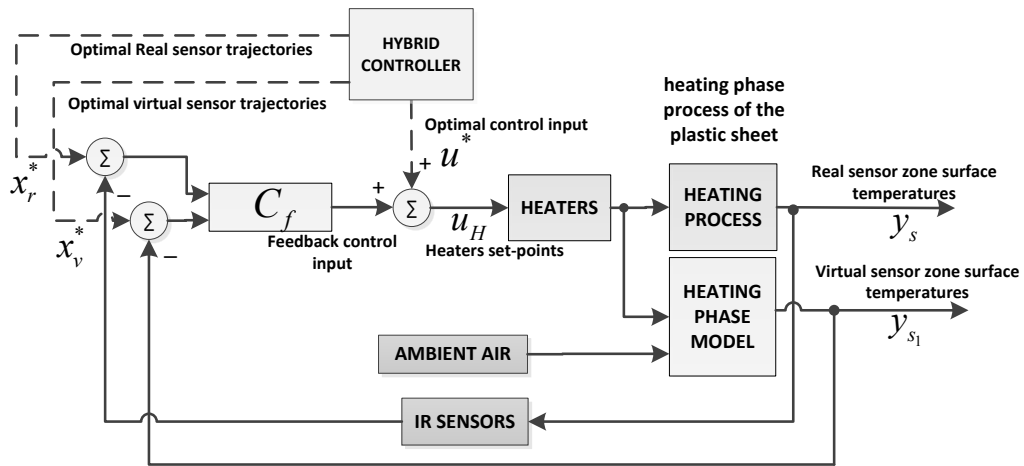


Figure 5.7. Proposed CLHC block diagram, providing robustness against perturbations

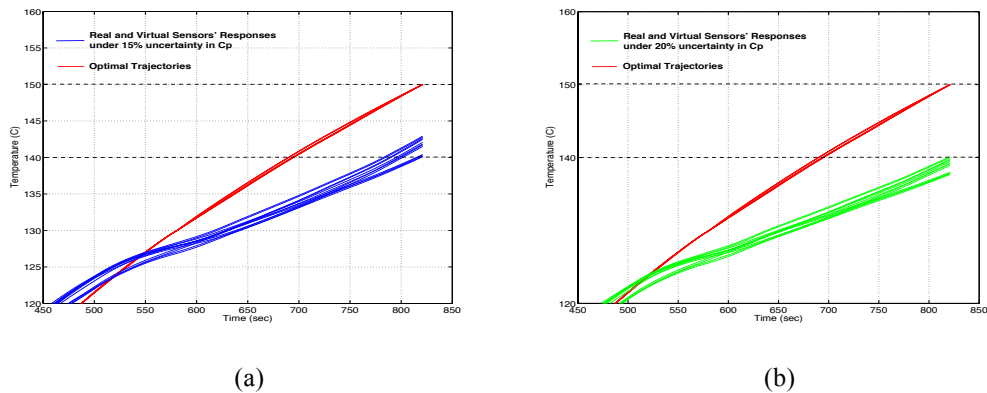


Figure 5.8. Open-loop response of the real and virtual measurement zones using the HOC generated control inputs: (a) under 15% uncertainty in C_p . (b) under 20% uncertainty in C_p .

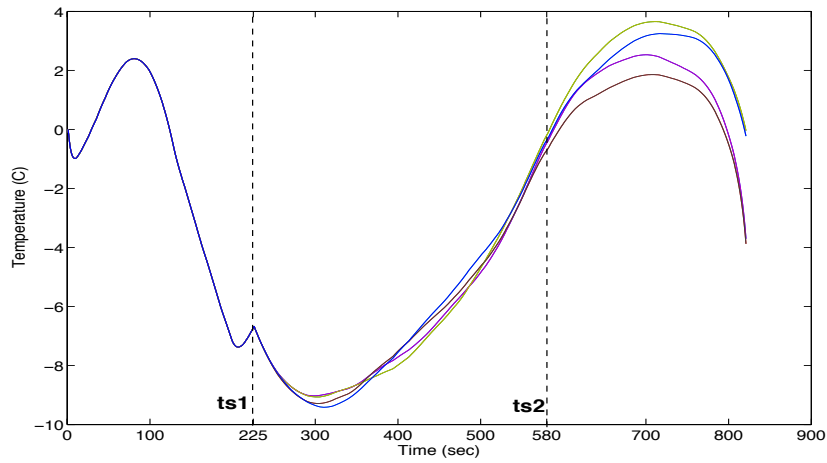


Figure 5.9. Using the open-loop HOC setup: The Difference between the optimal temperature trajectories and the temperature response of the real and virtual measurement zones. The difference remains in the $\pm 10^{\circ}\text{C}$ bound.

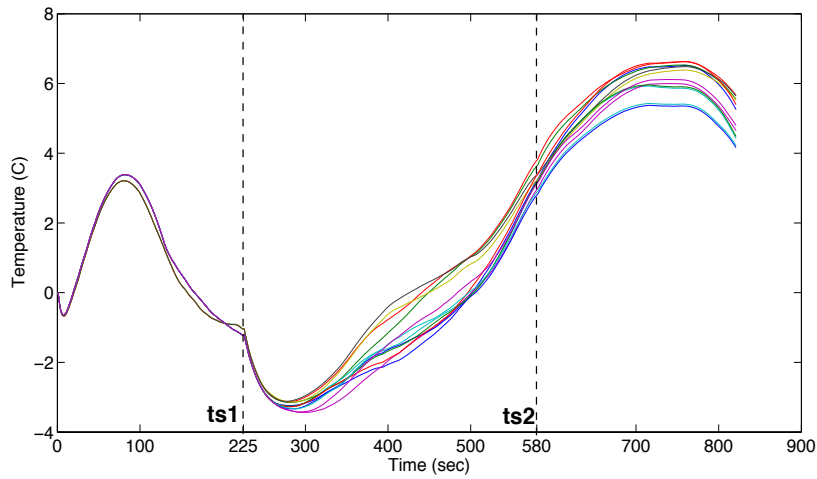


Figure 5.10. Using the CLHC setup: The Difference between the optimal temperature trajectories and the temperature response of the real and virtual measurement zones. Maximum difference is 6°C and showing close tracking.

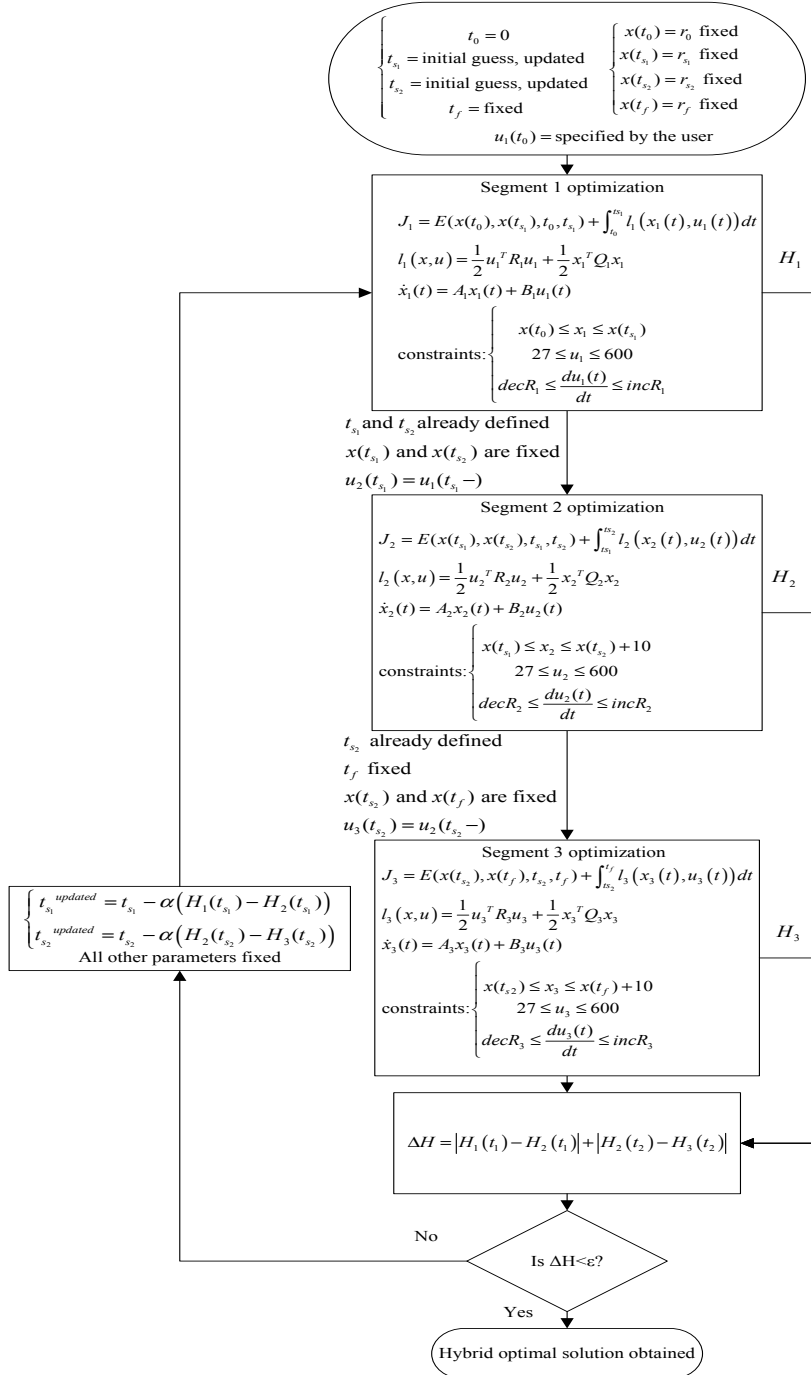
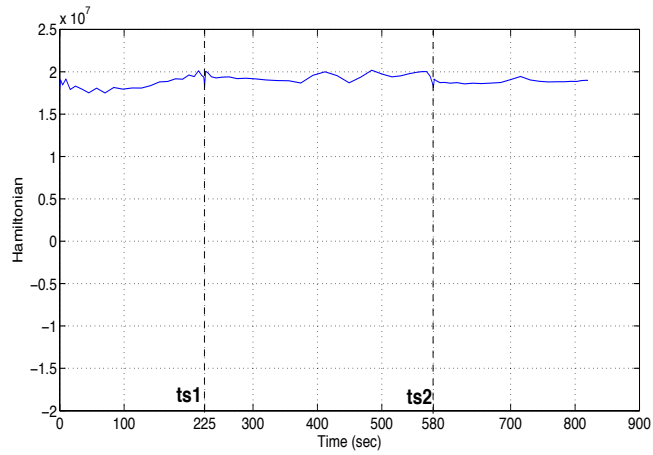
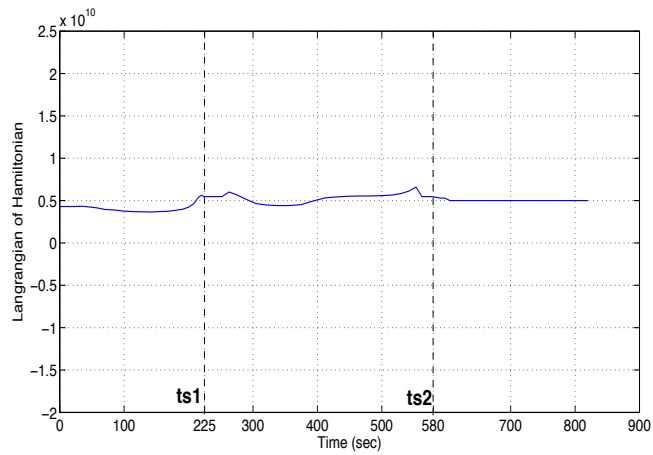


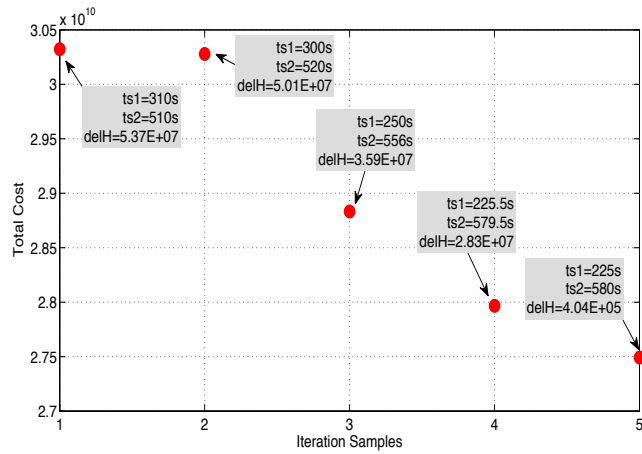
Figure 5.11. Proposed flowchart of the HOC algorithm used to solve the thermoforming heating phase tracking problem



(a)

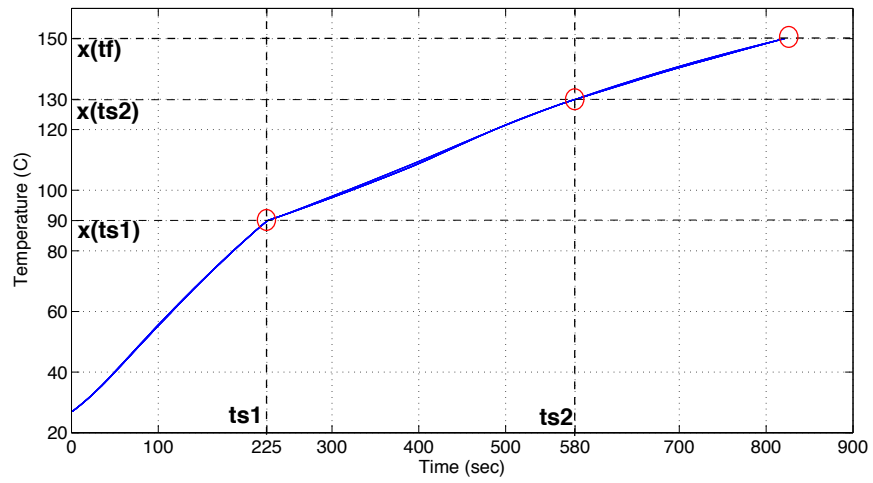


(b)

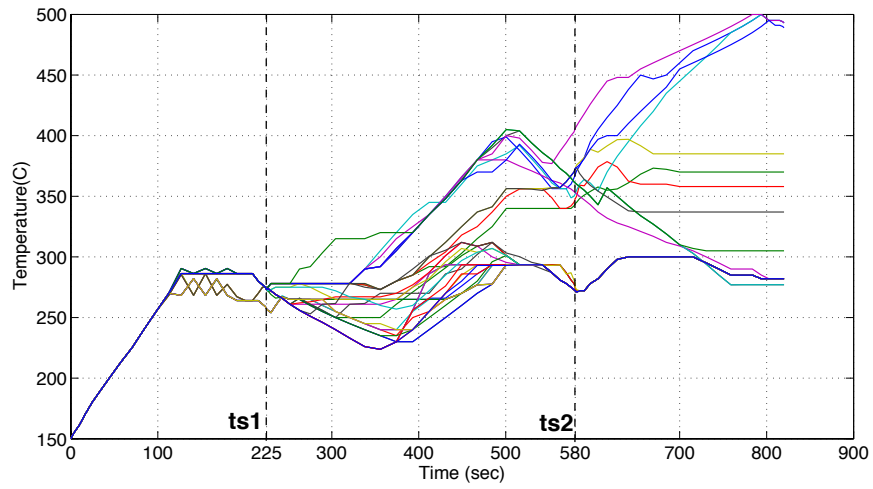


(c)

Figure 5.12. Resulting from the HOC algorithm: (a) The Hamiltonian plot of the three segments. (b) The Langrangian of the Hamiltonian for the three segments. (c) Total cost minimization curve.

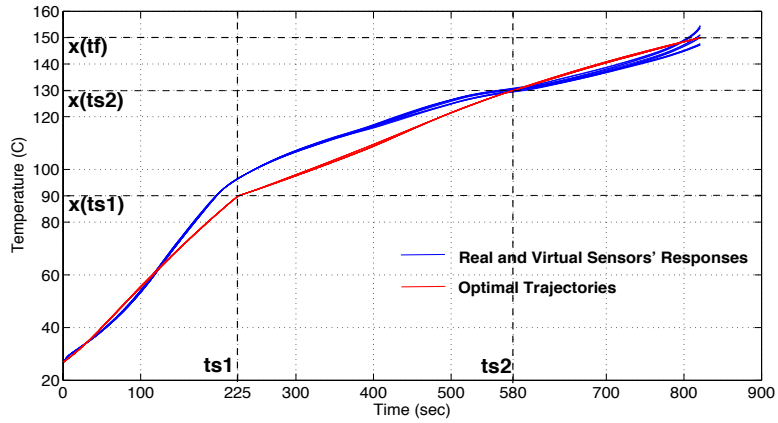


(a)

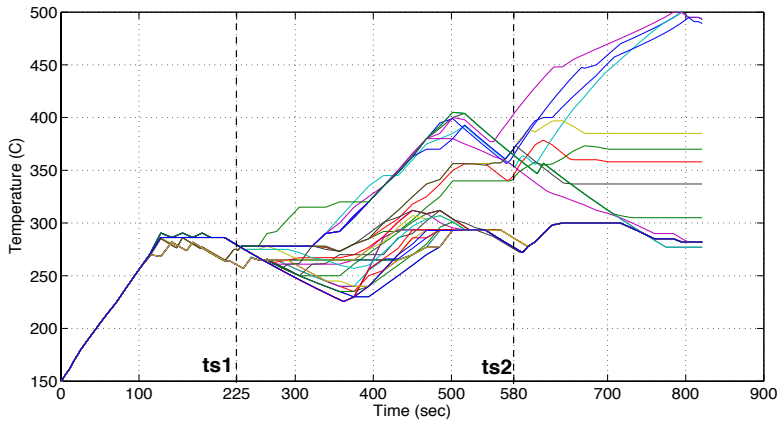


(b)

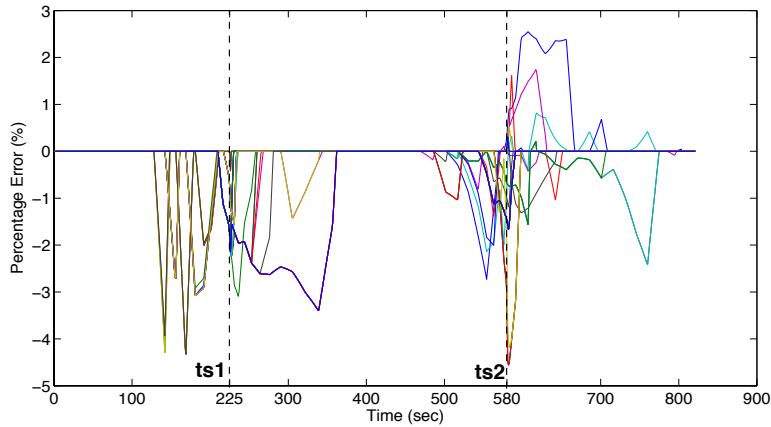
Figure 5.13. Resulting from the HOC algorithm: (a) the optimal temperature trajectories of the measurement zones. (b) Optimal control inputs for the heaters.



(a)

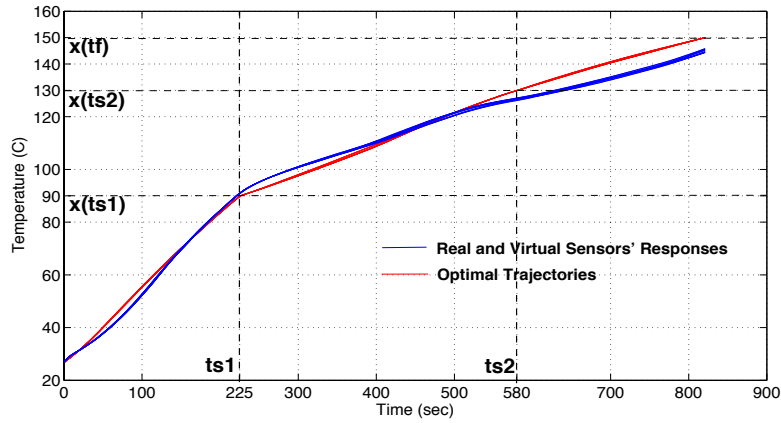


(b)

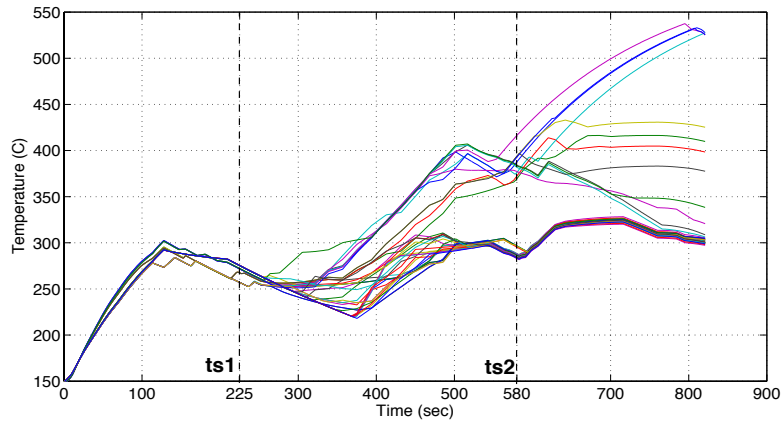


(c)

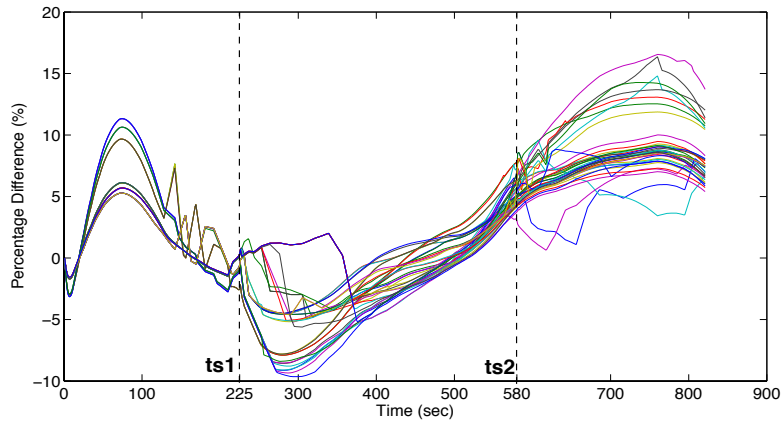
Figure 5.14. Simulating the HOC generated control inputs in open-loop: (a) The temperature response of the real and virtual measurement zones, closely tracking the optimal trajectories. (b) The response of the heaters to the HOC inputs. (c) The percentage error between the heaters' response and HOC generated control inputs, which shows 95% accuracy.



(a)



(b)



(c)

Figure 5.15. Under 20% uncertainty, simulating the HOC generated optimal temperature trajectories and control inputs using the proposed CLHC diagram: (a) The temperature response of the real and virtual measurement zones, closely tracking the optimal trajectories. (b) The response of the heaters. (c) The percentage error between the heaters' response and HOC generated control input, showing 85% accuracy, which means that the heaters are behaving similarly to HOC generated control inputs.

5.7 Conclusion

In this chapter, the parameter-varying heat transfer model of the heating phase was modeled in a hybrid optimal control framework. A constrained HMP-based HOC algorithm was presented to solve the large-scale, constrained, and parameter-varying temperature tracking problem, and to minimize the power consumption of the heaters in the process. The HOC algorithm resulted in optimal control inputs and state trajectories taking the nonlinear dynamics of the heaters into account, treating them as control box and path constraints. In this chapter, a CLHC block diagram was also proposed to provide robustness against perturbation. The HOC and CLHC were tested on an industrial thermoforming machine simulator, which included all the nonlinear dynamics, temperature-varying properties, and geometrical attributes of the thermoforming process. The performance, efficiency, and robustness of both of these methods were showcased as it was shown that the HOC and the CLHC successfully solve the temperature tracking problem of the heating phase.

In the next chapter, a summary of this thesis is given, and potential future research avenues are discussed.

6 Conclusion

6.1 Thesis Summary

In this thesis, a number of problems have been addressed towards improving the accuracy, autonomy, productivity and cost-effectiveness of the thermoforming heating phase. In parallel, certain control and sensing algorithms have been developed, which have the potential to be applied to other thermal applications.

In Chapter 2, MVBSs and virtual core-temperature observers were developed and combined in Fig. 2.5 to replace the closed-loop control block diagram of Fig. 1.1, used in previous thermoforming studies. It was shown that MBVSs introduce additional surface temperature measurement points in the feedback, leading to improved observability of the process since uneven and asymmetrical temperature profiles across plastic sheets can now be achieved in a cost-efficient way as the need for the use of extra IR sensors is eliminated. Core-temperature observers are another significant addition to the updated closed-loop block diagram as they provide accurate temperature estimates of the center-plane of the sheet, which ultimately result in the core of the plastic sheet to also be within the forming temperature window by the end of the cycle. Consequently, the implementation of the core-temperature observers results in reduction of scrap rates.

In Chapter 2, the updated control diagram (shown in Fig. 2.5) containing the MBVSs and the core-temperature observers was simulated on an industrial thermoforming machine simulator in order to assess the accuracy of the new estimation methods and to evaluate the performance and robustness of the overall system. The simulation study was conducted in two parts: 1) simulation under ordinary conditions and 2) simulation under 20% uncertainty in material properties. The simulation was conducted for zoned temperature (uneven temperature) ramp inputs, and measurements from the IR sensors, the MVBSs, and the core-temperature observers were presented. It was shown that under both cases of nominal and uncertain conditions, when compared to the responses of the IR sensors, the MVBSs and core-temperature observers provide accurate estimations of the temperature. It was also shown that zoned temperature tracking is achieved across and through the depth of the plastic sheet as the IR sensors, the MVBSs, and core-temperature observers all closely track the input references and remain within $\pm 10^{\circ}\text{C}$ of the

forming temperature. The robustness of the new control system (Fig. 2.5) was also shown as the IR sensors, the MVBSs, and the core-temperature observers all showed accurate tracking under 20% perturbations of the material properties included in the virtual sensor and core-temperature blocks.

Upon successful implementation of the MVBSs and core-temperature observers in the control system, the block diagram of the updated control system shown in Fig. 2.5 was used in the subsequent studies conducted in this thesis.

In Chapter 3, the application of the Watanabe-modified Smith predictor technique to improve the heating cycle (tracking time) of the thermoforming heating phase was studied. The Smith predictor is an internal-model control technique designed to compensate for input delays in the system. The motivation behind implementing this particular control method was based on the observation that the temperature response of a plastic sheet was exhibiting an input delay type of behavior. The source of the input delay was found to be in the sluggish and nonlinear dynamics of the heaters, as well as other ambient factors affecting the heating process.

In order to design the Watanabe-modified Smith predictor controllers for the heating phase, the heat transfer dynamics of the plastic measurement zones were modeled and represented using “first-order-plus-time-delay” (FOPTD) dynamics, followed by the Direct Synthesis design approach. The Watanabe-modified Smith predictor controllers were then added to the new control block diagram developed in Chapter 2 (Fig. 2.5) and simulated on a industrial thermoforming machine simulator. The aim of the simulation study was to assess the performance and robustness of the proposed control technique while also comparing the performance and robustness against existing control methods (PI controllers). The simulation study was conducted for zoned temperature set-points in two parts: 1) simulation under ordinary conditions and 2) simulation under 30% uncertainty in material properties. Under nominal conditions, it was shown that the Smith predictor control technique improved the tracking performance (heating cycle) compared to the PI control method. In the second scenario, under 30% uncertainty in the material properties, it was shown that the Smith predictor technique maintains robustness while additionally improving the tracking performance of the system, compared to the PI control method.

In Chapter 4, the objective was to introduce an automation technique for the thermoforming of multilayered plastic sheets. As it has been described before, multilayer plastic

sheets are gaining popularity in thermoforming since higher quality products, which are more elegant and eye appealing, can be produced. The vehicular, construction, and sanitary components seen today are all made of multilayer plastic sheets. Multilayer plastic sheets, however, are difficult to form as each layer of these sheets consists of a different rheological property and a designated forming temperature.

In Chapter 4, a practical model of the heating phase of multilayer plastic sheets was presented. This model can easily be linearized and used in various control schemes. More importantly, this model is a generalized model in the sense that it can account for any number or combination of plastic materials in a multilayer sheet. A discrete-time model predictive controller (DTMPC) was then proposed to solve the temperature tracking problem of multilayer plastic sheets in thermoforming, for the first time. The DTMPC method took into account the heat transfer model of all the layers along with the actuator nonlinearities associated with the heaters to successfully address the tracking problem for all the different layers within the multilayer plastic sheet. The control setup, presented in Chapter 2 (Fig. 2.5), containing the DTMPC method was simulated on an industrial thermoforming machine simulator, where it was shown that the proposed method provides superior tracking performance as well as lower energy consumption compared to classical control methods.

In Chapter 5, the heat transfer model of the heating phase in thermoforming, presented in [34] and [42] was revisited. Certain material properties incorporated in these models were found to be dependent on the temperature of the polymer. As studies suggest in [37] and [57], variations in some of these properties during the heating cycle is substantial. The specific heat capacity (C_p) is one of these material properties that varies up to nine times its initial value as the temperature of the plastic sheet is increasing. Therefore, as the studies in [57], [34] and [37] suggest, these temperature variations have to be incorporated in the heat transfer model of plastic sheets.

In Chapter 5, the parameter-varying heat transfer equations of the heating phase were modeled in a hybrid optimal control framework. A constrained Hybrid Minimum Principle (HMP) based hybrid optimal control (HOC) algorithm was presented in this chapter to solve the large-scale, constrained, and parameter-varying problem of temperature tracking, while minimizing the power consumption of the heaters in the process. The HOC algorithm produced the optimal control inputs and state trajectories taking the nonlinear dynamics of the heaters, in

the form of saturation and rate saturation limits, into account and treating these dynamics as control box and path constraints. In this chapter, a closed-loop hybrid control (CLHC) block diagram was also proposed to provide robustness against perturbation. The HOC and CLHC were subsequently tested on an industrial thermoforming machine simulator, which included all the nonlinear dynamics, temperature-varying properties, and geometrical attributes of the thermoforming process. The performance, efficiency, and robustness of both of these methods were showcased as it was shown that the HOC and the CLHC successfully solve the temperature tracking problem of the heating phase. Using the simulation study, it was also highlighted that the CLHC produces optimal control signals as long as the process is not overly perturbed, but even at the point where the perturbation percentage is high, the temperature response is forced to closely track the optimal trajectories produced by the HOC algorithm while the generated control inputs exhibit a similar pattern to the optimal control inputs.

Finally, successful implementation of the proposed HOC algorithm was a proof of concept to show that HMP-based hybrid optimal controllers can actually be implemented on complex industrial processes, which are large-scaled, comprise nonlinear constraints, and include parameter variations.

6.2 Future Research

Some of the areas, which can be subjects of future research in thermoforming and other related thermal processes, are briefly discussed in this section.

6.2.1 Inclusion of the Sag Effect in the Heat Transfer Model

As it was briefly alluded to in Chapter 1, in the heating phase, the plastic sheet starts to sag as its temperature nears the forming window. The sag affects the heat transfer model of the bottom surface layer of the plastic sheet and the infrared heat transmission through the interior layers, as the distance between the sheet and bottom heaters decreases. The reduction of distance between the bottom heaters and the sheet affects the values of the view factors, as the vertical distance between the sheet and the heaters plays an important role in determining the view factors (as defined in [42]), thus changing the dynamics of heat transfer model. Therefore, the Q_{RB_n} term in equation (3), presented in Chapter 5, will be a variable parameter since the view factors F_{ij} , used to determine Q_{RB_n} , will all be dependent on the sag effect.

This effect is yet to be incorporated and accounted for in the heat transfer model of the plastic sheet. One of the possible approaches to model this effect would be to consider the distance between the plastic sheet and the heaters below the sheet as a temperature-varying parameter so that as the temperature of the sheet increases, the distance between the plastic sheet and the heaters below decreases. This would model the sag effect dynamics of the heating phase on the plastic sheet.

In addition to the inclusion of the sag dynamics, a control method needs to be developed for the heating phase in the presence of the sag dynamics. A control scheme, similar to the HOC algorithm presented in Chapter 5, a model predictive controller, or a robust LPV control algorithm could then be developed to solve the temperature tracking problem of the heating phase, in the presence of the sag dynamics.

6.2.2 Future Research on Temperature-Dependent Material Properties

In Chapter 5, temperature control of the plastic sheet in the presence of temperature-dependent material properties was addressed. In this study, only the specific heat capacity (C_p), which was the most dominant temperature-dependent material property in terms of its variation range, was considered as a temperature-varying parameter.

For future work, it is suggested to incorporate all temperature-dependent parameters, as it has been investigated in [36] and [37], in the heating phase model and to subsequently develop a hybrid optimal control algorithm or other possibly applicable control schemes to solve the new temperature tracking problem.

It is also suggested to solve the temperature tracking problem in the presence of temperature-dependent parameters for multilayer plastic sheets. Every layer of the multilayer sheet will have its own set of temperature-dependent material properties, and the control algorithm has to consider all the layers' varying properties.

Zoned temperature tracking is also highly desirable in order to show that complex-shaped plastic products can be successfully formed.

Most importantly, in future avenues of research, virtual core-temperature observers have to be developed, similar to the ones developed in Chapter 2, for the parameter-varying model of the heating phase. Ultimately, a closed-loop block diagram, similar to the one shown in Fig. 2.5, needs to be developed in order to form a comprehensive observer-based system, which contains accurate model-based virtual sensors and core-temperature observers.

6.2.3 Cycle-to-Cycle Control

The ideas presented in this thesis mainly address the in-cycle temperature control in thermoforming. As it was briefly described in Chapter 2, extensive research has also been conducted with regards to the cycle-to-cycle control problem in thermoforming (see [42] and [43]).

An interesting problem to consider would be to design a cycle-to-cycle controller using terminal iterative learning control algorithms (TILC) or robust TILC, based on the ideas presented in [42] and [43], for the heating phase model containing the temperature-dependent parameters. This can further improve the productivity and throughput of the thermoforming process.

6.2.4 Thermoplastic Composite Thermoforming and Welding Processes

The thermoplastic composite market is fast growing, thanks to the increased usage of these products in the fields of transportation (automotive and aerospace) and construction [112]. Different methods of producing thermoplastic composite parts have been studied in the literature, including, thermoforming and welding. In [113] and [114], the heat transfer modeling of thermoplastic composite welding has been discussed and several optimization approaches have been suggested. In [115], optimal thermoforming of large thermoplastic composite parts has been studied. Based on the above studies, it has been observed that the heat transfer modeling of these manufacturing processes resembles the characteristics of the plastic thermoforming process.

Therefore, a potential way to improve the productivity and efficiency of thermoplastic composite manufacturing processes is to apply and tailor the control schemes and estimation methods developed in this thesis. This could be a new research direction in the field of thermoplastic composite manufacturing.

7 References

- [1] IBISWorld. (July 2015). Global Plastic Product & Packaging Manufacturing: Market Research Report. [Online]. Available: <http://www.ibisworld.com/industry/global/global-plastic-product-packaging-manufacturing.html>
- [2] SPI. (2015). Plastics' Contributions to the U.S. Economy [Online]. Available: <http://www.plasticsindustry.org/economicstats>
- [3] The Canadian Plastics Industry Association. (2015). Homepage [Online]. Available: <http://www.plastics.ca>
- [4] G. R. Goetz Klink, O. Wadivkar, B. Znojek. (2012). Plastics. The Future for Automakers and Chemical Companies [Online]. Available: <https://www.atkearney.com/documents/10192/244963/>.
- [5] J. L. Throne, *Understanding thermoforming*, 2nd ed. Cincinnati, OH: Hanser Gardner, 2008, pp. 1-5.
- [6] R. Stein. (2004). *Plastic* [Online]. Available: <http://www.encyclopedia.com/topic/Plastics.aspx>
- [7] BCC Research, "Thermoformed Plastics: Global Markets," PLS047C, Apr. 2014.
- [8] P. Girard, R. DiRaddo, V. Thomson, and B. Boulet, "Advanced In-cycle and Cycle-to cycle On-line adaptive Control for Thermoforming of large Thermoplastic Sheets," NRC Publications Archive, Boucherville, QC, 2005.
- [9] J. L. Throne, "Multilayer Polymers," in *Understanding Thermoforming*, 2nd ed. Cincinnati, OH: Hanser Gardner, 2008, pp. 193-194.
- [10] R. DiRaddo, W. I. Patterson, and M. R. Kamal, "Closed Loop Control of Parison Dimension Profiles in Extrusion Blow Molding," *International Polymer Processing*, vol. 6, no. 3, pp. 217-224, Sept. 1991.
- [11] R. DiRaddo and A. Garcia-Rejon, "In-cycle Deterministic and Stochastic Dynamics of Extrusion Blow Molding," *International Polymer Processing*, vol. 7, no. 3, pp. 257-266, Sept. 1992.
- [12] D. Laroche K. Kabanemi, L. Pecora, R. DiRaddo, "Integrated numerical modeling of the blow molding process," *Polymer Engineering & Science*, vol. 39, no. 7, pp. 1223-1233, July 1999.
- [13] G. Huang and H. Huang, "Optimizing parison thickness for extrusion blow molding by hybrid method," *Journal of Materials Processing Technology*, vol. 182, no. 1-3, pp. 512-518, Feb. 2007.
- [14] M. R. Kamal, W. I. Patterson, and V. G. Gomes, "An injection molding study. Part I: Melt and barrel temperature dynamics," *Polymer Engineering & Science*, vol. 26, no. 12, pp. 854-866, July 1986.
- [15] V. G. Gomes, W. I. Patterson, and M. K. Kamal, "An injection molding study. Part II: Evaluation of alternative control strategies for melt temperature," *Polymer Engineering & Science*, vol. 26, no. 12, pp. 867-876, July 1986.
- [16] R. Dubay, A. C. Bell, and Y. P. Gupta, "Control of plastic melt temperature: A multiple input multiple output model predictive approach," *Polymer Engineering & Science*, vol. 37, no. 9, pp. 1550-1563, Sept. 1997.

- [17] R. Dubay, Y. P. Gupta, and A. C. Bell, "Predictive control of plastic melt in heated zones with insulation," *The Journal of injection molding technology*, vol. 2, no. 1, pp. 37-45, 1998.
- [18] C. Diduch, R. Dubay, and W. G. Li, "Temperature control of injection molding. Part I: Modeling and identification," *Polymer Engineering & Science*, vol. 44, no. 12, pp. 2308-2317, Dec. 2004.
- [19] R. Dubay, C. Diduch, and W. G. Li, "Temperature control in injection molding. Part II: Controller design, simulation, and implementation," *Polymer Engineering & Science*, vol. 44, no. 12, pp. 2318-2326, Dec. 2004.
- [20] A. Gerber, R. Dubay, and A. Healy, "CFD-based predictive control of melt temperature in plastic injection molding," *Applied mathematical modelling*, vol. 30, 9, pp. 884-903, Sept. 2006.
- [21] M. Anbarasan, S. J. S. Prasad, R. Meenakumari, and P. A. Balakrishnan, "Modified PID controller for avoiding overshoot in temperature of barrel heating system," in *2013 International Conference on Emerging Trends in VLSI, Embedded System, Nano Electronics and Telecommunication System (ICEVENT)*, Madras, India, 2013, pp. 1-5.
- [22] L. Tao, Y. Ke, and G. Furong, "Identification and Autotuning of Temperature-Control System With Application to Injection Molding," *IEEE Transactions on Control Systems Technology*, vol. 17, no. 6, pp. 1282-1294, May 2009.
- [23] R. Dubay, B. Pramujati, J. Han, and F. Strohmaier, "An investigation on the application of predictive control for controlling screw position and velocity on an injection molding machine," *Polymer Engineering & Science*, vol. 47, no. 4, pp. 390-399, Mar. 2007.
- [24] P. Park, C. Schaper, and T. Kailath, "Control strategy for temperature tracking in rapid thermal processing of semiconductor wafers," in *Proceedings of the 31st IEEE Conference on Decision and Control*, Tucson, AZ, 1992, pp. 2568-2573.
- [25] C. Schaper, M. Moslehi, K. Saraswat, and T. Kailath, "Control of MMST RTP: repeatability, uniformity, and integration for flexible manufacturing [ICs]," *IEEE Transactions on Semiconductor Manufacturing*, vol. 7, no. 2, pp. 202-219, May 1994.
- [26] C. Schaper, M. Moslehi, K. Saraswat, and T. Kailath, "Modeling, Identification, and Control of Rapid Thermal Processing Systems," *Journal of The Electrochemical Society*, vol. 141, no. 11, pp. 3200-3209, Nov. 1994.
- [27] C. Tian and T. Fujii, "Nonlinear system identification of rapid thermal processing," *Control Engineering Practice*, vol. 13, no. 6, pp. 681-687, June 2005.
- [28] W. Cho, T. F. Edgar, and J. Lee, "Nonlinear Model Identification for Temperature Control in Single Wafer Rapid Thermal Processing," *Industrial & Engineering Chemistry Research*, vol. 47, no. 14, pp. 4791-4796, July 2008.
- [29] S. Aranovskiy, A. Kapitonov, A. Bobtsov, A. Pyrkin, E. Zavarin, D. Davydov, R. Ortega, "Robust control of rapid thermal processes applied to vapor deposition processing," in *2014 6th International Congress on Ultra Modern Telecommunications and Control Systems and Workshops (ICUMT)*, St. Petersburg, Russia, 2014, pp. 578-583.
- [30] K. Junghwan, L. Jongyeop, J. Sanghyun, L. Sungyong, and L. Kwang Soon, "Modeling and Optimal Design of a Glass RTP System," *IEEE Transactions on Semiconductor Manufacturing*, vol. 28, no. 4, pp. 545-550, Sept. 2015.
- [31] B. Moore, "In-cycle control of the thermoforming reheat process," M.Eng. thesis, Dept. of Electrical and Computer Engineering, McGill University, Montreal, Canada, 2002.

- [32] B. Moore, P. Girard, B. Boulet, and R. DiRaddo, "In-cycle dynamics of forming operations," in *American Control Conference*, Anchorage, Alaska, 2002, pp. 3349-3350.
- [33] A. Yousefi, A. Bendada, and R. DiRaddo, "Improved modeling for the reheat phase in thermoforming through an uncertainty treatment of the key parameters," *Polymer Engineering & Science*, vol. 42, no. 5, pp. 1115-1129, May 2002.
- [34] M. Ajersch, "Modeling and real-time control of sheet reheat phase in thermoforming," M.Eng. thesis, Department and Electrical and Computer Engineering, McGill University, Montreal, Canada, 2004.
- [35] G. Gauthier, M. Ajersch, B. Boulet, A. Haurani, P. Girard, R. DiRaddo, "A new absorption based model for sheet reheat in thermoforming," in *Proceedings of the Annual Technical Conference (ANTEC 2005)*, Cincinnati, OH, 2005, pp. 353-357.
- [36] V. Thomson, N. Bhuiyan, P. Girard, S. Khan. (2012). *Improved mathematical modeling for the sheet reheat phase during thermoforming*, Society of Plastics Engineers [Online]. Available: www.4spepro.org/pdf/003906/003906.pdf.
- [37] S. Khan, P. Girard, N. Bhuiyan, V. Thomson, "Improved mathematical modeling for the sheet reheat phase during thermoforming," *Polymer Engineering & Science*, vol. 52, no. 3, pp. 625-636, Mar. 2012.
- [38] B. Boulet. (Sept. 2011). *MAGI-THERM Industrial Controller for Thermoforming Operations* [Online]. Available: <http://www.magitherm.com>
- [39] M. M. I. Chy, B. Boulet, and A. Haidar, "A model predictive controller of plastic sheet temperature for a thermoforming process," in *American Control Conference (ACC)*, San Francisco, Cal, 2011, pp. 4410-4415.
- [40] M. M. I. Chy and B. Boulet, "A New Method for Estimation and Control of Temperature Profile over a Sheet in Thermoforming Process," in *Industry Applications Society Annual Meeting (IAS), 2010 IEEE*, 2010, pp. 1-8.
- [41] M. M. I. Chy and B. Boulet, "Estimation and control of temperature profile over a sheet in thermoforming process using non-equidistant temperature sensor," in *2011 IEEE Industry Applications Society Annual Meeting (IAS)*, Orlando, FL, 2011, pp. 1-8.
- [42] G. Gauthier, "Terminal iterative learning for cycle-to-cycle control of industrial processes," Ph.D. Dissertation, Department of Electrical and Computer Engineering, McGill University, 2008.
- [43] G. Gauthier and B. Boulet, "Robust design of terminal ILC with H-infinity mixed sensitivity approach for a thermoforming oven," *J. Control Sci. Eng.*, vol. 2008, no. 8, pp. 1-6, 2008.
- [44] O. J. Smith, "A controller to overcome dead time," *ISA Journal*, vol. 6, no. 2, pp. 28-33, 1959.
- [45] L. Roca, J. L. Guzman, J. E. Normey-Rico, M. Berenguel, L. Yebra, "Filtered Smith predictor with feedback linearization and constraints handling applied to a solar collector field," *Solar Energy*, vol. 85, no. 5, pp. 1056-1067, May 2011.
- [46] A. Núñez-Reyes, J. E. Normey-Rico, C. Bordons, and E. F. Camacho, "A Smith predictive based MPC in a solar air conditioning plant," *Journal of Process Control*, vol. 15, no. 1, pp. 1-10, Feb. 2005.
- [47] G. Díaz, M. Sen, K. T. Yang, and R. L. McClain, "Dynamic prediction and control of heat exchangers using artificial neural networks," *International Journal of Heat and Mass Transfer*, vol. 44, no. 9, pp. 1671-1679, May 2001.

- [48] K. Watanabe and M. Ito, "A process-model control for linear systems with delay," *IEEE Transactions on Automatic Control*, vol. 26, no. 6, pp. 1261-1269, Dec. 1981.
- [49] K. J. ASTROM, C. C. Hang, and B. Lim, "A new Smith predictor for controlling a process with an integrator and long dead-time," *IEEE transactions on Automatic Control*, vol. 39, no. 2, pp. 343-345, 1994.
- [50] W. Zhang, Y. Sun, and X. Xu, "Two degree-of-freedom Smith predictor for processes with time delay," *Automatica*, vol. 34, no. 10, pp. 1279-1282, Oct. 1998.
- [51] M. Bellet, M. H. Vantal, and B. Monasse, "Thermal Effects in the Numerical Simulation of the Thermoforming of Multilayered Polymer Sheets," *International Polymer Processing*, vol. 13, no. 3, pp. 299-308, Sept. 1998.
- [52] M.-H. Vantal, B. Monasse, and M. Bellet, "Numerical simulation of the thermoforming of multi-layer polymer sheets," in *Proceedings of 5th Int. Conf. on Numerical Methods in Industrial Forming Processes*, Ithaca, NY, United States, 1995, pp. 1089-1095.
- [53] R. De Keyser and J. Donald, "Model based predictive control in RTP semiconductor manufacturing," in *Proceedings of the 1999 IEEE International Conference on Control Applications*, 1999, Hawaii, US, pp. 1636-1641.
- [54] E. Dassau, B. Grosman, and D. R. Lewin, "Modeling and temperature control of rapid thermal processing," *Computers & Chemical Engineering*, vol. 30, no. 4, pp. 686-697, Feb. 2006.
- [55] R. Z. Freire, G. H. C. Oliveira, and N. Mendes, "Predictive controllers for thermal comfort optimization and energy savings," *Energy and Buildings*, vol. 40, no. 7, pp. 1353-1365, 2008.
- [56] M. Yudong, F. Borrelli, B. Hency, B. Coffey, S. Bengea, P. Haves, "Model Predictive Control for the Operation of Building Cooling Systems," *IEEE Transactions on Control Systems Technology*, vol. 20, no. 3, pp. 796-803, Mar, 2012.
- [57] W. Maalouf, "Robust Control in Thermoforming," M.Eng. thesis, Department of Electrical and Computer Engineering, McGill University, 2008.
- [58] N. Aouf, "Robust control techniques for aerospace vehicles," Ph.D. Dissertation, Department of Electrical and Computer Engineering, Montreal, Canada, 2001.
- [59] F. Wu, "Control of linear parameter varying systems," Ph.D. Dissertation, Department of Electrical Engineering, University of California at Berkeley, Berkley, CA, 1995.
- [60] F. Wu and K. Dong, "Gain-scheduling control of LFT systems using parameter-dependent Lyapunov functions," *Automatica*, vol. 42, no. 1, pp. 39-50, 2006.
- [61] P. Apkarian and R. J. Adams, "Advanced gain-scheduling techniques for uncertain systems," *IEEE Transactions on Control Systems Technology*, vol. 6, no. 1, pp. 21-32, 1998.
- [62] P. Apkarian, P. Gahinet, and G. Becker, "Self-scheduled H^∞ control of linear parameter-varying systems: a design example," *Automatica*, vol. 31, no. 9, pp. 1251-1261, 1995.
- [63] P. Apkarian, P. C. Pellanda, and H. D. Tuan, "Mixed H^2/H^∞ multi-channel linear parameter-varying control in discrete time," *Systems & Control Letters*, vol. 41, no.5, pp. 333-346, 2000.
- [64] E. Atam, D. Patteeuw, S. P. Antonov, L. Helsen, "Optimal Control Approaches for Analysis of Energy Use Minimization of Hybrid Ground-Coupled Heat Pump Systems," *IEEE Transactions on Control Systems Technology*, to be published.

- [65] L. Whei-Min, C. M. Hong, C. M. Huang, T. C. Ou, "Hybrid Control of a Wind Induction Generator Based on Grey-Elman Neural Network," *IEEE Transactions on Control Systems Technology*, vol. 21, no. 6, pp. 2367-2373, Nov. 2013.
- [66] G. Karer, G. Music, I. Skrjanc, and B. Zupancic, "Hybrid fuzzy model-based predictive control of temperature in a batch reactor," *Computers & Chemical Engineering*, vol. 31, no. 12, pp. 1552-1564, Jan. 2007.
- [67] A. Shamiri, S. W. Wong, M. F. Zamil, M. A. Hussain, and N. Mostoufi, "Modified two-phase model with hybrid control for gas phase propylene copolymerization in fluidized bed reactors," *Chemical Engineering Journal*, vol. 264, pp. 706-719, Mar. 2015.
- [68] N. H. McClamroch and I. Kolmanovsky, "Performance benefits of hybrid control design for linear and nonlinear systems," *Proceedings of the IEEE*, vol. 88, no. 7, pp. 1083-1096, July 2000.
- [69] A. Franco and D. Rivas, "Optimization of Multiphase Aircraft Trajectories Using Hybrid Optimal Control," *Journal of Guidance, Control, and Dynamics*, vol. 38, no. 3, pp. 452-467, Mar. 2015.
- [70] M. Soler, A. Olivares, and E. Staffetti, "Hybrid Optimal Control Approach to Commercial Aircraft Trajectory Planning," *Journal of Guidance, Control, and Dynamics*, vol. 33, no. 3, pp. 985-991, May 2010.
- [71] K. Namwook, C. Sukwon, and P. Huei, "Optimal Control of Hybrid Electric Vehicles Based on Pontryagin's Minimum Principle," *IEEE Transactions on Control Systems Technology*, *IEEE Transactions on*, vol. 19, no. 5, pp. 1279-1287, 2011.
- [72] A. Pakniyat and P. E. Caines, "The gear selection problem for electric vehicles: An optimal control formulation," in *13th International Conference on Control Automation Robotics & Vision (ICARCV)*, Singapore, 2014, pp. 1261-1266.
- [73] F. H. Clarke and R. B. Vinter, "Optimal Multiprocesses," *SIAM Journal on Control and Optimization*, vol. 27, no. 5, pp. 1072-1091, 1989.
- [74] M. Garavello and B. Piccoli, "Hybrid necessary principle," *SIAM Journal on Control and Optimization*, vol. 43, no. 5, pp. 1867-1887, Mar. 2005.
- [75] H. J. Sussmann, "A maximum principle for hybrid optimal control problems," in *13th International Conference on Decision and Control*, Pheonix, AZ, 1999, pp. 425-430.
- [76] M. Shahid Shaikh and P. E. Caines, "On the Hybrid Optimal Control Problem: Theory and Algorithms," *Automatic Control, IEEE Transactions on*, vol. 52, no. 9, pp. 1587-1603, Sept. 2007.
- [77] F. Taringoo and P. E. Caines, "Gradient geodesic and Newton geodesic HMP algorithms for the optimization of hybrid systems," *Annual Reviews in Control*, vol. 35, no. 2, pp. 187-198, Dec. 2011.
- [78] A. Pakniyat and P. E. Caines, "The Hybrid Minimum Principle in the presence of switching costs," in *2013 IEEE 52nd Annual Conference on Decision and Control (CDC)*, Florence, Italy, 2013, pp. 3831-3836.
- [79] X. Xu and P. J. Antsaklis, "Optimal control of switched systems based on parameterization of the switching instants," *Automatic Control, IEEE Transactions on*, vol. 49, no. 1, pp. 2-16, Jan. 2004.
- [80] A. Pakniyat and P. E. Caines, "Time Optimal Hybrid Minimum Principle and the Gear Changing Problem for Electric Vehicles," *IFAC-PapersOnLine*, vol. 48, no. 27, pp. 187-192, 2015.

- [81] Y. Wang, K. Ueda, and S. A. Bortoff, "A Hamiltonian approach to compute an energy efficient trajectory for a servomotor system," *Automatica*, vol. 49, no. 12, pp. 3550-3561, Jan. 2013.
- [82] J. Koller, A. G. Colin, B. Besselink, and K. H. Johansson, "Fuel-efficient control of merging maneuvers for heavy-duty vehicle platooning," in *Proceedings of the 18th IEEE International Conference on Intelligent Transportation Systems*, Las Palmas, Spain, 2015.
- [83] Q. Zhang and M. Canova, "Modeling air conditioning system with storage evaporator for vehicle energy management," *Applied Thermal Engineering*, vol. 87, pp. 779-787, Aug. 2015.
- [84] V. Kumar, "Estimation of absorptivity and heat flux at the reheat phase of thermoforming process," M.S. Thesis, Department of Mechanical Engineering, McGill University, Montreal, Canada, 2005.
- [85] M. G. Marangou, "Thermoforming of polystyrene sheets deformation and tensile properties," M.S. Thesis, Department of Chemical Engineering, McGill University, Montreal, Canada, 1986.
- [86] J. Tang, "Finite element analysis of nonlinear viscoelastic membranes in relation to thermoforming," M.S. Thesis, Department of Civil Engineering, McGill University, Montreal, Canada, 1991.
- [87] R. L. Wu, "Finite element and experimental analyses of the inflation of membranes in relation to thermoforming," M.S. Thesis, Department of Mechanical Engineering, McGill University, Montreal, Canada, 1984.
- [88] C.-T. Chen, *Linear system theory and design*, 3rd ed., New York, NY: Oxford University Press, 1999, pp. 247-268.
- [89] J. Florian, *Practical Thermoforming: Principles and Applications*, 2nd ed., New York: M. Dekker, 1996.
- [90] F. Erchiqui, M. Souli, and R. B. Yedder, "Nonisothermal finite-element analysis of thermoforming of polyethylene terephthalate sheet: Incomplete effect of the forming stage," *Polymer Engineering & Science*, vol. 47, no. 12, pp. 2129-2144, 2007.
- [91] P. News. (Mar. 08, 2011). *FYI Charts* [Online]. Available: <http://www.plasticnews.com/fyi-charts/index.html>
- [92] R. Modirnia and B. Boulet, "Model-based virtual sensors and core temperature observers in thermoforming applications," in *Industry Applications Society Annual Meeting (IAS), 2011 IEEE*, Orlando, Fl, 2011, pp. 1-8.
- [93] D. Seborg, T. F. Edgar, and D. Mellichamp, *Process dynamics & control*, 2nd ed., New York: John Wiley & Sons, 2006.
- [94] IHS Inc. (Sept. 2013). *America's New Energy Future: The Unconventional Oil and Gas Revolution and the US Economy*. Available: <http://www.ihs.com/info/ecc/a/americas-new-energy-future-report-vol-3.aspx>
- [95] R. Modirnia and B. Boulet, "Model-Based Virtual Sensors and Core-Temperature Observers in Thermoforming Applications," *Industry Applications, IEEE Transactions on*, vol. 49, no. 2, pp. 721-730, Feb. 2013.
- [96] R. Modirnia and B. Boulet, "Application of the Watanabe-modified Smith predictor control technique in thermoforming," in *2012 American Control Conference (ACC)*, Montreal, Canada, 2012, pp. 6448-6454.

- [97] R. Fletcher, *Practical methods of optimization*, 2nd ed., New York: John Wiley & Sons, 2013.
- [98] L. Wang, *Model predictive control system design and implementation using MATLAB®*, London: Springer Science & Business Media, 2009.
- [99] D. Dimitrov, P.B. Wieber, O. Stasse, H. J. Ferreau, H. Diedam, "An Optimized Linear Model Predictive Control Solver," in *Recent Advances in Optimization and its Applications in Engineering*, M. Diehl, F. Glineur, E. Jarlebring, and W. Michiels, Eds., New York: Springer, 2010, pp. 309-318.
- [100] S. A. Ashter, *Thermoforming of single and multilayer laminates plastic films technologies, testing, and applications*, Waltham, MA: William Andrew, 2014.
- [101] R. Modirnia, B. Boulet, "Modeling and Model Predictive Control of Multilayered Plastic Sheets in Thermoforming", submitted for publication.
- [102] A. Bensoussan and J. Menaldi, "Hybrid control and dynamic programming," *Dynamics of Continuous Discrete and Impulsive Systems*, vol. 3, no. 4, pp. 395-442, 1997.
- [103] M. S. Branicky, V. S. Borkar, and S. K. Mitter, "A unified framework for hybrid control: model and optimal control theory," *IEEE Transactions on Automatic Control*, vol. 43, no. 1, pp. 31-45, 1998.
- [104] P. E. Caines, F. H. Clarke, X. Liu, and R. B. Vinter, "A Maximum Principle for Hybrid Optimal Control Problems with Pathwise State Constraints," in *2006 45th IEEE Conference on Decision and Control*, San Diego, CA, 2006, pp. 4821-4825.
- [105] J. Lygeros, "On reachability and minimum cost optimal control," *Automatica*, vol. 40, no. 6, pp. 917-927, 2004.
- [106] A. Pakniyat and P. E. Caines, "On the relation between the Minimum Principle and Dynamic Programming for Hybrid systems," in *2014 IEEE 53rd Annual Conference on Decision and Control (CDC)*, 2014, pp. 19-24.
- [107] F. Taringoo and P. Caines, "On the Optimal Control of Impulsive Hybrid Systems on Riemannian Manifolds," *SIAM Journal on Control and Optimization*, vol. 51, no. 4, pp. 3127-3153, Jan. 2013.
- [108] S. Dharmatti and M. Ramaswamy, "Hybrid Control Systems and Viscosity Solutions," *SIAM Journal on Control and Optimization*, vol. 44, no. 4, pp. 1259-1288, 2005.
- [109] I. M. Ross, "A Beginner's Guide to DIDO (Ver. 7.3), A MATLAB Application Package for Solving Optimal Control Problems," Elissar LLC, Monterey, California, 2007.
- [110] I. M. Ross and F. Fahroo, "Legendre Pseudospectral Approximations of Optimal Control Problems," in *New Trends in Nonlinear Dynamics and Control and their Applications*. vol. 295, W. Kang, C. Borges, and M. Xiao, Eds., Berlin: Springer Berlin Heidelberg, 2003, pp. 327-342.
- [111] I. M. Ross and F. Fahroo, "Pseudospectral Knotting Methods for Solving Nonsmooth Optimal Control Problems," *Journal of Guidance, Control, and Dynamics*, vol. 27, no. 3, pp. 397-405, May 2004.
- [112] D. Gay, *Composite materials: design and applications*, Boca Ranton, Florida: CRC press, 2014.
- [113] É. Talbot, P. Hubert, M. Dubé, and A. Yousefpour, "Optimization of thermoplastic composites resistance welding parameters based on transient heat transfer finite element modeling," *Journal of Thermoplastic Composite Materials*, vol. 26, no. 5, pp. 699-717, June 2013.

- [114] A. Levy, S. Le Corre, and I. Fernandez Villegas, "Modeling of the heating phenomena in ultrasonic welding of thermoplastic composites with flat energy directors," *Journal of Materials Processing Technology*, vol. 214, no. 7, pp. 1361-1371, July 2014.
- [115] K. Karjust, M. Pohlak, and J. Majak, "Technology Route Planning of Large Composite Parts," *International Journal of Material Forming*, vol. 3, no. 1, pp. 631-634, Apr. 2010.
- [116] D. Kipp, *Plastic Material Data Sheets*, Blacksburg, VA: MatWeb, Division of Automation Creation, 2010.
- [117] M. Sepe. (2015). *MATERIALS: The Trouble with Data Sheets*, Plastics Technology [Online]. Available: www.ptonline.com/columns/materials-the-trouble-with-data-sheets
- [118] R. Krache and I. Debah, "Some Mechanical and Thermal Properties of PC/ABS Blends," *Materials Sciences and Applications*, vol. 2, no. 5, pp. 404-410, May 2011.
- [119] K. Kaniappan and S. Latha, "Certain Investigations on the Formulation and Characterization of Polystyrene / Poly(methyl methacrylate) Blends," *International Journal of ChemTech Research*, vol. 3, no. 2, pp. 708-717, Apr. 2011.
- [120] American Chemical Society National Historic Chemical Landmarks. (Mar. 2016). Polypropylene and High-density Polyethylene. [Online]. Available: <http://www.acs.org/content/acs/en/education/whatischemistry/landmarks/polypropylene.html>
- [121] P. Alvarado, "Steel vs. Plastics: The Competition for Light-Vehicle Fuel Tanks," *The Journal of the Materials, Metals & Materials Society*, vol. 48, no. 7, pp. 22-25, 1996.
- [122] Polyvance. (2016). *PLASTIC IDENTIFICATION* [Online]. Available: www.polyvance.com/identify.php

Appendix A The Industrial Thermoforming Machine Simulator

In this Appendix, we describe the thermoforming simulator used to evaluate the performance of the methods and algorithms presented in this thesis.

We would like to first acknowledge the efforts of the former students, working in the thermoforming research group at McGill University, for the initial development of the MATLAB/Simulink® simulator. These esteemed colleagues are: Ben Moore, Mark Ajersch, Guy Gauthier, Alexandre Boyer, Gino Lalli, and many other researchers who have immensely contributed to the advancement of this line of research.

The simulator initially developed for the thermoforming project was representative of a AAA thermoforming machine, which consisted of a total of 12 heaters (6 on top and 6 below the plastic sheet) and incorporated between 4 to 7 IR sensors depending on the type of study, as shown in [31], [34], [42].

The simulator was based on the heat transfer models presented in equations (1), (2), (3), (4), (5) presented in Chapter 2 of this thesis. The material properties of the plastic sheet, namely the density of the plastic sheet ρ , the specific heat capacity of the sheet C_p , the thermal conduction k , the emissivity ε_{eff} , and the convection coefficient h were all kept constant during the simulation, where in fact these values are temperature dependent. In order to compensate for the temperature variation of these material properties and to make sure that the heat transfer model of the plastic sheet accurately mimics the actual process, the values of the material properties had to be carefully tuned, which are within the variation range of these parameters. In [34], Ajersch conducted an experimental study, as the operating temperature range for the heaters was set from 280°C to 420°C, and reported a set of parameter tunings, which resulted in 2% accuracy comparing the model's sheet temperature response with actual experimental ones.

With regards to the heaters, which are indeed the actuators of this process, the AAA machine uses ceramic heaters as described in [34]. Moore modeled the dynamics of the heaters in [31] using a second-order model while Ajersch presented an experimental graph showcasing the heating and cooling rate dynamics of the heaters [34]. The heating rate was achieved by

setting the power of heater to 100% while the cooling rate was attained by completely shutting off the heater.

Therefore, the simulator was built based on the heat transfer equations, the set of tunings presented by Ajersch, and the experimental heating and cooling rates models representing the dynamics of the heaters. This type of simulator was successfully utilized by Gauthier in [42] to verify the functionality and performance of the cycle-to-cycle controller developed for thermoforming.

For our simulation study, we have expanded the simulator to represent a Brown rotary thermoforming machine. The Brown rotary machine is on the industrial scale because of its size, the number of heaters, and the sheet size dimensions. This simulator contains 108 heaters (54 placed on top and 54 placed on the bottom), uses ceramic heaters, and can fit plastic sheets with dimensions of up to 1.5mX2m.

This simulator consists of 20 IR (infrared) sensors (10 on top and 10 on the bottom) and 24 model-based virtual sensors (12 on top and 12 on the bottom), which were presented in Chapter 2. The configuration of the heaters, the IR, and the virtual sensors is showcased in Fig. 2.7, in which the 2D position grid of the IR sensors and the virtual sensors relative to the heaters is presented. The vertical distance between the top and bottom heaters and the plastic sheet is considered as 20 cm on each side.

In the next section we present the schematic of the simulator and will provide descriptions of different blocks.

A.1 The Thermoforming Simulator Blocks

In this section, we present the schematic of the industrial simulator. The general schematic of this simulator is based on the block diagram of the closed-loop control system presented in Fig. 2.5. Fig. A.1 shows the block schematic, originally showcased in Fig. 2.5, implemented in Simulink®. In Fig. A.1, the controller block is a discrete time model predictive controller (DTMPC) although this block is replaced in each chapter by the particular controller in study. The Simulator consists of various blocks which are listed below:

1. The “HEATERS” block: shown in red and contains the nonlinear dynamics of the heaters. The nonlinear dynamics of the heaters are: 1) the saturation limits, presented by equation (21) in Chapter 5, and 2) the heating and cooling rate saturation limits, presented by equation (23) in Chapter 5.

2. The top and bottom “Ambient Air Blocks”: shown in orange, representing the heat transfer dynamics of the ambient air, presented by equations (8) and (9) in Chapter 4.
3. The “Heating Phase Model”: shown in dark blue, representing the heating phase model of the measurement zones, which are created by the presence of IR sensors.
 - a. In Chapter 2, the heating phase model is derived from equations (1), (2), (3), (4), and (5), defined in Chapter 2.
 - b. In Chapter 3, the heating phase model is derived from equations (1), (2), (3), (4), and (5), defined in Chapter 2.
 - c. In Chapter 4, the heating phase model is derived from equations (1), (3), (4), (5), and (6), defined in Chapter 4.
 - d. In Chapter 5, the heating phase model is derived from equations (5), (6), and (7), defined in Chapter 5.

It should be noted that the nonlinearities and the absorption coefficients associated with the radiation term are incorporated in the “Heating Phase Model” block.

4. The “Virtual Heating Phase Model”: shown in light blue, representing the heating phase model of the measurement zones, which are created by the presence of virtual model-based sensors, presented in Chapter 2. The heat transfer models are incorporated in a similar fashion as stated in the “Heating Phase Model” block.
5. The “Luenberger” and “virtual Luenberger observer” blocks: shown in pink, representing the virtual core-temperature observer presented in Chapter 2.
6. The “feedback” block: shown in green, collecting the feedback data required by the controller. In the case of DTMPC, all states of the system need to be fed back (as discussed in Chapter 4). For the case of PI, Smith predictor, and hybrid optimal controllers, only the surface temperature measurements of IR and virtual sensors need to be fed back.
7. The “controller” block: shown in cyan blue. As mentioned before this block changes in every chapter. Different controller blocks will be discussed in subsequent sections.

In the following figures, we extensively uncover the schematic each of the block diagrams shown in Fig. A.1.

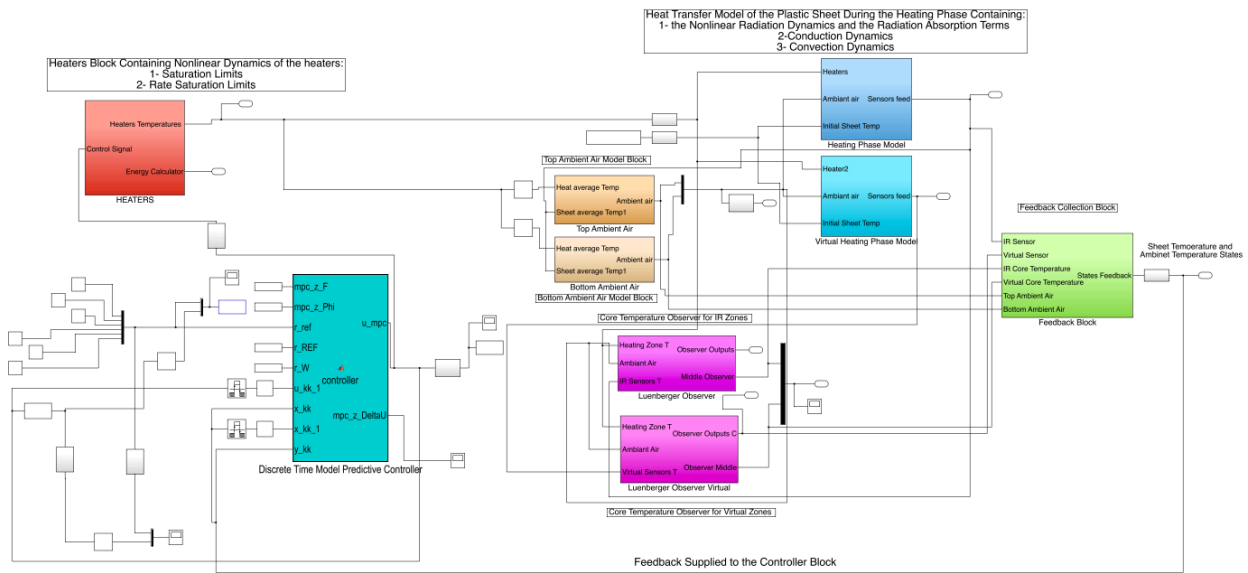


Figure A.1. The General Simulator Schematic

A.1.1 The Heaters Block

Fig. A.2 shows the contents of the “Heaters” block. As it can be seen, a saturation block is initially placed to account for the saturation dynamics defined in (21) in Chapter 5, followed by the two green and purple blocks, which are placed to model the heating and cooling rate saturation limits for each of the 108 heaters. As mentioned before, the equations for the heating and cooling rates are presented in (23) of Chapter 5. The green block takes the derivative of heaters’ temperatures and feeds them to the purple block. The purple block is shown in detail in Fig. A.3, for each heater, as the heating and cooling saturation rates are implemented.

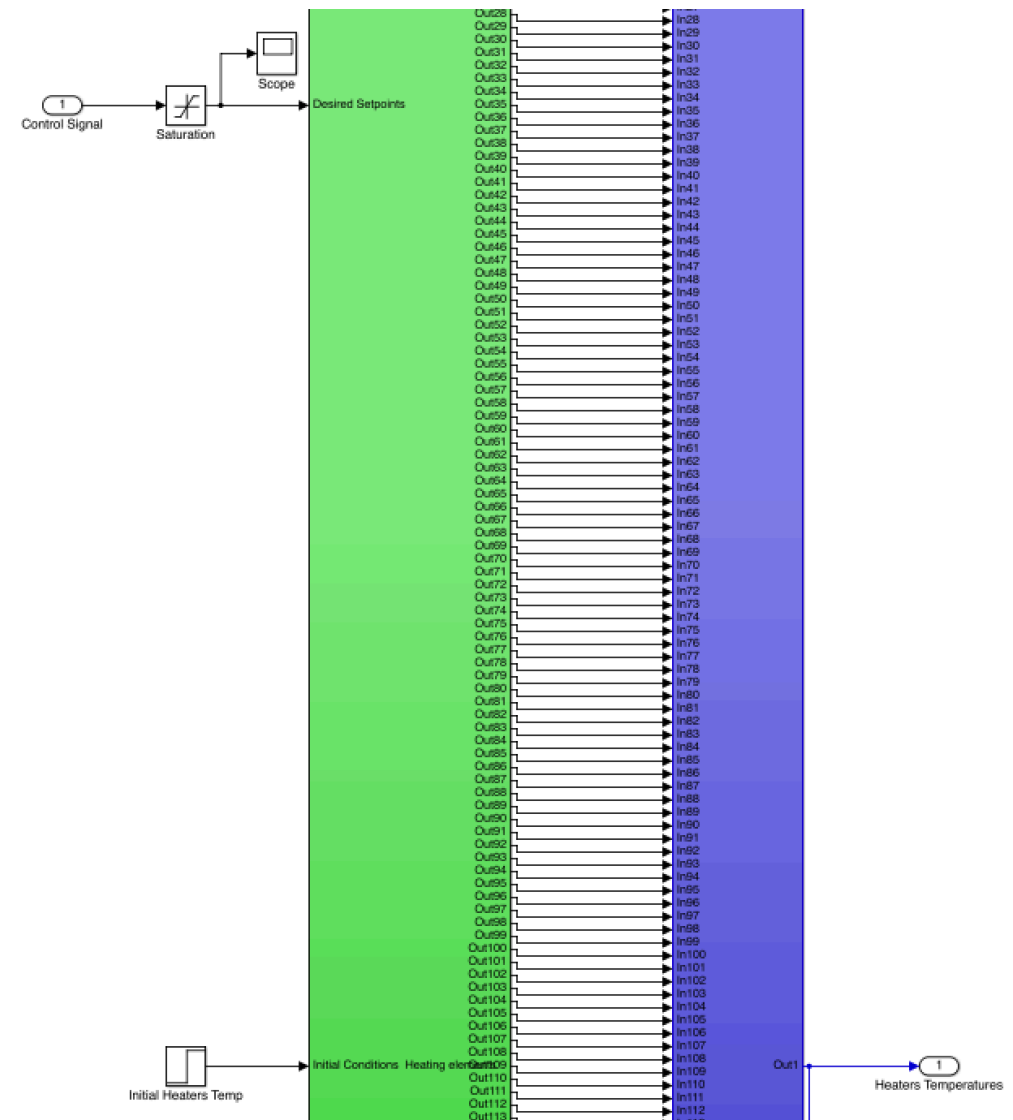


Figure A.2. The Heaters Block

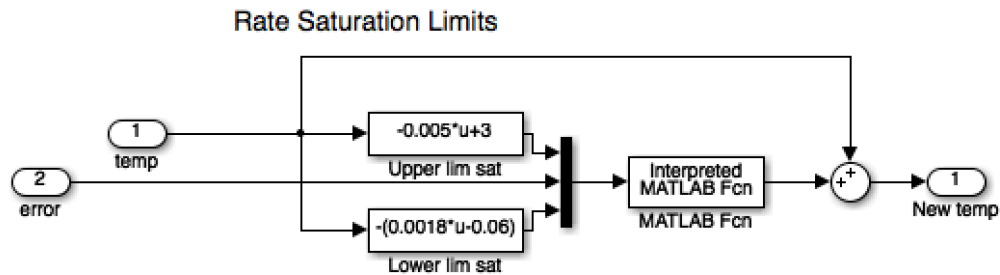


Figure A.3. Heating and Cooling rate saturation blocks

A.1.2 The Heating Phase Model Block

Fig. A.4 shows the contents inside the “Heating Phase Model” Block, and it can be observed that each measurement zone has its own block. Fig. A.5 and Fig. A.6 show the blocks inside each measurement zone block, where it is demonstrated that the measurement zone is being vertically divided into five different layers in order to achieve more accurate measurements through the depth of the plastic sheet.

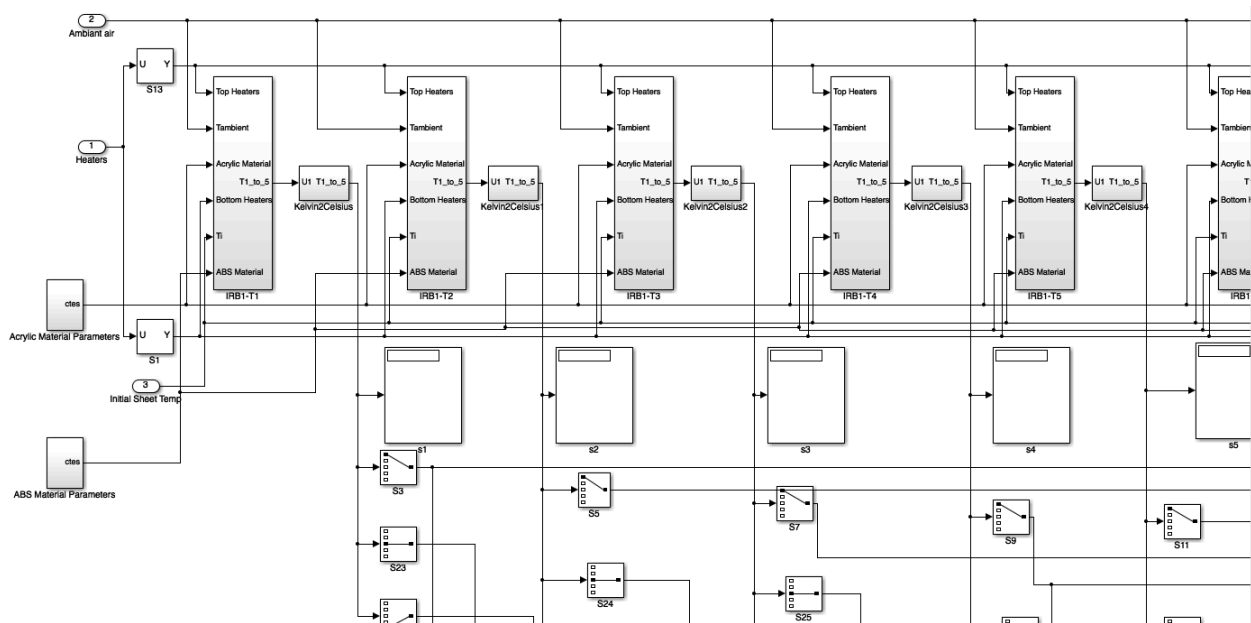


Figure A.4. The block of the heating phase model

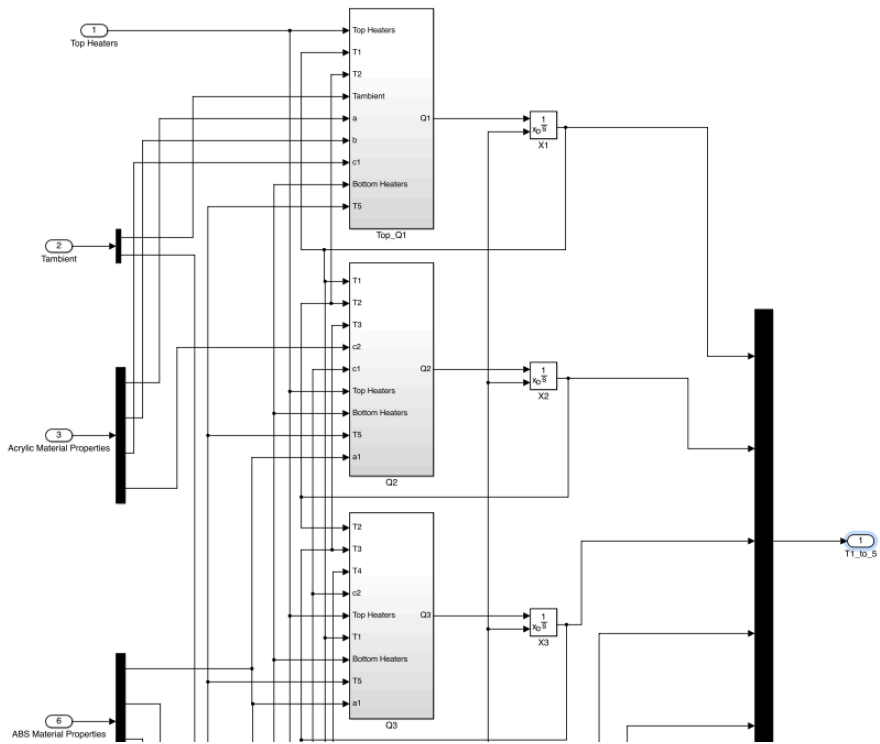


Figure A.5. The heat transfer model block for every measurement zone divided in five fictitious layers

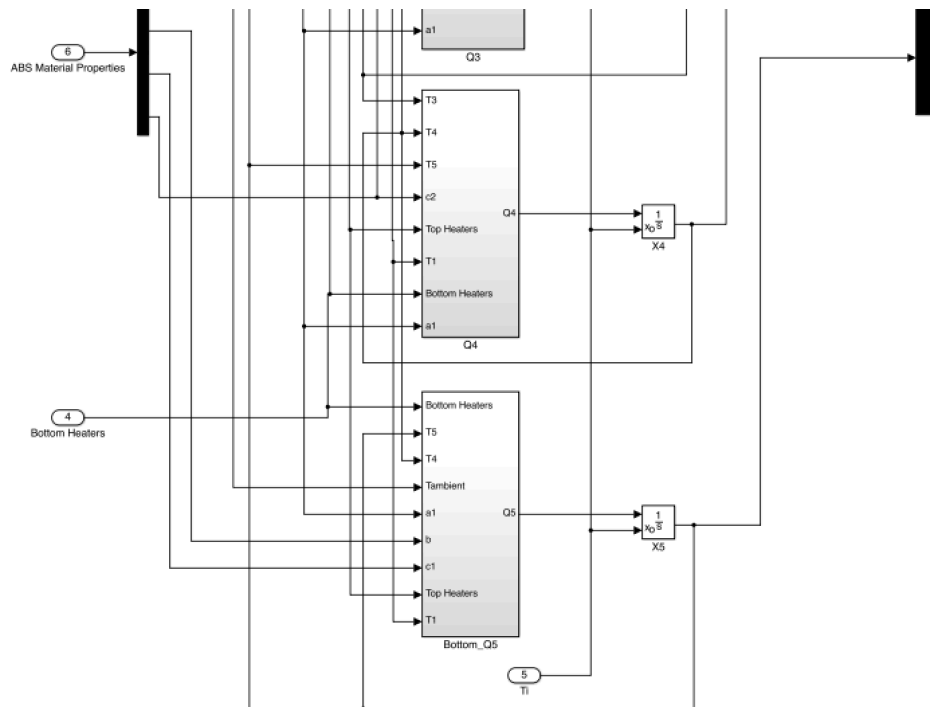


Figure A.6. The heat transfer model block for every measurement zone divided in fictitious layers (continued)

Fig. A.7, Fig. A.8, Fig. A.9, Fig. A.10, and Fig. A.11 show the contents inside of each measurement zone block. These figures implement the heat transfer models presented in each chapter as previously discussed. Fig. A.5, Fig. A.6, Fig. A.7, Fig. A.8, and Fig. A.9 show the radiation transmission coefficients being included in each of the layer blocks, as well as the nonlinearities associated with the radiation terms.

The “Virtual Heating Phase Model” block also has the same structure as the “Heating Phase Model” block although the difference is that the placement of virtual sensors is different than the placement of IR sensors.

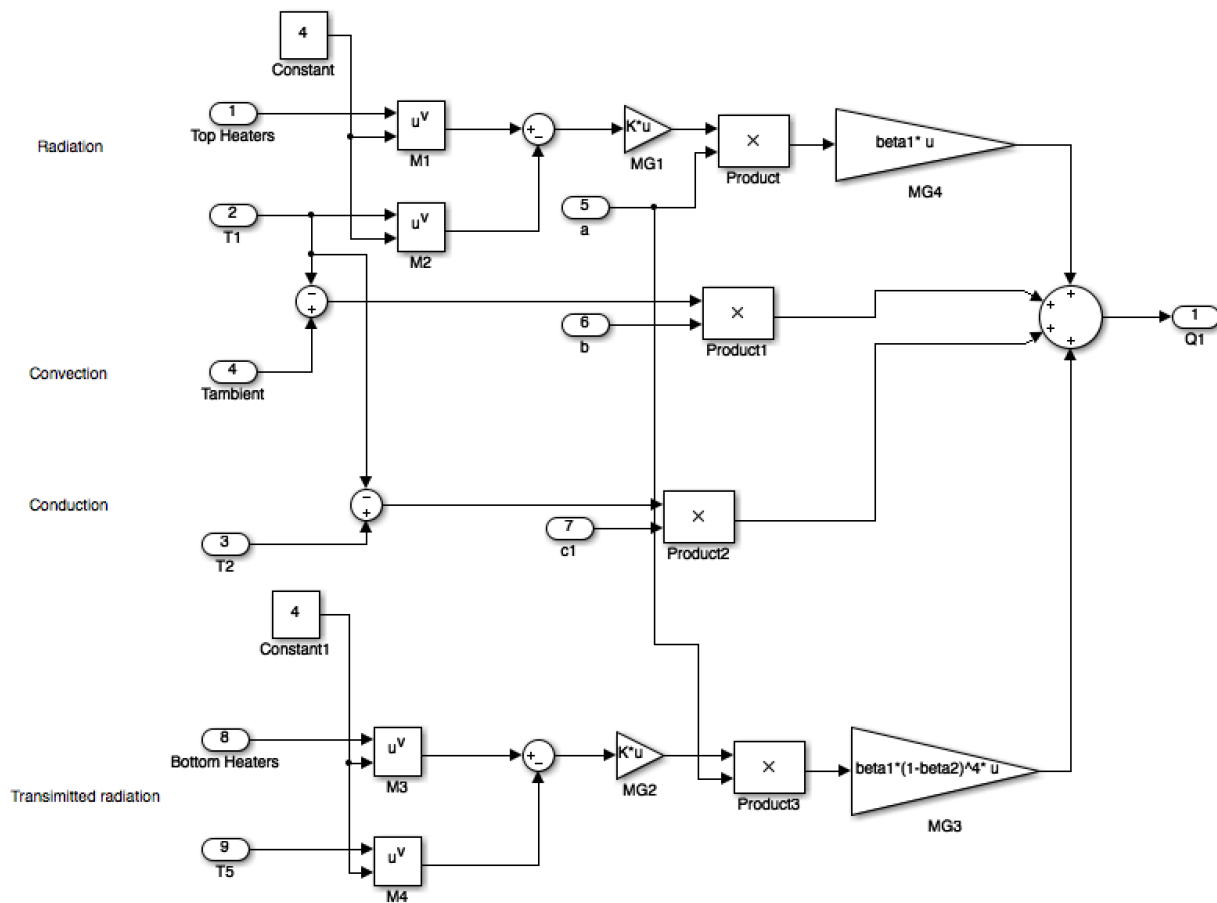


Figure A.7. The heat transfer model of the first layer

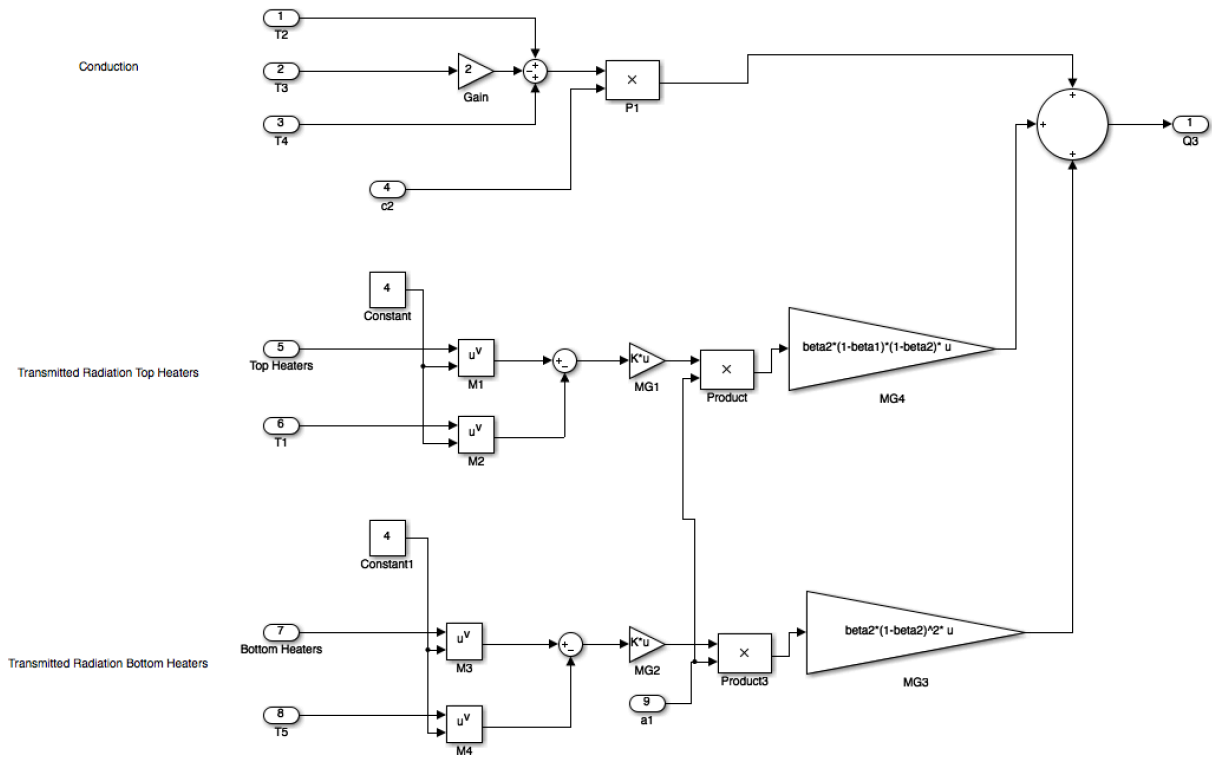


Figure A.10. The heat transfer model of the fourth layer

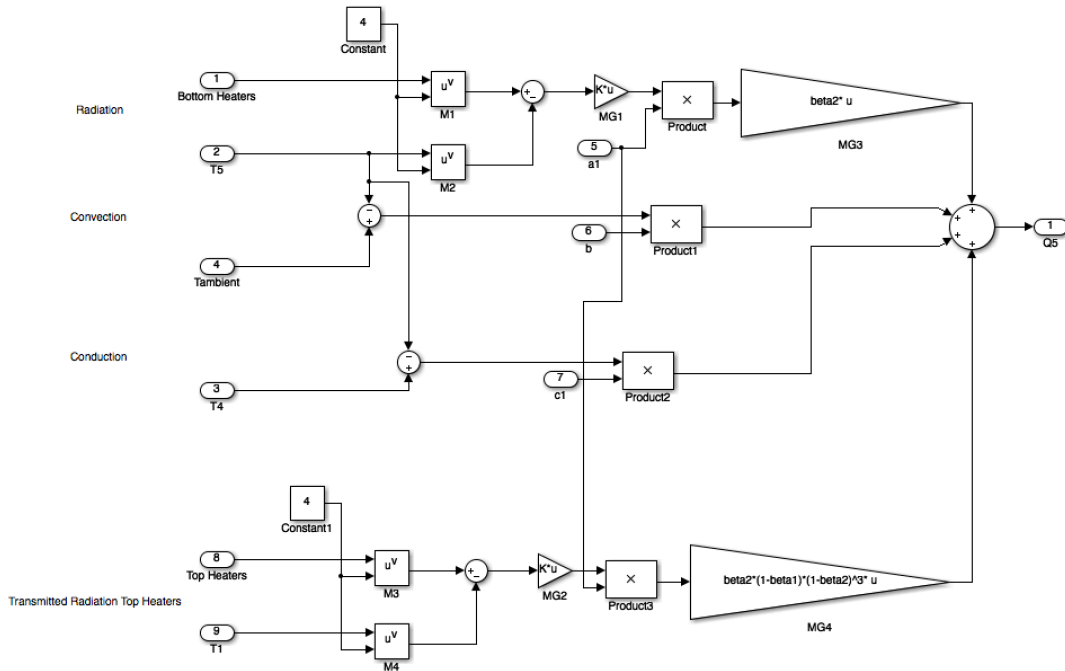


Figure A.11. The heat transfer model of the fifth layer

A.1.3 The Ambient Air Blocks

Fig. A.12 shows the contents of the “Ambient Air” blocks. This Figure exactly demonstrates the ambient air heat equation model presented in equations (8) and (9), which was presented in Chapter 4. It should be mentioned that this model contains the nonlinear radiation terms, presented in equations (8) and (9), in the Top_Q1 block (shown in Fig. A.12).

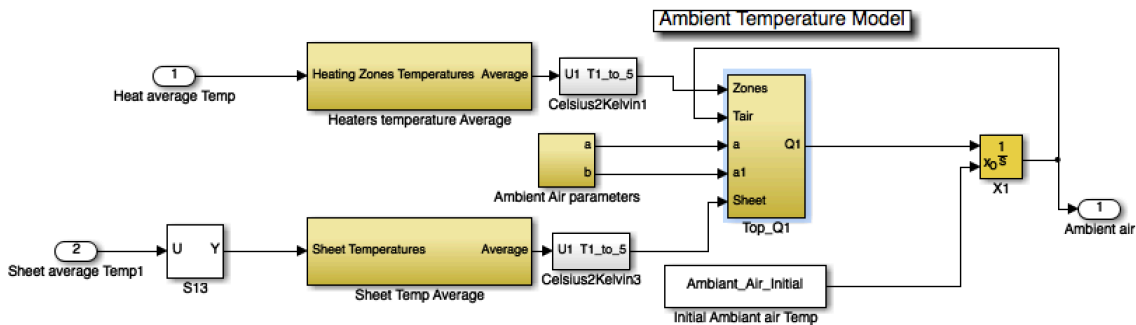


Figure A.12. Inside the ambient air block

A.1.4 Luenberger Observer Blocks

Fig. A.13 shows the contents of one of the “Luenberger Observer” blocks as the “Luenberger Observer Virtual” is shown here. The Luenberger observers are described in detail in Chapter 2. The feedback of the virtual observer block is produced by subtracting the temperature estimates generated by the virtual heating phase model from the observer outputs generated by the “Luenberger Observer Virtual” block.

With regards to the “Luenberger observer”, the feedback is produced by subtracting the temperatures generated by the heating phase model from the observer outputs generated by the “Luenberger Observer” block.

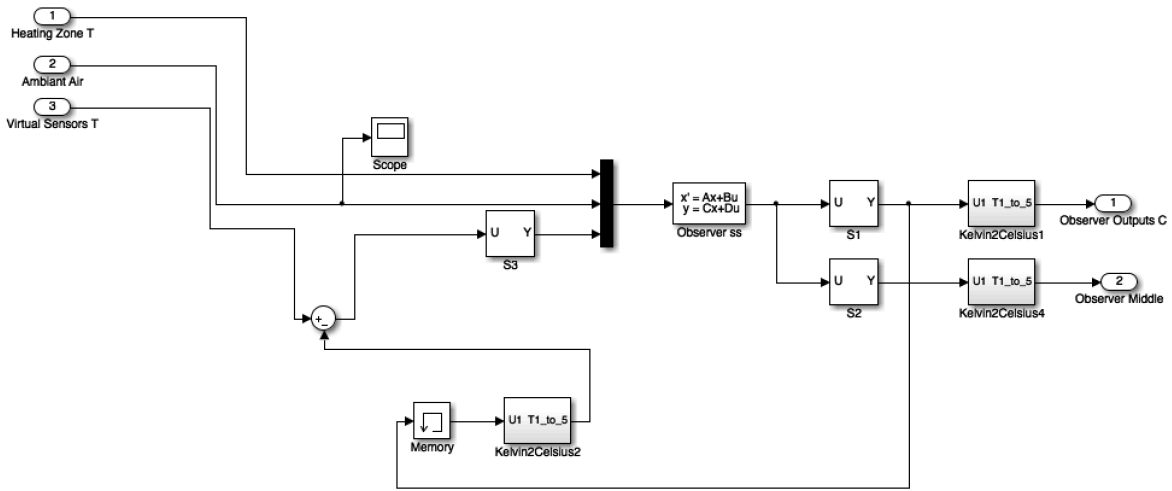


Figure A.13. Inside the observers block

A.2 Chapter 2 Simulator Blocks

In this section, we showcase the PI controller block, utilized in Chapter 2 to provide temperature tracking for the plastic sheet. The overall setup will maintain its general structure as shown in Fig. A.1, but the controller block is now replaced with PI controllers and a coupling matrix. The modified setup is shown in Fig. A.14 as the PI controller block is shown in pink.

Fig. A.15 shows the contents inside the “PI controllers” block. This Simulink® setup is extensively discussed in Chapter 2 as Fig. 2.2 explains the methodology. Essentially for each IR or virtual measurement zone, a PI controller is assigned to take the error between the feedback measurement and the input reference in order to produce a control effort for the same zone. These zone control signals are then converted into heater temperature set-points via a coupling matrix (shown in Fig. 2.2). The coupling matrix is made of view factor elements, which determine the fractions of the radiant energy exchanged between each of the heaters and the particular measurement zone on the plastic sheet. The view factors are discussed in Chapter 2, and the reader can also refer to [42] for a more extensive elaboration on the view factors. Finally,

in Fig. A.15, an anti windup feedback is also realized in order to improve the stability and performance of the PI controllers.

The contents inside the “PID Controllers” and “PID Controllers V” block are shown in Fig. A.16, as it is displayed that a distinct PI controller is designated for each of the real and virtual measurement zones. Therefore, there exist a total of 20 PI controllers for the IR measurement zones, as well as a total of 24 PI controllers for the virtual measurement zones.

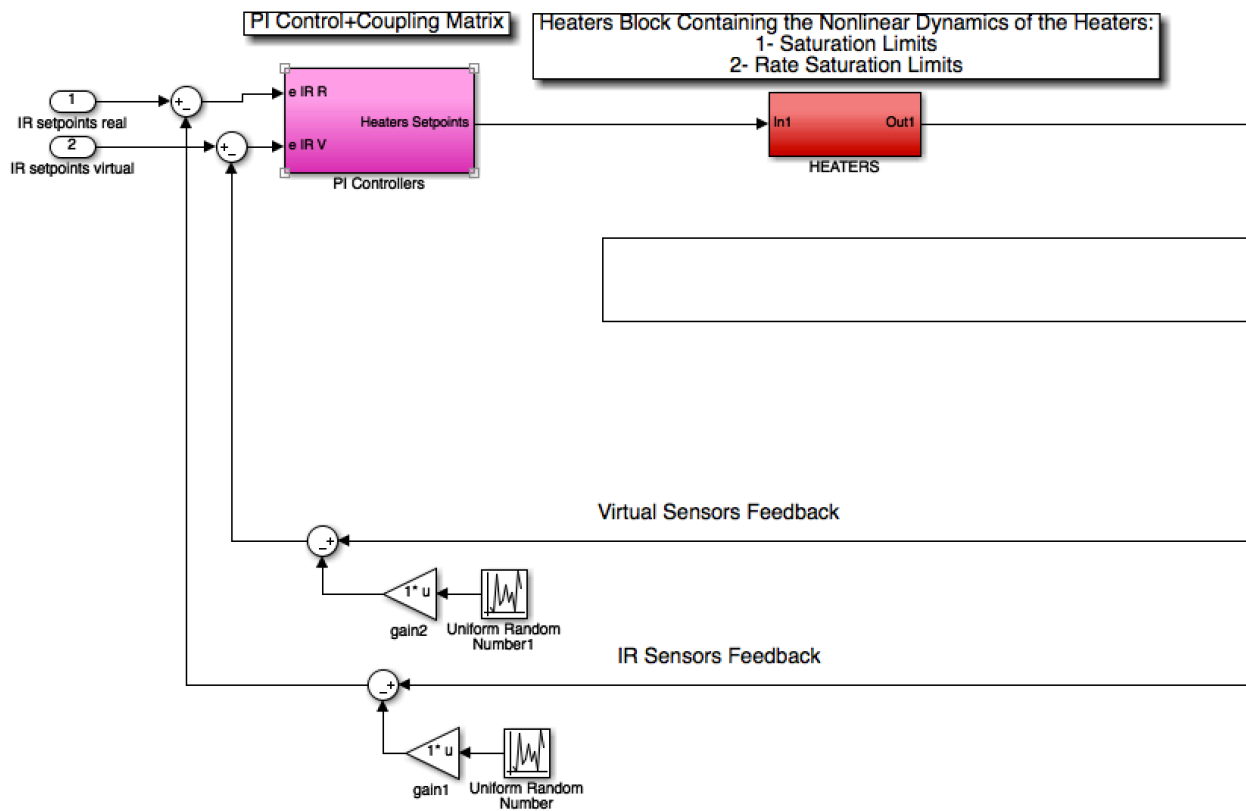


Figure A.14. The simulator in the presence of PI controllers

Controllers with Anti Windup for the IR and Virtual Sensor Measurement Zones

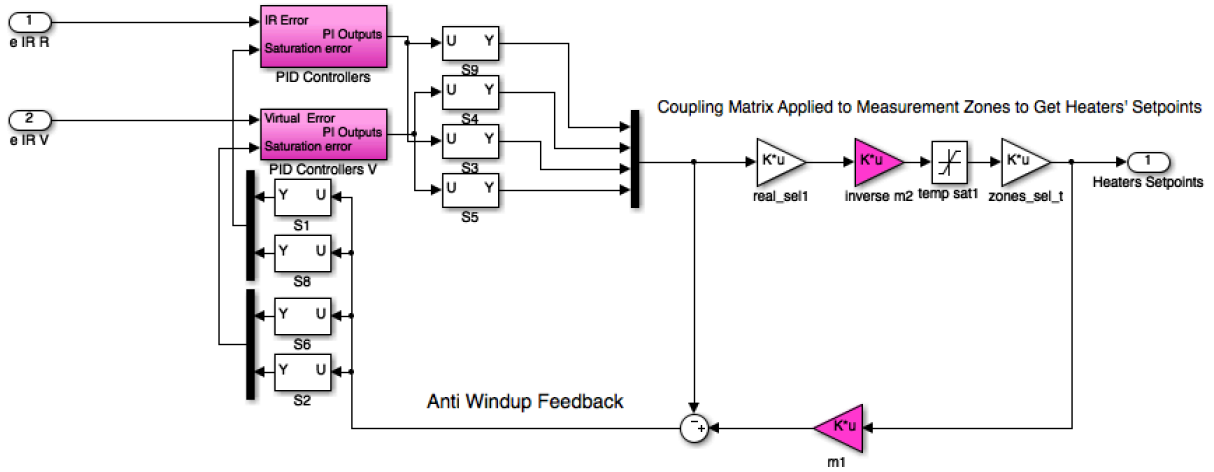


Figure A.15. Inside the PI control block

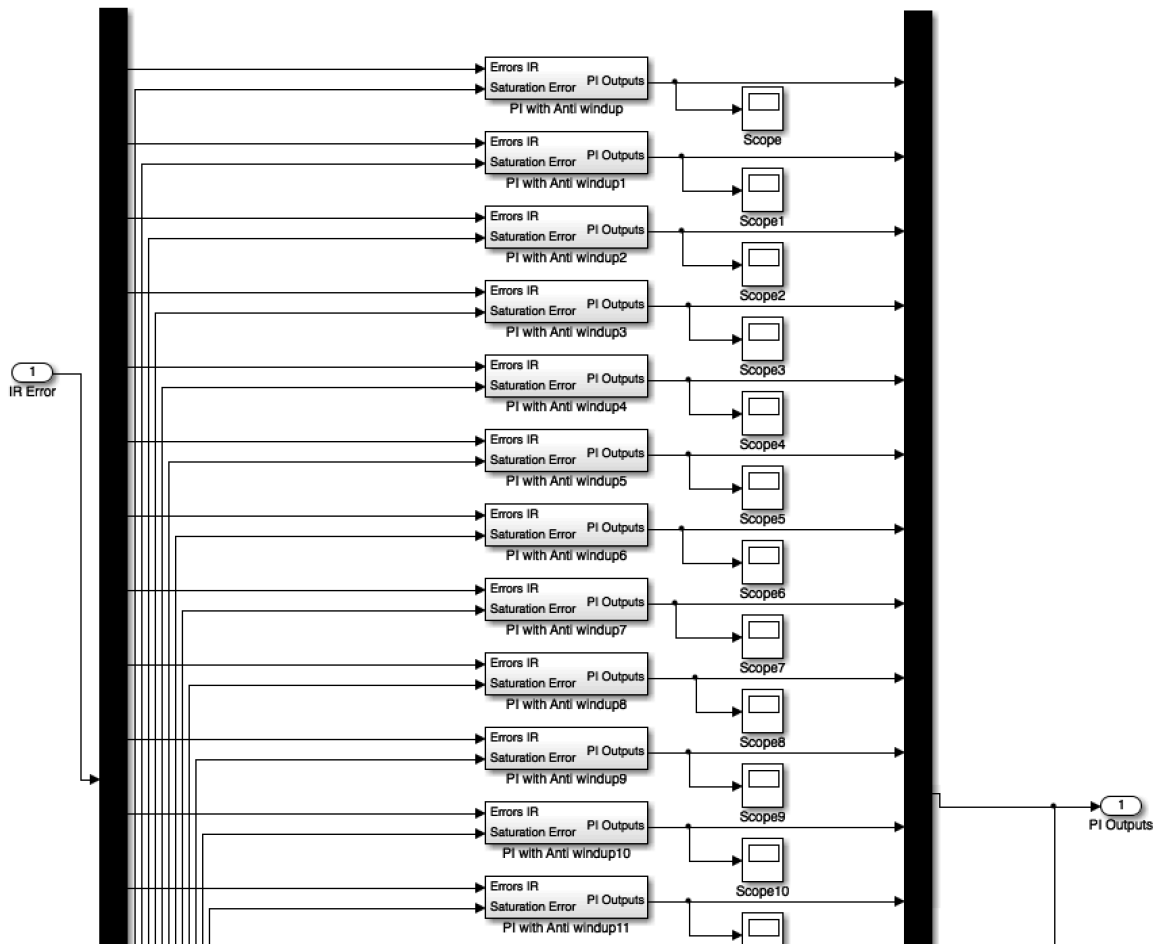


Figure A.16. The PI controllers blocks designated for each measurement zone

A.3 Chapter 3 Simulator Blocks

In this section, we present the Simulink® implementation of the Watanabe-modified Smith predictor scheme, implemented in Chapter 3. The simulation structure and the controller block are similar to the structures shown in Fig. A.14 and Fig. A.15. However, the contents inside the “PID Controllers” block and the “PID Controllers V” are different as the Watanabe-modified Smith predictor controllers replace the PI controllers. Fig. A.17 shows these Smith predictor controllers, designed for each measurement zone, while Fig. A.18 shows the contents inside each of the Smith predictor controller blocks.

The concept behind the simulation schematic shown in Fig. A.18 is extensively covered in Chapter 3. Fig. 3.2 provides an adequate explanation as to how this setup works, and the rest of the chapter discusses the design process for this control scheme. It should be noted that in Fig. A.18, the D term in the PID controller block is set to zero.

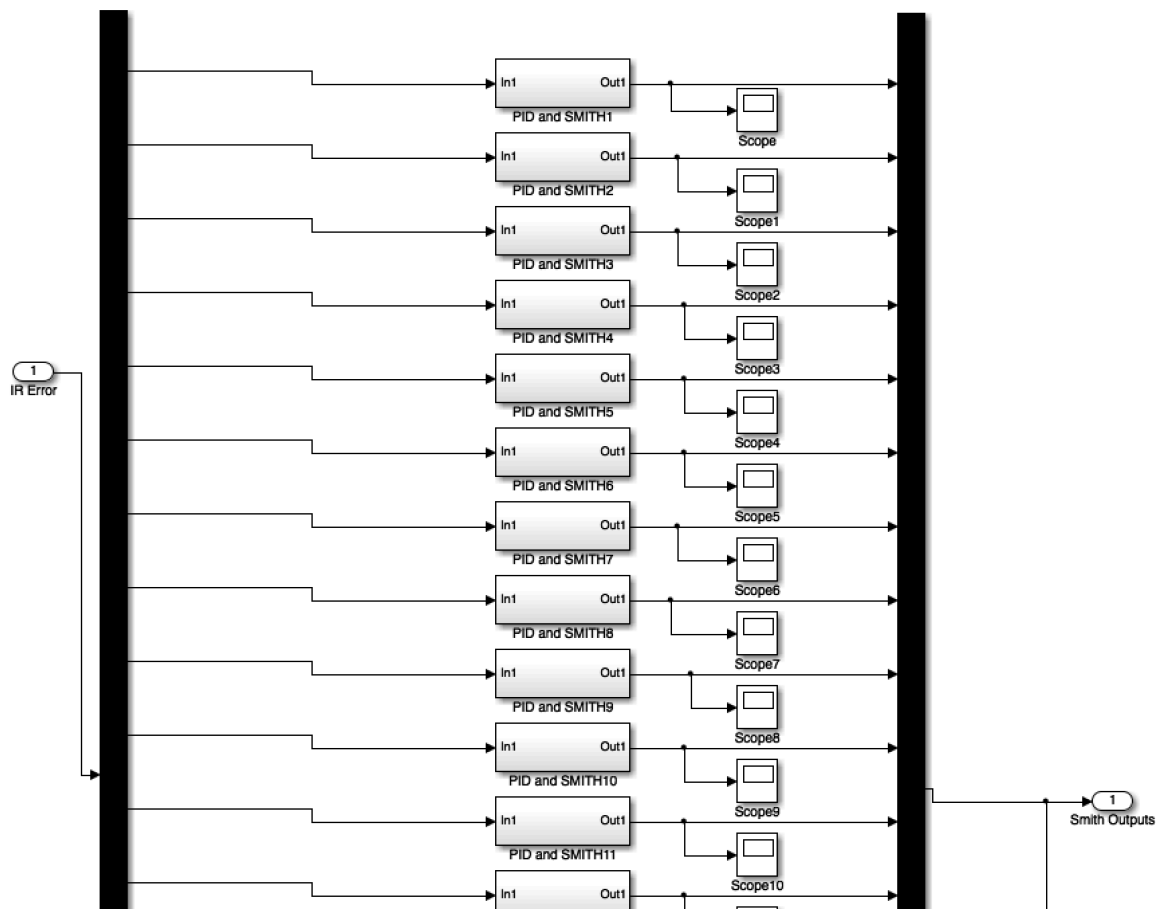


Figure A.17. The Smith predictor setup along with PI controllers designed for each measurement zone

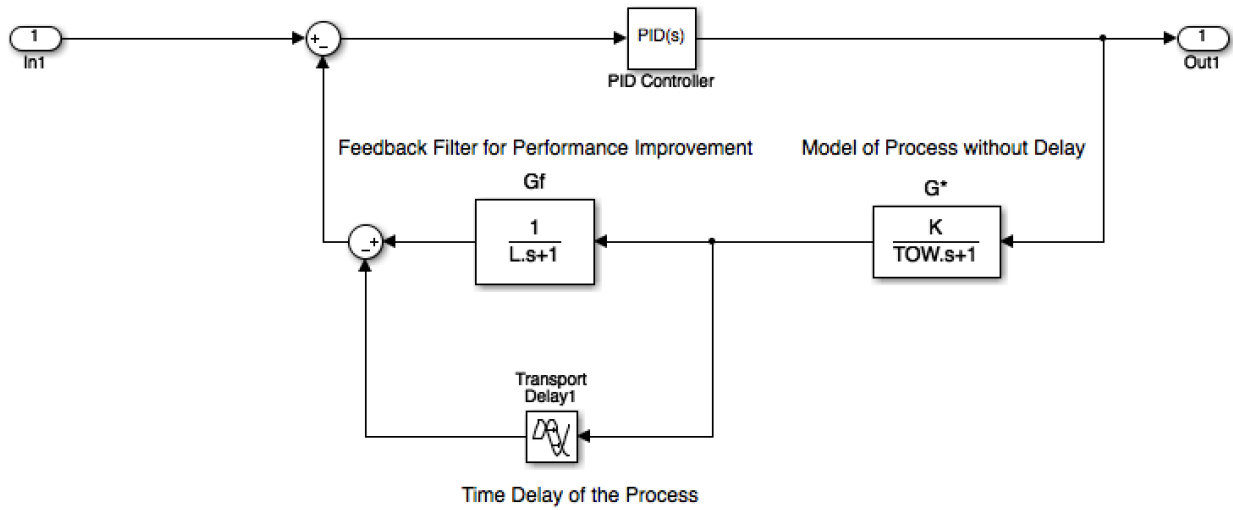


Figure A.18. Inside the block of each Smith predictor scheme

A.4 Chapter 4 Simulator Blocks

In this section, we present the Simulink® implementation of the discrete time model predictive controller (DTMPC), discussed in Chapter 4. The cyan blue block represents the DTMPC algorithm, which is coded in MATLAB and is applied to Simulink® in real-time via the “Discrete Time Model Predictive Controller” block.

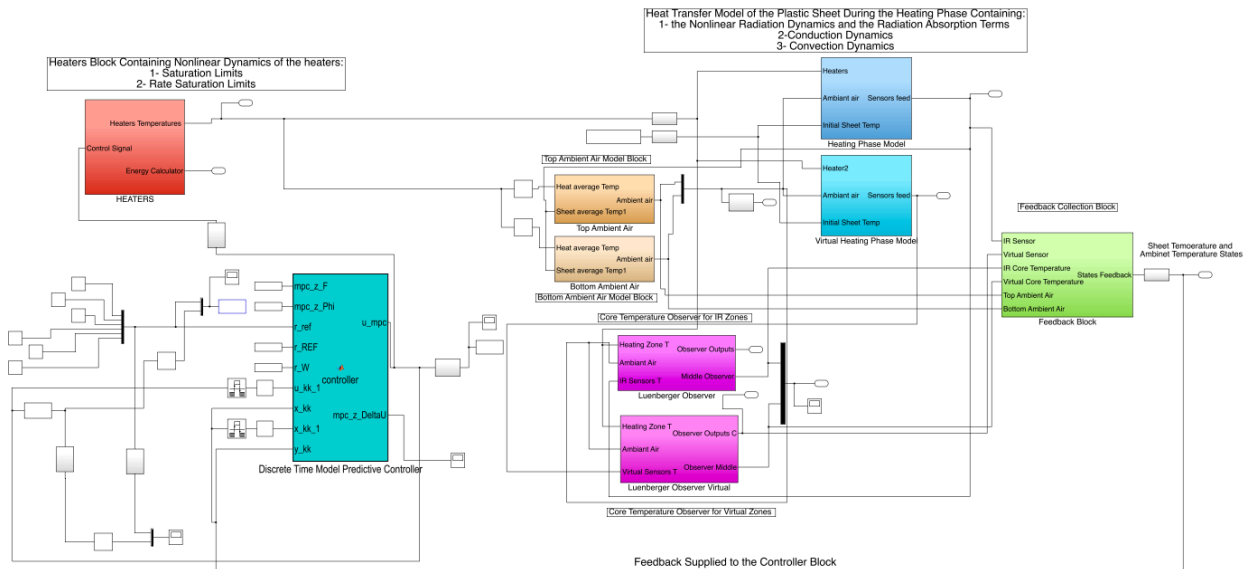


Figure A.19. The simulator in the presence of the discrete time model predictive controller

A.5 Chapter 5 Simulator Blocks

In this section, the hybrid optimal control simulation setup, studied in Chapter 5, is discussed. In Chapter 5, we conduct simulation studies for two different control schemes: 1) open-loop hybrid optimal control, for which the block diagram is shown in Fig. 5.6, and 2) closed-loop hybrid control, for which the block diagram is shown in Fig. 5.7.

The simulation blocks are similar to the ones discussed in section A1, with the exception that in the “Heating Phase Model” and “Virtual Heating Phase Model” blocks, the specific heat capacity C_p varies in real-time according to the sheet temperature in each measurement zone. Thus, the heat transfer equations used in these blocks are presented in equations (5), (6), and (7) in Chapter 5. The variation curve chosen for C_p is shown in Fig. 5.2 (shown in Chapter 5).

Also, in Chapter 5, we consider the thermoforming machine to be of a smaller size, consisting of 36 heaters (18 on top and 18 on the bottom), while considering six IR sensors (three on top and three on the bottom) and six virtual sensors (three on top and three on the bottom). The 2D position grid of the IR sensors and the virtual sensors relative to the heaters is shown in Fig. 5.5, and the vertical distance between the top and bottom heaters and the plastic sheet is considered as 20 cm on each side. The simulator is designed to fit sheets with dimensions of up to 1.5mX0.9m. In this chapter, a smaller simulator was used because the execution and the convergence of the hybrid design algorithm could become time consuming using a personal computer. Therefore, in order to expedite the design process, we used a reduced-sized model to get admissible results in a faster time.

In the simulator schematic, both control schemes are implemented in one setup as shown in Fig. A.20. Observing Fig. A.20, the cyan blue blocks are respectively the optimal control signals and the optimal trajectories generated by the hybrid optimal control algorithm. The switch implemented before the “Heaters” block is set to switch between the open-loop scheme (shown in Fig. 5.6) and the closed-loop scheme (shown in Fig. 5.7). The green block represents the feedback controller used in the closed-loop scheme (presented in Fig. 5.7). If the closed-loop scheme is in effect, the controller output will be the superposition of the hybrid optimal control signals and the control signal generated by the feedback controller. On the other hand, if the open-loop scheme is acting on the system, only the hybrid optimal control signals are applied to the heaters, and thus there is no feedback in the setup.

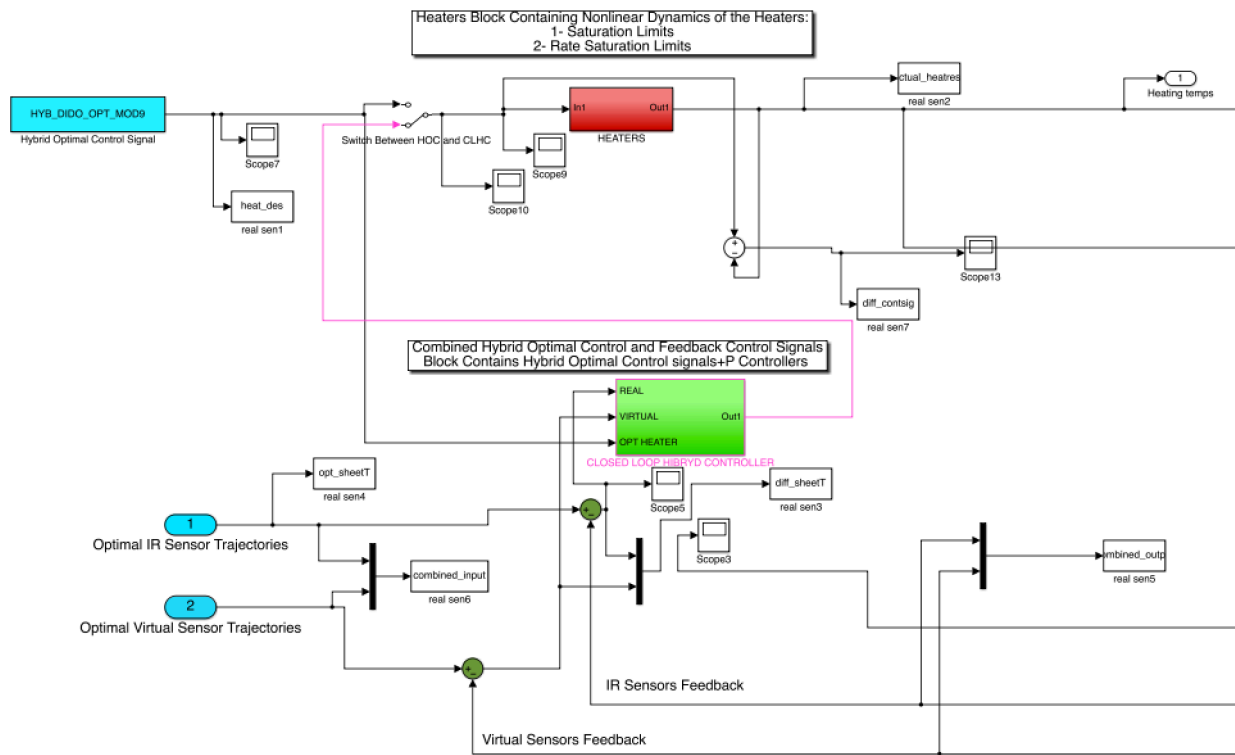


Figure A.20. The simulator in the presence of the hybrid optimal and feedback controllers

A.6 Table of Material Properties

In this section, we present the table of tuned material properties for the black HDPE sheet used in Chapters 2, 3, and 5, as well as the table of tuned material properties for the transparent (non-opaque) Acrylic and ABS plastics that form the multilayer sheet, as presented in Chapter 4. These values are obtained from [116] and from the tunings presented by Ajersch in [34].

Table A-1 Table of tuned material properties for HDPE

Material Properties	Units	Values
Density	kg/m ³ .	950
Specific Heat Capacity	J/(kg.K)	1838 (varying in Chapter 5)
Effective Emissivity		0.45
Average absorptivity		300
Conduction Coefficient	W/(m.K)	0.4
Convection Coefficient	W/(m ² .K)	6

Table A-2 Table of tuned material properties for Acrylic

Material Properties	Units	Values
Density	kg/m ³ .	1185
Specific Heat Capacity	J/(kg.K)	1500
Effective Emissivity		0.45
Average absorptivity		300
Conduction Coefficient	W/(m.K)	0.21
Convection Coefficient	W/(m ² .K)	6

Table A-3 Table of tuned material properties for ABS

Material Properties	Units	Values
Density	kg/m ³ .	1057
Specific Heat Capacity	J/(kg.K)	1200
Effective Emissivity		0.45
Average absorptivity		300
Conduction Coefficient	W/(m.K)	0.17
Convection Coefficient	W/(m ² .K)	6

A.7 Simulator Discussion

As it was elaborated before, for most of the thesis, the values for the material properties are tuned so that the simulator can mimic the actual process. Also, as it was previously mentioned, in the case of the HDPE sheet, Ajersch introduced tunings in [34], which resulted in $\pm 2\%$ percent error between the simulation and experiment results for heaters varying in the range of 280°C to 420°C. In case the heaters temperatures go above the specified range, the error could be higher. In terms of the validation of the simulator, we used the tunings presented by Ajersch in [34] and adjusted the controller gains (whenever possible) so that the heaters did not exceed the 420°C upper limit, as the goal was to maintain a $\pm 2\%$ error between the simulation and the actual process. However, there may have been instances when this range has been violated.

Therefore, one of the potential shortcomings of the simulator could be that the material properties are tuned and not treated as temperature dependent. However, the tracking results

obtained in all the chapters of this thesis are precise enough that in case we have larger errors between the model and the actual process, the temperature responses may still fall within the $\pm 10^\circ\text{C}$ forming window, and so proper forming could still occur.

More importantly, the methodologies and algorithms developed in this thesis are not affected if the heat transfer model of the plastic sheet contains variable material properties. Here we discuss the validity of each method if in the simulator setup, the model with variable material properties replaces the current model.

In Chapter 2, the proposed virtual model-based sensors would still provide accurate estimations since there are no limitations in implementing a model with varying material properties in the virtual sensor algorithm. This is also showcased in the simulation study as a 20% perturbation is acting on the system, yet the virtual sensors are unfazed by these perturbations.

In Chapter 3, the proposed Watanabe-modified Smith predictor scheme would still provide accurate tracking since the heating phase model containing varying material properties would still manifest first-order dynamics as shown by Khan *et al.* in [37]. Moreover, in the simulation study, we have applied a 30% perturbation to the system, and the results are again unaffected by these perturbations.

In Chapter 4, as it can be observed from Fig. 4.8(b), the heaters are operating within the range of 100°C to 310°C as the proposed discrete time model predictive controller (DTMPC) does not allow the heaters' temperatures to go to high values due to the prediction and control horizons, the incorporation of the heaters dynamics, and the inclusion of control output minimizing terms in the cost function in (25). Also, the r_w gain in equation (23) of Chapter 4 can be always systematically adjusted so that for all types of plastic sheets, the heaters temperatures do not exceed the 420°C limit. This will allow the DTMPC algorithm to be admissible in an actual experimental setting. As it was discussed in Chapter 6, in case the need to deal with a heat transfer model with variable material properties arises, the DTMPC could be replaced by a nonlinear model predictive controller, which contains similar characteristics to the DTMPC. This could be investigated as future research avenue.

Nevertheless in [37], Khan *et al.* suggest an error of approximately 5°C between a sheet temperature varying model and a model with constant material properties, for the heater temperature range of 280°C to 320°C , and larger errors outside of this window. This is why we

have started the process of developing controllers for models with temperature varying material properties, as this was studied in Chapter 5 for a temperature-varying specific heat capacity C_p , which varies the most amongst all the material properties. As it was shown in Chapter 5 through the simulation study, where the real-time variations of C_p are implemented in the simulator, the hybrid optimal controller provides precise temperature tracking for the temperature varying heat transfer model. In fact, the hybrid optimal controller has the potential to account for the dynamics of all the temperature varying material properties, such as the density ρ and the thermal conductivity k , and is ultimately able to produce control signals to provide accurate temperature tracking. As a future avenue of research, we will design the hybrid controller for the full temperature varying model, presented by Thomson *et al.* in [36] and by Khan *et al.* in [37], to conclude the control design investigations.

In summary, the simulator is comprehensive in terms of accounting for the nonlinearities associated with the heaters' dynamics and the radiation terms, as well as accounting for radiation absorption coefficients through the layers of the plastic sheet. In terms of the material properties, with the proper set of tunings, the simulator could mimic the actual process with a $\pm 2\%$ error for a certain range of heaters, but there may have been instances where this range has been violated. However, as it was described in detail, this does not affect the validity of the methodologies and algorithms proposed in this thesis, and the legitimacy of the methods proposed in this thesis remains intact.